

# **Noise Filtering in Quantum Information**

Todd James Green

*A thesis submitted to*

The University of Sydney

*in partial fulfillment of the  
requirements for the degree of*

Doctor of Philosophy

School of Physics  
The University of Sydney  
October 2016



## Abstract

The parallel developments of quantum mechanics, information theory and computer science, over the course of the 20th century, have led to proposals for new technologies that leverage the peculiar characteristics of quantum systems to perform information processing tasks that would otherwise be infeasible. However, a significant impediment to the construction of practical quantum information processing (QIP) devices is the fragility of the coherent quantum states on which their successful operation depends, in the presence of noise generated by interactions with the environment. These interactions not only induce errors that adversely affect the capacity to store and process information reliably, they can lead to the complete destruction of desirable quantum properties. Without the development of strategies to characterize and suppress errors due to realistic, temporally correlated noise, practical, large-scale QIP technologies are therefore unlikely to ever be realized.

In this thesis, we present novel techniques for modeling and mitigating the effects of time-dependent noise created by interactions between a quantum system and its environment, and by errors in applied controls. Our scope encompasses quantum storage (memory) and nontrivial QIP tasks in both single and multi-qubit systems, with a particular focus on control operations applied to trapped-ion qubits. The work begins with the introduction of a computationally efficient approach to characterizing the impact of time-dependent noise in single-qubit systems. We show that the fidelity of an arbitrary control operation can be expressed in terms of the spectral characteristics of the noise (an experimentally relevant parameter) and a set of *generalized filter functions* that capture the action of the control in frequency space. In conjunction with brute-force numerical simulation, we use this analytical technique to model the evolution of a noisy single-qubit system subject to an arbitrary piecewise-constant control sequence. We also determine the extent to which known composite pulses, devised to correct for static control errors, continue to be robust when subject to time-dependent non-Markovian noise. In addition, by accurately predicting the effects of experimentally engineered noise in single-qubit trapped ion systems, we demonstrate the practical utility of the method in analyzing the operation of arbitrary control protocols as spectral filters.

In the second half of the work, we obtain a number of new and important results that extend the range of utility of state-preserving ‘bang-bang’ dynamical decoupling (DD) control sequences. Firstly, we show that, via the repetition of an appropriately chosen high-order base DD sequence, the coherence of an arbitrary single-qubit state can be made to saturate at a fixed non-zero value. On the basis of both analytical and numerical calculations, we conclude that it is possible to maintain this ‘fidelity plateau’ for a significant period of time, even in the presence of realistic experimental imperfections. These device-independent results provide a means to create a practically useful high-fidelity, long-time quantum memory. Importantly, we show how this approach can be generalized, through the imposition of appropriate symmetry conditions, to obtain similar results for multi-qubit systems and for non-Gaussian noise environments. In the process, we devise multi-qubit DD sequences that can ensure maximum high-order error suppression in both the time and the frequency domains, using exponentially fewer pulses than existing sequences. Finally, we explain how, given the freedom to arbitrarily and quasi-instantaneously change the phase of the interaction between a system of qubits and a finite collection of oscillators, frequency-specific phase modulation protocols can be implemented that decouple the qubits from targeted oscillator modes at pre-determined times. This technique can be used to generate fast, high-fidelity multi-qubit entangling operations in, for example, ion trap QIP devices. Via concatenation, these DD-like sequences can also be used to simultaneously suppress the deleterious effects of fluctuations in the strength of the coupling field.



# Attribution Statements

## Chapter 3

The contents of this chapter have been published as:

T. J. Green, H. Uys and M. J. Biercuk, “High-order noise filtering in nontrivial quantum logic gates”, Physical Review Letters **109**, 020501 (2012).

With the exception of some minor reformatting, the work has been reproduced without alteration.

*Contribution* - The idea of extending the existing filter function formalism to non-trivial control operations was conceived by M. J. Biercuk. I developed the analytical method presented in the publication and H. Uys was responsible for the numerical contribution. All three authors collaborated on the writing of the work.

## Chapter 4

The contents of this chapter (excluding the post-publication addendum, section 4.9) have been published as:

T. J. Green, J. Sastrawan, H. Uys and M. J. Biercuk, “Arbitrary quantum control of qubits in the presence of universal noise”, New Journal of Physics **15**, 095004 (2013).

With the exception of some minor reformatting, and the above-mentioned additional section, the work has been reproduced without alteration.

*Contribution* - I developed the analytical method presented in the publication. J. Sastrawan made contributions to the formalism for the description of decoupling sequences in section 5, and H. Uys was responsible for undertaking the numerical work. I wrote the text with guidance from M. J. Biercuk.

## Chapter 5

The contents of this chapter have been published as:

C. Kabytayev, T. J. Green, K. Khodjasteh, M. J. Biercuk, L. Viola and K. R. Brown, “Robustness of composite pulses to time-dependent control noise”, Physical Review A **90**, 012316 (2014).

With the exception of some minor reformatting, the work has been reproduced without alteration.

*Contribution* - I made major contributions to the analytical work presented and to the writing of the paper.

## **Chapter 6**

The contents of this chapter have been published as:

A. Soare, H. Ball, D. Hayes, J. Sastrawan, M. C. Jarratt, J. J. McLoughlin, X. Zhen, T. J. Green and M. J. Biercuk, “Experimental noise filtering by quantum control”, *Nature Physics* **10**, 825 (2014).

With the exception of some minor reformatting, the work has been reproduced without alteration.

*Contribution* - A. Soare, H. Ball, D. Hayes and M. J. Biercuk conceived and performed the experiments, built experimental apparatus, contributed to data analysis and wrote the manuscript. I conceived and developed a major part of the theoretical toolkit used, and provided guidance in linking theoretical objects to measurement results, working with H. Ball, who led data analysis. J. Sastrawan, M. C. Jarratt and X. Zhen assisted with development of the experimental system and data collection. J. J. McLoughlin assisted with data collection.

## **Chapter 7**

The contents of this chapter have been published as:

K. Khodjasteh, J. Sastrawan, D. Hayes, T. J. Green, M. J. Biercuk and L. Viola, “Designing a practical high-fidelity long-time quantum memory”, *Nature Communications* **4**, 2045 (2013).

With the exception of some minor reformatting, the work has been reproduced without alteration.

*Contribution* - I collaborated with J. Sastrawan and D. Hayes on developing analytical and numerical approaches to modeling the effect of deviations from ideal, instantaneous control pulses. This work leveraged the analytical toolkit for filter transfer functions that I developed and used code that I had originally written.

## **Chapter 8**

The contents of this chapter have been published as:

G. A. Paz-Silva, S.-W. Lee, T. J. Green and L. Viola, “Dynamical decoupling sequences for multi-qubit dephasing suppression and long-time quantum memory”, *New Journal of Physics* **18**, 073020 (2016).

With the exception of some minor reformatting, the work has been reproduced without alteration.

*Contribution* - As co-author of the paper, I collaborated with my fellow co-authors G. A. Paz-Silva, S.-W. Lee and L. Viola on the analytical methods and results presented, and on the structure and text of the publication. I was also responsible for writing section 5.2, in which the effects of deviations from the idealized theoretical model are discussed.

## **Chapter 9**

The bulk of the contents of this chapter have been published as:

T. J. Green and M. J. Biercuk, “Phase-modulated decoupling and error suppression in qubit-oscillator systems”, Physical Review Letters **114**, 120502 (2015).

The subsections entitled ‘Example phase modulation sequence’, ‘Entangling phases for a piecewise-constant phase-modulation sequence’ and ‘The Molmer Sorensen gate’, which appeared in the *Supplementary material* of the original publication have been incorporated into the main text, to improve readability. Otherwise, the work has been reproduced without alteration.

*Contribution* - The idea of using phase-modulation to generate multi-mode entangling operations was conceived by M. J. Biercuk. I developed the analytical method presented, performed all supporting calculations, and wrote the text/prepared the figures, with guidance from M. J. Biercuk.

## Acknowledgements

I would firstly like to thank my supervisor, Assoc. Prof. Michael Biercuk. Without his guidance, encouragement and (most importantly) patience, it's unlikely that I would have even embarked on a PhD in theoretical physics, let alone completed it. I'm also extremely grateful to my co-supervisor, Assoc. Prof. Andrew Doherty for his willingness to cheerfully answer any and all questions, no matter how poorly articulated they may have been. Much thanks also to all past and present students and staff of the Quantum Control Laboratory (QCL). In particular, those in the QCL team with whom I've worked on one project or another over the past few years: Harrison Ball, Sandeep Mavadia, Claire Edmunds, Alistair Milne, Jarrah Sastrawan, David Hayes, Alexander Soare, Marie Claire Jarratt, Xinglong Zhen and Will De Ferranti. Thanks also to external co-authors Hermann Uys, Kaveh Khodjasteh and Ken Brown.

I'm also greatly indebted to my *unofficial* co-supervisor (and official co-author), Prof. Lorenza Viola, whose enthusiasm for theoretical physics, for gelato, and for life in general, made my time at Dartmouth so enjoyable. Thanks to Peter Kaplar for his hospitality during my stay in Hanover, to my Dartmouth officemates Peter (Johnson) and Sebastian, and to Seung-Woo, Gerardo, Chingiz, Roberto, Marjan, and all staff and students at Dartmouth.

Much thanks also to friends John, Allan, Lance and Deb, for their great generosity and encouragement.

Lastly, I would like to dedicate this work to the memories of my father Jeffery Edwin Green and my Grandfather Edward Bernard Green, neither of whom had the opportunity to pursue higher education, despite their lifelong love of learning. I like to think that they would be proud of this achievement, had they known about it. And to my late friend Mark Horniman with whom I embarked on this ill-advised journey into physics, and whose dark humor helped me through many difficult moments – ‘It doesn’t get any better than this.’



## **A note on style & content**

The major part of this thesis consists of previously published material – each chapter essentially being made up of a single published work, with a modicum of reformatting to improve readability. While this choice of style has inevitably resulted in some (very minor) variations in nomenclature and notation from chapter to chapter, each published work, and therefore each chapter, is self-contained, in the sense that all terminology and notational conventions are fully explained as they arise.

Chapter 2 is intended to provide the background material to bridge any gaps in knowledge that may exist, assuming the reader has at least a couple of years of undergraduate physics behind them. It also serves the more general purpose of providing some context for the chapters that follow.



*There's joy in repetition.*

Prince Rogers Nelson

(1958-2016)



# Contents

<b>1</b>	<b>Introduction</b>	<b>1</b>
<b>2</b>	<b>Background theory</b>	<b>5</b>
2.1	Quantum formalism . . . . .	5
2.1.1	Measurements & states . . . . .	6
2.1.2	Operators & changes of state . . . . .	7
2.1.3	Mixed states . . . . .	8
2.1.4	Bipartite systems & entanglement . . . . .	9
2.1.5	Dynamics . . . . .	10
2.2	Quantum information processing . . . . .	12
2.2.1	Qubits & the Bloch sphere representation . . . . .	12
2.2.2	Quantum logic gates . . . . .	13
2.3	Decoherence . . . . .	14
2.3.1	The quantum model . . . . .	15
2.3.2	The semiclassical model . . . . .	16
2.3.3	Dephasing noise . . . . .	17
2.4	Classical control & noise filtering . . . . .	18
2.4.1	Linear systems & controllability . . . . .	18
2.4.2	Filters in the time & frequency domains . . . . .	19
2.5	Dynamical quantum error suppression . . . . .	22
2.5.1	Open-loop quantum control . . . . .	22
2.5.2	Coherent averaging . . . . .	23
2.5.3	General dephasing DD sequences & spectral overlap . . . . .	26
2.5.4	General DQES control setting . . . . .	28
2.6	Relevance of this work . . . . .	33
<b>3</b>	<b>High-order noise filtering in nontrivial quantum logic gates</b>	<b>34</b>
3.1	Introduction . . . . .	34
3.2	Theoretical model . . . . .	35
3.2.1	The error vector . . . . .	35
3.2.2	Entanglement fidelity . . . . .	36
3.2.3	Fourier space representation . . . . .	37
3.3	Conclusion . . . . .	40
<b>4</b>	<b>Arbitrary quantum control of qubits in the presence of universal noise</b>	<b>42</b>
4.1	Introduction . . . . .	42
4.2	Quantum control in realistic environments . . . . .	44
4.2.1	Single-qubit dynamics and the Bloch sphere . . . . .	44

4.2.2	Capturing the effects of noise . . . . .	46
4.2.3	Geometric treatment of decoherence: the error vector and control matrix	47
4.2.4	Magnus expansion of the error vector . . . . .	47
4.3	Operational fidelity . . . . .	48
4.3.1	Moving to the Fourier domain . . . . .	50
4.4	Evaluating the control matrix . . . . .	50
4.4.1	Universal noise . . . . .	51
4.4.2	Dephasing noise . . . . .	52
4.5	Pulse effects in dynamical decoupling sequences . . . . .	54
4.5.1	Separating pulses from the pulse sequence . . . . .	55
4.5.2	Pulse forms: Standard $\pi_X$ -pulses and dynamically corrected gates . . . . .	56
4.5.3	Interpreting the filter function . . . . .	57
4.5.4	The full filter functions: DD + DCG . . . . .	57
4.6	Limits of approximation . . . . .	58
4.6.1	Convergence of the Magnus expansion . . . . .	59
4.6.2	Numerical simulations and the first-order approximation . . . . .	59
4.7	Conclusion . . . . .	62
4.8	Appendix . . . . .	63
4.9	Addendum . . . . .	67
<b>5</b>	<b>Robustness of composite pulses to time-dependent control noise</b>	<b>69</b>
5.1	Introduction . . . . .	69
5.2	Theoretical framework . . . . .	70
5.2.1	Control protocols . . . . .	70
5.2.2	Time-dependent error model . . . . .	72
5.3	Results . . . . .	73
5.3.1	Analytical results and geometric picture . . . . .	73
5.3.2	Comparison with numerical results . . . . .	77
5.4	Conclusion . . . . .	78
5.5	Appendix . . . . .	79
<b>6</b>	<b>Experimental noise filtering by quantum control</b>	<b>81</b>
6.1	Introduction . . . . .	81
6.2	Results . . . . .	82
6.3	Conclusion . . . . .	86
6.4	Appendix A . . . . .	88
6.5	Appendix B . . . . .	89
<b>7</b>	<b>Designing a practical high-fidelity long-time quantum memory</b>	<b>108</b>
7.1	Introduction . . . . .	108
7.2	Results . . . . .	109
7.2.1	Model . . . . .	109
7.2.2	Quantum memory requirements . . . . .	110
7.2.3	Quantum memory via periodic repetition . . . . .	111
7.2.4	Realistic effects . . . . .	114
7.3	Discussion . . . . .	117
7.4	Appendix . . . . .	118

<b>8</b>	<b>Dynamical decoupling sequences for multi-qubit dephasing suppression</b>	<b>122</b>
8.1	Introduction . . . . .	122
8.2	Multi-qubit controlled dephasing dynamics . . . . .	124
8.2.1	Gaussian versus non-Gaussian dephasing models . . . . .	124
8.2.2	Control protocols . . . . .	128
8.2.3	Exact representation of the controlled dynamics and fundamental filter functions . . . . .	130
8.3	Dynamical decoupling vs. multi-qubit dephasing noise: short-time memory . .	134
8.3.1	Non-selective multi-qubit control sequences . . . . .	134
8.3.2	Selective two-qubit control sequences . . . . .	135
8.3.3	Selective multi-qubit control sequences . . . . .	142
8.4	Dynamical decoupling vs. multi-qubit dephasing noise: long-time storage . .	146
8.4.1	Fidelity plateau conditions for multi-qubit classical stationary dephasing	146
8.4.2	Fidelity plateau conditions for multi-qubit classical plus spin-boson dephasing . . . . .	149
8.5	Further considerations . . . . .	153
8.5.1	Controlled entanglement generation and storage . . . . .	153
8.5.2	Realistic considerations . . . . .	154
8.6	Conclusion . . . . .	157
8.7	Appendix A: Controlled two-qubit dynamics under Gaussian dephasing . . .	158
8.8	Appendix B: Two-qubit fidelity plateau under symmetry breaking timing errors	160
<b>9</b>	<b>Phase-modulated decoupling and error suppression in qubit-oscillator systems</b>	<b>163</b>
9.1	Introduction . . . . .	163
9.2	Theoretical model . . . . .	164
9.3	Entangling phases for a piecewise-constant phase-modulation sequence . .	168
9.4	Example implementation . . . . .	169
9.5	Conclusion . . . . .	171
9.6	Appendix . . . . .	172
<b>10</b>	<b>Conclusion</b>	<b>176</b>

# Chapter 1

## Introduction

Beginning in the early years of last century, the development of the modern theory of quantum mechanics has reshaped our view of the physical world, and the way in which we interact with it. The tangible certainties of the classical past have been superseded by a paradigm of probabilities and potentialities in which we, as observers, play an irreducible part. At a fundamental level, quantum mechanics seems to be saying something quite profound about the nature of reality and, more particularly, about the division between subjective and objective knowledge. While this might appear to be of mainly esoteric interest, it has had, and continues to have, an impact at the more practical level. Working scientists have learned to be somewhat wary of concrete statements about the properties of physical systems, outside of their actually being measured. Notwithstanding, what one can say with some degree of confidence is that quantum mechanics is, at the very least, a theory of knowledge. In particular, it is a theory of how the process of observation changes our state of knowledge, i.e., it is a theory of information [1, 2, 3].

Remarkably, while quantum theory was still in its infancy, and its implications were still being understood, two emerging disciplines, communications theory and computer science, were contributing to the development of a rigorous, quantitative theory of information and of information processing. In 1948, Claude Shannon, in a landmark work on the capacity of classical communication channels, established the mathematical foundations of the modern theory of information [4]. In the process, he introduced the fundamental unit of information – the *bit* (binary digit) – a physical system that can exist in only one of two possible stable states, usually labeled 0 and 1. More than a decade earlier, Alan Turing had employed a similar minimal symbolic alphabet in a work that described a universal computing device (now known as a Turing machine) that has come to be seen as the theoretical blueprint for all modern computers [5].

In combination, communications theory and computer science have provided the rigorous theoretical underpinning for what has become known as the ‘information age’. However, while quantum theory has played a significant role to date, in allowing for the design and construction of smaller and more efficient components, information processing and transmitting technologies still operate on the basis of classical physics. It is only very recently that the possibility of genuinely *quantum* information processing (QIP) devices has provoked serious scientific and commercial interest. The physical principle that differentiates QIP from orthodox, classical information processing is that of the superposition of states. Like the classical bit, the fundamental unit of QIP, the qubit (*qu-antum bit*), can be observed in just one of two mutually exclusive states. However, unlike the classical bit, its behaviour can be explained fully only by assuming that, when it is not being observed, it can exist in a *coherent superposition*

$$|\psi\rangle = c_0|0\rangle + c_1|1\rangle \quad (1.1)$$

of the two observable states (denoted here by the ‘kets’  $|0\rangle$  and  $|1\rangle$ ) where  $c_0$  and  $c_1$  are complex

numbers for which  $|c_0|^2 + |c_1|^2 = 1$ . It is the possibility of such superpositions that gives QIP its extraordinary potential power [6]. For example, given a quantum register of  $n$  qubits, it is, in principle, a simple matter to produce a state that is an equally weighted superposition of all possible register values (i.e., all possible strings of 0s and 1s). Loosely speaking, subsequent QIP operations can then be executed on all register values simultaneously, a feat of parallel processing that is difficult to match using classical computing technology, for any significant number of bits. Unfortunately, the superposition principle also has a ‘down side’ in that it can result in the *entanglement* of the QIP system and its environment, leading to the degradation of encoded quantum information.

While the possibility of completely isolating a physical system from its surroundings is a useful simplifying assumption for the theorist, any real physical system will interact with its environment to some degree. Classically, there is no reason to suppose that this coupling cannot, at least in principle, be reduced to a level below which it does not significantly affect the system’s measurable properties. By contrast, quantum theory predicts that even the weakest of interactions can generate entangled system-environment states, *fundamentally* altering the observable behaviour of the system and culminating in the complete suppression of interference effects – a process referred to as *decoherence* [7, 8]. Along with the advent of experimental techniques that have enabled researchers to study the mechanisms of coherence decay in real quantum systems [9, 10, 11], the rapidly growing interest in the development of quantum coherent technologies, to which decoherence-induced errors constitute a major impediment, has focused renewed attention on the understanding and mitigation of environment-induced noise effects in QIP systems.

One of the more obvious ways to address the decoherence problem, assuming all possible steps have been taken to reduce undesirable interactions at the level of device design, is to simply transplant existing classical error correction techniques into the quantum context. In a classical error-correcting code, information is encoded into logical bits, each of which is composed of several physical bits, and it is this redundancy that enables errors to be detected and corrected. Unfortunately, there are several difficulties deriving from the ‘quantumness’ of QIP systems that limit the direct application of classical error correction techniques: (i) the *no-cloning theorem*, which prohibits the copying of arbitrary quantum states – ruling out the naive application of classical redundant encoding methods [12, 13]; (ii) while classical bits are (by definition) *digital*, suffering only from discrete ‘bit-flip’ errors, the states of a qubit, and therefore the possible errors that may arise, form a continuum and are thus essentially *analogue* in character; and (iii) merely observing a QIP system in order to detect errors will, in general, change its state, creating precisely the sort of unwanted evolution we wish to counter.

Surprisingly, in the mid-1990s it was shown that it was possible to create a class of *quantum* error correction codes (QECs) that ‘discretized’ the continuum of errors, operated without the need to directly measure the quantum state, and employed redundancy in a way that circumvented the no-cloning theorem [14, 15, 16]. However, issues associated with the practical implementation of QECs limit their application to physical systems in which maximum error rates are of the order of  $\sim 10^{-4}$  [17, 18, 6]. Thus, while QECs will be an essential element of any future QIP technology, they do not, on their own, appear to solve the decoherence problem.

A different, and indeed complementary, approach to combating the effects of noise in general, and of decoherence in particular, is to attempt to suppress the resulting errors at the *physical level*, before they reach the logical level at which QEC is applied.<sup>1</sup> In the main, the focus of this work is the assessment and generalization of an approach to physical-layer error reduction

---

<sup>1</sup>In fact, limitations on the capacity to experimentally isolate a controlled quantum system and the aforementioned acceptable error rates for QECs would seem to mandate some form of active error suppression at the physical level.

called *dynamical quantum error suppression* (DQES). Inspired by the well-established coherent averaging techniques of nuclear magnetic resonance (NMR) spectroscopy [19, 20, 21], DQES takes advantage of the fact that no physical process, including any that may manifest as noise, can take place instantaneously. There is therefore always some time interval relative to which any change can be regarded as ‘slow’. If experimental quantum control hardware is such that this timescale can be accessed, i.e., if control operations can be executed before significant change has occurred, then the evolution of the target quantum system can be manipulated in such a way that errors generated during different intervals of time can be ‘averaged out’. DQES methods therefore operate most effectively in strongly non-Markovian noise environments in which correlation times are large on experimentally accessible timescales.

The temporal description of the interplay between noise and control processes is complemented by the *spectral* description, which allows for a useful alternative way of thinking about the design of control and/or signal processing systems [22, 23, 24]. Envisioning a complex signal as a composition of simpler periodic signals can often make its salient properties easier to grasp than does a direct temporal analysis. In frequency space, error suppression can be thought of as a filtering process by which particularly damaging frequency components are removed from the noise signal. Transferring this noise filtering perspective into the QIP context allows one to make use of this intuitively appealing perspective and to take advantage of the wealth of hard-won knowledge accumulated by the control theory and signal processing communities. Quantum control can then be viewed as a filtering operation that may be tailored, via the tuning of applied control fields, to perform optimally in particular noise frequency environments. The concept of filtering can also be abstracted to include *symmetrization*, a process by which control protocols are contrived to generate an *effective* evolution of the target system that preserves quantum information in the short-time limit.

The principle aims of this work are to further advance our understanding of the effects of time-dependent noise on QIP systems, from both spectral and temporal perspectives, and to develop novel physical-layer error suppression strategies, based on DQES principles, to counter these effects. Particular emphasis is placed on direct application of these strategies in real experimental settings and on their interpretation as frequency-domain noise filters. A key motivation is the extension of the existing, operationally limited, filter function formalism to arbitrary continuous-time control protocols and realistic, universal noise environments. We also seek to generalize existing DQES approaches to perform crucial QIP tasks such as long-time storage of information and entanglement generation.

The thesis begins in earnest in Chapter 2, with a summary of basic quantum mechanics and of elements of QIP. We also outline some of the more relevant aspects of classical control and quantum control theory. This is followed by a short discussion of simple decoherence models in quantum systems. The principles of DQES are then described, with an emphasis on decoherence suppression as a form of noise filtering. While the discussion in this chapter is brief, it is hoped that it will to provide the reader with sufficient theoretical background to put the ensuing material into context. Chapters 3 and 4 introduce single-qubit *generalized filter functions*, which can be used to describe the frequency-space action of arbitrary control operations in a broad range of noise environments. In chapter 5 we demonstrate the practical utility of this generalized noise filtering approach by accurately modeling the performance of composite pulse sequences in time-dependent noise environments. In chapter 6 we use this analytical approach in conjunction with experimental techniques to assess the efficacy of control protocols as noise filters.

Chapter 7 begins the second half of the thesis in the which range of application of idealized ‘bang bang’ dynamical decoupling (DD) sequences is extended beyond short-time preservation of single-qubit states in Gaussian dephasing environments. Here, we show that a practical long-time quantum memory can be generated via the periodic repetition of appropriately chosen DD

sequences. In chapter 8, efficient DD state-preservation protocols are devised for multi-qubit systems, subject to arbitrary non-Gaussian dephasing noise. The principle of using sequence repetition to create long-time quantum memory is then shown to be applicable to the multi-qubit case, subject to certain symmetry constraints. In chapter 9, we show that DD-like instantaneous ‘phase-flip’ sequences can be used to decouple a system of qubits from a collection of oscillators, after a pre-determined interaction time, generating high-fidelity inter-qubit entangling operations.

# Chapter 2

## Background theory

It's an obvious truth that no physical control operation can be carried out entirely without error. There are always imperfections of one kind or another that, if not accounted for, may prevent a control objective from being achieved with an acceptable degree of precision. In the language of communications theory, such imperfections reduce the capacity of a signal to transfer information reliably, i.e., they generate *noise*. This problem is particularly acute in quantum information processing (QIP) where, due to the analogue nature of quantum states and the limitations of error correcting codes, information processing tasks must be executed with an exceptionally high degree of fidelity. It is therefore crucial that the requisite quantum control operations be designed to be robust in the presence of noise.

While all processes that contribute to the degradation of stored quantum information ought to be considered, if the potential of QIP is to be realized, those that stem from the impossibility of completely isolating a controlled physical system from its surroundings have particularly unusual and deleterious effects in the quantum context. For this reason, and because an intuitive understanding of the nature of other sources of noise can largely be carried over from the classical setting, the principle aim of this chapter is to provide the background material necessary for an appreciation of the theoretical and practical challenges associated with the modeling and mitigation of environment-induced decoherence effects. With this in mind, we begin with a very brief summary of elementary quantum theory and of relevant aspects of QIP. We go on to consider simple quantum and semiclassical decoherence models, before introducing some useful concepts in classical control theory and signal processing. This is followed by a broad discussion of the principles of dynamical quantum error suppression (DQES), with an emphasis on its interpretation as quantum noise filtering.

### 2.1 Quantum formalism

From a purely operationalist standpoint, quantum mechanics is a set of rules for calculating the probabilities of measurement outcomes. This is not an especially remarkable statement, afterall, the same might be said of any physical theory. What is remarkable is that the uncertainty that gives rise to probabilities in quantum mechanics does not seem to be susceptible to a simple ignorance interpretation. That is to say, by contrast with classical systems, we can't assume that a quantum system possesses a complete set of real physical properties, each having a pre-existing value that can be revealed, however imperfectly, via measurement [25]. The philosophical implications of this have been, and continue to be, the subject of much debate. Fortunately, for the future of QIP, the theoretical understanding that underlies our capacity to control quantum systems is not contingent on the outcome of these discussions. As long as we can predict the way

in which the probabilities of measurement outcomes will change as a quantum system evolves, under both controlled and uncontrolled influences, we can, in principle, design and implement a protocol that will ‘steer’ the system to execute some desirable QIP task.

### 2.1.1 Measurements & states

The probabilities of the outcomes of all possible measurements that might be performed on a quantum system define its *state*. Clearly, the state of any particular system depends on its history, i.e., on how it was *prepared*. However, different preparation procedures need not lead to different states. Formally, then, a quantum state is to be regarded as an *equivalence class* of preparation procedures [2]. Two quantum systems that share the same set of probability assignments are, therefore, said to share the same state. A particularly simple example of a quantum state is one for which the measurement of some physical observable  $A$  always yields the same value, say  $a_1$ . Using ‘bra-ket’ notation, the mathematical representative of this state is a vector  $|a_1\rangle$  residing in a complex vector space  $\mathcal{H}$ , called the Hilbert space of the system [26]. Similarly, if an alternative preparation procedure results in always obtaining a value  $a_2 \neq a_1$  for the same observable, then we assign to this state the vector  $|a_2\rangle \in \mathcal{H}$ . The ‘quantumness’ of the system manifests when it is prepared in such a way that the outcome of any single measurement is either  $a_1$  or  $a_2$ , but we cannot predict which beforehand. That is, each outcome has a nonzero probability of being obtained.

Classically, we might simply conclude that this indeterminacy is only apparent and that, in principle, we could obtain sufficient information about the preparation procedure to regain our ability to predict the outcome perfectly. However, quantum mechanics allows for situations in which there is no way of knowing, even in principle, which of the outcomes will occur without fundamentally changing the nature of the experiment. The consequence of this is that, if the system is effectively ‘informationally isolated’ from the rest of the universe, then, until the point at which it is measured, we cannot assign to it one or other of the states  $|a_1\rangle$  or  $|a_2\rangle$  associated with the two perfectly distinguishable, i.e., mutually exclusive, measurement outcomes [1]. Instead, the state of the system must be described by a superposition

$$|\psi\rangle = c_1|a_1\rangle + c_2|a_2\rangle, \quad (2.1)$$

where  $c_1$  and  $c_2$  are complex numbers,  $c_1, c_2 \in \mathbb{C}$ .

#### The inner product and the Born rule

The distinguishability of measurement outcomes is formalized via an inner product,  $\langle \cdot | \cdot \rangle : \mathcal{H} \times \mathcal{H} \rightarrow \mathbb{C}$ , that maps any two vectors  $|\phi_1\rangle, |\phi_2\rangle$  in the system Hilbert space to a complex number  $\langle\phi_1|\phi_2\rangle$ , such that:

1.  $\langle\phi_1|\phi_2\rangle^* = \langle\phi_2|\phi_1\rangle$ , for all  $|\phi_1\rangle, |\phi_2\rangle \in \mathcal{H}$ , where  $(\cdot)^*$  denotes the complex conjugate;
2.  $\langle\psi|(c_1|\phi_1\rangle + c_2|\phi_2\rangle) = c_1\langle\psi|\phi_1\rangle + c_2\langle\psi|\phi_2\rangle$ , for all  $|\psi\rangle, |\phi_1\rangle, |\phi_2\rangle \in \mathcal{H}$  and  $c_1, c_2 \in \mathbb{C}$ ;
3.  $\langle\psi|\psi\rangle > 0$ , for all nonzero  $|\psi\rangle \in \mathcal{H}$ .

The last condition allows one to associate a magnitude, or *norm*  $\| |\psi\rangle \| = \sqrt{\langle\psi|\psi\rangle}$ , with each vector in the space. To be consistent with the conventions of probability theory, the vectors representing the physical states of quantum systems are normalized so that  $\langle\psi|\psi\rangle = 1$ . However, this does not uniquely define a particular vector as being *the* representative of the state. Rather, since it can be shown that global phase shifts do not affect observable properties, all vectors that differ by some complex phase factor are treated as equivalent state representatives.

Two states, such as  $|a_1\rangle$  and  $|a_2\rangle$  in equation (2.1), that are perfectly distinguishable are defined as having a vanishing inner product,  $\langle a_1|a_2\rangle = 0$ , and are said to be *orthogonal*. If we also wish to make it clear that the states are normalized, then we say that they are *orthonormal*. Given the properties of the inner product, and the orthonormality of  $|a_1\rangle$  and  $|a_2\rangle$ , we can make the all-important connection between the abstract superposition  $|\psi\rangle$  in equation (2.1) and the outcomes of measurements performed on the system in a laboratory.<sup>1</sup> Specifically, the complex coefficients in (2.1) are given by the inner products of the superposition state  $|\psi\rangle$  with each of the component states, i.e.,  $c_i = \langle a_i|\psi\rangle$ , for  $i = 1, 2$ . And the square moduli of these inner products, defined such that  $|c_1|^2 + |c_2|^2 = 1$ , give the probabilities of obtaining the corresponding measurement outcomes. In more practical terms,  $|c_i|^2 = |\langle a_i|\psi\rangle|^2$  can be interpreted as the limiting value of the relative frequency of outcome  $a_i$  in a long sequence of measurements made on identically prepared quantum systems. This is the so-called *Born rule* for assigning probabilities [27]. Generalization to the case of  $n$  possible measurement outcomes  $\{a_i\}_{i=1}^n$  is made by defining a set of  $n$  corresponding orthogonal states  $\{|a_i\rangle\}_{i=1}^n$ , where  $\langle a_i|a_j\rangle = \delta_{ij}$ .<sup>2</sup> An arbitrary state of such a system is expressible as

$$|\psi\rangle = \sum_{i=1}^n c_i |a_i\rangle, \quad (2.2)$$

where  $\sum_{i=1}^n |c_i|^2 = 1$ . And the set of states  $\{|a_i\rangle\}_{i=1}^n$  is said to form a basis for the  $n$ -dimensional Hilbert space  $\mathcal{H}$  of the quantum system. Once the basis is defined, the state of the system can be represented by the column vector  $(c_1, c_2, \dots, c_n)^T = (\langle a_1|\psi\rangle, \langle a_2|\psi\rangle, \dots, \langle a_n|\psi\rangle)^T$  of complex coefficients (the superscript  $T$  denotes the transpose).

### 2.1.2 Operators & changes of state

A change in the state of a quantum system manifests mathematically as a map from an initial to a final vector in its associated Hilbert space  $\mathcal{H}$ , i.e., it takes the form of an operator (in general, because we would like these changes to respect superpositions, we require that operators be linear.) A particularly stark change occurs when the system is measured. Given an initial state of the form (2.2), a measurement of observable  $A$  will return one of the outcomes  $\{a_i\}_{i=1}^n$ , say  $a_1$ . The continuity of our experience of reality would suggest that a second measurement, immediately following the first, would yield the same result. Hence, we might say that the measurement process has *projected* the superposition state  $|\psi\rangle$  onto the basis state  $|a_1\rangle$ . This process can be absorbed into the Hilbert space formalism by defining, for each possible outcome, a linear projection operator  $P_i \equiv |a_i\rangle\langle a_i|$ , that acts to ‘project out’ the  $i$ -th component of  $|\psi\rangle$ , i.e.,  $P_i|\psi\rangle = (|a_i\rangle\langle a_i|)|\psi\rangle = |a_i\rangle(\langle a_i|\psi\rangle)$ . In the language of projection operators, the probability of obtaining  $a_i$ , given that the system is in state  $|\psi\rangle$ , can be expressed as  $\langle\psi|P_i|\psi\rangle$ .

In practice, given the probabilistic nature of measurement outcomes, it is the average value of an observable  $A$  that is the quantity most relevant in the laboratory. A convenient shorthand for such averages, or *expectation values*, is obtained by introducing an operator representation of  $A$ , defined by attaching to each projection operator the associated (real-valued) measurement outcome, and summing over all possibilities:<sup>3</sup>

$$A = \sum_{i=1}^n a_i P_i = \sum_{i=1}^n a_i |a_i\rangle\langle a_i|. \quad (2.3)$$

---

<sup>1</sup>“Quantum phenomena do not occur in a Hilbert space, they occur in a laboratory” - Asher Peres [2]

<sup>2</sup> $\delta_{ij} = 1$ , for  $i = j$  and is equal to zero otherwise

<sup>3</sup>We have used the same notation for the observable and its operator representation. This is is unlikely to lead to any misunderstandings in this work, but one should be cognisant of the difference.

It is then easy to show that, given the system is in state  $|\psi\rangle$ , the expectation value of observable  $A$  is simply  $\langle\psi| A |\psi\rangle$ . It is also easy to show that, like all operators representing observables,  $A$  has the property of being *Hermitian*, i.e.,  $A = A^\dagger$ , where the *adjoint*,  $A^\dagger$ , of  $A$  is defined such that

$$\langle\phi_1| A^\dagger |\phi_2\rangle = \langle\phi_2| A |\phi_1\rangle^* \quad (2.4)$$

for all  $|\phi_1\rangle, |\phi_2\rangle \in \mathcal{H}$ . Hermitian operators are particularly suited to representing measurable quantities because, for finite-dimensional systems, they can always be written in the form (2.3), where the set of vectors  $\{|a_i\rangle\}_{i=1}^n$  forms an orthonormal *eigenbasis* for  $\mathcal{H}$ , and the *eigenvalues*  $\{a_i\}_{i=1}^n$  are real numbers, suitable for representing measured values of physical observables.

A particularly important set of Hermitian operators in QIP are the Pauli operators  $\{\sigma_x, \sigma_y, \sigma_z\}$  which, along with identity (the ‘do nothing’ operator)  $I$ , form a basis for all operators acting on the state space of a two-dimensional quantum system. The Pauli operators have eigenvalues  $\pm 1$  and are most often written in terms of the  $\sigma_z$  eigenbasis,  $\{|0\rangle, |1\rangle\}$  (it is the convention in QIP that these states are labeled by 0 and 1, rather than by their eigenvalues):

$$\sigma_x = |0\rangle\langle 1| + |1\rangle\langle 0|, \quad \sigma_y = i |1\rangle\langle 0| - i |0\rangle\langle 1|, \quad \sigma_z = |0\rangle\langle 0| - |1\rangle\langle 1|. \quad (2.5)$$

Defining the *commutator* of two operators  $A$  and  $B$  as  $[A, B] \equiv AB - BA$ , the Pauli operators are found to satisfy the following useful commutation relations:

$$[\sigma_i, \sigma_j] = 2i\varepsilon_{ijk}\sigma_k, \quad (2.6)$$

where the Levi-Civita tensor  $\varepsilon_{ijk}$  has the value 1 for the ordered triple of indices  $(i, j, k) = (x, y, z)$  and cyclic permutations thereof, vanishes when any two indices match, and is equal to  $-1$  otherwise. In addition, one can show that

$$\sigma_x^2 = \sigma_y^2 = \sigma_z^2 = I. \quad (2.7)$$

Each Pauli operator is therefore not only Hermitian, it is also its own inverse, so that we can write  $\sigma_k^\dagger \sigma_k = \sigma_k \sigma_k^\dagger = I$ , for  $k = x, y, z$ . More generally, any operator  $U$  for which  $U^\dagger U = UU^\dagger = I$  holds is called a *unitary* operator. Crucially, unitary operators do not affect the distinguishability of quantum states and, as such, are used to represent information preserving changes to quantum systems (see section 2.1.5).

Finally, we note that any operator  $M$  can be defined by its *matrix elements*  $M_{ij} \equiv \langle a_i| M |a_j\rangle$  with respect to a particular basis  $\{|a_i\rangle\}_{i=1}^n$ . An operator equation such as  $|\phi\rangle = M|\psi\rangle$  is then equivalent to a matrix equation

$$\begin{pmatrix} \langle a_1|\phi\rangle \\ \cdot \\ \cdot \\ \cdot \\ \langle a_n|\phi\rangle \end{pmatrix} = \begin{pmatrix} \langle a_1| M |a_1\rangle & \cdot & \cdot & \cdot & \langle a_1| M |a_n\rangle \\ \cdot & \ddots & & & \cdot \\ \cdot & & \ddots & & \cdot \\ \cdot & & & \ddots & \cdot \\ \langle a_n| M |a_1\rangle & \cdot & \cdot & \cdot & \langle a_n| M |a_n\rangle \end{pmatrix} \begin{pmatrix} \langle a_1|\psi\rangle \\ \cdot \\ \cdot \\ \cdot \\ \langle a_n|\psi\rangle \end{pmatrix}. \quad (2.8)$$

### 2.1.3 Mixed states

It is often the case that we have less than maximal information about the state of a quantum system. Instead, we may know only that it has some probability  $p_j$  of being in state  $|\psi_j\rangle$ , for  $j = 1, \dots, m$  (these states need not be orthogonal.) If we wish to calculate the expected value of an observable  $A$ , given this scenario, we need to account for both quantum and classical sources of uncertainty. Letting  $\langle\cdot\rangle$  denote the expectation value, one finds that

$$\langle A \rangle = \sum_{j=1}^m p_j \langle \psi_j | A | \psi_j \rangle. \quad (2.9)$$

This expression can be made a little more compact by defining the *density matrix*

$$\rho = \sum_{j=1}^m p_j |\psi_j\rangle\langle\psi_j| \quad (2.10)$$

associated with the system. Equation (2.9) is then equivalent to

$$\langle A \rangle = \text{Tr} [\rho A], \quad (2.11)$$

where  $\text{Tr}[\cdot]$  indicates that the *trace* of the expression within the brackets is to be taken. The trace is a linear transformation that maps Hilbert space operators to scalars by summing over expectation values with respect to a complete set of basis states  $\{|a_i\rangle\}_{i=1}^n$ , i.e.,

$$\text{Tr} [M] \equiv \sum_{i=1}^n \langle a_i | M | a_i \rangle, \quad (2.12)$$

for any operator  $M \in \mathcal{H}$ .

Density matrices are the most general way to represent quantum states as they encompass both pure states, of which we have maximal knowledge, and so-called *mixed states*, for which there is some additional uncertainty. The density matrix for a pure state  $|\psi\rangle$  is a simple projection operator  $|\psi\rangle\langle\psi|$ . For a mixed state, as the name suggests, the density matrix can be thought of as a classical *mixture* of projection operators, as in (2.10).

For an operator  $\rho$  to be a valid density matrix for a quantum system, it must have the following properties:

- $\langle\psi|\rho|\psi\rangle \geq 0$  for all  $|\psi\rangle \in \mathcal{H}$  (this condition of *positivity* also implies that  $\rho^\dagger = \rho$ , so that density operators are Hermitian); and
- $\text{Tr}[\rho] = 1$  (necessary for a consistent statistical interpretation.)

Density matrices that represent mixed states have the addition property that  $\text{Tr}[\rho^2] < 1$ .

### 2.1.4 Bipartite systems & entanglement

A *bipartite* quantum system is made up of two component systems  $\mathcal{S}_1$  and  $\mathcal{S}_2$ , each having its own Hilbert space;  $\mathcal{H}_{\mathcal{S}_1}$  and  $\mathcal{H}_{\mathcal{S}_2}$ . According to quantum theory, the appropriate representation for the state space of the combined system  $\mathcal{S}_1 + \mathcal{S}_2$  is the *tensor product* space  $\mathcal{H}_{\mathcal{S}_1+\mathcal{S}_2} \equiv \mathcal{H}_{\mathcal{S}_1} \otimes \mathcal{H}_{\mathcal{S}_2}$ , which consists of all linear combinations of products of the form  $|\psi\rangle \otimes |\chi\rangle$ , where  $|\psi\rangle \in \mathcal{H}_{\mathcal{S}_1}$  and  $|\chi\rangle \in \mathcal{H}_{\mathcal{S}_2}$ . If  $\{|v_i\rangle\}_{i=1}^{n_{\mathcal{S}_1}}$  is a basis for  $\mathcal{H}_{\mathcal{S}_1}$  and  $\{|w_i\rangle\}_{i=1}^{n_{\mathcal{S}_2}}$  is a basis for  $\mathcal{H}_{\mathcal{S}_2}$ , then a basis for  $\mathcal{H}_{\mathcal{S}_1+\mathcal{S}_2}$  consists of all products  $|v_i\rangle \otimes |w_j\rangle$ , where  $i = 1, \dots, n_{\mathcal{S}_1}$ , and  $j = 1, \dots, n_{\mathcal{S}_2}$ . Given that the dimensions of the component spaces are  $n_{\mathcal{S}_1}$  and  $n_{\mathcal{S}_2}$ , the composite space  $\mathcal{H}_{\mathcal{S}_1+\mathcal{S}_2}$  has dimension  $n = n_{\mathcal{S}_1} n_{\mathcal{S}_2}$ .

The inner product  $(\cdot, \cdot)$  on  $\mathcal{H}_{\mathcal{S}_1} \otimes \mathcal{H}_{\mathcal{S}_2}$  is defined in terms of the subsystem inner products:

$$(|\psi_1\rangle \otimes |\chi_1\rangle, |\psi_2\rangle \otimes |\chi_2\rangle) \equiv \langle\psi_1|\psi_2\rangle\langle\chi_1|\chi_2\rangle \quad (2.13)$$

for  $|\psi_1\rangle, |\psi_2\rangle \in \mathcal{H}_{\mathcal{S}_1}$  and  $|\chi_1\rangle, |\chi_2\rangle \in \mathcal{H}_{\mathcal{S}_2}$ . Similarly, any two operators  $M_1$  and  $M_2$ , acting on  $\mathcal{H}_{\mathcal{S}_1}$  and  $\mathcal{H}_{\mathcal{S}_2}$  respectively, define an operator  $M_1 \otimes M_2$  that acts on  $\mathcal{H}_{\mathcal{S}_1} \otimes \mathcal{H}_{\mathcal{S}_2}$  via the rule

$$(M_1 \otimes M_2) (|\psi\rangle \otimes |\chi\rangle) = (M_1 |\psi\rangle) \otimes (M_2 |\chi\rangle), \quad (2.14)$$

which can be generalized to arbitrary bipartite states and operators by linearity (we note here that, for the sake of simplifying notation, the tensor product symbol  $\otimes$  is often dropped from operator and state products, so that, for example,  $M_1 \otimes M_2$  becomes  $M_1 M_2$ , and  $|\psi\rangle \otimes |\chi\rangle$  becomes  $|\psi\rangle |\chi\rangle$  or  $|\psi, \chi\rangle$ .)

## Entangled states

Of central importance to QIP are those states of a bipartite quantum system that are classified as being *entangled*. An entangled state is most easily defined as a state that is not *separable*, where separability implies that the state of the composite system  $\mathcal{S}_1 + \mathcal{S}_2$ , given that it is pure, can be expressed as the tensor product of pure states of the component systems, i.e., if  $|\phi\rangle$  is the state of  $\mathcal{S}_1 + \mathcal{S}_2$ , then we can write

$$|\phi\rangle = |\psi\rangle \otimes |\chi\rangle, \quad (2.15)$$

where  $|\psi\rangle \in \mathcal{H}_{\mathcal{S}_1}$  and  $|\chi\rangle \in \mathcal{H}_{\mathcal{S}_2}$ . A composite quantum system in a separable state is therefore describable in terms of the states of its component systems. A system in an entangled (i.e., nonseparable) state, on the other hand, *cannot* be described in this way.

In the formalism of density matrices, a bipartite system in a state  $\rho_{\mathcal{S}_1 + \mathcal{S}_2}$  is separable if it can be decomposed as a convex sum

$$\rho_{\mathcal{S}_1 + \mathcal{S}_2} = \sum_i q_i \rho_{\mathcal{S}_1}^{(i)} \otimes \rho_{\mathcal{S}_2}^{(i)}, \quad (2.16)$$

where  $\{q_i\}$  is a set of nonnegative numbers such that  $\sum_i q_i = 1$ , and  $\{\rho_{\mathcal{S}_1}^{(i)}\}$  and  $\{\rho_{\mathcal{S}_2}^{(i)}\}$  are sets of density matrices defined on Hilbert spaces  $\mathcal{H}_{\mathcal{S}_1}$  and  $\mathcal{H}_{\mathcal{S}_2}$ , respectively.

### 2.1.5 Dynamics

The time-evolution of a closed quantum system (i.e., one from which there is no transfer of information to the rest of the universe) is represented by a unitary evolution operator, or propagator,  $U(t, t_0)$  that acts on the Hilbert space  $\mathcal{H}$  to map the system state vector at time  $t_0$  to its state vector at some later time  $t$ :

$$|\psi(t)\rangle = U(t, t_0)|\psi(t_0)\rangle. \quad (2.17)$$

This transformation conserves inner products and so does not change the distinguishability of states - reflecting the reversibility of the system evolution. More generally, for the larger class of states, representable as density matrices, this mapping takes the form

$$\rho(t) = U(t, t_0)\rho(t_0)U^\dagger(t, t_0). \quad (2.18)$$

The propagator is generated by the quantum Hamiltonian, i.e., the Hermitian operator representing the energy of the system, via the Schrodinger equation

$$i\hbar \frac{d}{dt}U(t, t_0) = H(t)U(t, t_0) \quad (2.19)$$

which has a formal solution given by the Dyson series [28]

$$U(t, t_0) = I + \sum_{n=1}^{\infty} \left(\frac{-i}{\hbar}\right)^n \int_{t_0}^t dt_1 \int_{t_0}^{t_1} dt_2 \dots \int_{t_0}^{t_{n-1}} dt_n H(t_1)H(t_2)\dots H(t_n). \quad (2.20)$$

Introducing an operator,  $\mathcal{T}_+$ , that preserves the time-ordering of operator products, equation (2.20) may be written more compactly as

$$U(t, t_0) = \mathcal{T}_+ \exp \left\{ -i \int_{t_0}^t dt' H(t')/\hbar \right\}. \quad (2.21)$$

However, if the Hamiltonian commutes with itself at different times ( $[H(t), H(t')] = 0$  for all  $t, t'$ ), then the time ordering becomes redundant and the propagator reduces to a complex exponential of the time-integrated Hamiltonian [29].

## The interaction picture

A transformation to the so-called *interaction picture*, or *interaction frame*, can often be advantageous, particularly for perturbative calculations. The transformation assumes a Hamiltonian of the form

$$H(t) = H_1(t) + H_2(t) \quad (2.22)$$

where, typically,  $H_2(t)$  is small in comparison to  $H_1(t)$ . The basic idea is then to remove any *direct* contribution from the large term  $H_1(t)$ .

If  $U(t, t_0)$  is the solution of the Schrodinger equation (2.19) for the full Hamiltonian (2.22) and  $U_1(t, t_0)$  is the solution for  $H_1(t)$  only, then we define the interaction picture evolution operator as  $\tilde{U}(t, t_0) \equiv U_1^\dagger(t, t_0)U(t, t_0)$  (this may be interpreted as a transformation to a frame that moves with the unperturbed dynamics, defined by  $H_1(t)$ .) This operator satisfies the following modified Schrodinger equation:

$$i\hbar \frac{d}{dt} \tilde{U}(t, t_0) = \tilde{H}_2(t) \tilde{U}(t, t_0), \quad (2.23)$$

where  $\tilde{H}_2(t) \equiv U_1^\dagger(t, t_0)H_2(t)U_1(t, t_0)$  defines the interaction picture Hamiltonian. This Hamiltonian has a magnitude determined by the small term  $H_2(t)$ , rather than the ‘full-strength’ Hamiltonian  $H(t)$ .

The interaction picture transformation is often used when two quantum systems interact weakly and we want to remove the direct dependence on the internal Hamiltonian of one or both of the systems. However, it also appears in the guise of the ‘toggling’ or ‘control’ frame transformation, where it is used to transfer the direct effect of a strong applied control field to a modulating effect on the autonomous Hamiltonian.

## Open systems

In addressing the issue of decoherence, we are faced with the problem of describing the evolution of a target quantum system  $\mathcal{S}$  that becomes entangled with a secondary system, referred to as its *environment*, or simply as the *bath*,  $\mathcal{B}$  (section 2.3). In the process, the bath gains information about the state of  $\mathcal{S}$ , the evolution of which becomes irreversible and therefore no longer unitary. However, we can still choose to treat the larger, composite system  $\mathcal{S} + \mathcal{B}$  as if it were closed and evolving unitarily. Assuming the component systems are initially unentangled and that the density matrix of  $\mathcal{S} + \mathcal{B}$  is (letting  $t_0 = 0$ )

$$\rho_{\mathcal{S}+\mathcal{B}}(0) = \rho_{\mathcal{S}}(0) \otimes \rho_{\mathcal{B}}(0), \quad (2.24)$$

the state at a later time  $t > 0$  is, using the closed system evolution rule (2.18),

$$\rho_{\mathcal{S}+\mathcal{B}}(t) = U(t) (\rho_{\mathcal{S}}(0) \otimes \rho_{\mathcal{B}}(0)) U^\dagger(t), \quad (2.25)$$

where we’ve used the standard shorthand  $U(t) \equiv U(t, 0)$ .

This evolution becomes irreversible at the level of the system  $\mathcal{S}$  because, not having access to the bath, we are forced to ‘average over’ its degrees of freedom. This process leads to a loss of information or, equivalently, an increase in entropy. Mathematically, the averaging takes the form of a *partial trace*  $\text{Tr}_{\mathcal{B}}[\cdot]$ , with respect to a complete set of basis states of the bath (in contrast to the usual trace operation  $\text{Tr}[\cdot]$ , as it would be applied to the composite system, the states of  $\mathcal{S}$  are not summed over.) The result is a final system state

$$\rho_{\mathcal{S}}(t) = \text{Tr}_{\mathcal{B}} [U(t) (\rho_{\mathcal{S}}(0) \otimes \rho_{\mathcal{B}}(0)) U^\dagger(t)]. \quad (2.26)$$

For a fixed initial bath state, equation (2.26) defines a *superoperator*  $\Xi_{(t,0)}$  that acts on the space of density matrices on  $\mathcal{H}_S$ :

$$\rho_S(t) = \Xi_{(t,0)} [\rho_S(0)]. \quad (2.27)$$

It can be shown that this superoperator, called a *dynamical map*, preserves all the important properties of the density matrix [30].

## 2.2 Quantum information processing

Like any physical system, a quantum system can, in principle, be used to store and process information. However, the possibility of superposed states, the nonlocality of quantum entanglement and the indeterminacy of the measurement process bestow QIP with unique characteristics that justify its treatment as field of study of its own, quite distinct from its classical equivalent. For this reason, we won't attempt anything like a comprehensive survey of the subject here. Rather, we present a very brief discussion of some of the QIP concepts and terminology that will arise in the ensuing chapters of the thesis.

### 2.2.1 Qubits & the Bloch sphere representation

The physical systems into which information is encoded for the purpose of QIP are most often collections of simple two-state quantum systems called *qubits*. Any pure state of a single qubit is expressible as a superposition

$$|\psi\rangle = c_0|0\rangle + c_1|1\rangle \quad (2.28)$$

of two appropriately chosen *computational basis states*  $|0\rangle$  and  $|1\rangle$ . While the pair of complex coefficients in (2.28) represents four real numbers, the normalization condition  $|c_0|^2 + |c_1|^2 = 1$ , along with the physical irrelevance of any global phase factor, reduces the number of real parameters needed to specify a single-qubit state to just two. This can be made explicit by rewriting the state (2.28) in the equivalent form

$$|\psi\rangle = \cos(\vartheta/2)|0\rangle + e^{i\varphi} \sin(\vartheta/2)|1\rangle. \quad (2.29)$$

This parsimonious parameterization allows us to visualize the state as a unit vector

$$\mathbf{v} = (\sin \vartheta \cos \varphi, \sin \vartheta \sin \varphi, \cos \vartheta), \quad (2.30)$$

called a *Bloch vector*, defined by angles  $(\vartheta, \varphi)$ , relative to a three-dimensional Cartesian coordinate system [6]. In this way, the entire space of pure single-qubit states can be mapped to the surface of a sphere of unit radius - *the Bloch sphere* (figure 2.1).

Mixed states can be incorporated into the Bloch sphere picture in a relatively straightforward manner by observing that an arbitrary single-qubit density matrix can be written as

$$\rho = \frac{1}{2} [I + v_x \sigma_x + v_y \sigma_y + v_z \sigma_z], \quad (2.31)$$

where  $v_a = \text{Tr}(\sigma_a \rho)$  is the quantum mechanical expectation value of the operator  $\sigma_a$ , for  $a = x, y, z$ . For a pure state  $|\psi\rangle$ , the vector  $\mathbf{v} = (v_x, v_y, v_z)$  is simply the unit vector (2.30). For a mixed state, on the other hand, it is easy to show that the magnitude of the Bloch vector must be less than one,  $v_x^2 + v_y^2 + v_z^2 < 1$ . We can therefore associate every point within the Bloch sphere, in addition to all points on the surface, with a valid single-qubit state (and vice versa).

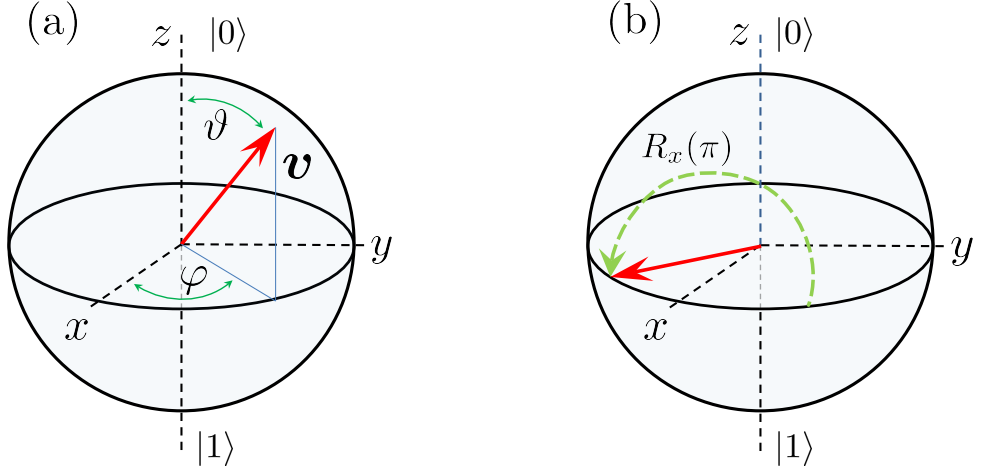


Figure 2.1: (Bloch sphere) - (a) A single-qubit pure state, defined by the parameters  $(\vartheta, \varphi)$ , is represented by the Bloch vector  $\mathbf{v} = (\sin \vartheta \cos \varphi, \sin \vartheta \sin \varphi, \cos \vartheta)$ . (b) ‘ $\pi$ -rotation’ of a Bloch vector about the  $x$ -axis, enacted by the rotation operator  $R_x(\pi)$ .

### 2.2.2 Quantum logic gates

A quantum computation begins with a system of  $n$  qubits, prepared in some initial state, usually designated as the  $|0, 0, \dots, 0\rangle \equiv |0\rangle_1 \otimes |0\rangle_2 \otimes \dots \otimes |0\rangle_n$  state. To this state is applied a unitary operator  $U_{alg}$  that enacts the desired QIP algorithm, transforming the system to a final target state

$$|\psi_f\rangle = U_{alg} |0, 0, \dots, 0\rangle. \quad (2.32)$$

However, rather than treat the unitary algorithm  $U_{alg}$  as a single operation, its design and execution can be made easier by constructing it as a sequence of discrete one- and two-qubit unitary operators called *gates*.

#### Single-qubit gates

Ignoring global phase factors, any single-qubit gate can be written in the form

$$U(\hat{\mathbf{n}}, \theta) = \exp[-i\theta \hat{\mathbf{n}} \cdot \boldsymbol{\sigma}/2] = \cos(\theta/2)I - i \sin(\theta/2)\hat{\mathbf{n}} \cdot \boldsymbol{\sigma} \quad (2.33)$$

where  $\hat{\mathbf{n}} = (n_x, n_y, n_z)$  is a real row vector of unit length and  $\boldsymbol{\sigma} = (\sigma_x, \sigma_y, \sigma_z)^T$  is a column vector of Pauli spin operators. Within the Bloch sphere picture, the effect of this operator is to rotate a Bloch vector representing some initial state, about the axis defined by  $\hat{\mathbf{n}}$ , through an angle  $\theta$ , to a Bloch vector representing the final state. In this sense, the unitary operator  $U(\hat{\mathbf{n}}, \theta)$  can be associated with a rotation operator  $R_{\hat{\mathbf{n}}}(\theta)$  that acts directly on the three-dimensional space of Bloch vectors, rather than on the abstract single-qubit Hilbert space (see figure 2.1).

Three simple, but important families of single-qubit gates are generated by the Pauli operators, and map to rotations about the  $x$ ,  $y$  and  $z$  axes of the Bloch sphere:

$$U(\hat{\mathbf{x}}, \theta) = \cos(\theta/2)I - i \sin(\theta/2)\sigma_x \Rightarrow R_x(\theta) \quad (2.34)$$

$$U(\hat{\mathbf{y}}, \theta) = \cos(\theta/2)I - i \sin(\theta/2)\sigma_y \Rightarrow R_y(\theta) \quad (2.35)$$

$$U(\hat{\mathbf{z}}, \theta) = \cos(\theta/2)I - i \sin(\theta/2)\sigma_z \Rightarrow R_z(\theta). \quad (2.36)$$

(NB: the one-to-one correspondence between single-qubit gates and rotation operators means that there is usually no problem in equating the two, so that, for example,  $\Rightarrow$  can be replaced by  $=$  in the above.)

In Chapter 5 of the thesis, in which error suppressing *composite gates* are discussed, rotations about arbitrary axes lying in the  $xy$ -plane of the Bloch sphere play a central role. These rotations are defined by a unit vector  $\hat{n}(\phi) = (\cos \phi, \sin \phi, 0)$ , fixing the axis of rotation, and a rotation angle  $\theta$ . The corresponding rotation operator in this case is designated  $R(\theta, \phi)$ .

## Two-qubit gates

Using products of single-qubit gates only, we cannot, given a collection of  $n$  qubits in a separable multi-qubit state

$$|\psi\rangle = |\psi_1\rangle \otimes |\psi_2\rangle \otimes \dots |\psi_n\rangle \quad (2.37)$$

create an entangled state. We therefore need to introduce a class of genuinely multi-qubit gates whose action on one set of qubits is conditioned on the state of another. In fact, it can be shown that any  $n$ -qubit gate can be constructed from one- and two-qubit gates alone [6], so it suffices to consider only the  $n = 2$  case.

The most commonly encountered class of two-qubit gates in QIP are the *controlled* gates in which a single-qubit unitary operator  $U$  is applied to a *target* qubit when the state of a second *control* qubit is in the  $|1\rangle$  state. Conversely, if the state of the control qubit is  $|0\rangle$ , the identity operation  $I$  is applied to the target qubit. The general form of a controlled two-qubit gate is

$$U_C = |0\rangle\langle 0| \otimes I + |1\rangle\langle 1| \otimes U. \quad (2.38)$$

Specific examples are the CNOT gate

$$U_{\text{CNOT}} = |0\rangle\langle 0| \otimes I + |1\rangle\langle 1| \otimes \sigma_x \quad (2.39)$$

that applies a single-qubit NOT gate that ‘flips’ the state of the target qubit when the control qubit is in the  $|1\rangle$  state, and the CPHASE gate

$$U_{\text{CPHASE}} = |0\rangle\langle 0| \otimes I + |1\rangle\langle 1| \otimes \sigma_z \quad (2.40)$$

that applies a  $\pi$  phase shift to the  $|1\rangle$  state of the target qubit, conditioned on the state of the control.

## 2.3 Decoherence

One of the more confronting differences between the quantum mechanical world view and that provided by classical physics is that quantum theory predicts the existence of entangled states, i.e., states that exhibit strong non-local quantum correlations. And it is the phenomenon of quantum entanglement that facilitates the extraordinary information processing power of quantum computers. Unfortunately, producing entangled states suitable for QIP is far from straightforward (see Chapter 9, for example). While entanglement is not hard to generate (indeed, the appearance of the classical world of everyday experience seems to be evidence of its ubiquity), it is very difficult to control. Even weakly interacting systems can become thoroughly entangled very rapidly. As a consequence, any information that may initially be localized within a particular quantum system has a strong tendency to ‘diffuse’ into surrounding systems (i.e., the environment), becoming delocalized and unavailable to an observer with the ability to measure

the initial system only. Alternatively, information can simply be lost by failing to track the evolution of an otherwise well-defined quantum state. This can occur when, for example, random fluctuations in an effectively classical environment act differently on each element of an ensemble of qubits. In this section, we present a brief discussion of the effects of both quantum and classical environments on the capacity of an open quantum system to store and process quantum information.

### 2.3.1 The quantum model

The loss of localized quantum information brought about by entanglement between a quantum system and its environment is tantamount to a loss of quantum coherence, i.e., the very property that imbues the system with ‘quantumness’. This process, one of the main impediments to QIP, is referred to as *environment-induced decoherence* or simply *decoherence* [31, 8]. As an example of how decoherence comes about, consider a quantum system  $\mathcal{S}$  that interacts with a large, uncontrolled environment, or bath,  $\mathcal{B}$ , via a simple linear interaction Hamiltonian

$$H_{\mathcal{S}\mathcal{B}} = S \otimes B, \quad (2.41)$$

where  $S$  ( $B$ ) is a Hermitian operator acting on the system (bath) Hilbert space  $\mathcal{H}_{\mathcal{S}}$  ( $\mathcal{H}_{\mathcal{B}}$ ). This Hamiltonian generates the time evolution operator (unless otherwise indicated,  $\hbar = 1$  throughout the remainder of the discussion)

$$U(t) = \exp\{-i(S \otimes B)t\}, \quad (2.42)$$

where  $U(t) \equiv U(t, 0)$ .

If we suppose that the initial state vector of the combined system  $\mathcal{S} + \mathcal{B}$  is of the separable form  $|\phi(0)\rangle = |\psi(0)\rangle \otimes |\chi(0)\rangle$ , where  $|\psi(0)\rangle$  ( $|\chi(0)\rangle$ ) is the initial state of the system (bath), then, expanding  $|\psi(0)\rangle$  in the eigenbasis  $\{|s_i\rangle\}$  of  $S$ , the initial density matrix may be written as

$$\rho_{\mathcal{S}+\mathcal{B}}(0) = \left( \sum_{ij} c_i c_j^* |s_i\rangle \langle s_j| \right) \otimes |\chi(0)\rangle \langle \chi(0)|. \quad (2.43)$$

At a time  $t > 0$ , the dynamics induced by (2.41) result in a final state

$$\begin{aligned} \rho_{\mathcal{S}+\mathcal{B}}(t) &= U(t) \rho_{\mathcal{S}+\mathcal{B}}(0) U^\dagger(t) \\ &= \sum_i |c_i|^2 |s_i\rangle \langle s_i| \otimes |\chi_i(t)\rangle \langle \chi_i(t)| + \sum_{i \neq j} c_i c_j^* |s_i\rangle \langle s_j| \otimes |\chi_i(t)\rangle \langle \chi_j(t)| \end{aligned} \quad (2.44)$$

where  $|\chi_j(t)\rangle \equiv \exp\{-is_j B t\} |\chi(0)\rangle$  ( $s_i$  is the eigenvalue associated with eigenstate  $|s_i\rangle$ ). Upon tracing out the bath degrees of freedom, one obtains the final, reduced density matrix

$$\rho_{\mathcal{S}}(t) = \sum_i |c_i|^2 |s_i\rangle \langle s_i| + \sum_{i \neq j} c_i c_j^* |s_i\rangle \langle s_j| \langle \chi_j(t) | \chi_i(t) \rangle, \quad (2.45)$$

representing the state of our knowledge of the system  $\mathcal{S}$  at time  $t$ .

From equation (2.45), we see that the coherence between the system basis states  $|s_i\rangle$  and  $|s_j\rangle$  depends on the overlap  $\langle \chi_j(t) | \chi_i(t) \rangle$  between the relative bath states. This overlap, which tends to decrease with both the strength of the interaction and the total interaction time  $t$ , is a simple measure of the distinguishability of the environmental states. In other words, it is a measure of how much information about the state of  $\mathcal{S}$  has been transferred to the environment. At a point at which the overlap vanishes, it becomes possible, if only in principle, to obtain complete

knowledge of the system state by performing a measurement on the environment. The system will then fail to exhibit any quantum coherence effects in the  $\{|s_i\rangle\}$  basis.

It is important to note that the simple interaction Hamiltonian (2.41) ignores both the internal Hamiltonians of the system  $H_S$  and of the bath  $H_B$ . While, for many of the systems considered in this work, the former is assumed to be well understood and can be accounted for in a relatively straightforward manner, the internal bath evolution, over which we have no control, can complicate matters greatly by providing a genuinely dynamical element to the interaction. This can be made plain by introducing an internal bath Hamiltonian to (2.41), so that the total Hamiltonian becomes  $H_{SB} + I_S \otimes H_B$ , where  $I_S$  is the identity operator on  $\mathcal{H}_S$ . Transforming to the interaction picture with respect to the bath evolution (see section 2.1.5) produces an obviously time-dependent interaction (assuming  $H_B$  doesn't commute with  $B$ )

$$\tilde{H}_{SB}(t) = S \otimes (e^{iH_B t} B e^{-iH_B t}). \quad (2.46)$$

This additional time-dependence does not change the conclusions drawn from the simple description above in a *qualitative* way, however, as we will see in the sequel, it does make the *quantitative* analysis significantly more complicated, as it does the design of protocols aimed at combating the effects of decoherence.

### 2.3.2 The semiclassical model

Beyond making the dynamical influence of the bath apparent, a further advantage of the interaction picture transformation is that it facilitates a unified treatment of the quantum model of decoherence, described above, and the *semiclassical* model.<sup>4</sup> Formally, the semiclassical equivalent of the quantum interaction Hamiltonian (2.46) can be obtained by replacing the fluctuating *quantum* variable with a fluctuating *classical* variable, yielding

$$H_{S+B} = S \otimes \beta_S(t) I_B. \quad (2.47)$$

In this expression, the presence of the bath identity operator  $I_B$  reflects the lack of back-action effects from the system to the bath, while the random process  $\beta_S(t)$  models the effect of the bath on the system. The one-way nature of the interaction means that the bath Hilbert space is essentially redundant (all operations on the environment being trivial), so that it is often more convenient to ignore it altogether and simply write (2.47) as

$$H_S = \beta_S(t) S. \quad (2.48)$$

This simple Hamiltonian generates the time evolution operator

$$U(t) = \exp \left\{ -iS \int_0^t dt' \beta_S(t') \right\} \quad (2.49)$$

which, when applied to the initial density matrix

$$\rho_S(0) = \sum_{ij} c_i c_j^* |s_i\rangle \langle s_j| \quad (2.50)$$

has the effect of multiplying each of the eigenstates  $\{|s_i\rangle\}$  by a state-dependent random phase factor.

---

<sup>4</sup>It can be argued that the semiclassical model does not represent ‘true’ decoherence, as there is no entanglement between system and bath [7]. Here, we take an operationalist view of decoherence as essentially any process that results in a diminution of observable coherence effects.

The final density matrix of the ensemble system  $\mathcal{S}$  is obtained by averaging over all possible phase values (here, this averaging process is denoted by  $\mathbb{E}\{\cdot\}$ ):

$$\rho_{\mathcal{S}}(t) = \sum_i |c_i|^2 |s_i\rangle\langle s_i| + \sum_{i \neq j} c_i c_j^* |s_i\rangle\langle s_j| \mathbb{E}\{e^{-i\phi(t)(s_i-s_j)}\}, \quad (2.51)$$

where  $\phi(t) \equiv \int_0^t dt' \beta_S(t')$ . In most cases of interest, the ensemble average phase factors in equation (2.51) will decay over time, leading to a loss of observable coherence effects in the  $\{|s_i\rangle\}$  basis. In contrast to the quantum decoherence model, this should be interpreted as a loss of information about the system, rather than as a transfer of information from the system to the bath.

The semiclassical decoherence model has proved to be extremely effective in capturing key aspects of experimental reality in a range of QIP settings, ranging from ion traps [32] to solid state superconducting devices [33]. In general, it is applicable when the environment can be assumed to be sufficiently large and/or at a high enough effective temperature that it may affect the state of  $\mathcal{S}$  without itself being significantly perturbed.

### 2.3.3 Dephasing noise

When the system-environment interaction commutes with the internal Hamiltonian of the system,  $[H_{\mathcal{S}}, H_{SB}] = 0$ , as it does trivially in the preceding examples, then the populations of the energy eigenstates of  $\mathcal{S}$  are unaffected by the interaction. There is therefore no net energy exchange between the system and the bath. We refer to this kind of interaction as a pure *dephasing* interaction (or *dephasing noise*). In the simple case of a single-qubit system in which the two basis states are, in the absence of any interaction, separated by a fixed energy  $E_0$ , the semiclassical pure dephasing Hamiltonian can be written as

$$H_{\mathcal{S}}(t) = (E_0 + \beta_z(t)) \sigma_z / 2. \quad (2.52)$$

Transforming to the interaction picture with respect to the intrinsic system evolution  $H_{\mathcal{S},0} \equiv E_0 \sigma_z / 2$ , equation (2.52) reduces to the simple form of (2.48), discussed in the previous section. Following the procedure outlined therein, we find that, after a period  $t$  of noisy evolution, and upon averaging over the ensemble of noise realizations, the off-diagonal component,  $\rho_{01}(t) \equiv \langle 0 | \rho_{\mathcal{S}}(t) | 1 \rangle$ , of the single-qubit density matrix (a.k.a. the ‘coherence’) becomes

$$\rho_{01}(t) = \rho_{01}^*(t) = \rho_{01}(0) \mathbb{E}\{e^{-i\phi(t)}\} \quad (2.53)$$

where  $\phi(t) \equiv \int_0^t dt' \beta_z(t')$ , and  $\rho_{01}(0)$  is the initial coherence. If we assume that  $\beta_z(t)$  is a zero-mean Gaussian noise process with an approximately ‘white’ spectrum (i.e., a spectrum in which all noise frequencies contribute equally), then we find that we can write (2.53) as

$$\rho_{01}(t) = \rho_{01}(0) e^{-t/T_2} \quad (2.54)$$

where  $T_2$  is a constant that characterizes the loss of phase coherence. This result remains approximately true to the extent that the correlation time of the environment is small relative to the dynamics of the system, i.e., in the so-called *Markovian* limit.

While a characteristic ‘dephasing time’  $T_2$  will seldom be as clearly defined as it is in the Markovian limit, and any real interaction will also involve energy transfer between the system and the environment, producing additional *relaxation* effects on some timescale  $T_1$ , there are good reasons for focusing attention on dephasing noise models when contemplating error suppression strategies in QIP systems. Firstly, in many of the systems of interest, it can be shown

that  $T_1 \gg T_2$ , so that a great deal of progress can be made by directing attention away from the effects of the complex system-environment interaction as whole, towards the relatively simpler problem of dephasing. Secondly, due to the technological limitations of quantum control hardware, the dynamical quantum error suppression (DQES) strategies considered in this work are most effective for noise that is slowly varying, or low-frequency dominated. The dephasing time  $T_2$  is very sensitive to low-frequency noise, especially in the long-time limit. Consequently, DQES can yield marked improvements in this simple decoherence metric.

## 2.4 Classical control & noise filtering

Control theory is concerned with selecting, from a set of possible alternatives, a plan of action aimed at achieving some pre-determined objective. The objective is typically defined in terms of the observable behaviour of a target *system*. In quantum control theory, as it is applied in QIP, the systems of interest are quantum systems, typically collections of qubits, and the objective is the performance of some information processing task. While, as we will see in the sequel, some of the broader concepts of orthodox control theory can be applied directly to QIP, a more detailed analysis reveals the limitations of classical, linear methods in the quantum setting. In this and the following section, we will highlight some important areas of commonality and of difference between quantum and classical control paradigms, beginning with a very brief discussion of notions of *controllability* and of *filtering* in the classical context.

### 2.4.1 Linear systems & controllability

In simple mathematical terms, a classical control system maps an input, or control signal, described by an  $n$ -dimensional vector of real-valued functions  $\mathbf{u}(t) \in \mathbb{R}^n$ , to an output signal  $\mathbf{y}(t) \in \mathbb{R}^m$  [22, 23]. The control signal  $\mathbf{u}(t)$  represents those influences that can be used to ‘steer’ the system towards the control objective. There are two broad approaches to selecting a control strategy, or protocol, defined by a particular choice of  $\mathbf{u}(t)$ . If a protocol is selected solely on the basis of the control objective and of prior knowledge of the system, then it is referred to as an *open-loop* control protocol. By contrast, a *closed-loop*, or *feedback*, protocol is one in which information gained from the output  $\mathbf{y}(t)$ , during execution, is used to modify  $\mathbf{u}(t)$  (see figure 2.2). Both approaches have advantages and disadvantages. Specifically, open-loop protocols are often less resource intensive, yet they can be ineffective if the system behaviour is not well understood or if there are unexpected disturbances. Conversely, closed-loop protocols are better able to cope with unanticipated behaviour, but have the disadvantages of requiring greater control resources and of introducing an additional element of measurement error.

In general, knowledge of the input function over some time interval  $[0, t]$  is not sufficient to specify the output over the same interval. An additional set of variables  $\mathbf{x}(0) \in \mathbb{R}^p$ , representing the *state* of the system at the initial time, is required to uniquely define the output. For linear time-invariant (LTI) systems,<sup>5</sup> the relationships between inputs, outputs and states are summarized by the following set of equations [22]:

$$\dot{\mathbf{x}}(t) = \mathbf{A}\mathbf{x}(t) + \mathbf{B}\mathbf{u}(t) \quad (2.55)$$

$$\mathbf{y}(t) = \mathbf{C}\mathbf{x}(t) + \mathbf{D}\mathbf{u}(t), \quad (2.56)$$

---

<sup>5</sup>A control system is linear if the combinations of input vectors  $\lambda_1\mathbf{u}_1(t) + \lambda_2\mathbf{u}_2(t)$  and of initial state vectors  $\lambda_1\mathbf{x}_1(0) + \lambda_2\mathbf{x}_2(0)$  produce an output vector  $\lambda_1\mathbf{y}_1(t) + \lambda_2\mathbf{y}_2(t)$ , for  $\lambda_1, \lambda_2 \in \mathbb{R}$  and  $t \geq 0$ . A system is time-invariant if a temporal translation of both the initial state and the input signal produces a corresponding translation of the output.

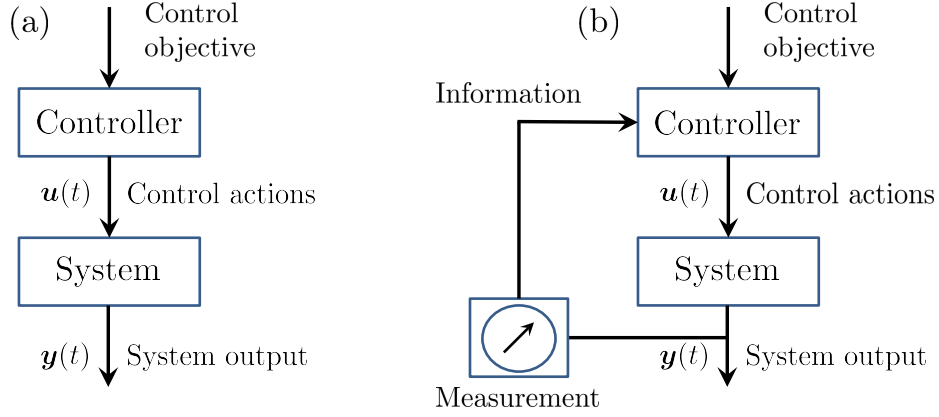


Figure 2.2: (*Open-loop vs. Closed-loop control*) - Control protocols can be divided into two classes: (a) *Open-loop control protocols*, which are not modified on the basis of information obtained via measurement; and (b) *closed-loop protocols* in which the control actions are contingent on the outcomes of measurements made during execution.

where  $\dot{\mathbf{x}} = d\mathbf{x}/dt$ , and  $\mathbf{A}, \mathbf{B}, \mathbf{C}$  and  $\mathbf{D}$  are matrices of appropriate dimensions. These equations have the solutions

$$\mathbf{x}(t) = e^{\mathbf{A}t}\mathbf{x}(0) + \int_0^t dt' e^{\mathbf{A}(t-t')}\mathbf{B}\mathbf{u}(t') \quad (2.57)$$

and

$$\mathbf{y}(t) = \mathbf{C}e^{\mathbf{A}t}\mathbf{x}(0) + \mathbf{C} \int_0^t dt' e^{\mathbf{A}(t-t')}\mathbf{B}\mathbf{u}(t') + \mathbf{D}\mathbf{u}(t), \quad (2.58)$$

from which one can derive the criterion for controllability.

In short, a system is *controllable* if an input can be found that will transfer any initial state to any final state in a finite time. More formally, if, given any initial state  $\mathbf{x}_i = \mathbf{x}(0)$  and any final state  $\mathbf{x}_f$ , there exists an input signal such that, for some finite  $t > 0$ ,  $\mathbf{x}(t) = \mathbf{x}_f$ , then the system is said to be controllable. Using equation (2.57), it can be proved that the LTI system (2.55)-(2.56) is controllable if the  $p \times p$  matrix ( $p$  being the dimension of the state vector)

$$\mathbf{W}(t) = \int_0^t dt' e^{\mathbf{A}t'} \mathbf{B} \mathbf{B}^T e^{\mathbf{A}^T t'} \quad (2.59)$$

has a nonzero determinant, for any  $t > 0$ .

While solutions of the form (2.57) can be derived in the *quantum* control context using time-dependent perturbation theory [34], their application is limited to very weak control fields. As we will see in section 2.5.1, for the more general, and practical, case in which the applied controls cannot be treated perturbatively, the relevant equations for an open-loop quantum control system are *nonlinear* and assessing its controllability is less straightforward.

## 2.4.2 Filters in the time & frequency domains

Returning to equation (2.58), it is frequently the case that there is no direct contribution from the control to the output, so that  $\mathbf{D} = 0$ . If the initial state also vanishes,  $\mathbf{x}(0) = 0$ , then we

obtain the simple *input-output* representation of the control system:

$$\mathbf{y}(\tau) = \int_0^\tau dt' \mathbf{g}(t-t') \mathbf{u}(t'), \quad (2.60)$$

where

$$\mathbf{g}(t) = \mathbf{C} e^{\mathbf{A} t} \mathbf{B} \quad (2.61)$$

is the system's *impulse response* function. Via the convolution (2.60), the impulse response function completely determines the nature of the system's output  $\mathbf{y}(t)$ , given an arbitrary input  $\mathbf{u}(t)$ . The system can be seen as acting to *filter* the input signal to obtain the output signal. Here, the filter is characterized entirely by the impulse response function  $\mathbf{g}(t)$ .

Additional insights into the behaviour of LTI control systems, and into the design and construction of filters, can be obtained by a transformation to the frequency domain. Taking the Laplace transform of the convolution (2.60) yields

$$\mathbf{y}(s) = \mathbf{g}(s) \mathbf{u}(s) \quad (2.62)$$

where  $\mathbf{y}(s)$  and  $\mathbf{u}(s)$  are, respectively, the Laplace transforms of the output and input signals, defined on the plane of the complex frequency variable  $s = \sigma + i\omega$ , and

$$\mathbf{g}(s) = \mathbf{C} [s\mathbf{I} - \mathbf{A}]^{-1} \mathbf{B} \quad (2.63)$$

is the Laplace transform of the impulse response function, referred to as the *transfer function*. From the form of the transfer function, particularly the placement of its poles and zeros, one can extract important information about the filtering characteristics of the system [22, 23].

## Accumulation & difference filters

For our purposes, we drop the matrix notation and consider only single-input/single-output (SISO) systems. We also assume a slightly modified representation of a filter that is more consistent with the terminology and notation we will use in the subsequent section. And, rather than use the complex Laplace frequency, we let  $s = i\omega$  and work in the more familiar Fourier frequency space.

Specifically, we consider the following simple filtering system

$$\phi(\tau, 0) = \int_0^\tau dt \beta(t) = \int_{-\infty}^\infty dt r_{[0, \tau]}(t) \beta(t), \quad (2.64)$$

in which, rather than being a controlled variable, the input signal  $\beta(t)$  is a zero-mean random process representing pure noise, so that any output  $\phi(\tau, 0)$  is to be regarded as an error. In the expression on the far right of equation (2.64), the integral is restricted to the interval  $[0, \tau]$  by the rectangular impulse response function  $r_{[0, \tau]}(t)$  that has unit value for  $t \in [0, \tau]$  and vanishes otherwise. The system is a simple continuous-time *accumulation* or *averaging* filter. Intuitively, its effect is to 'average out' those components of the noise that fluctuate rapidly compared to the operation time  $\tau$ , so that quasi-static contributions become progressively more dominant as  $\tau$  increases, i.e., it acts as a (quite inefficient) *low-pass filter*.

This intuitive picture of the action of the filter can be made concrete by defining a suitable measure for the 'size' of the random output. A convenient metric is the mean square value, or variance [35]:

$$\mathbb{E}\{\phi^2(\tau, 0)\} = \int_{-\infty}^\infty dt' \int_{-\infty}^\infty dt'' r_{[0, \tau]}(t') r_{[0, \tau]}(t'') \mathbb{E}\{\beta(t') \beta(t'')\} \quad (2.65)$$

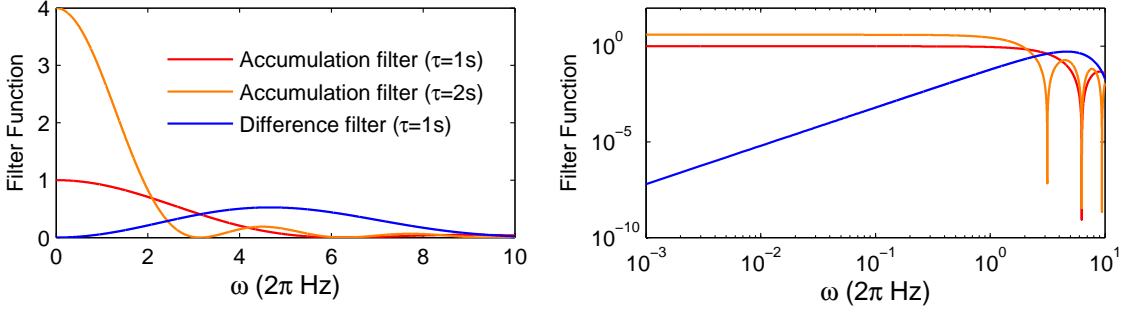


Figure 2.3: (Left) Comparison of frequency space behaviour of accumulation filters of duration  $\tau = 2\text{s}$  (orange) and  $\tau = 1\text{s}$  (red), and a difference filter of duration  $\tau = 1\text{s}$  (blue). (Right) Log-log plot of the same data, highlighting low-frequency behaviour.

If we assume the noise is wide-sense stationary,<sup>6</sup> then we can use the Wiener–Khintchine theorem to write [36]

$$\mathbb{E}\{\beta(t')\beta(t'')\} = \frac{1}{2\pi} \int_{-\infty}^{\infty} d\omega S_{\beta}(\omega) e^{i\omega(t'-t'')}, \quad (2.66)$$

where  $S_{\beta}(\omega)$  is the *power spectral density* of the noise process  $\beta(t)$ . Substituting (2.66) into (2.65) yields

$$\mathbb{E}\{\phi^2(\tau, 0)\} = \frac{1}{2\pi} \int_{-\infty}^{\infty} d\omega S_{\beta}(\omega) |r_{[0,\tau]}(\omega)|^2, \quad (2.67)$$

where

$$r_{[0,\tau]}(\omega) \equiv \int_{-\infty}^{\infty} dt r_{[0,\tau]}(t) e^{i\omega t} = e^{i\omega\tau/2} \tau \frac{\sin(\omega\tau/2)}{\omega\tau/2}. \quad (2.68)$$

From equation (2.67), the size of the output, and therefore of the error, is determined by the overlap between the power spectrum and the frequency space representation of the simple accumulation filter  $|r_{[0,\tau]}(\omega)|^2$ . In figure 2.3, the form of the latter is plotted for total operation times  $\tau = 1\text{s}$  and  $\tau = 2\text{s}$ , showing that lower frequency noise components do indeed become more dominant as the operation time increases.

In attempting to suppress the erroneous output signal, particularly the lower frequency contributions, we assume that our capacity to change the impulse response function is limited to the possibility of ‘flipping’ its sign at  $t = \tau/2$ , halfway through the operation time. We can therefore apply, to the existing continuous-time accumulation filter, an additional very simple *digital filter* [24]. The output in this case is

$$\phi(\tau, 0) = \sum_{\ell=-\infty}^{\infty} r_{\ell} \phi_{\ell}, \quad (2.69)$$

where  $\phi_{\ell} \equiv \int_{\ell\tau/2}^{(\ell+1)\tau/2} dt \beta(t)$ , and the digital filter coefficients (the discrete-time impulse response function) on the RHS are such that  $r_0 = 1$  and  $r_1 = \pm 1$ , depending on whether or not we choose to flip the sign for the second period of evolution, otherwise  $r_{\ell} = 0$ . The expression for the magnitude of the output signal, in the frequency domain, is identical to equation (2.67),

---

<sup>6</sup>A random process is wide-sense stationary if its mean value is independent of time and the two-time autocorrelation function depends only on the difference between the two time points [35].

with the exception of the following substitution

$$|r_{[0,\tau]}(\omega)|^2 \Rightarrow \left| \sum_{\ell=-\infty}^{\infty} r_\ell e^{i\ell\omega\tau/2} \right|^2 |r_{[0,\tau/2]}(\omega)|^2, \quad (2.70)$$

that is, the frequency-space action of the continuous-time accumulation filter is modified by the square modulus of the discrete-time Fourier transform (DTFT) of the digital filter.

If we choose  $r_1 = 1$ , so that there is no change of sign, then we implement a digital accumulation filter that, when combined with the continuous-time filter on which it acts, restores the original accumulation filter of equation (2.64). However, if we choose  $r_1 = -1$ , then we implement a digital *difference filter* which will reduce contributions from those components of the noise that don't change significantly from one subinterval to the next. This is confirmed by evaluating its DTFT:

$$\sum_{\ell=-\infty}^{\infty} r_\ell e^{i\ell\omega\tau/2} = -2ie^{i\omega\tau/4} \sin(\omega\tau/4) \quad (2.71)$$

which, as it goes to zero as  $\omega \rightarrow 0$ , acts to suppress the low frequency noise (see figure 2.3). Perhaps surprisingly, this elementary switch from an accumulation filter to a difference filter forms the basis of *dynamical quantum error suppression*, a method, or suite of methods, for suppressing noise in quantum systems.

## 2.5 Dynamical quantum error suppression

Dynamical quantum error suppression (DQES) is an approach to quantum control that originates in the refocusing and decoupling techniques employed in nuclear magnetic resonance (NMR) spectroscopy [20, 21]. By cleverly manipulating the dynamical evolution of nuclear spin states in a target material, via the application of strong radio-frequency (rf) pulses, the effects of unwanted interactions can be significantly reduced, vastly improving the quality of observed NMR spectra. DQES protocols use a similar methodology to generate high-fidelity quantum control operations with a ‘built-in’ robustness against errors. In contrast to both quantum feedback control and QEC, they are formulated solely on the basis of prior knowledge of available control resources and of system dynamics, rather than information obtained from the controlled system during execution. They can therefore be understood as a form of *open-loop* quantum control. Because there is no measurement required, nor are large numbers of ancillary qubits necessary, DQES protocols are relatively easy to implement experimentally and, indeed, have been shown to be effective in a range of physical systems [37, 38, 39, 32]. Although, on its own, DQES doesn’t solve the decoherence problem, it does hold great promise for the reduction of error rates to levels below which QECs are effective.

### 2.5.1 Open-loop quantum control

Depending on the particular physical setting, there are a variety of ways to model the evolution of a controlled quantum system [40]. Here, we consider *open-loop* quantum control only. We also assume that control devices do not become entangled with the target system and that their actions can be modeled semiclassically. Further, our interest is in generating desirable unitary operators, or gates, rather than particular quantum states. Given these conditions, the appropri-

ate model is one in which the controlled dynamics are generated via a *bilinear*<sup>7</sup> equation [41]

$$i\frac{dU(t)}{dt} = [H_0(t) + H_c(t)] U(t) \quad (2.72)$$

where  $H_0(t)$  is the uncontrolled *drift* Hamiltonian and

$$H_c(t) \equiv \sum_m H_m u_m(t) \quad (2.73)$$

defines the form of the *control Hamiltonian*. Here, the time-independent Hermitian operators  $\{H_m\}$  and the set of real-valued modulation functions  $\{u_m(t)\}$  are determined by the assumptions made regarding the control resources. For example, realistic control profiles are constrained by limited ‘pulse-shaping’ capabilities that will impose an upper bound  $u_{max}$  on the achievable control strength and a minimum timescale for control modulation  $\tau_{min}$ .

A closed quantum system, described by equation (2.72), is said to be *operator controllable* (the brand of controllability most relevant to QIP) if there exists a set of control modulation functions  $\{u_m(t)\}$  such that any final unitary operator  $U_f$  can be generated from the identity  $U(0) = I$  in a finite time. The mathematical criterion for assessing controllability may be expressed in terms of Lie algebras, a discussion of the details of which would take us to far afield, suffice it to say that while it is easy to state, proving that the criterion is met can be difficult for specific systems, particularly those of larger dimension. For an open system, in which control is restricted to the system Hilbert space  $(H_c(t) \otimes I_B)$ , the evolution of the target system  $\mathcal{S}$  is no longer unitary, which further complicates the issue of controllability [42]. Since the aim of DQES is to reduce the nonunitary contribution and its effect on the controllability of the target system, we generally only need assume that the target system is controllable in the absence of interactions (i.e., when it is closed).

### 2.5.2 Coherent averaging

All DQES protocols, no matter how complex, are based ultimately on the relatively simple idea of *coherent averaging*, the essence of which can be readily grasped by considering a generalization of its earliest incarnation; the ‘spin-echo’ technique, first proposed by Hahn in 1950 [19]. Let us suppose that our aim is to restore, at some time  $t = \tau > 0$ , the original state of an ensemble of spin-1/2 nuclei (our target system  $\mathcal{S}$ ), immersed in a magnetic field of unknown (possibly time-dependent) magnitude, directed along the  $z$ -axis. In mathematical terms, the aim is to implement the identity operation  $I_S$  on the system Hilbert space  $\mathcal{H}_S \cong \mathbb{C}^2$ . The dynamics of this ensemble system are modeled by a semiclassical Hamiltonian of the form (2.52) which, transforming to the interaction picture defined by the mean value of the magnetic field, becomes

$$H_S = \beta_z(t)\sigma_z/2. \quad (2.74)$$

Here, the zero-mean random process  $\beta_z(t)$  represents the variation in the precessional Larmor frequency across the ensemble, induced by the fluctuating inhomogeneity of the field.

At the start of the experiment, at time  $t = 0$ , all spins are assumed to be in the same pure state,  $|\psi(0)\rangle = |+y\rangle$ , corresponding to a unit-length Bloch vector  $v(0) = \hat{y}$  aligned along the positive  $y$ -axis of the Bloch sphere (see figure 2.4(a)). Over a time interval  $[0, \tau]$ , and in the absence of any control, the Hamiltonian (2.74) generates the free evolution propagator

$$U_0(\tau, 0) = \exp \{-i\phi(\tau, 0)\sigma_z/2\}, \quad (2.75)$$

---

<sup>7</sup>The equation is called bilinear because it contains the product of the control and the propagator.

where the random variable  $\phi(\tau, 0) \equiv \int_0^\tau ds \beta_z(s)$  can be interpreted as the output of a simple accumulation filter (see section 2.4.2). At the level of the individual spins, (2.75) prescribes a rotation of the  $i$ -th spin in the ensemble, about the  $z$ -axis, through an angle  $\phi^{(i)}(\tau, 0) \equiv \int_0^\tau ds \beta_z^{(i)}(s)$ , dictated by the particular realization  $\beta_z^{(i)}(t)$  of the fluctuating magnetic field it experiences. The resulting action on the associated Bloch vector can be expressed as

$$\mathbf{v}^{(i)}(\tau) = R_z(\phi^{(i)}) \hat{\mathbf{y}}, \quad (2.76)$$

where  $\phi^{(i)} \equiv \phi^{(i)}(\tau, 0)$ , and  $R_z(\phi^{(i)})$  is a three-dimensional rotation operator (see section 2.2.1). The ensemble as a whole is now no longer representable by a single pure state, or a single Bloch vector. Instead, we have a nontrivial distribution of states.

The relevant mathematical object for the description of such a system is the ensemble average density matrix  $\rho_S(\tau)$  or, equivalently, the ensemble average Bloch vector  $\mathbf{v}_S(\tau) \equiv \mathbb{E}\{\mathbf{v}(\tau)\}$ , where  $\mathbf{v}(\tau)$  is the *random vector* representing the ensemble. Assuming Gaussian distributed noise, and following the analysis in section 2.3.2, we find that the magnitude of the system Bloch vector decays to an extent determined by the variance of the Gaussian random variable  $\phi \equiv \int_0^\tau ds \beta_z(s)$  (figure 2.4(b)), i.e.,

$$\mathbf{v}_S(\tau) = e^{-\mathbb{E}\{\phi^2\}/2} \hat{\mathbf{y}}. \quad (2.77)$$

The result is an undesirable loss of coherence and of quantum information. From the frequency space representation of the variance  $\mathbb{E}\{\phi^2\}$  given in equation (2.67), the degree of coherence loss is determined by the overlap of the noise power spectrum and an accumulation filter function that tends to amplify low-frequency noise as  $\tau$  increases. The coherence of this simple quantum control system is therefore particularly sensitive to low-frequency noise.

The key to reducing this sensitivity and, in the ideal case, restoring the initial state of  $S$ , lies in recognizing that the Hamiltonian (2.74) has opposite sign for the  $|0\rangle$  and the  $|1\rangle$  eigenstates. If the noise does not vary significantly over the interval  $[0, \tau]$ , i.e., it is *quasi-static*, then by instantaneously ‘flipping’ the spin at  $t = \tau/2$ , we might expect to be able to reverse the evolution undergone before the flip (figure 2.4(b)-(c)). Physically, a spin-flip is executed via the application of a short, strong rf-pulse, inducing a  $\pi$ -rotation of the Bloch vector about the  $x$ -axis (figure 2.1(b)). In the idealized ‘bang-bang’ limit, in which the pulse is assumed to be instantaneous and infinitely strong, the operation can be represented by the Pauli operator  $\sigma_x$ . In order to fully restore the initial state, the spin must be flipped a second time at the conclusion of the operation (figure 2.4(d)-(e)). The total propagator for this two-pulse control sequence is

$$U(\tau, 0) = \sigma_x U_0(\tau, \tau/2) \sigma_x U_0(\tau/2, 0). \quad (2.78)$$

Applying the identity  $M_2 \exp\{M_1\} M_2^{-1} = \exp\{M_2 M_1 M_2^{-1}\}$ , valid for any operator  $M_1$  and invertible operator  $M_2$ , (2.78) becomes

$$U(\tau, 0) = \exp\{-i\phi(\tau, \tau/2)\sigma_x\sigma_z\sigma_x/2\} \exp\{-i\phi(\tau/2, 0)\sigma_z/2\} \quad (2.79)$$

which, using  $\sigma_x\sigma_z\sigma_x = -\sigma_z$ , reduces to

$$U(\tau, 0) = \exp\{-i[\phi(\tau/2, 0) - \phi(\tau, \tau/2)]\sigma_z/2\}. \quad (2.80)$$

The total evolution operator therefore now depends on the *difference* between the random phases accumulated over the two periods of free evolution, as do all quantities derived from it.

We can summarize the change from free-evolution to pulse-controlled evolution by writing a generic evolution operator that encompasses both cases:

$$U(\tau, 0) = \exp\left\{-i\left(\sum_{\ell=-\infty}^{\infty} r_\ell \phi_\ell\right) \sigma_z/2\right\}, \quad (2.81)$$

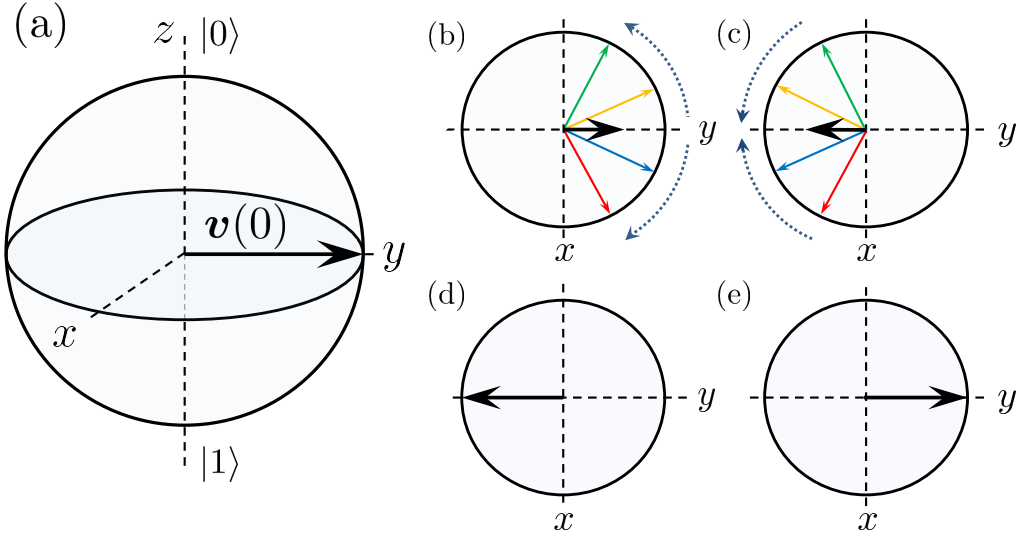


Figure 2.4: (Simple 2-pulse decoupling sequence) - (a) An ensemble of single-qubit systems shares the common initial state  $|+y\rangle$ , represented by the Bloch vector  $\mathbf{v}(0) = \hat{\mathbf{y}}$ . (b) (Looking down on the ‘equatorial plane’ of the Bloch sphere.) Subject to quasi-static noise over an interval  $[0, \tau/2]$ , each member of the ensemble (represented by the coloured arrows) acquires some randomly distributed phase. As a consequence, the ensemble average Bloch vector (black arrow) shrinks, signifying a loss of coherence. (c)-(d) After a  $\pi$ -rotation about the  $x$ -axis, applied at  $t = \tau/2$ , the ensemble is ‘refocused’. (e) A second  $\pi$ -rotation restores the initial coherent state at  $t = \tau$ .

where  $\phi_\ell \equiv \int_{\ell\tau/2}^{(\ell+1)\tau/2} dt \beta_z(t)$  and  $\{r_\ell\}$  are the coefficients of the digital filter described in section 2.4.2. If no pulse is applied, then  $r_0 = r_1 = 1$  and the result is a simple accumulation filter. If we apply a pulse, on the other hand, then  $r_0 = 1$  and  $r_1 = -1$  and, via the application of a carefully chosen control operation, we implement, at the level of the exponent of the unitary evolution operator, a digital difference filter. If the noise does not change significantly over the operation time  $\tau$ , then the exponent in (2.81) will be small, as will the decay of the Bloch vector. Indeed, in the ideal limit that the phase is time-independent, we find that  $U(\tau, 0) = I_S$  and the control objective is achieved with perfect fidelity.

A similar analysis applies for a single-spin system  $\mathcal{S}$  interacting with a quantum bath  $\mathcal{B}$ , though the presence of non-commuting operators can make a simple frequency space description of the action of the control protocol difficult, even for quite simple interactions (see reference [43] and Chapter 8 for more discussion of these issues as well as considerations of non-stationary and non-Gaussian noise environments). The quantum analogue of the semiclassical dephasing Hamiltonian (2.74), defined on the tensor product space  $\mathcal{H}_{\mathcal{S}+\mathcal{B}} = \mathcal{H}_{\mathcal{S}} \otimes \mathcal{H}_{\mathcal{B}}$ , is

$$H = \sigma_z \otimes B_z/2 + I_S \otimes H_{\mathcal{B}}. \quad (2.82)$$

Here,  $B_z$  and  $H_{\mathcal{B}}$  are operators acting on the bath Hilbert space  $\mathcal{H}_{\mathcal{B}}$ . This Hamiltonian generates a free evolution propagator (dropping the explicit tensor product notation)

$$U_0(t, 0) = \exp \{-i(\sigma_z B_z/2 + H_{\mathcal{B}})t\}, \quad (2.83)$$

which represents a pure dephasing action that leads to a loss of coherence similar to that observed for the classical dephasing environment. Again, assuming that the goal is to counter this and execute the identity operation on  $\mathcal{S}$ , we execute the control sequence (2.78). In this case,

(2.83) defines free evolution, and the control operation  $\sigma_x$  is applied to  $\mathcal{S}$  only. This produces the sequence propagator

$$U(\tau, 0) = \exp \{-i(-\sigma_z B_z/2 + H_{\mathcal{B}})\tau/2\} \exp \{-i(\sigma_z B_z/2 + H_{\mathcal{B}})\tau/2\}. \quad (2.84)$$

which, if  $[B_z, H_{\mathcal{B}}] = 0$ , simplifies to

$$U(\tau, 0) = I_{\mathcal{S}} \otimes \exp \{-iH_{\mathcal{B}}\tau\}, \quad (2.85)$$

so that, indeed, the state of  $\mathcal{S}$  is unaffected by the independent evolution of the environment.

When  $[B_z, H_{\mathcal{B}}] \neq 0$ , we can use the Baker-Campbell-Hausdorff expansion,  $e^{M_1}e^{M_2} = e^{M_1+M_2+[M_1,M_2]/2+\dots}$  [44], to rewrite (2.84) as

$$U(\tau, 0) = \exp \{-iH_{\mathcal{B}}\tau + \sigma_z[B_z, H_{\mathcal{B}}]\tau^2/8 + \dots\}. \quad (2.86)$$

In general, this is only approximately equal to (2.85) in the limit that  $\|B_z\|\|H_{\mathcal{B}}\|\tau^2 \ll 1$ , where  $\|\cdot\|$  denotes an appropriate unitarily invariant norm quantifying the ‘size’ or ‘strength’ of its argument [45]. In essence,  $\|B_z\|$  quantifies the strength of the coupling between  $\mathcal{S}$  and  $\mathcal{B}$ , while  $\|H_{\mathcal{B}}\|$  quantifies the rate at which  $\mathcal{B}$  evolves. In cases where  $\|H_{\mathcal{B}}\| > \|B_z\|$ , we can use the simpler, and more conservative, condition  $\|H_{\mathcal{B}}\|\tau \ll 1$  [46].

From both semiclassical and quantum examples of the application of a paradigmatic two-pulse *dynamical decoupling* (DD) sequence, we see that for coherent averaging, and hence DQES, to be effective, the information lost from the system state must be somehow ‘retrievable’ on the timescale of the applied control,  $\tau$ . Loosely speaking, the environment must retain some memory of its initial state for the duration of the protocol. A rough measure of the capacity to retain such information is the noise correlation time  $\tau_c$ , which can often be associated directly with the effective cutoff frequency  $\omega_c$  of the noise spectrum, i.e.,  $\tau_c \sim \omega_c^{-1}$ . In the ideal Markovian limit, the relevant correlation time of the environment is assumed to be so short in comparison to the rate of system evolution that the coherence information is effectively lost immediately [30]. Thus, we might say that a necessary condition for the efficacy of DQES is that the environment be non-Markovian, while a sufficient condition is  $\tau \ll \tau_c, (\omega_c^{-1})$ .

### 2.5.3 General dephasing DD sequences & spectral overlap

The treatment of the effect of a simple two-pulse sequence on an ensemble of spins in a classical dephasing environment can be extended quite straightforwardly to single-qubit systems in arbitrary initial states, subject to an arbitrary number of pulses, and in an expanded noise setting that includes an important subclass of quantum environments. The general form for the Hamiltonian of such a system is

$$H_{\mathcal{S}}(t) = \frac{1}{2}\sigma_z \otimes B_z(t), \quad (2.87)$$

where we allow for the environment to be modeled as either a quantum or a classical system by not specifying whether the time dependence in (2.87) is a result of a transformation to the interaction picture, with respect to a quantum bath  $\mathcal{B}$ , or due to the fluctuations of a classical random process. The distinction between quantum and classical analyses is reduced further by considering only interactions for which  $[B_z(t), B_z(t')] = cI_{\mathcal{B}}$ , for  $c \in \mathbb{R}$ ,  $t \neq t'$ , so that non-commuting operators contribute no more than a global phase factor.

With the aim of state preservation, a sequence of instantaneous parity reversing  $\pi$ -pulses is applied at times  $t_\ell$ , for  $\ell = 1, \dots, n$ , with  $\tau \equiv t_{n+1}$  and  $t_0 \equiv 0$ . The total propagator for such a sequence is

$$U(\tau, 0) = (\sigma_x)e^{-i\int_{t_n}^{t_{n+1}} dt B_z(t)\sigma_z/2} \dots \sigma_x e^{-i\int_{t_1}^{t_2} dt B_z(t)\sigma_z/2} \sigma_x e^{-i\int_{t_0}^{t_1} dt B_z(t)\sigma_z/2} \quad (2.88)$$

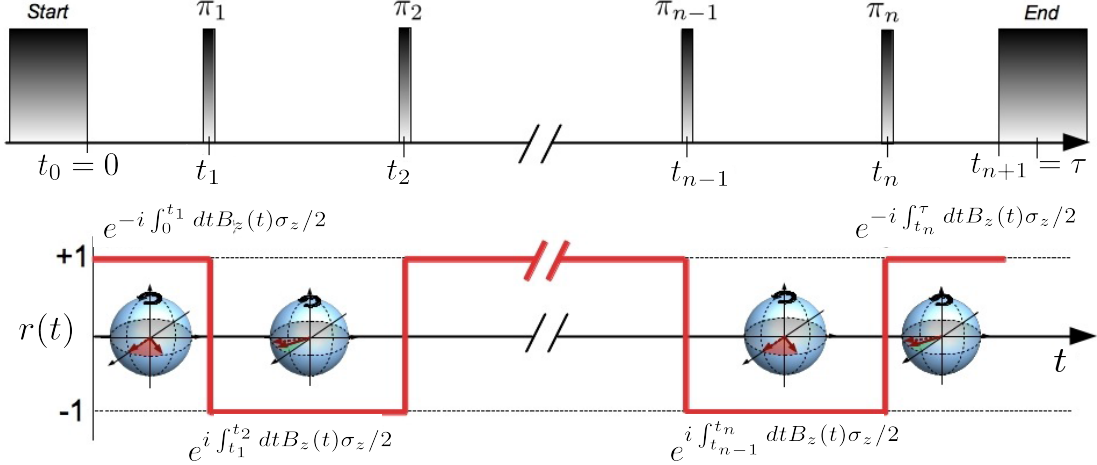


Figure 2.5: *Schematic representation of a single-axis dynamical decoupling pulse sequence and its relation to the switching function  $r(t)$ . Pulse width is represented as being nonzero for clarity and total sequence duration is  $\tau$ . (Top) Representation of the time-domain application of  $\pi$ -pulses. (Bottom) Phase accumulation ‘winds’ and ‘unwinds’ during successive free-evolution periods. [Adapted, with permission, from figure 1 in reference [47].]*

where the last  $\sigma_x$  pulse is required for odd  $n$  to ensure that the control propagator produces the identity, preserving an arbitrary state (NB: if the control objective is to preserve an eigenstate of  $\sigma_x$ , the additional pulse is not required.) Since all operator exponents commute, modulo an irrelevant constant, we may write the following compact expression for the propagator

$$U(\tau, 0) = \exp \left\{ -i\sigma_z \int_{-\infty}^{\infty} r(t)B_z(t)/2 \right\}, \quad (2.89)$$

where the impulse response, or ‘switching’, function

$$r(t) = \begin{cases} (-1)^{\ell+1} & , \text{for } t_\ell \leq t < t_{\ell+1} \\ 0 & , \text{for } t < t_0 \& t_{n+1} < t \end{cases} \quad (2.90)$$

alternates between values of +1 and -1 as consecutive pulses are applied, periodically reversing the evolution (see figure 2.5). As in the previous section, we can express this in terms of a digital filter  $\{r_\ell\}$ , by writing:

$$r(t) = \sum_{\ell=-\infty}^{\infty} r_\ell r_{[t_\ell, t_{\ell+1}]}(t), \quad (2.91)$$

where  $r_{[t_\ell, t_{\ell+1}]}(t)$  has unit value for  $t \in [t_\ell, t_{\ell+1}]$ , and the filter coefficients  $\{r_\ell\}$  encode the pattern of sign flips in (2.90).

Assuming an initial separable state  $\rho_{S+B} = \rho_S \otimes \rho_B$  for the case of a quantum bath, the density matrix of the system at the conclusion of the pulse sequence is

$$\begin{aligned} \rho_S(\tau) = & \rho_{00}(0) |0\rangle\langle 0| + \rho_{11}(0) |1\rangle\langle 1| \\ & + \rho_{01}(0) |0\rangle\langle 1| \langle e^{-i \int_{-\infty}^{\infty} dt r(t) B_z(t)} \rangle_{q,c} + \rho_{10}(0) |1\rangle\langle 0| \langle e^{i \int_{-\infty}^{\infty} dt r(t) B_z(t)} \rangle_{q,c} \end{aligned} \quad (2.92)$$

where we've accounted for both classical and quantum environments by letting  $\langle \cdot \rangle_c \equiv \mathbb{E}\{\cdot\}$  denote the classical ensemble average and  $\langle \cdot \rangle_q \equiv \text{Tr}_{\mathcal{B}}[\cdot \rho_{\mathcal{B}}]$  denote the quantum mechanical expectation value with respect to the bath. In general, for both quantum and classical cases, the coherence between computational basis states will be reduced by the magnitude of the factor  $\langle e^{-i \int_{-\infty}^{\infty} dt r(t) B_z(t)} \rangle_{q,c}$ .

If we make some additional assumptions about the nature of the environment then we can gain insight into the efficacy of the pulse sequence through a switch to the frequency domain. In the case of classical *Gaussian* dephasing noise ( $B_z(t) = \beta_z(t) I_{\mathcal{B}}$ ), we obtain the general form of the result alluded to in the previous section, though not stated explicitly:

$$\langle e^{-i \int_{-\infty}^{\infty} dt r(t) B_z(t)} \rangle_c = \mathbb{E}\{e^{-i \int_{-\infty}^{\infty} dt r(t) B_z(t)}\} = e^{-\chi(\tau)} \quad (2.93)$$

where

$$\chi(\tau) = \frac{1}{2\pi} \int_0^\infty \frac{d\omega}{\omega^2} S_{\beta_z}(\omega) F(\omega) \quad (2.94)$$

and

$$F(\omega) \equiv \omega^2 \left| \int_{-\infty}^{\infty} dt r(t) e^{i\omega t} \right|^2 \quad (2.95)$$

defines the so-called *filter function* that captures the effect of the control on the coherence of the noise-affected single-qubit system. If, in equation (2.87), the environment consists of a quasi-continuum of bosonic oscillator modes at thermal equilibrium at a temperature  $T$ , then

$$B_z(t) = \sum_i \left( g_i e^{i\omega_i t} b_i^\dagger + g_i^* e^{-i\omega_i t} b_i \right), \quad (2.96)$$

where  $g_i$  describes the coupling strength between the qubit and bosonic bath mode  $i$ , and  $b_i$  ( $b_i^\dagger$ ) is an operator annihilating (creating) an excitation of that mode. The expression for the coherence in this case is again  $e^{-\chi(\tau)}$ , however the exponent is now [48]

$$\chi(\tau) = \int_0^\infty \frac{d\omega}{\omega^2} J(\omega) \coth[\omega/(2k_B T)] F(\omega). \quad (2.97)$$

Here,  $T$  is the temperature of the bath,  $k_B$  is Boltzmann's constant and  $J(\omega)$  quantifies the density of oscillator modes as a function of frequency.

For both classical and quantum environments, the degree of coherence loss over the period of the controlled evolution is determined by the overlap between the spectral characteristics of the modulation imparted by the control and the noise power spectrum. It is worth noting here that Kurizki et. al. [49, 50, 51] have shown that, for a more general class of quantum control systems, the net susceptibility of a given protocol to weak environmental noise can be expressed in this way. And that it was Uhrig [52] and Cywinski et al. [53] who showed that, for DD sequences, the control could be expressed in terms of a simple temporal switching function, as described above, and that by changing the number and timing of the pulses the frequency space representation of the switching function could be modified to alter its noise filtering characteristics, particularly in the low frequency regime.

## 2.5.4 General DQES control setting

Having established the basic principles on which DQES is based, through a discussion of dynamical decoupling in fairly simple noise environments, we now briefly outline the way in which the approach is extended to more general QIP settings. Typically, the control object is a finite-dimensional quantum system  $\mathcal{S}$  (usually a collection of qubits) coupled to an uncontrolled

environment  $\mathcal{B}$ . The autonomous evolution of the composite system  $\mathcal{S} + \mathcal{B}$  is assumed to be generated by a Hamiltonian of the form

$$H_0 = H_{\mathcal{S}} \otimes I_{\mathcal{B}} + H_{\mathcal{S}\mathcal{B}} + I_{\mathcal{S}} \otimes H_{\mathcal{B}} \quad (2.98)$$

acting on the tensor product space  $\mathcal{H} = \mathcal{H}_{\mathcal{S}} \otimes \mathcal{H}_{\mathcal{B}}$ , where  $\mathcal{H}_{\mathcal{S}}$  ( $\mathcal{H}_{\mathcal{B}}$ ) is the system (bath) Hilbert space and  $I_{\mathcal{S}}$  ( $I_{\mathcal{B}}$ ) denotes the identity operation on  $\mathcal{H}_{\mathcal{S}}$  ( $\mathcal{H}_{\mathcal{B}}$ ). The Hamiltonians  $H_{\mathcal{S}}$  and  $H_{\mathcal{B}}$  account for the internal dynamics of the system and bath, respectively, while  $H_{\mathcal{S}\mathcal{B}}$  describes their interaction. The state of  $\mathcal{S} + \mathcal{B}$  at an arbitrary time  $t > 0$  is captured by the density operator  $\rho_{\mathcal{S}+\mathcal{B}}(t) = U(t)\rho_{\mathcal{S}+\mathcal{B}}(0)U^\dagger(t)$ , where  $\rho_{\mathcal{S}+\mathcal{B}}(0)$  is the initial state and  $U(t) = \exp\{-iH_0t\}$  is the evolution operator generated by (2.98). In the absence of any interaction,  $U(t)$  factorizes into a simple tensor product  $U(t) = U_{\mathcal{S}}(t) \otimes U_{\mathcal{B}}(t)$  of local operators acting separately on the system ( $U_{\mathcal{S}}(t)$ ) and the bath ( $U_{\mathcal{B}}(t)$ ). Given an initial separable state of the form  $\rho_{\mathcal{S}+\mathcal{B}}(0) = \rho_{\mathcal{S}}(0) \otimes \rho_{\mathcal{B}}(0)$ , for some initial system (bath) state  $\rho_{\mathcal{S}}(0)$  ( $\rho_{\mathcal{B}}(0)$ ),  $\mathcal{S}$  and  $\mathcal{B}$  will each evolve independently and unitarily according to its own internal dynamics. In contrast, a nonzero interaction term will, in general, cause  $\mathcal{S}$  and  $\mathcal{B}$  to become entangled and the observable quantum properties of  $\mathcal{S}$  will diminish.

The effects of externally applied control fields are modeled by a semi-classical control Hamiltonian  $H_c(t)$  acting on the system alone.<sup>8</sup> The control Hamiltonian generates the propagator

$$U_c(t) = \mathcal{T}_+ \exp \left\{ -i \int_0^t ds H_c(s) \right\} \quad (2.99)$$

which, because it represents that part of the evolution of the composite system over which we have direct control, is the central DQES design object.

Assuming no part of the system's internal evolution is required to achieve complete controllability, all evolution generated by the interaction Hamiltonian (2.98) may be regarded as noise. Henceforth, we define it as the ‘error Hamiltonian’,  $H_e \equiv H_0$ , and rewrite it in the more convenient form

$$H_e = \sum_a S_a \otimes B_a + I_{\mathcal{S}} \otimes H_{\mathcal{B}}, \quad (2.100)$$

for appropriately defined bath  $\{B_a\}$  operators and traceless system operators  $\{S_a\}$  (any error due to the internal ‘drift’ of the system  $H_{\mathcal{S}}$  can be absorbed by letting  $B_a = I_{\mathcal{B}}$ , for some value of  $a$ ). Since DQES protocols are effective only for sufficiently weak interactions, the bath operators  $\{B_a\}$  and  $H_{\mathcal{B}}$  are assumed to be bounded in the appropriate norm but are otherwise potentially unspecified. In addition to the pure bath Hamiltonian  $H_{\mathcal{B}}$ , the error Hamiltonian  $H_e$  contains all contributions that act to cause the total propagator

$$U(t) = \mathcal{T}_+ \exp \left\{ -i \int_0^t ds (H_c(s) + H_e) \right\} \quad (2.101)$$

to induce unwanted evolution.

For a general semiclassical decoherence model, the error Hamiltonian can be written in the explicitly time-dependent form

$$H_e(t) = \sum_a \beta_a(t) S_a, \quad (2.102)$$

---

<sup>8</sup>In general, experimental imperfections will cause  $H_c(t)$  to differ from its nominal form. To account for this, we could write  $H_c(t) = H_{c,0}(t) + H_{c,e}(t)$ , where  $H_{c,0}(t)$  represents the ideal control and  $H_{c,e}(t)$  represents the error. However, as our focus here is system-environment interaction noise, and for the sake of simplifying the discussion, we won't consider the effect of control errors explicitly, unless otherwise stated.

where the real-valued stochastic functions of time  $\{\beta_a(t)\}$  represent the action of the classical noise field in each of the ‘directions’ defined by the set of system operators  $\{S_a\}$ . As described in section 2.3.2, in this case, the final state of the system is obtained by taking the average over an ensemble of system density matrices, rather than by tracing out the degrees of freedom of the environment.

## Control objectives

For a particular control model and set of available resources, a variety of control objectives may be of interest. Here, we are interested in synthesizing a target *unitary* operation  $Q$  (not necessarily the identity operation) on an open quantum system  $\mathcal{S}$ . In the absence of any ‘error generators’  $\{S_a\}$  in (2.100), the total propagator (2.101) reduces to the simple tensor product

$$U(t) = U_c(t) \otimes \exp\{-iH_B t\} \quad (2.103)$$

The target operation can then be achieved, over a some predetermined time interval  $[0, \tau]$ , if the available control resources allow for the execution of a control protocol such that  $Q = U_c(\tau)$  (the independent evolution of the bath being irrelevant.)

For the general case, a simple decomposition of the form (2.103) is not possible and  $U(t)$  will induce additional system evolution. The task then becomes one of eliminating this undesirable evolution, subject to the constraint that  $Q = U_c(\tau)$ . To tackle the problem, we use the form of the ideal case (2.103) as a guide and write

$$U(\tau) = Q \exp\{-i\Phi(\tau)\}, \quad (2.104)$$

where the ideal control operation  $Q$  and the extraneous evolution  $\exp\{-i\Phi(\tau)\}$ ,<sup>9</sup> have been formally separated. The Hermitian operator  $\Phi(\tau)$  is referred to as the *error action* operator and may be expressed in terms of the control modulated error Hamiltonian  $\tilde{H}_e(t) \equiv U_c(t)^\dagger H_e(t) U_c(t)$  via the relation [46, 55]

$$\exp\{-i\Phi(\tau)\} = \mathcal{T}_+ \exp\left\{-i \int_0^\tau ds \tilde{H}_e(s)\right\}. \quad (2.105)$$

In general, the error action operator will be the sum of a component  $\Phi_{SB}(\tau)$  that includes system operators, and a component  $\Phi_B(\tau)$  containing only bath terms. Mathematically, the norm  $\|\Phi_{SB}(\tau)\|$  provides an upper bound for any fidelity loss due to a discrepancy between the ideal and the actual evolution on  $\mathcal{S}$  and, as such, can be used to quantify the error per gate (EPG) [45, 54]. For naive gate implementation the EPG scales linearly with the operation time:

$$\text{EPG}^{[0]} = \mathcal{O}[\tau]. \quad (2.106)$$

DQES protocols are designed to improve this scaling by canceling the dependence on  $\tau$  up to some desired order of accuracy.

## Filtering via symmetrization

Control propagators for DQES protocols described in this thesis are frequently defined piecewise over the control interval  $[0, \tau]$ . In these cases, the total sequence time is divided into  $n$  subintervals such that some ‘primitive gate’  $P_j$  is executed over the subinterval  $[t_{j-1}, t_j]$ , for

---

<sup>9</sup>This unitary is simply the ‘toggling’ frame propagator, written as an exponential function of the anti-Hermitian operator  $-i\Phi(\tau)$ . It is always possible to write a unitary in this form.

$j = 1, \dots, n$ , where  $t_n \equiv \tau$  and  $t_0 \equiv 0$ . Primitive gates are readily executable gates used to construct more complex transformations and, in the simplest case, may be generated by turning on and off selected control Hamiltonians in the available set  $\{H_m\}$ . The primitive gates combine to form a ‘control block’ that executes the target operation  $Q$ , i.e.  $Q = P_n P_{n-1} \dots P_1$ . The presence of system operators in the error Hamiltonian  $H_e$  means that each primitive gate  $P_j$  will be implemented with some error. Thus, the actual primitive operation can be expressed in terms of the ideal operation  $P_j$  and an error term. So, we write  $U(t_j, t_{j-1}) = P_j \exp\{-i\Phi_j\}$ , where

$$\exp\{-i\Phi_j\} \equiv \mathcal{T}_+ \exp \left\{ -i \int_{t_{l-j}}^{t_j} ds \tilde{H}_e(s) \right\} \quad (2.107)$$

The total propagator for the control block can then be written as

$$U(\tau) = P_n e^{-i\Phi_n} P_{n-1} e^{-i\Phi_{n-1}} \dots P_1 e^{-i\Phi_1} \quad (2.108)$$

from which, upon introducing the cumulative operators  $Q_l \equiv P_{l-1} P_{l-2} \dots P_0$ , where  $P_0 \equiv I_S$  and  $Q = Q_{n+1}$ , we can obtain the following expression for the net error action of a control block [55]

$$e^{-i\Phi} = e^{-iQ_n^\dagger \Phi_n Q_n} e^{-iQ_{n-1}^\dagger \Phi_{n-1} Q_{n-1}} \dots e^{-iQ_1^\dagger \Phi_1 Q_1}. \quad (2.109)$$

The Baker-Campbell-Hausdorff formula [44] provides a series expansion for the total error action

$$\Phi = \sum_{\nu=1}^{\infty} \Phi^{[\nu]}, \quad (2.110)$$

where

$$\Phi^{[1]} = \sum_{i=1}^n Q_i^\dagger \Phi_i Q_i \quad (2.111)$$

and the sum of all terms of order  $\nu$  and higher scales as

$$\left\| \sum_{\nu} \Phi^{[\nu]} \right\| = \mathcal{O}[\max \|\Phi_j\|^{\nu}]. \quad (2.112)$$

If  $n(\max \|\Phi_j\|) < \pi$ , then the series converges [56].

To the extent that the evolution in the ‘toggling’ frame can be regarded as being due to the first order term (2.111) only (i.e., assuming that the error associated with each control segment in the sequence is sufficiently small), it is possible to interpret the action of a DQES protocol as ‘symmetrizing’ the system evolution, so that those components of the system-environment interaction that would otherwise produce unwanted evolution are rendered ineffective [57, 58]. In essence, this symmetrization process is a generalization of the digital difference filter (section 2.4.2), in that it removes those error contributions that do not vary throughout the execution of the protocol.

To make this plain, note that a quantum system evolving in accordance with a Hamiltonian  $H$  is said to possess a *dynamical symmetry* with respect to a unitary transformation  $Q_j$  if

$$[Q_j, H] = 0. \quad (2.113)$$

It is a simple matter to verify that the set  $\mathcal{G}$  of all symmetry transformations satisfying (2.113) contains the identity  $I$  (trivially), and is closed under multiplication ( $Q_i, Q_j \in \mathcal{G} \Rightarrow Q_i Q_j \in \mathcal{G}$ ) and inversion ( $Q_i \in \mathcal{G} \Rightarrow Q_i^{-1} = Q_i^\dagger \in \mathcal{G}$ ). Thus  $\mathcal{G}$  forms a group with respect to the usual

rules of operator multiplication.<sup>10</sup> A direct consequence of (2.113) is that  $U^\dagger(t)Q_jU(t) = Q_j$ , where  $U(t)$  is the propagator generated by  $H$ . The implication of this is that all expectation values of the symmetry operators  $\{Q_j\}$  are conserved. Since any quantum state may be defined by a catalogue of expectation values, the existence of a symmetry group can be associated with a set of preserved states. In the extreme limit that the group forms a basis for the entire operator space, all states are preserved. Due to closure under multiplication, the group-averaged *effective* Hamiltonian

$$H_{\text{eff}} \equiv \frac{1}{|\mathcal{G}|} \sum_i Q_i^\dagger H Q_i \quad (2.114)$$

commutes with all  $Q_i \in \mathcal{G}$  (here,  $|\mathcal{G}|$  is simply the number of elements in the group.) Hence, if we can drive the system to evolve as though its dynamics were governed by this effective Hamiltonian, then the set of operators  $\{Q_i\}$ , and the associated states, will be preserved. One can then say that the evolution has been *symmetrized* with respect to  $\mathcal{G}$ .

In the case of interacting systems, it is possible for the natural interaction Hamiltonian to exhibit intrinsic symmetries. In principle, information may then be encoded in so-called *decoherence free subspaces* (DFS's), i.e., sets of system states that are immune to decoherence [59]. In practice, real quantum interactions rarely allow for the existence of DFS's capable of preserving quantum information with acceptably low error rates for operationally useful lengths of time. However, through the implementation of DQES control protocols, we can effectively engineer DFS's by *imposing* a symmetry structure on the dynamics of the system via the action of an external controller. Returning to equation (2.111), and assuming higher order terms can be neglected, we can define an effective Hamiltonian

$$H_{\text{eff}} \equiv \frac{1}{\tau} \Phi^{[1]} = \frac{1}{\tau} \sum_{i=1}^n Q_i^\dagger \Phi_i Q_i \quad (2.115)$$

that, to first order, describes the system's evolution over the interval  $[0, \tau]$ . If we can contrive a control sequence such that  $\Phi_i = \tilde{\Phi}$ , for all  $i$ , then

$$H_{\text{eff}} = \frac{1}{\tau} \sum_{i=1}^n Q_i^\dagger \tilde{\Phi} Q_i \quad (2.116)$$

also commutes with all  $Q_i \in \mathcal{G}$ , preserving the associated states.

That the two-pulse DD sequence, discussed in section 2.5.2, is in fact an example of this process can be made apparent by considering the case of static noise, where the system Hamiltonian is  $H_S = \beta_z \sigma_z / 2$ . The propagator (2.79) can then be written as  $U(\tau, 0) = \exp \{-i\bar{H}_S \tau\}$  where  $\bar{H}_S$  is a time-independent effective Hamiltonian defined by

$$\bar{H}_S \equiv \frac{1}{2} [I_S H_S I_S + \sigma_x H_S \sigma_x]. \quad (2.117)$$

It is easy to show that the pair of unitary operators  $\{I_S, \sigma_x\}$  constitutes a group, so that (2.117) is a particular instance of (2.114) (in fact, the group  $\{I_S, \sigma_x\}$  is isomorphic to the difference filter.) We therefore conclude that, whereas the original system Hamiltonian commuted with only the  $\sigma_z$  operator:

$$[\sigma_z, H_S] = 0, \quad (2.118)$$

reflecting the rotational symmetry of the system about the  $z$  axis. The effective Hamiltonian  $\bar{H}_S$ , which in this simple case actually vanishes, also commutes with  $\sigma_x$  and  $\sigma_y \propto \sigma_x \sigma_z$ , ensuring the preservation of arbitrary system states.

---

<sup>10</sup>To be precise,  $\mathcal{G}$  is a unitary representation of an abstract group, however this distinction is usually not important and it is generally safe to identify group and group representation.

More generally, for an arbitrary time-independent error Hamiltonian  $H_e$ , periodic DD (PDD) sequences produce first order decoupling by symmetrizing the evolution on  $\mathcal{S}$  with respect to a ‘decoupling group’  $\mathcal{G}$ . The  $n$  pulses that comprise a PDD sequence of duration  $\tau$  are assumed to be equally spaced, so that the error action  $\Phi_j = H_e \Delta t$ , for all  $j = 1, \dots, n$  [58, 60]. Consequently, to first order in  $\tau$ , the total propagator  $U(\tau)$  induces no evolution on  $\mathcal{S}$  so that the system has been effectively decoupled from its environment. This implies that decoherence induced by an arbitrary, and potentially unknown, quantum environment may be suppressed in the limit  $\tau \rightarrow 0$ . Crucially, the same principles can be extended to include more realistic bounded control decoupling sequences, in the form of *Eulerian dynamical decoupling* (EDD) [61], and to error robust *dynamically corrected gates* (DCGs) that enact nontrivial control operations [55]. Thus, by generalizing the concept of a filter to groups of operators in a system Hilbert space, we can continue to view DQES protocols through the lens of noise filtering.

## 2.6 Relevance of this work

In the following chapters, we generalize the theoretical constructs outlined in this chapter, with a particular emphasis on expanding the practically useful conception of DQES sequences as filters in frequency space, making fruitful connections, where possible, with the existing theoretical apparatus of classical control theory and signal processing. We also enlarge the field of application of DQES methods to encompass long-time storage of quantum information and, crucially, efficient state preservation and entanglement generation in *multi-qubit* systems. The results we derive constitute an important addition to the existing literature on quantum control and error suppression techniques and, it is hoped, will contribute to the eventual realization of practical, error-robust QIP technologies.

# Chapter 3

## High-order noise filtering in nontrivial quantum logic gates

Treating the effects of a time-dependent classical dephasing environment during quantum logic operations poses a theoretical challenge, as the application of non-commuting control operations gives rise to both dephasing and depolarization errors that must be accounted for in order to understand total average error rates. We develop a treatment based on effective Hamiltonian theory that allows us to efficiently model the effect of classical noise on nontrivial single-bit quantum logic operations composed of arbitrary control sequences. We present a general method to calculate the ensemble-averaged entanglement fidelity to arbitrary order in terms of noise filter functions, and provide explicit expressions to fourth order in the noise strength. In the weak noise limit we derive explicit filter functions for a broad class of piecewise-constant control sequences, and use them to study the performance of dynamically corrected gates, yielding good agreement with brute-force numerics.

The contents of this chapter have been published as: T. Green, H. Uys and M. J. Biercuk, “High-order noise filtering in nontrivial quantum logic gates”, *Physical Review Letters* **109**, 020501 (2012). This work extends the simple ‘bang bang’ decoupling filter function formalism, described in section 2.5.3, to account for the effects of dephasing noise on realistic finite-width control operations, introducing the concept of *generalized filter functions*. The results presented herein are expounded upon, and widened to include universal (multi-axis) noise, in the following chapter.

### 3.1 Introduction

Dynamical error suppression strategies have been demonstrated as a means by which errors due to decoherence may be suppressed during qubit memory operations [48, 58, 57, 62, 63, 64, 65, 66]. In such cases, a filter-design framework [33, 67, 53, 32, 47] has successfully shown how to precisely estimate average error rates in the presence of classical, time-dependent noise. Expanding this analysis beyond the identity operator has proved challenging due to the need for efficient techniques to treat a random, time-varying noise term that does not commute with the applied control field. Understanding the influence of such time-dependent processes during control operations is vital, however, as environmental decoherence sets the lower-bound on achievable gate error rates in a quantum informatic setting.

In this chapter, we address the challenge of characterizing and mitigating decoherence due to

classical noise during nontrivial single-qubit operations. We calculate the ensemble-averaged entanglement fidelity for an arbitrary control sequence to fourth order in the noise strength, incorporating terms to the third order of the Magnus Expansion in an effective Hamiltonian treatment. For concreteness we explicitly calculate the filter functions to lowest nontrivial order for sequences composed of  $\pi$ -rotations about Cartesian axes with arbitrary rotation rates - a class including dynamically corrected gates (DCGs). Our results permit detailed calculation of the generic (amplitude and phase) errors that result from applying a quantum control operation in the presence of pure-dephasing noise, and validate perturbative predictions of an increased order of error suppression [68, 55]. This straightforward analytical approach is compared against brute-force numerical calculations of the evolution of the Bloch vector, and shows excellent agreement.

## 3.2 Theoretical model

We consider the canonical dephasing environment in which the system evolves freely under a Hamiltonian of the form  $H = \frac{1}{2}[\Omega + \eta(t)]\sigma_z$ , where  $\Omega$  is the unperturbed qubit splitting,  $\eta$  is a time-dependent classical random variable, and  $\sigma_z$  is a Pauli operator. In the case of free-evolution the presence of a nonzero  $\eta(t)$  produces dephasing in an ensemble average. However, during driven operations where one applies a control field proportional to  $\sigma_x$  or  $\sigma_y$ , the presence of a pure-dephasing noise environment yields both polarization damping and dephasing effects. Both must be considered in a full treatment of gate errors. This accounts for the most significant *correctable* forms of decoherence in experiment; most remaining polarization-damping errors are due to stochastic processes that cannot be corrected through dynamical error suppression.

The total Hamiltonian (in the rotating frame at  $\Omega$ ) is  $H(t) = H_0(t) + H_c(t)$ , over  $t \in [0, \tau]$ . The operator  $H_0(t) = \eta(t)\sigma_z/2$  represents a time-varying dephasing environment, while  $H_c(t)$  describes an interaction between the system and an external control device that, in principle, may be used to implement arbitrary rotations of the Bloch vector. In general, evaluating the total propagator  $U(t) = T \exp(-i \int_0^t H(t')dt')$  explicitly for  $H_0(t) \neq 0$  is difficult due to noncommuting terms in  $H(t)$ . We therefore proceed by factoring out that part of the qubit evolution that is due solely to the control and expressing the residual ‘error propagator’  $\tilde{U}(\tau)$  in terms of a *time-independent* effective Hamiltonian that can then be evaluated, following a general procedure laid out in reference [58].

### 3.2.1 The error vector

Defining the control propagator  $U_c(t) = T \exp(-i \int_0^t H_c(t')dt')$ , it can be shown that  $\tilde{U}(t) = U_c^\dagger(t)U(t)$  satisfies the equation of motion

$$i \frac{d\tilde{U}(t)}{dt} = \tilde{H}_0(t)\tilde{U}(t), \quad (3.1)$$

where  $\tilde{H}_0(t) \equiv U_c^\dagger(t)H_0(t)U_c(t)$  [20, 21]. If  $H_c(t)$  enacts a target unitary operation  $Q$  in the absence of decoherence, then we may write the total noise-affected operation as  $U(\tau) = Q\tilde{U}(\tau)$ . The error propagator can then be expressed in terms of a time-independent effective Hamiltonian  $H_{\text{eff}}$ , defined by  $\tilde{U}(\tau) \equiv \exp(-iH_{\text{eff}}\tau)$ .

For a dephasing Hamiltonian we have

$$\tilde{H}_0(t) = \frac{\eta(t)}{2}U_c^\dagger(t)\sigma_zU_c(t); \quad (3.2)$$

the term  $U_c^\dagger(t)\sigma_z U_c(t)$  is a rotation of the  $\sigma_z$  operator due to the control. We may therefore define a time-dependent ‘control vector’ in a Cartesian basis ( $l = x, y, z$ ),  $\mathbf{s}_1(t) = \sum_l s_{1,l}(t)\hat{l}$ , where  $|\mathbf{s}_1(t)| = 1$ ,  $\forall t \in [0, \tau]$ , such that

$$\tilde{H}_0(t) = \frac{\eta(t)}{2}\mathbf{s}_1(t) \cdot \boldsymbol{\sigma}. \quad (3.3)$$

Since  $\tilde{H}_0(t)$  belongs to the Lie algebra  $su(2)$ ,  $\forall t \in [0, \tau]$ , the effective Hamiltonian  $H_{\text{eff}}$  derived from it is also in  $su(2)$ . We may now write  $U(\tau) = Q \exp[-i\mathbf{a}(\tau) \cdot \boldsymbol{\sigma}]$ , where the effect of the noise on the ideal operation  $Q$  is encoded in the ‘error vector’  $\mathbf{a}(\tau)$ . Here  $\mathbf{a}(\tau) = \sum_l a_l(\tau)\hat{l}$  represents error contributions to  $Q$  due to terms in  $H_{\text{eff}}$  proportional to the Cartesian components of the Pauli operator. In general, the action of the control converts pure-dephasing noise to arbitrary rotations of the qubit’s Bloch vector, producing both dephasing and polarization damping errors.

In most cases, an explicit expression for  $\exp[-i\mathbf{a}(\tau) \cdot \boldsymbol{\sigma}]$  can only be found using approximation methods. For our purposes, it is desirable that the simple exponential form of the operator be retained to any level of approximation. This can be achieved through the use of the Magnus expansion [69, 70]. Using this method, the exponent is expanded in an infinite series of time-integrals over nested commutators of  $\tilde{H}_0(t)$  at different times. In conjunction with the identity  $[\mathbf{u} \cdot \boldsymbol{\sigma}, \mathbf{v} \cdot \boldsymbol{\sigma}] = 2i(\mathbf{u} \times \mathbf{v}) \cdot \boldsymbol{\sigma}$ ,  $\mathbf{u}, \mathbf{v} \in \mathbb{R}^3$ , we find that we can write  $\mathbf{a}(\tau) \cdot \boldsymbol{\sigma} = \sum_{i=1}^{\infty} \mathbf{a}_i \cdot \boldsymbol{\sigma}$  to all orders  $i$ . The first three terms in the series expansion of the error vector are

$$\mathbf{a}_1(\tau) = \frac{1}{2} \int_0^\tau dt \eta(t) \mathbf{s}_1(t), \quad (3.4)$$

$$\mathbf{a}_2(\tau) = \frac{1}{4} \int_0^\tau dt_2 \int_0^{t_2} dt_1 \eta(t_1) \eta(t_2) \mathbf{s}_2(t_1, t_2) \quad (3.5)$$

and

$$\mathbf{a}_3(\tau) = \frac{1}{12} \int_0^\tau dt_3 \int_0^{t_3} dt_2 \int_0^{t_2} dt_1 \eta(t_1) \eta(t_2) \eta(t_3) \mathbf{s}_3(t_1, t_2, t_3). \quad (3.6)$$

Here, high-order commutators in the Magnus expansion have been reduced to vector cross products of the control vector at different times,  $\mathbf{s}_2(t_1, t_2) \equiv \mathbf{s}_1(t_2) \times \mathbf{s}_1(t_1)$  and  $\mathbf{s}_3(t_1, t_2, t_3) \equiv \mathbf{s}_1(t_3) \times [\mathbf{s}_1(t_2) \times \mathbf{s}_1(t_1)] + [\mathbf{s}_1(t_3) \times \mathbf{s}_1(t_2)] \times \mathbf{s}_1(t_1)$ .

### 3.2.2 Entanglement fidelity

We evaluate the net effect of the gate operation  $Q$  in the presence of noise via the ensemble average entanglement fidelity [71],  $\langle \mathcal{F}(\tau) \rangle = \langle |\text{Tr}(QU(\tau)/2)|^2 \rangle$  which, when written in terms of the error vector, becomes

$$\langle \mathcal{F}(\tau) \rangle = \frac{1}{2} [\langle \cos[2|\mathbf{a}|] \rangle + 1]. \quad (3.7)$$

To evaluate the fidelity we write  $|\mathbf{a}| = (\sum_l a_l^2)^{1/2}$ , express the cosine term as a Taylor series and substitute the Magnus expansion  $a_l = \sum_{i=1}^{\infty} a_{i,l}$  for each component of the error vector. The result is an infinite series of multi-dimensional integrals over products of multiple-time noise correlation functions and components of the control vector  $\mathbf{s}_1(t)$ . For example, the lowest order effects of the noise are captured by

$$\langle a_{1,l}^2 \rangle = \int_{-\infty}^{\infty} \int_{-\infty}^{\infty} s_{1,l}(t_1) s_{1,l}(t_2) \langle \eta(t_1) \eta(t_2) \rangle dt_1 dt_2, \quad (3.8)$$

for  $l = x, y, z$ .

Assuming the noise is Gaussian, only correlation functions  $\langle \eta(t_1) \dots \eta(t_n) \rangle$  for which  $n$  is even contribute. Further, applying the Gaussian moment theorem, each of these can be written in terms of simple *two-point* correlation functions. Using the root mean square deviation of the noise,  $\Delta\eta \equiv \sqrt{\langle \eta(t)^2 \rangle}$ , as a measure of the noise strength, we can define a parameter  $\xi \equiv \Delta\eta\tau/2$  which provides an upper bound for the magnitude of each term in the series expansion of the cosine function.<sup>1</sup> If we restrict our analysis to weak-noise/efficient-control conditions under which  $\xi < 1$ , then higher-order terms provide diminishing contributions to the total error and we may truncate the series. To fourth order in  $\xi$  we find that

$$\langle \cos[2|\mathbf{a}|] \rangle = 1 - 2\xi^2 \left\{ \overline{\langle a_{1,l}^2 \rangle} \right\} - 2\xi^4 \left\{ \frac{1}{4} \left( 3\overline{\langle a_{2,l}^2 \rangle} + 2\overline{\langle a_{1,l}a_{3,l} \rangle} \right) - \overline{\langle a_{1,l}^2 a_{1,l'}^2 \rangle} \right\} \quad (3.9)$$

where sums are implicitly performed over  $l$  and  $l'$ . An overline indicates that the maximum magnitude of the term has been factored out. For example, we find that the maximum value of  $|\langle a_{1,l}^2 a_{1,l'}^2 \rangle|$  is  $3\xi^4$ , so that  $\overline{\langle a_{1,l}^2 a_{1,l'}^2 \rangle} \equiv \langle a_{1,l}^2 a_{1,l'}^2 \rangle / (3\xi^4)$  and  $|\overline{\langle a_{1,l}^2 a_{1,l'}^2 \rangle}| \leq 1$ . Equation (3.9) includes terms to *third* order in the Magnus expansion as they contribute to the same order in  $\xi$  as the second order term.

### 3.2.3 Fourier space representation

The various contributions to equation (3.9) may be calculated explicitly by Fourier transforming the noise and control. For instance, we may write

$$\langle a_{1,l}^2 \rangle = \frac{1}{4\pi} \int_0^\infty |y_{1,l}(\omega)|^2 \frac{S(\omega)}{\omega^2} d\omega, \quad (3.10)$$

with  $y_{1,l}(\omega) = -i\omega \int_{-\infty}^\infty s_{1,l}(t) e^{i\omega t} dt$ , capturing terms proportional to  $\sigma_l$ . We sum over  $l$  to write  $F_1(\omega) = \sum_l F_{1,l} = \sum_l |y_{1,l}(\omega)|^2$ , corresponding to the terms in the first line of equation (3.9). Similarly, we account for the proliferation of higher order terms arising from the vector cross product by defining  $F_{p,2}(\omega, \omega', \tau)$ , where  $p$  is an index over terms proportional to  $\xi^4$  in equation (3.9). These terms contain four-point correlation functions in time,  $\langle \eta(t_1)\eta(t_2)\eta(t_3)\eta(t_4) \rangle$ , which may be explicitly evaluated using the Gaussian moment theorem. We may then compactly write the entanglement fidelity

$$\begin{aligned} \langle \mathcal{F} \rangle = 1 &- \frac{1}{4\pi} \int_0^\infty \frac{d\omega}{\omega^2} S(\omega) F_1(\omega, \tau) \\ &- \frac{1}{(4\pi)^2} \sum_p \int_0^\infty \frac{d\omega}{\omega^2} S(\omega) \int_0^\infty \frac{d\omega'}{\omega'^2} S(\omega') F_{p,2}(\omega, \omega', \tau). \end{aligned} \quad (3.11)$$

Terms to all orders in  $\xi$  may be evaluated using the same procedure.

With these expressions we have reduced the effect of a time-dependent dephasing environment and a time-dependent control Hamiltonian to integrals incorporating only stationary

---

<sup>1</sup>If the power spectral density  $S(\omega)$  of the noise has a sharp high-frequency cutoff  $\omega_c$ , then  $\Delta\eta$  becomes an increasing function of the cutoff frequency,  $\Delta\eta = \Delta\eta(\omega_c)$ . Additionally, the total sequence time  $\tau$  is inversely related to the minimum value of the bandwidth  $\Omega_{\text{ctrl}}$  of the control [72]. The parameter  $\xi$  can then be written as  $\xi = c\Delta\eta(\omega_c)/\Omega_{\text{ctrl}}$ , where  $c$  is a constant. For example, in the case of white noise,  $S(\omega) = \alpha\Theta(\omega_c - \omega)$ , we have  $\xi = c\alpha\sqrt{\omega_c}/\Omega_{\text{ctrl}}$ . Thus the requirement that  $\xi \ll 1$  corresponds to a the regime in which the control is sufficiently ‘fast’ relative to the noise.

statistical properties of the system: the noise power spectral density and the spectral functions to arbitrary order,  $F_i$ . These terms contain all relevant information about the applied control, and the explicit inclusion of terms proportional to all  $\sigma_l$  captures both dephasing and polarization-damping errors produced during control operations. We refer to the terms  $F_i$  as the *filter functions* for the total control operation, in analogy with previous work on dynamical decoupling [67, 53, 32, 47]. The leading nontrivial term is closely related to the idea of spectral overlap functions between control and noise that has been studied previously [73, 51, 74], but a generalized derivation to high order has not appeared to the best of our knowledge.

We now consider a specific case for concreteness that is germane to many coherent control experiments, including the implementation of dynamically corrected gates. We define  $H_c(t)$  as piecewise-constant over a total of  $k \in \mathbb{N}$  consecutive time bins, such that during the  $j$ -th time bin the control is intended to execute  $\sigma_{l_j}$ , restricted here to either the identity  $I$ , or a rotation of the qubit Bloch vector through  $\pm\pi$  about one of the three Cartesian directions. In this notation,  $l_j = I, x, y, z$ . The control propagator may be written explicitly such that during the  $j$ th driven operation we have

$$U_c^{(j)} = \exp[-i\Omega_R^{(j)}(t - t_{j-1})\sigma_{l_j}/2]\sigma_{\forall j-1}, \quad (3.12)$$

where  $\Omega_R^{(j)}$  gives the driven rotation rate about axis  $\hat{l}$  in time-bin  $j$ . The operator  $\sigma_{\forall j-1} = \sigma_{l_{j-1}}\sigma_{l_{j-2}}\dots\sigma_{l_1}$  describes the cumulative effect of all completed rotations in the preceding time segments.

We restrict our presentation to terms in the entanglement fidelity of order  $\xi^2$ , appropriate for the case of weak dephasing noise. Higher order contributions are straightforward to calculate explicitly, but involve many dozens of terms. In this case we only require first-order components of the error vector and may approximate

$$\langle \mathcal{F}(\tau) \rangle \approx \frac{1}{2} \left[ e^{-2\sum \langle a_{1,l}^2 \rangle} + 1 \right]. \quad (3.13)$$

Using the first-order filter functions we have  $\langle \mathcal{F}(\tau) \rangle \approx \frac{1}{2} [\exp(-\chi(\tau)) + 1]$ , where

$$\chi(\tau) = \frac{1}{2\pi} \int_0^\infty F_1(\omega) \frac{S(\omega)}{\omega^2} d\omega. \quad (3.14)$$

For piecewise-constant control as described above, the terms contributing to  $F_{1,l}(\omega)$  may be written:

$$y_{1,x}(\omega) = \sum_{j=1}^k (-1)^{N_{y,z}^{[j]}+1} \frac{i\omega\Omega_R^{(j)}}{\omega^2 - (\Omega_R^{(j)})^2} (e^{i\omega t_j} + e^{i\omega t_{j-1}}) \delta_{l_j y} \quad (3.15)$$

$$y_{1,y}(\omega) = \sum_{j=1}^k (-1)^{N_{x,z}^{[j]}} \frac{i\omega\Omega_R^{(j)}}{\omega^2 - (\Omega_R^{(j)})^2} (e^{i\omega t_j} + e^{i\omega t_{j-1}}) \delta_{l_j x} \quad (3.16)$$

$$y_{1,z}(\omega) = \sum_{j=1}^k (-1)^{N_{x,y}^{[j]}} \left[ \frac{\omega^2}{\omega^2 - (\Omega_R^{(j)})^2} (e^{i\omega t_j} + e^{i\omega t_{j-1}}) (\delta_{l_j x} + \delta_{l_j y}) + (e^{i\omega t_{j-1}} - e^{i\omega t_j}) (\delta_{l_j z} + \delta_{l_j I}) \right] \quad (3.17)$$

where  $\delta_{\alpha\beta} = 1$  for  $\alpha = \beta$  and is zero otherwise. Here  $N_{\alpha,\beta}^{[j]}$  represents the number of times  $\sigma_\alpha$  or  $\sigma_\beta$  appear in the sequence up to the  $j$ -th interval. We note that the prefactors in these equations

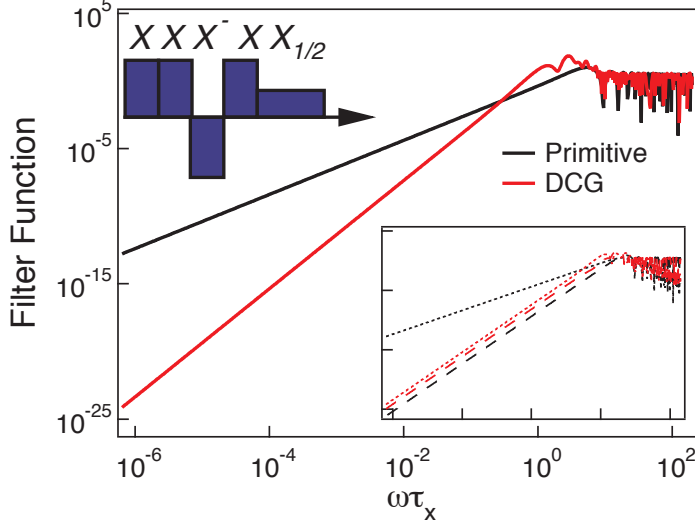


**Figure 3.1:** *Filter functions for primitive  $X$  and  $X_{DCG}$ , based on equation (3.17). Upper inset, schematic construction of  $X_{DCG}$  [68].  $X^-$  is a  $X$  rotation with  $\pi$  phase shift. Lower inset, Amplitude,  $F_{1,x}$  (dotted), and Phase  $F_{1,z}$  (dashed) filter functions for the same gates, denoted by color. Tick marks same as main panel.*

are similar to those derived from the steady-state master-equation treatment of a driven two-level system in the presence of dissipation [30].

Using this approach we are able to analyze the effects of classical noise on a complete set of both primitive (standard) and dynamically protected single-qubit gates of interest for quantum logic. As an example, in figure 3.1 we show the total filter functions derived from this treatment for  $X$  operations in primitive and DCG formulations [61, 68]. Consistent with previous perturbative treatments of quantum-mechanical baths, we find that the order of error suppression, given by the low-frequency rolloff of  $F_1(\omega)$ , is increased in the DCG relative to the primitive gate [47, 75]. The extension of the duration of  $X_{DCG}$  relative to  $X$  is manifested as a decrease in  $\omega_{F1}$ , the frequency above which the filter function takes value unity and noise is passed largely unimpeded. By examining the phase and amplitude components of the filter function independently ( $F_{1,z}$  and  $F_{1,x}$ ), we see that for a DCG we improve the order of error suppression primarily in the term that commutes with the control operation (e.g. amplitude for an  $X$  gate). The form of the filter functions for other operations and their DCG constructions (e.g.  $Z_\theta$ ,  $H$ ) show similar behavior. Dynamical decoupling (dynamically protected  $I$ ) may also be treated using equation (3.17).

Using the lowest-order approximation for the entanglement fidelity and the specific forms of the filter functions for  $X_{DCG}$  we calculate the error probability for different noise environments and plot these in figure 3.2. As expected, in an environment given by  $S(\omega) = \alpha/\omega^2$ , with  $\alpha$  a scaling factor (c.f. reference [76]), we find significant benefits from using the DCG construction. By contrast, in a white noise environment with a sharp high-frequency cutoff ( $S(\omega) = \alpha\Theta(\omega_c - \omega)$ ) the significant high-frequency spectral components of the noise and the extended duration of the DCG construction can yield a net performance degradation in the event of long  $\tau_x$  and large  $\omega_c$ . The relationship between these two quantities thus provides a dominant practical limit on the applicability of DCG construction in realistic settings; so long as  $\omega_c \lesssim \tau_x^{-1}$  the DCG provides net performance enhancement.

Validation for the assumptions and approximations made in this treatment comes from performing detailed brute-force numerical simulation of the evolution of the Bloch vector in the presence of a noisy environment, and averaging over multiple trajectories,  $\eta(t)$  (figure 3.2(c)).

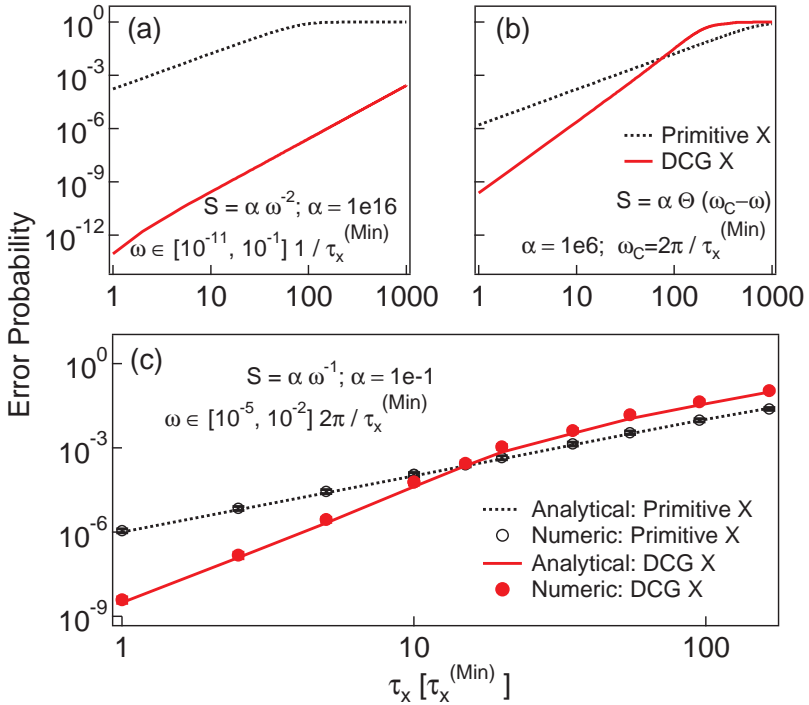


Figure 3.2: Calculated error rates for primitive  $X$  and  $X_{DCG}$  gates in the presence of noise. (a) Calculated error rates in the presence of noise similar to that observed in reference [76], appropriate for decoherence due to nuclear spin diffusion in solid-state singlet-triplet qubits. Data are plotted in dimensionless units of the minimum  $\tau_x$  value. (b) Similar to (a), but using a white noise power spectral density up to a sharp high-frequency cutoff. (c) Comparison of calculated error rates based on analytical filter functions derived herein and brute-force numerics. Noise strength in numerics is set using  $\Delta = 0.008 \left( \tau_x^{(\text{Min})} \right)^{-1}$ , guaranteeing convergence of the Magnus expansion for this range of  $\tau_x$ . Each data point averages over 50 randomly generated noise trajectories whose statistical properties reproduce  $S(\omega)$ . Error bars are derived from the root-mean-square deviation of the individual trajectory results, but are small compared to the marker size.

The trajectories are chosen to exhibit the statistical properties of a desired power spectral density. Calculations involving only the terms in equation (3.17) accurately reproduce numerically calculated error probabilities to within  $\sim 20\%$  for the  $X$  gate. In complex DCG sequences efficient decoupling reduces leading-order terms until residual contributions become comparable to higher-order terms. We observe that the lowest-order filter functions underestimate error and deviation from numerics grows with more complex sequences or stronger noise, but remains a factor of order unity for the cases we have studied.

### 3.3 Conclusion

In summary, we have developed a theoretical treatment permitting the calculation of error rates due to time-varying classical noise during arbitrary control operations, to arbitrary order. We have explicitly produced a general high-order approximation to the qubit's entanglement fidelity and using the first three orders of the Magnus expansion. Building on these results we

have presented an example case of piecewise-constant control, and given simple, leading-order expressions for the filter function. This allows any experimentalist to evaluate expected error rates to the correct order of magnitude *during nontrivial control operations*, accounting for the fact that pure dephasing noise can result in both dephasing and polarization damping errors during control operations. Included in this class of control sequences are dynamically corrected gates, and we have validated previous perturbative calculations for DCG performance through an intuitive noise-filtering approach.

We believe that this experimentally accessible and rigorously tested method for understanding the influence of classical noise in single-qubit logic operations will prove valuable to the community and will open new pathways for the development of error-robust quantum control strategies. We emphasize that our approach is technology independent and these methods apply to any quantum system.

*Acknowledgements:* The authors thank A.C Doherty, K. Khodjasteh, and L. Viola for useful discussions. This work partially supported by the US Army Research Office under Contract Number W911NF-11-1-0068, and the Australian Research Council Centre of Excellence for Engineered Quantum Systems CE110001013.

# Chapter 4

## Arbitrary quantum control of qubits in the presence of universal noise

We address the problem of deriving analytic expressions for calculating universal decoherence-induced errors in qubits undergoing arbitrary, unitary, time-dependent quantum-control protocols. We show that the fidelity of a control operation may be expressed in terms of experimentally relevant spectral characteristics of the noise and of the control, over all Cartesian directions. We formulate control matrices in the time domain to capture the effects of piecewise-constant control, and convert them to generalized Fourier-domain filter functions. These generalized filter functions may be derived for complex temporally modulated control protocols, accounting for susceptibility to rotations of the qubit state vector in three dimensions. Taken together, we show that this framework provides a computationally efficient means to calculate the effects of universal noise on arbitrary quantum control protocols, producing results comparable to those obtained via time-consuming simulations of Bloch vector evolution. As a concrete example, we apply our method to treating the problem of dynamical decoupling incorporating realistic control pulses of arbitrary duration or form, including the replacement of simple  $\pi$ -pulses with complex dynamically corrected gates.

The contents of this chapter have been published as: T. Green, J. Sastrawan, H. Uys and M. J. Biercuk, “Arbitrary quantum control of qubits in the presence of universal noise”, New Journal of Physics **15**, 095004 (2013). This work is intended to ‘flesh out’ the generalized filter function approach introduced in the previous short chapter/publication, providing a very detailed derivation of the formalism, and several illustrative and useful example applications.

### 4.1 Introduction

A basic requirement for the realization of practical quantum coherent technologies, in particular quantum information processing (QIP) devices, is the capacity to efficiently manipulate quantum states with a high degree of precision. This prerequisite has given rise to the development of the field of Quantum Control Theory [77, 78, 79, 80, 81, 82, 83]. Significant research attention has been devoted to this discipline due to the remarkable promise of quantum coherent technologies for future applications including quantum computation, quantum-enabled sensing, and quantum-enhanced metrology.

One of the primary challenges being addressed by the research community is the understanding and mitigation of decoherence processes in quantum systems. In these processes,

uncontrolled interaction with the environment leads to randomization of a system's state, effectively destroying its ‘quantumness.’ This phenomenon is especially important in quantum information settings where net error rates deep below fault-tolerance thresholds ( $\sim 10^{-4}$ ) are required in order to build scalable quantum computers [17, 84, 6].

A variety of methods have been developed to characterize the performance of quantum control protocols, with an eye towards estimating error rates due to decoherence in realistic, experimentally relevant noise environments. One of the most interesting, from a practical perspective, is the concept of spectral overlap formalized by Kofman and Kurizki [49, 85]. In this general approach, the net susceptibility of a given quantum control protocol to environmental noise is given by the overlap in frequency between the noise power spectral density and the spectral characteristics of the modulation imparted by the control. Such insights have been particularly important for the field of dynamical error suppression (DES), which seeks to provide error robustness to quantum hardware at the physical level. These techniques address both implementation of quantum memory (dynamical decoupling (DD)) [86, 48, 58, 57, 62] as well as nontrivial quantum logic gates [87, 68, 55] and exploit interference trajectories to effectively time-reverse the accumulation of error.

The concepts of the spectral overlap were expanded in the context of DD by Uhrig [67] and Cywinski *et al* [53], in attempting to understand the efficacy of these protocols in suppressing decoherence in Non-Markovian environments. It was shown that, in considering DES broadly, the relevant control protocol could be thought of as a noise *filter*, and the efficiency of a particular control sequence deduced simply by an examination of the relevant filter transfer function [47]. This general approach has been repeatedly validated in experiments using a variety of technologies - from trapped atomic ions to semiconductor spin qubits [88, 32, 89, 90, 91]. Remarkable agreement has been demonstrated between simple theoretical expressions for error derived from the so-called ‘filter-function’ and experimentally measured noise power spectra - so much so that inverting this approach has allowed DES protocols to be used in noise spectroscopy [92, 93, 94].

Despite these capabilities, there remains a significant gap in our understanding of how to efficiently calculate expected operational fidelities and error rates for complex quantum control protocols and for situations in which universal (i.e. multi-axis) time-dependent noise sources are present. For instance, relatively little is known about how to account for the accumulation of error due to pulse non-idealities in DD sequences; the bang-bang limit is still widely assumed in analytic treatments.

Generally, while it is understood that spectral overlap techniques may be employed in order to evaluate error rates, it is not known how to efficiently produce analytic filter functions appropriate for such complex quantum control protocols. This is largely due to that fact that the analytic complexity of deriving such functions grows significantly as soon as non-commuting operators appear in the control Hamiltonian - as would be the case in DD with nonzero-duration control pulses or other nontrivial control operations.

In this chapter, we address this challenge by developing a generalized method for evaluating the effects of universal, semiclassical decoherence on a quantum system undergoing an arbitrary unitary control protocol. By adopting an approach in which the effect of the applied control is described by a three-dimensional control matrix [95, 96, 97], the effect of universal decoherence on an effective spin-1/2 qubit is given a geometric interpretation. In the presence of weak decohering noise, we show how all Cartesian contributions to the resulting operational fidelity may be calculated using noise power spectral densities along with the Fourier-space representations of the elements of the control matrix. Further, we show how it is possible to simply construct generalizations of the filter function for arbitrary control protocols by assuming piecewise-constant controls. As an example of the utility of this approach we study DD incorporating both realistic ‘primitive’  $\pi$ -pulses and more complicated dynamically corrected

gates. We are able to derive first order filter functions for the incorporation of arbitrary control pulses into a DD sequence and validate the performance of dynamically corrected gates in mitigating pulse errors in these sequences.

The remainder of the chapter is organized as follows. In section 4.2 we first provide some relevant background theory before introducing a framework for quantum control in noisy environments and a geometric interpretation of decoherence, leading to the derivation of analytic expressions for the fidelity in section 4.3. Section 4.4 then provides a concrete method to evaluate the control matrix (and hence the generalized filter functions) for the case of piecewise-constant control in the presence of universal and pure-dephasing noise. To demonstrate the practical utility of our method this approach is applied to the problem of finite-pulse effects in DD in section 4.5. Our framework permits us to efficiently separate out contributions to the filter function from the pulse *locations* from effects arising from the pulse *form* in a dephasing environment. We follow with a discussion of the limits of the filter function approach and a comparison between this analytic framework and detailed numeric simulations in section 4.6, before offering a conclusion.

## 4.2 Quantum control in realistic environments

According to quantum theory, an initially coherent quantum system  $\mathcal{S}$  and its environment  $\mathcal{B}$  can, via physical interaction, become entangled, forming a single composite quantum system  $\mathcal{S} + \mathcal{B}$ . From the perspective of an observer, with the capacity to measure only  $\mathcal{S}$ , coherence is effectively lost [7]. If unaddressed, this process of *decoherence* can occur very rapidly, making the long term retention and accurate processing of information impossible. Similar effects may be derived using a model in which environmental interaction is introduced via a fluctuating classical noise field. In this case, loss of coherence is understood as occurring via a process of randomization across an ensemble of identical quantum systems, each subject to a different realization of the noise. This semi-classical approach, often also referred to generically as decoherence, has the advantage of not requiring a detailed knowledge of the system-environment interaction Hamiltonian. Further, it has been shown repeatedly that such phenomenological noise models can accurately represent important aspects of experimental reality [32].

In this section, we outline a mathematical treatment of a controlled qubit affected by classical fields that serve to randomize the phase and probability amplitudes of the quantum state, while preserving the vector norm (i.e., we omit leakage from the computational state space).

### 4.2.1 Single-qubit dynamics and the Bloch sphere

Broadly speaking, a qubit is a quantum system that exhibits two possible outcomes for the measurement of a particular physical observable: the  $z$ -component of the intrinsic angular momentum of a spin-1/2 particle being the archetypal example. Letting  $|0\rangle$  and  $|1\rangle$  denote the states in which one or other of these outcomes are returned with certainty, and assuming maximal knowledge of the system, an arbitrary qubit state may be written as a linear combination

$$|\psi\rangle = \cos(\vartheta/2)|0\rangle + e^{i\varphi}\sin(\vartheta/2)|1\rangle \quad (4.1)$$

The angles  $(\vartheta, \varphi)$  define a three-dimensional unit vector, the Bloch vector, that provides a convenient pictorial representation of the state [6]. Interpreting all possible states in this way, the two-dimensional qubit state space is mapped to a sphere of unit radius, called the Bloch sphere (figure 4.1).

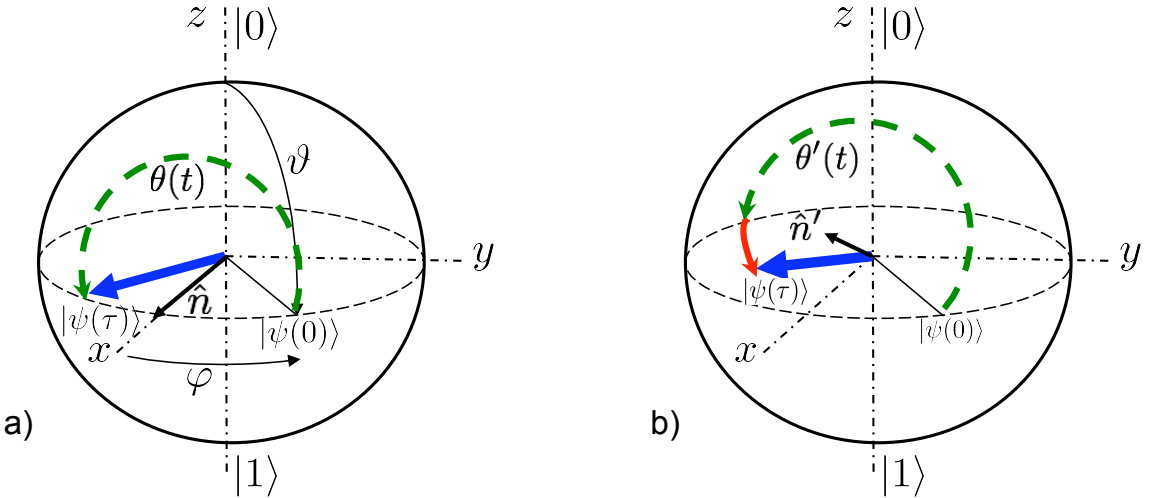


Figure 4.1: The Bloch sphere: showing a  $\pi$ -rotation about the  $x$ -axis, transforming an initial state  $|\psi(0)\rangle$  to a final state  $|\psi(t)\rangle$ , for a) ideal and b) the noise-affected control operations. The thick arrow indicates the final qubit state, the solid black arrow indicates the rotation axis, and the dotted path indicates the rotation angle. In b) the rotation axis and angle are both changed by the presence of the noise. Red extension of the path indicates over-rotation in path  $\theta'(t)$ . See text.

The temporal evolution of the qubit is described by the propagator  $U(t, 0)$ , a unitary operator that transforms some initial state  $|\psi(0)\rangle$  to a final state  $|\psi(t)\rangle = U(t, 0)|\psi(0)\rangle$ , for  $t \geq 0$ . Within the Bloch sphere picture, this ‘length-preserving’ transformation corresponds to a simple rotation of the qubit Bloch vector. The propagator satisfies the Schrodinger equation ( $\hbar = 1$ )

$$i \frac{d}{dt} U(t, 0) = H(t)U(t, 0) \quad (4.2)$$

where  $H(t)$  is the Hamiltonian operator, which we may assume to be traceless (i.e.,  $\text{Tr}(H(t)) = 0$ ), for all  $t$ . Disregarding irrelevant global phase factors, the set of all single qubit propagators, in conjunction with the usual operator product, forms the Lie group  $SU(2)$  [98].

That a geometrical interpretation of the action of a propagator is possible in terms of a rotation of the Bloch vector is a consequence of the homomorphism (structure-preserving map) that may be constructed between  $SU(2)$  and the group of three-dimensional rotation operators,  $SO(3)$  [98]. In short, the action of each propagator  $U \in SU(2)$  (and its physically equivalent negative  $-U$ ) on a single-qubit state  $|\psi\rangle$  can be represented by the action of a rotation operator  $R \in SO(3)$  on the Bloch vector corresponding to  $|\psi\rangle$ . To make this relationship explicit, we note that an arbitrary solution to (4.2) may be written in the form

$$U(t, 0) = \exp[-i\theta(t)\hat{n}(t)\boldsymbol{\sigma}/2], \quad (4.3)$$

where  $\hat{n}(t) = (n_x(t), n_y(t), n_z(t))$  is a real row vector of unit length,  $\boldsymbol{\sigma} = (\sigma_x, \sigma_y, \sigma_z)^T$  is a column vector comprised of the Pauli spin operators, and  $\theta(t)$  is a real function of time. The rotation operator in  $SO(3)$  corresponding to  $U(t, 0)$  is that which rotates the Bloch vector through an angle  $\theta(t)$ , about an axis defined by  $\hat{n}(t)$ . Thus, any single-qubit propagator may be thought of as acting to cause a simple rotation of the Bloch vector.

## 4.2.2 Capturing the effects of noise

To model the effect of noise on the capacity to control the evolution of a simple quantum system, we consider an ensemble of identically prepared noninteracting qubits evolving according to a Hamiltonian

$$H(t) = H_0(t) + H_c(t) \quad (4.4)$$

Here, the effect of the environment is modeled by the generalized noise Hamiltonian

$$H_0(t) = \boldsymbol{\sigma} \boldsymbol{\beta}(t), \quad (4.5)$$

where  $\boldsymbol{\beta}(t) = (\beta_x(t), \beta_y(t), \beta_z(t))$  is a three-element row vector, each component of which is a random process modeling classical noise in one of the three spatial dimensions. Control over the state of the qubit can be achieved through the application of an external field, represented by a control Hamiltonian

$$H_c(t) = \mathbf{h}(t)\boldsymbol{\sigma}, \quad (4.6)$$

where the components of the vector  $\mathbf{h}(t) = (h_x(t), h_y(t), h_z(t))$  describe the strength and direction of the control field as a function of time.

The presence of the noise term in (4.4) will, in general, affect adversely the ability to accurately ‘steer’ the qubit state via the control Hamiltonian  $H_c(t)$ . As a simple illustration, consider the application of a constant control Hamiltonian  $H_c(t) = \Omega\sigma_x/2$  to an otherwise isolated qubit, where  $\Omega \equiv \pi/\tau$  for some positive real number  $\tau$ . Under these circumstances, the total Hamiltonian is independent of time and equation (4.2) is easily integrated to give

$$U(\tau, 0) = \exp[-i\pi\sigma_x/2]. \quad (4.7)$$

Thus, over a time interval  $[0, \tau]$  the control field generates a rotation of the qubit Bloch vector through an angle of  $\pi$  radians, about the  $x$ -axis (a ‘ $\pi_X$ -pulse’), as shown in figure 4.1(a). If we allow for nonzero but constant ‘noise’ by letting  $\boldsymbol{\beta}(t) = (0, 0, \beta_z)$ , for example, then

$$U(\tau, 0) = \exp[-i\pi(\sigma_x + \nu\sigma_z)/2], \quad (4.8)$$

where  $\nu \equiv 2\beta_z/\Omega$ . The propagator now describes a rotation through an angle  $\theta' > \pi$ , about an axis that is tilted away from the  $xy$ -plane (figure 4.1(b)). The noise therefore causes both a change in the angle of rotation and a shift of the rotational axis, so that the final qubit state will not be the one intended.

In general, for noise that is time-dependent, deriving a simple closed-form expression for the propagator  $U(t)$  is not possible, as the Hamiltonian will generally not commute with itself at different times (from here on we omit the first argument of a propagator when it is zero). Therefore, rather than attempt to solve (4.2) directly, we introduce the ‘control propagator’  $U_c(t)$ , defined as the solution to the *noise-free* Schrodinger equation

$$i\frac{d}{dt}U_c(t) = H_c(t)U_c(t). \quad (4.9)$$

We may then write  $U(t) = U_c(t)\tilde{U}(t)$ , with the ‘error propagator’  $\tilde{U}(t)$  capturing any deviation from the control evolution due to noise [68, 56]. Substituting  $U(t) = U_c(t)\tilde{U}(t)$  into (4.2), and defining the ‘toggling frame’ Hamiltonian

$$\tilde{H}_0(t) \equiv U_c^\dagger(t)H_0(t)U_c(t) \quad (4.10)$$

we find that  $\tilde{U}(t)$  satisfies the modified Schrodinger equation

$$i\frac{d}{dt}\tilde{U}(t) = \tilde{H}_0(t)\tilde{U}(t) \quad (4.11)$$

In the absence of noise, executing a target operation  $Q$  over a time interval  $[0, \tau]$  simply requires one to engineer a control Hamiltonian such that  $U_c(\tau) = Q$ . More generally, we retain the requirement that  $U_c(\tau) = Q$ , so that  $U(\tau) = Q\tilde{U}(\tau)$ . The goal of dynamical error suppression is then to reduce  $\tilde{U}(\tau)$  to the identity  $I$ .

### 4.2.3 Geometric treatment of decoherence: the error vector and control matrix

The error propagator  $\tilde{U}(\tau)$ , being an element of  $SU(2)$ , may be interpreted as a rotation of the qubit Bloch vector through some angle  $2a(\tau)$ , about an axis  $\hat{\mathbf{a}}(\tau)$ . Hence

$$\tilde{U}(\tau) = \exp [-i\mathbf{a}(\tau)\boldsymbol{\sigma}], \quad (4.12)$$

where  $\mathbf{a}(\tau) \equiv a(\tau)\hat{\mathbf{a}}(\tau)$  is the real-valued ‘error vector’ with components  $a_i(\tau)$ , for  $i \in \{x, y, z\}$ , and magnitude  $|a(\tau)| = (\mathbf{a}(\tau)\mathbf{a}^T(\tau))^{1/2}$ .

From equations (4.10-4.12), we see that the error vector is determined by the toggling frame Hamiltonian  $\tilde{H}_0(t)$ , which itself derives from the action of the control propagator  $U_c(t)$  on  $H_0(t)$ . The aforementioned homomorphism between  $SU(2)$  and  $SO(3)$  enables us to identify  $U_c(t)$  with a three-dimensional ‘control matrix’  $\mathbf{R}(t) \in SO(3)$  [95]

$$\tilde{H}_0(t) = \sum_{i=x,y,z} \beta_i(t) U_c^\dagger(t) \sigma_i U_c(t) \quad (4.13)$$

$$= \sum_{i,j=x,y,z} \beta_i(t) R_{ij}(t) \sigma_j \quad (4.14)$$

$$= \boldsymbol{\beta}(t) \mathbf{R}(t) \boldsymbol{\sigma}. \quad (4.15)$$

Using the orthogonality of the Pauli operators with respect to the Hilbert-Schmidt inner product, the elements of  $\mathbf{R}(t)$  are

$$R_{ij}(t) \equiv [\mathbf{R}(t)]_{ij} = \text{Tr} (U_c^\dagger(t) \sigma_i U_c(t) \sigma_j) / 2 \quad (4.16)$$

for  $i, j \in \{x, y, z\}$ .

The control matrix may be written compactly as  $\mathbf{R}(t) \equiv (\mathbf{R}_x(t), \mathbf{R}_y(t), \mathbf{R}_z(t))^T$ , where  $\mathbf{R}_i(t) \equiv (R_{ix}(t), R_{iy}(t), R_{iz}(t))$  is a row vector comprised of the  $i$ -th row of the control matrix. Using this notation, (4.15) becomes

$$\tilde{H}_0(t) = \sum_{i=x,y,z} \beta_i(t) \mathbf{R}_i(t) \boldsymbol{\sigma}. \quad (4.17)$$

We will use this form in below, where we seek to write the error vector in terms of the noise components and elements of the control matrix.

### 4.2.4 Magnus expansion of the error vector

An explicit expression for the error vector  $\mathbf{a}(\tau)$  can be calculated by finding a solution to (4.11) that has the exponential form (4.12). At the cost of expressing the exponent as an infinite series, the Magnus expansion gives the desired result [69, 70, 99]. Specifically, given equation (4.11), we may write  $\tilde{U}(\tau) = \exp [-i\Phi(\tau)]$ , where

$$\Phi(\tau) = \sum_{\mu}^{\infty} \Phi_{\mu}(\tau). \quad (4.18)$$

The first three terms in the expansion are

$$\Phi_1(\tau) = \int_0^\tau dt \tilde{H}_0(t), \quad (4.19)$$

$$\Phi_2(\tau) = -\frac{i}{2} \int_0^\tau dt_1 \int_0^{t_1} dt_2 \left[ \tilde{H}_0(t_1), \tilde{H}_0(t_2) \right], \quad (4.20)$$

$$\begin{aligned} \Phi_3(\tau) = -\frac{1}{6} \int_0^\tau dt_1 \int_0^{t_1} dt_2 \int_0^{t_2} dt_3 & \left\{ \left[ \tilde{H}_0(t_1), \left[ \tilde{H}_0(t_2), \tilde{H}_0(t_3) \right] \right] \right. \\ & \left. + \left[ \tilde{H}_0(t_3), \left[ \tilde{H}_0(t_2), \tilde{H}_0(t_1) \right] \right] \right\} \end{aligned} \quad (4.21)$$

with higher order terms involving increasingly complicated multiple integrals of nested commutators.

Substituting the toggling frame Hamiltonian (4.17) into the Magnus expansion, and using the vector identity  $[\mathbf{u}\sigma, \mathbf{v}\sigma] = 2i(\mathbf{u} \times \mathbf{v})\sigma$ , for  $\mathbf{u}, \mathbf{v} \in \mathbb{R}^3$ , we find that we are able to write the error vector in the form of an infinite series

$$\mathbf{a}(\tau) = \sum_{\mu}^{\infty} \mathbf{a}_{\mu}(\tau), \quad (4.22)$$

where

$$\mathbf{a}_1(\tau) = \sum_{i=x,y,z} \int_0^\tau dt \beta_i(t) \mathbf{R}_i(t), \quad (4.23)$$

$$\mathbf{a}_2(\tau) = \sum_{i,j=x,y,z} \int_0^\tau dt_1 \int_0^{t_1} dt_2 \beta_i(t_1) \beta_j(t_2) \tilde{\mathbf{R}}_{ij}(t_1, t_2), \quad (4.24)$$

$$\mathbf{a}_3(\tau) = \frac{2}{3} \sum_{i,j,k=x,y,z} \int_0^\tau dt_1 \int_0^{t_1} dt_2 \int_0^{t_2} dt_3 \beta_i(t_1) \beta_j(t_2) \beta_k(t_3) \tilde{\mathbf{R}}_{ijk}(t_1, t_2, t_3). \quad (4.25)$$

Here, we've introduced the vectors  $\tilde{\mathbf{R}}_{ij}(t_1, t_2) \equiv [\mathbf{R}_i(t_1) \times \mathbf{R}_j(t_2)]$  and  $\tilde{\mathbf{R}}_{ijk}(t_1, t_2, t_3) \equiv [\mathbf{R}_i(t_1) \times [\mathbf{R}_j(t_2) \times \mathbf{R}_k(t_3)]] + [\mathbf{R}_k(t_3) \times [\mathbf{R}_j(t_2) \times \mathbf{R}_i(t_1)]]$ . Generally, the  $n$ -th order term is an  $n$ -fold integral over the sum of all possible products of the form

$$\beta_{i_1}(t_1) \beta_{i_2}(t_2) \dots \beta_{i_n}(t_n) \tilde{\mathbf{R}}_{i_1 i_2 \dots i_n}(t_1, t_2, \dots, t_n), \quad (4.26)$$

where the vector  $\tilde{\mathbf{R}}_{i_1 i_2 \dots i_n}(t_1, t_2, \dots, t_n)$  is a sum of multiple vector cross products of rows of the control matrix  $\mathbf{R}(t)$ , evaluated at times  $t_1, t_2, \dots, t_n$ .

Given (4.22-4.25), we have a series expansion for the error vector in which the components of the noise vector and the elements of the control matrix appear explicitly. By defining an appropriate metric for the fidelity of a control operation, in terms of the error vector, we can use these results to evaluate the impact of noise on an arbitrary control operation on an ensemble of identical non-interacting qubits.

### 4.3 Operational fidelity

One way of measuring how well a given propagator  $V_1$  approximates a target operation  $V_2$  is to take the Hilbert-Schmidt inner product

$$(V_2, V_1) \equiv \frac{1}{2} \text{Tr}\{(V_2^\dagger V_1)\} \quad (4.27)$$

which, by analogy with the usual inner product of state vectors, effectively measures the ‘overlap’ between the two operators. Taking the square modulus of the inner product of  $U(\tau) = Q\tilde{U}(\tau)$  and  $Q$  gives  $\mathcal{F}(\tau) \equiv \frac{1}{4}|\text{Tr}(\tilde{U}(\tau))|^2$ . This metric serves to quantify the accuracy of a control operation subject to a particular realization of the noise vector  $\beta(t)$ . Experimentally, however, it is usually only the ensemble average (denoted by the angular brackets  $\langle \dots \rangle$ ) of  $\mathcal{F}(\tau)$ , taken over all realizations of the noise Hamiltonian (4.5), that is measured. We therefore refer to

$$\mathcal{F}_{av}(\tau) \equiv \frac{1}{4}\langle |\text{Tr}(\tilde{U}(\tau))|^2 \rangle \quad (4.28)$$

as determining the ‘fidelity’ of a particular control operation.

With the error propagator written in terms of the error vector (4.12), and suppressing the explicit  $\tau$ -dependence, one finds

$$\mathcal{F}_{av} = \frac{1}{2}[\langle \cos(2a) \rangle + 1] \quad (4.29)$$

so that, for each qubit in the ensemble, the fidelity is determined by the magnitude of the angle through which the noise causes the control operation to be *rotated* away from the target operation  $Q$ . Expanding the cosine term in a Taylor series we obtain

$$\mathcal{F}_{av} = \frac{1}{2} \left[ 1 + \sum_{m=0}^{\infty} (-1)^m \frac{2^{2m}}{(2m)!} \langle a^{2m} \rangle \right]. \quad (4.30)$$

Considering the first nontrivial term ( $m = 1$ ) in the expansion, recalling that  $a^2 = \mathbf{a}\mathbf{a}^T$ , and using the Magnus expansion of the error vector (4.23), we may write

$$\langle a^2 \rangle = \sum_{\mu\nu} \langle \mathbf{a}_\mu \mathbf{a}_\nu^T \rangle = [\langle a_1^2 \rangle + \langle a_2^2 \rangle + \dots + 2(\langle \mathbf{a}_1 \mathbf{a}_2^T \rangle + \langle \mathbf{a}_1 \mathbf{a}_3^T \rangle + \langle \mathbf{a}_2 \mathbf{a}_3^T \rangle + \dots)] , \quad (4.31)$$

where  $a_1^2 \equiv \mathbf{a}_1 \mathbf{a}_1^T$ , and  $\mu, \nu$  are indices indicating the order of the Magnus expansion. Calculating the terms  $\langle a^{2m} \rangle$  for  $m > 1$  in a similar way, we arrive at a series expansion for the fidelity

$$\mathcal{F}_{av} = 1 - \langle a_1^2 \rangle - 2\langle \mathbf{a}_1 \mathbf{a}_2^T \rangle - \left[ \langle a_2^2 \rangle + 2\langle \mathbf{a}_1 \mathbf{a}_3^T \rangle - \frac{\langle a_1^4 \rangle}{3} \right] + \dots \quad (4.32)$$

with  $a_2^2 \equiv \mathbf{a}_2 \mathbf{a}_2^T$  and  $a_1^4 \equiv (\mathbf{a}_1 \mathbf{a}_1^T)^2$ .

The fidelity is thus expressed explicitly in terms of noise correlations and the control matrix. For instance, the second term in (4.32)

$$\langle a_1^2 \rangle = \sum_{i,j=x,y,z} \int_0^\tau dt_2 \int_0^\tau dt_1 \langle \beta_i(t_1) \beta_j(t_2) \rangle \mathbf{R}_i(t_1) \mathbf{R}_j^T(t_2) \quad (4.33)$$

$$= \sum_{i,j,k=x,y,z} \int_0^\tau dt_2 \int_0^\tau dt_1 \langle \beta_i(t_1) \beta_j(t_2) \rangle R_{ik}(t_1) R_{jk}(t_2) \quad (4.34)$$

contains all two-point noise cross-correlation functions  $\langle \beta_i(t_1) \beta_j(t_2) \rangle$ , for  $i, j \in \{x, y, z\}$ , while the third contains all those evaluated at three time points, and the terms in square brackets all involve four-point correlation functions (this is determined by the sum of subscript indices, as they indicate the expansion-order of the error vector in (4.23-4.25). For noise that is weak, the general trend will be for terms involving higher-order correlation functions to have less of an effect on the fidelity. Explicit forms for these terms, in the case that the components of the noise vector are independent Gaussian processes, may be found in the appendix of this paper and, for purely dephasing noise (i.e.  $H_0(t) = \beta_z(t)\sigma_z$ ), in [100].

### 4.3.1 Moving to the Fourier domain

The individual terms in the series expansion of the fidelity (4.32) rely on time-domain correlation and cross-correlation functions and convolution with the multidimensional control matrix. Using the properties of the Fourier transform, it is experimentally more convenient to rewrite these terms in the frequency domain. Generally, we can define the Fourier transform  $\mathcal{S}_{i_1 \dots i_n}(\omega_1, \dots, \omega_n)$  of an  $n$ -point cross-correlation function via

$$\langle \beta_{i_1}(t_1)\beta_{i_2}(t_2)\dots\beta_{i_n}(t_n) \rangle \equiv \frac{1}{(2\pi)^n} \int d\omega_1 \dots \int d\omega_n \mathcal{S}_{i_1 \dots i_n}(\omega_1, \dots, \omega_n) e^{i(\omega_1 t_1 + \dots + \omega_n t_n)}. \quad (4.35)$$

The fidelity (4.32) can then be rewritten as

$$= 1 - \sum_{n=2}^{\infty} \left\{ \frac{1}{(2\pi)^n} \sum_{i_1 \dots i_n} \int d\omega_1 \dots \int d\omega_n \mathcal{S}_{i_1 \dots i_n}(\omega_1, \dots, \omega_n) \mathcal{R}_{i_1 \dots i_n}(\omega_1, \dots, \omega_n) \right\}, \quad (4.36)$$

where  $\mathcal{R}_{i_1 \dots i_n}(\omega_1, \dots, \omega_n)$  is determined solely by the control matrix.

For noise that is sufficiently weak, the  $n = 2$  term in (4.36) will be the dominant contributor to fidelity loss in the short term. If the noise is also *wide sense stationary* then the two-point cross-correlation functions depend only on the time difference  $t_2 - t_1$ , so that

$$\langle \beta_i(t_1)\beta_j(t_2) \rangle = \frac{1}{2\pi} \int_{-\infty}^{\infty} d\omega S_{ij}(\omega) e^{i\omega(t_2 - t_1)}, \quad (4.37)$$

where  $S_{ij}(\omega)$  is the cross-power spectral density between the random variables  $\beta_i(t)$  and  $\beta_j(t)$ . We then have

$$\mathcal{F}_{av} \simeq 1 - \frac{1}{2\pi} \sum_{i,j,k=x,y,z} \int_{-\infty}^{\infty} \frac{d\omega}{\omega^2} S_{ij}(\omega) R_{jk}(\omega) R_{ik}^*(\omega), \quad (4.38)$$

where

$$R_{ij}(\omega) \equiv -i\omega \int_0^\tau dt R_{ij}(t) e^{i\omega t} \quad (4.39)$$

are the elements of the control matrix in the frequency domain (again we suppress the explicit dependence on the total time  $\tau$ ). The form of (4.38) is reminiscent of the filter function introduced in previous literature on dynamical error suppression, to which we will return later. Thus, in the weak noise regime (to be defined in the appendix, for Gaussian noise), it is possible to understand the fidelity of a qubit's unitary evolution in terms of spectral properties of the noise and the control [49, 67].

In the next section we will show how the control matrix may be evaluated for the paradigmatic case of a piecewise constant control sequence. In doing so, we explicitly demonstrate the connection between our generalized approach and the well known filter-function formalism.

## 4.4 Evaluating the control matrix

In general, for arbitrary continuous-time modulation of  $H_c(t)$ , the control matrix can be evaluated only approximately. However, under the simplifying assumption of piecewise-constant control it becomes possible to find an exact analytic form. The result can be applied to DD (state preservation) sequences, as well as a variety of nontrivial control operations such as piecewise-defined dynamically corrected gates and composite pulses [101, 87].

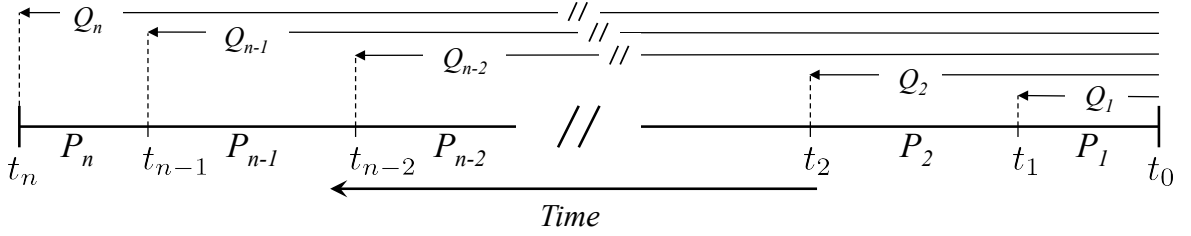


Figure 4.2: Explanatory diagram for a piecewise-defined control sequence. During each interval  $[t_{l-1}, t_l]$ , a control operation  $P_l$  is executed. The operators  $Q_l$  are the control propagator evaluated at the start of the  $l$ -th pulse, for  $l = 1, 2, \dots, n$ .

#### 4.4.1 Universal noise

For a sequence of  $n$  consecutive unitary control operations (or control ‘pulses’)  $P_1, \dots, P_n$ , we divide the total sequence time  $\tau$  into  $n$  corresponding time intervals, such that the  $l$ -th operation  $P_l$  is executed over the interval  $[t_{l-1}, t_l]$ , i.e.,  $P_l = U_c(t_l, t_{l-1})$ , for  $l \in \{1, 2, \dots, n\}$ , where  $t_n \equiv \tau$  and  $t_0 \equiv 0$  (figure 4.2). Letting  $P_0 \equiv I$ , and defining the cumulative operators  $Q_l \equiv P_l P_{l-1} \dots P_0$  so that  $Q \equiv Q_n$ , the elements of the control matrix (4.16) take the form

$$R_{ij}(t) = \frac{1}{2} \sum_{l=1}^n G^{(l)}(t) \text{Tr}\left(Q_{l-1}^\dagger U_c^\dagger(t, t_{l-1}) \sigma_i U_c(t, t_{l-1}) Q_{l-1} \sigma_j\right) \quad (4.40)$$

where the function  $G^{(l)}(t) \equiv \Theta[t - t_{l-1}] - \Theta[t - t_l]$  has unit value within the  $l$ -th time interval and is zero elsewhere.

Equation (4.40) can be rewritten in terms of the individual control matrices  $\mathbf{R}^{P_l}(t - t_{l-1})$  for each of the  $n$  operations  $P_l$  in the sequence, defined relative to the pulse start times  $t_{l-1}$ , by letting

$$U_c^\dagger(t, t_{l-1}) \sigma_i U_c(t, t_{l-1}) = \sum_{j=x,y,z} R_{ij}^{P_l}(t - t_{l-1}) \sigma_j \quad (4.41)$$

for  $i \in \{x, y, z\}$ . Again, the components of  $\mathbf{R}^{P_l}(t - t_{l-1})$  are obtained from the Hilbert-Schmidt inner product

$$R_{ij}^{P_l}(t - t_{l-1}) \equiv [\mathbf{R}^{P_l}(t - t_{l-1})]_{ij} = \frac{1}{2} \text{Tr}\left(U_c^\dagger(t, t_{l-1}) \sigma_i U_c(t, t_{l-1}) \sigma_j\right) \quad (4.42)$$

for  $i, j \in \{x, y, z\}$ . Substituting (4.41) into (4.40), and using the linearity of the trace operation, we find that we can write the control matrix for the pulse sequence in the compact form

$$\mathbf{R}(t) = \sum_{l=1}^n G^{(l)}(t) \mathbf{R}^{P_l}(t - t_{l-1}) \boldsymbol{\Lambda}^{(l-1)} \quad (4.43)$$

where the matrix  $\boldsymbol{\Lambda}^{(l-1)}$  has components

$$\Lambda_{ij}^{(l-1)} \equiv [\boldsymbol{\Lambda}^{(l-1)}]_{ij} = \frac{1}{2} \text{Tr}\left(Q_{l-1}^\dagger \sigma_i Q_{l-1} \sigma_j\right) \quad (4.44)$$

for  $i, j \in \{x, y, z\}$ . Using (4.39) to define the control matrix in the frequency domain, we have

$$\mathbf{R}(\omega) = \sum_{l=1}^n e^{i\omega t_{l-1}} \mathbf{R}^{P_l}(\omega) \boldsymbol{\Lambda}^{(l-1)} \quad (4.45)$$

where

$$\mathbf{R}^{P_l}(\omega) \equiv -i\omega \int_0^{t_l-t_{l-1}} dt e^{i\omega t} \mathbf{R}^{P_l}(t) \quad (4.46)$$

is the frequency domain control matrix for the  $l$ -th pulse,  $P_l$ .

With the above expressions and a knowledge of the statistical properties of the noise we can, in combination with the results of section 4.3, find an approximate value for the fidelity of an arbitrary piecewise-defined control sequence in a weak noise environment. This approach is straightforward to implement by hand or via numerics. Ultimately the computational efficiency of calculating the control matrix and spectral overlap integrals far exceeds that of brute-force numerical simulations of the evolution of the Bloch vector [100].

#### 4.4.2 Dephasing noise

In many of the physical systems with the potential for use in nascent quantum information technologies, the characteristic single-qubit dephasing time  $T_2$  is considerably smaller than the relaxation time  $T_1$ , and governed by different physical processes. It is important, therefore, that we understand the effects of purely dephasing noise on single-qubit control. To this end, we consider a model system in which the noise vector  $\beta(t)$  has only a  $z$ -component and the noise Hamiltonian (4.5) reduces to

$$H_0(t) = \beta_z(t)\sigma_z \quad (4.47)$$

In this context, only the third row of the control matrix is required to calculate the fidelity, and we refer to the corresponding row vector  $\mathbf{R}_z(t) \equiv (R_{zx}(t), R_{zy}(t), R_{zz}(t))$  as the ‘control vector’. From (4.38), the lowest-order contribution of noise to the fidelity (4.32) is captured by the term

$$\langle a_1^2 \rangle = \frac{1}{2\pi} \int_{-\infty}^{\infty} \frac{d\omega}{\omega^2} S_z(\omega) F_z^{(1)}(\omega) \quad (4.48)$$

where the first order dephasing ‘filter function’  $F_z^{(1)}(\omega)$  is simply the square modulus of the frequency domain control vector

$$F_z^{(1)}(\omega) \equiv \sum_{i=x,y,z} |R_{zi}(\omega)|^2 \quad (4.49)$$

If we further assume that the noise is Gaussian, with a mean value of zero, then all correlation functions  $\langle \beta_z(t_1) \dots \beta_z(t_n) \rangle$  for which  $n$  is odd are equal to zero. The Gaussian moment theorem also allows us to write all remaining higher-order correlations in terms of only the simplest two-point correlation function (see the appendix). In the frequency domain, the statistical properties of the noise are then captured entirely by the power spectral density  $S_z(\omega)$ , and the fidelity (4.32) can be written as the infinite sum [100]

$$\begin{aligned} \mathcal{F}_{av} = 1 - & \left[ \frac{1}{2\pi} \int_{-\infty}^{\infty} \frac{d\omega}{\omega^2} S_z(\omega) F_z^{(1)}(\omega) \right. \\ & \left. + \frac{1}{(2\pi)^2} \int_{-\infty}^{\infty} \frac{d\omega}{\omega^2} S_z(\omega) \int_{-\infty}^{\infty} \frac{d\omega'}{\omega'^2} S_z(\omega') F_z^{(2)}(\omega, \omega') + \dots \right] \end{aligned} \quad (4.50)$$

Here, the effect of the control on the qubit fidelity is described by the functions  $F_z^{(p)}$ , for  $p = 1, 2, \dots$ , which depend only on the control vector  $\mathbf{R}_z$ . The complexity of the filter functions increases rapidly with increasing order. However,  $F_z^{(1)}(\omega)$  can be quite simple in form and reasonably straightforward to calculate. In the weak noise regime we ignore the higher order terms in (4.50) and write

$$\mathcal{F}_{av}(\tau) \simeq \frac{1}{2} \{1 + \exp[-\chi(\tau)]\} \quad (4.51)$$

where the rate of fidelity decay is given by

$$\chi(\tau) \equiv \langle a_1^2 \rangle = \frac{1}{\pi} \int_0^\infty \frac{d\omega}{\omega^2} S_z(\omega) F_z^{(1)}(\omega) \quad (4.52)$$

Thus, the decay rate is determined by a simple overlap integral between the power spectrum of the noise and a ‘filter function’ representing the control in the Fourier domain. This result is similar to the familiar expression for the coherence of a dynamical decoupling sequence in the case of unbounded controls [67] (see also section 4.5). The difference here being that the filter function  $F_z^{(1)}$  captures only the lowest order nontrivial effect of the control on the fidelity in a dephasing environment, rather than providing an exact solution in the bang-bang limit.

For a piecewise-defined control sequence, subject to purely dephasing noise, equation (4.40) reduces to the following expression for the components of the control vector

$$R_{zi}(t) = \frac{1}{2} \sum_{l=1}^n G^{(l)}(t) \text{Tr} \left( Q_{l-1}^\dagger U_c^\dagger(t, t_{l-1}) \sigma_z U_c(t, t_{l-1}) Q_{l-1} \sigma_i \right) \quad (4.53)$$

Similarly, (4.45) and (4.46) become

$$\mathbf{R}_z(\omega) = \sum_{l=1}^n e^{i\omega t_{l-1}} \mathbf{R}_z^{P_l}(\omega) \boldsymbol{\Lambda}^{(l-1)} \quad (4.54)$$

and

$$\mathbf{R}_z^{P_l}(\omega) \equiv -i\omega \int_0^{t_l - t_{l-1}} dt e^{i\omega t} \mathbf{R}_z^{P_l}(t) \quad (4.55)$$

respectively, where the components of the  $l$ -th pulse control vector are

$$R_{zj}^{P_l}(t - t_{l-1}) = \frac{1}{2} \text{Tr} \left( U_c^\dagger(t, t_{l-1}) \sigma_z U_c(t, t_{l-1}) \sigma_j \right) \quad (4.56)$$

for  $j \in \{x, y, z\}$ .

If we assume that during each of the  $n$  time intervals comprising the sequence the applied control effects a steady rotation of the qubit Bloch vector through an angle  $\theta_l$ , about an axis  $\hat{\mathbf{n}}_l = \cos(\phi_l)\hat{\mathbf{x}} + \sin(\phi_l)\hat{\mathbf{y}}$  in the  $xy$ -plane, then for  $t \in [t_{l-1}, t_l]$

$$U_c(t, t_{l-1}) = \exp \left[ \frac{-i}{2} \Omega_l (t - t_{l-1}) \sigma_{\phi_l} \right] \quad (4.57)$$

where  $\Omega_l \equiv \theta_l/(t_l - t_{l-1})$  is the rotation rate and  $\sigma_{\phi_l} \equiv \cos(\phi_l)\sigma_x + \sin(\phi_l)\sigma_y$ . From (4.56) and (4.55) we can show that the frequency domain control vector for the  $l$ -th operation has components

$$R_{zj}^{P_l}(\omega) = \frac{\omega}{\omega^2 - \Omega_l^2} \{ \delta_{zj} [i\Omega_l g_l(\omega) - \omega f_l(\omega)] + [\Omega_l f_l(\omega) - i\omega g_l(\omega)] \text{Tr}(\sigma_{\phi_l} \sigma_z \sigma_j) \} \quad (4.58)$$

where  $f_l(\omega) \equiv e^{i\omega(t_l - t_{l-1})} \cos(\theta_l) - 1$  and  $g_l(\omega) \equiv e^{i\omega(t_l - t_{l-1})} \sin(\theta_l)$ . Although (4.58) has been derived assuming rotations take place about axes in the  $xy$ -plane only, periods of free evolution (no rotation) and  $z$ -axis rotations are easily accounted for by setting  $\theta_l = 0$  and  $\Omega_l = 0$  in (4.58), whenever one of these operations occurs in the sequence. This is possible simply because, for dephasing noise, both of these operations commute with the noise operator.

With these analytical tools, the process for finding the operational fidelity of an arbitrary piecewise-constant control sequence in the presence of dephasing noise may be summarized as follows:

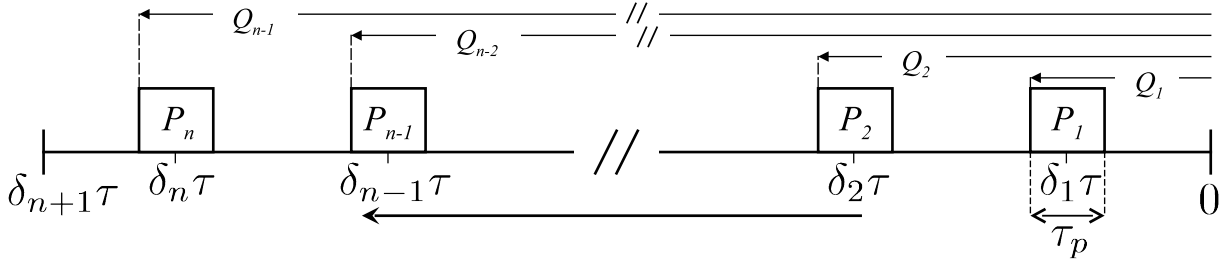


Figure 4.3: *Dynamical decoupling sequence for  $n$  identical pulses, each of width  $\tau_p$ , centered at times  $\delta_l\tau$ , for  $l = 1, 2, \dots, n$ .*

1. Calculate the matrix defined in equation (4.44) for each step in the chain of control operations;
2. Substitute the above result and equation (4.58) into (4.54);
3. Repeat for all time steps  $l \in \{1, \dots, n\}$  to find the control vector in the Fourier domain;
4. Find the first-order filter function from (4.49);
5. Use (4.51) and (4.52) to calculate approximate expression for the fidelity valid for weak dephasing noise.

In the next section we employ this approach to study the impact of pulse imperfections on the performance of DD sequences used in quantum memory.

## 4.5 Pulse effects in dynamical decoupling sequences

DD sequences are control protocols aimed at implementing the identity operation ( $Q = I$ ), and thus preserving the initial state of the qubit. In the limit of instantaneous control pulses it has been shown that, for both semi-classical dephasing noise and quantum spin-boson models, it is possible to write the qubit coherence at the end of an arbitrary DD sequence, given preparation of the system in a superposition of eigenstates of  $\sigma_z$ , as  $W = e^{-\chi(\tau)}$  [52, 88]. In this expression, the effects of both the noisy dephasing environment and the control modulation are contained in the overlap integral

$$\chi(\tau) = \frac{1}{\pi} \int_0^\infty \frac{d\omega}{\omega^2} S_z(\omega) F_z(\omega) d\omega. \quad (4.59)$$

The statistical properties of the noise in the Fourier domain are captured via the noise power spectrum  $S_z(\omega)$ , and the action of the control sequence via the filter function  $F_z(\omega)$ . We note that (4.59) is formally identical to (4.52) above, with the exception that, because the control pulses are assumed to be unbounded in strength with vanishing duration (the so-called ‘bang-bang’ approximation), the filter function in (4.59) is exact. The bang-bang approximation is, however, unphysical and has been shown in experiment to neglect important contributions to the net error arising from realistic pulses of nonzero width (see figure 4.3).

In this section we apply the techniques we have developed to evaluate the fidelity of dynamical decoupling sequences when considering physical constraints - such as the incorporation of realistic control pulses - in a purely dephasing noise environment.

### 4.5.1 Separating pulses from the pulse sequence

Beyond the bang bang limit, the effectiveness of a DD sequence will depend on both the temporal spacing and form of the pulses used. To find optimal error-suppressing sequences for a given environment or physical system, either of these variables may be changed independently of the other, and these differences should be easily separated in an analytical framework. We are therefore motivated to express the sequence control vector  $\mathbf{R}_z(\omega)$  in terms that can be separated into those dependent only on pulse *location* and those dependent on pulse *type* (expressed in terms of the individual *pulse* control vectors  $\mathbf{R}_z^{P_l}(\omega)$ ).

As in section 4.4, we start with a piecewise constant sequence of  $n$  pulses, however, to model a DD sequence we allow for a period of free evolution (i.e., no control operation) both before and after each pulse, so that immediately following the  $l$ -th pulse, we have  $Q_l = P_l I P_{l-1} I \dots I P_0$ , for  $l \in \{1, 2, \dots, n\}$ . Within the total sequence time  $\tau$  (including both control pulses and free evolution periods), the  $l$ -th pulse has a width  $\tau_{p_l}$  and is centered at a time  $\delta_l \tau$ , where  $0 \leq \delta_l \leq 1$  and  $\delta_{n+1} = 1$  (see figure 4.3). Using this notation the sequence control vector is

$$\begin{aligned} \mathbf{R}_z(\omega) = \hat{\mathbf{z}} & \left[ 1 - e^{i\omega\tau} + \sum_{l=1}^n e^{i\omega\delta_l\tau} \left( e^{i\omega\tau_{p_l}/2} \Lambda^{(l)} - e^{-i\omega\tau_{p_{l-1}}/2} \Lambda^{(l-1)} \right) \right] \\ & + \sum_{l=1}^n e^{i\omega\delta_l\tau - \tau_{p_l}/2} \mathbf{R}_z^{P_l}(\omega) \Lambda^{(l-1)} \end{aligned} \quad (4.60)$$

the form of the pulse appearing explicitly only in the last term.

While DD sequences have traditionally been composed of identical  $\pi$ -pulses executed about a common axis, equation (4.60) is quite general. The only restriction being that, in the absence of noise, the net effect is to execute the identity operation. Hence, it may be applied to the analysis of unusual DD schemes such as the recently proposed KDD (Knill dynamical decoupling), based on the Knill pulse [102]. However, since our aim here is simply to provide an example application of our method, we will limit our attention to more conventional sequences. Specifically, we assume identical pulses, each of width  $\tau_p$  and executing a net  $\pi$ -rotation of the qubit Bloch vector about the  $x$  axis, i.e.,  $P_l = \sigma_x$ , for  $l \in \{1, 2, \dots, n\}$ . In this case, the pulse control vector  $\mathbf{R}_z^{P_l}(\omega)$  is independent of  $l$  and has only  $z$  and  $y$  components. The matrix  $\Lambda^{(l-1)}$  is diagonal with  $\Lambda_{yy}^{(l-1)}$  and  $\Lambda_{zz}^{(l-1)}$  alternating between 1 and  $-1$  with each successive pulse. The resulting sequence control vector has the two components

$$R_{zz}(\omega) = 1 - e^{i\omega\tau} + [2 \cos(\omega\tau_p/2) - e^{-i\omega\tau_p/2} R_{zz}^P(\omega)] \sum_{l=1}^n (-1)^l e^{i\omega\delta_l\tau} \quad (4.61)$$

and

$$R_{zy}(\omega) = -e^{-i\omega\tau_p/2} R_{zy}^P(\omega) \sum_{l=1}^n (-1)^l e^{i\omega\delta_l\tau} \quad (4.62)$$

It is worth noting here that, when the form of the pulse is ignored altogether (i.e., when both  $R_{zy}^P(\omega)$  and  $R_{zz}^P(\omega)$  go to zero), the control vector reduces to a single component

$$R_{zz}(\omega) = 1 - e^{i\omega\tau} + 2 \cos(\omega\tau_p/2) \sum_{l=1}^n (-1)^l e^{i\omega\delta_l\tau}. \quad (4.63)$$

a result derived previously by assuming finite-width pulses during which noise was ignored [32, 88]. And, in the bang-bang limit of infinitely narrow pulses ( $\tau_p \rightarrow 0$ ) we have the standard

result (for even  $n$ )

$$R_{zz}(\omega) = 1 - e^{i\omega\tau} + 2 \sum_{l=1}^n (-1)^l e^{i\omega\delta_l\tau}. \quad (4.64)$$

with  $F_z(\omega) = |R_{zz}(\omega)|^2$ .

Equations (4.61) and (4.61) capture modification of dephasing dynamics due to the duration and form of the pulses as well as depolarization effects occurring due to pulse-errors derived from a fluctuating detuning from resonance (i.e., the impact of dephasing noise). We will move forward using these expressions in order to treat experimentally relevant cases of DD incorporating various pulse forms including error-suppressing dynamically corrected gates.

## 4.5.2 Pulse forms: Standard $\pi_X$ -pulses and dynamically corrected gates

For a DD sequence we are interested in physical control operations that implement a logical NOT gate. The simplest approach is to employ ‘primitive’  $\pi_X$ -pulses, implemented by applying the ideal control Hamiltonian  $H_c = \Omega\sigma_x/2$  over a time interval  $[0, \tau_\pi]$ , where  $\Omega \equiv \pi/\tau_\pi$ . This induces a simple rotation of the Bloch vector through an angle of  $\pi$  radians about the  $x$ -axis. In the presence of time-varying dephasing noise, the bare gate is modified by an error term that, to first order, results in a small additional rotation about an axis that has both  $y$  and  $z$ -components. From equations (4.54) and (4.58) we find that the two corresponding components of control vector are

$$R_{zz}^P \equiv R_{zz}^{(Prim)}(\omega) = \frac{\omega^2}{\omega^2 - \Omega^2} (e^{i\omega\tau_\pi} + 1) \quad (4.65)$$

and

$$R_{zy}^P \equiv R_{zy}^{(Prim)}(\omega) = \frac{i\omega\Omega}{\omega^2 - \Omega^2} (e^{i\omega\tau_\pi} + 1) \quad (4.66)$$

It is interesting to note the correspondence between the prefactors here and those arising in a master-equation treatment of a driven quantum system in the presence of dissipation [30].

Moving beyond the standard  $\pi_X$ -pulse of finite duration, we consider a gate that has been designed to provide robustness in the presence of random gate errors - the dynamically corrected gate. In previous work we demonstrated how such gates provide enhanced resistance to error in the presence of time-varying dephasing noise [100]. Here we include expressions for a dynamically corrected logical NOT gate consisting of three successive  $\pi_X$  pulses, the second of which is executed at a rotation rate  $\Omega/2$ , half that of the other two [103]. The control Hamiltonian for this gate is

$$H_c(t) = \begin{cases} \Omega\sigma_x/2 & 0 \leq t < \tau_\pi \\ \Omega\sigma_x/4 & \tau_\pi \leq t < 3\tau_\pi \\ \Omega\sigma_x/2 & 3\tau_\pi \leq t \leq 4\tau_\pi, \end{cases} \quad (4.67)$$

so that  $\tau_p = 4\tau_\pi$ . In the case of dephasing noise, the control vector again has two components:

$$R_{zz}^P \equiv R_{zz}^{(DCG)}(\omega) = \omega^2 \left[ \frac{p_1(\omega)}{\omega^2 - \Omega^2} - \frac{p_2(\omega)}{\omega^2 - (\Omega/2)^2} \right], \quad (4.68)$$

$$R_{zy}^P \equiv R_{zy}^{(DCG)}(\omega) = i\omega\Omega \left[ \frac{p_1(\omega)}{\omega^2 - \Omega^2} - \frac{p_2(\omega)/2}{\omega^2 - (\Omega/2)^2} \right], \quad (4.69)$$

where  $p_1(\omega) \equiv e^{4i\omega\tau_\pi} + e^{3i\omega\tau_\pi} + e^{i\omega\tau_\pi} + 1$  and  $p_2(\omega) \equiv e^{3i\omega\tau_\pi} + e^{i\omega\tau_\pi}$ .

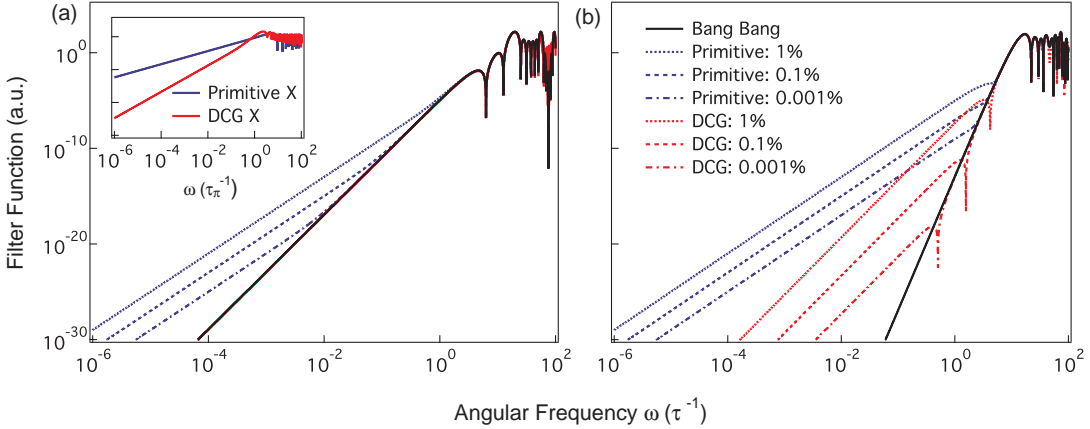


Figure 4.4: *First order filter functions as a function of dimensionless frequency. The inset of a) compares filter functions for primitive (blue) and dynamically corrected (red) NOT gates while the main plot shows filter functions for a 6 pulse CP sequence. The results for primitive NOT pulses are shown in blue, while those for dynamically corrected pulses are shown in red. Plot b) shows the same set of results for the 6 pulse UDD sequence. Black lines represent filter functions for sequences in the bang-bang limit.*

### 4.5.3 Interpreting the filter function

The inset to figure 4.4(a) shows the filter functions,  $F_z(\omega) \equiv |R_{zy}^P(\omega)|^2 + |R_{zz}^P(\omega)|^2$ , for the primitive and dynamically corrected logical NOT operations described above, as a function of the angular frequency in units of  $\tau_\pi^{-1}$ . The rate of growth of the filter function with  $\omega$ , captures the low-frequency ‘filtering’ performance of DD sequences. Beyond a certain frequency  $F_z(\omega) \rightarrow 1$ , above which noise is passed unimpeded. This corresponds to the physical observation that fluctuations fast relative to the shortest interpulse period cannot be effectively suppressed by dynamical decoupling.

The filter function’s behavior near zero frequency captures the leading-order error susceptibility. We may express  $F_z(\omega) \propto (\omega\tau_\pi)^{2(\alpha+1)}$  as  $\omega\tau_\pi \rightarrow 0$ , then  $\alpha$  is the order of error suppression for the sequence [75]. Using these expressions, an examination of figure 4.4 reveals that the relative performance of the primitive and dynamically corrected gates is captured in the slope of the filter function as plotted on a log-log scale [47]; higher slope corresponds to a higher order of error suppression (for noise near zero frequency). In a filter-design framework we may refer to this slope as a filter rolloff in the stopband, using the relation that the rolloff is  $6(\alpha + 1)$  dB/octave. At low frequencies the primitive  $\pi_X$ -pulse filter function is approximately quadratic, i.e.  $F_z(\omega) \propto (\omega\tau_\pi)^2$ , resulting in  $\alpha = 0$  - the same as for free evolution. This is not a surprising result, since there is no error suppression built into the primitive gate. By contrast the DCG filter function scales as  $F_z(\omega) \propto (\omega\tau_\pi)^4$ , giving  $\alpha = 1$ , as expected for a construction designed to suppress error to first order.

### 4.5.4 The full filter functions: DD + DCG

We now combine the control vectors derived for the pulses themselves with those obtained for the generic DD sequences, considering three paradigmatic cases: (1) bang-bang decoupling, (2) standard pulses with nonzero  $\tau_p$ , (3) DCGs. This is accomplished by calculating  $\mathbf{R}_z^P$  and inserting the relevant Cartesian components into (4.61) and (4.62) for the full DD sequence. This study reveals how it is possible to evaluate complex perturbations to quantum control

protocols in a straightforward manner using our method.

We compare the error-suppressing performance of CP (Carr and Purcell) and UDD (Uhrig dynamical decoupling) sequences as illustrative examples, accounting for each of the cases outlined above. The CP sequence, devised in the context of NMR [104], is a straightforward extension of the original Hahn spin echo [19]. In an  $n$ -pulse CP sequence, the  $l$ -th pulse has the fractional location  $\delta_l = (l - 1/2)/n$ . The bang-bang limit CP filter function for  $n = 6$  is shown as a black line in figure 4.4(a) for  $n = 6$ . It exhibits an order of error suppression of  $\alpha = 2$ , as do all CP sequences with  $n \geq 2$ , giving a roll-off of 18 dB/octave. This is a limiting case in which pulse effects are entirely ignored.

If we now take into account the width of the pulses by assuming that they take the form of primitive NOT gates of width  $\tau_p$ , as described above, then the components of the pulse control vector  $\mathbf{R}_z^P(\omega)$  are given by equations (4.65) and (4.66). The resulting filter functions, indicated by the blue lines in figure 4.4(a), show a reduced order of error suppression  $\alpha = 2 \rightarrow 1$ , with a corresponding reduction of the filter rolloff to 12dB/octave. As the pulse width grows as a fraction of the entire sequence, the relative importance of the pulses grows, as expected. This is manifested as an expansion of the range over which the modification to the filter-function due to pulse effects dominates the bang-bang filter function.

Despite the reduction in the order of error suppression, there is still noise cancelation, regardless of the pulse width, since the sequence is in essence an Eulerian dynamical decoupling (EDD) sequence [61]. Replacing the primitive pulses with dynamically corrected composite gates and the components of the pulse control vector with (4.68) and (4.69), we almost completely restore the original 18dB/octave roll-off for the CP sequences (figure 4.4(a)). These filter functions lie approximately beneath the bang-bang filter function in this figure. This observation confirms that the DCG provides one order of error cancellation during the applied pulses. In essence, the deleterious effect of error accumulation during nonzero-duration control pulses can be mitigated by choosing a compensating pulse design.

Studying UDD is more instructive because the  $n$ -pulse UDD sequence, with relative pulse locations given by  $\delta_l = \sin^2[\pi l/(2n + 2)]$ , ensures that (in the bang bang limit) the first  $n$ -derivatives of  $R_{zz}(\omega)$  vanish at  $\omega = 0$  [67, 52], giving an order of error suppression that increases linearly with  $n$ . The effects of pulse width and shape on a UDD sequence are therefore potentially more dramatic. For sufficiently long pulses we see, from figure 4.4(b), that the general benefits derived from the use of a UDD sequence can largely be destroyed as the error-susceptibility of the pulses dominates the suppression provided by the pulse timing. Again, we observe that the reduction in the order of error suppression arising from addition of nonzero-duration  $\pi_X$ -pulses can be partially offset by use of a DCG. However, the fact that by design, the DCG used here only provides first-order error suppression, reduces our ability to recover the original order of error suppression provided by a UDD sequence with large  $n$ .

Nonetheless, these results indicate that judicious choice of DCG or other compensating pulse protocols within DD sequences provides a path to mitigate the effects of pulse errors in DD sequences. This is especially important in long-storage settings where large pulse numbers may be employed in order to effectively suppress dephasing errors [105]. These observations represent an important validation of our method, and show that it provides a straightforward approach to account for a variety of pulse-duration, modulation, and shape effects.

## 4.6 Limits of approximation

In deriving (4.38) in section 4.3, we assumed both that the Magnus expansion converges and that truncating the additional series expansion of the fidelity (4.32) introduces no significant error. In this section we examine these assumptions more closely and discuss their limits of

validity.

### 4.6.1 Convergence of the Magnus expansion

A sufficient condition for the convergence of the Magnus expansion is [106]

$$\int_0^\tau dt \|\tilde{H}_0(t)\|_{op} < \pi \quad (4.70)$$

The operator norm  $\|\tilde{H}_0(t)\|_{op}$  is the smallest number  $K \geq 0$  such that  $\|\tilde{H}_0(t)|\psi\rangle\|_{\mathcal{H}_S} \leq K\|\psi\rangle\|_{\mathcal{H}_S}$  for all  $|\psi\rangle \in \mathcal{H}_S$ , where  $\|\psi\rangle\|_{\mathcal{H}_S} \equiv \sqrt{\langle\psi|\psi\rangle}$  is the usual vector norm defined on the system Hilbert space  $\mathcal{H}_S$  [107]. It is a simple matter to derive the intuitively obvious result that

$$\|\tilde{H}_0(t)\|_{op} = \|\boldsymbol{\beta}(t)\| = (\beta_x(t)^2 + \beta_y^2(t) + \beta_z^2(t))^{1/2} \quad (4.71)$$

i.e., the ‘size’ of the toggling frame Hamiltonian is measured by the magnitude of the noise vector.

In an experiment, for each physical realization of the noise process, the  $i$ -th noise component  $\beta_i(t)$  will have some maximum absolute value  $\beta_i^{(m)}$ , over the interval  $[0, \tau]$ . We can then write  $\|\boldsymbol{\beta}(t)\| \leq \|\boldsymbol{\beta}^{(m)}\|$ , for all  $t$ , where  $\boldsymbol{\beta}^{(m)} = (\beta_x^{(m)}, \beta_y^{(m)}, \beta_z^{(m)})$ . It immediately follows that

$$\int_0^\tau dt \|\boldsymbol{\beta}(t)\| \leq \|\boldsymbol{\beta}^{(m)}\| \tau \quad (4.72)$$

and convergence is assured if  $\|\boldsymbol{\beta}^{(m)}\| \tau < \pi$ . The problem is, of course, that the maxima  $\beta_i^{(m)}$  are unknown quantities. Nonetheless, if the noise is stationary and has well-defined root mean square values  $\delta\beta_i \equiv (\langle\beta_i(0)^2\rangle)^{1/2}$ , for  $i = x, y, z$ , then for small total operation times  $\tau$ , letting  $\beta_i^{(m)} = C_m \delta\beta_i$ , for a sufficiently large value of  $C_m > 0$ , will mean that contributions from elements of the ensemble not satisfying the convergence condition

$$\xi < \pi/C_m \quad (4.73)$$

where  $\xi \equiv \langle\boldsymbol{\beta}(0)\boldsymbol{\beta}(0)^T\rangle^{1/2}\tau$ , can be ignored without significant error.

It can be shown (see appendix) that this same parameter  $\xi$  represents a bound on the strength of high-order terms in the expansion for the fidelity (4.32) and serves as ‘smallness parameter’ providing insight into when the first-order filter-function is sufficient to obtain a good approximation for the overall fidelity. Essentially, we require  $\xi^2 \ll 1$  for the first order approximation to hold. In general, this is sufficient to guarantee convergence of the Magnus expansion for all but a statistically insignificant proportion of qubits in the ensemble.

### 4.6.2 Numerical simulations and the first-order approximation

Finally we present an instructive example to illustrate that our techniques are amenable to detailed understanding of the limits of applicability and scaling behaviours of the calculated operational fidelity. To this end we compare the performance of our analytical expressions with numerical simulations in which we explicitly time-evolve the Schrodinger equation. As a test case, we simulate a primitive NOT-gate ( $\pi_X$ -pulse), in the presence of pure dephasing noise,  $H(t) = \beta(t)\hat{\sigma}_z/2 + \Omega_R\hat{\sigma}_x/2$ , and study the behaviour of the fidelity (4.32) as a function of the control field strength.

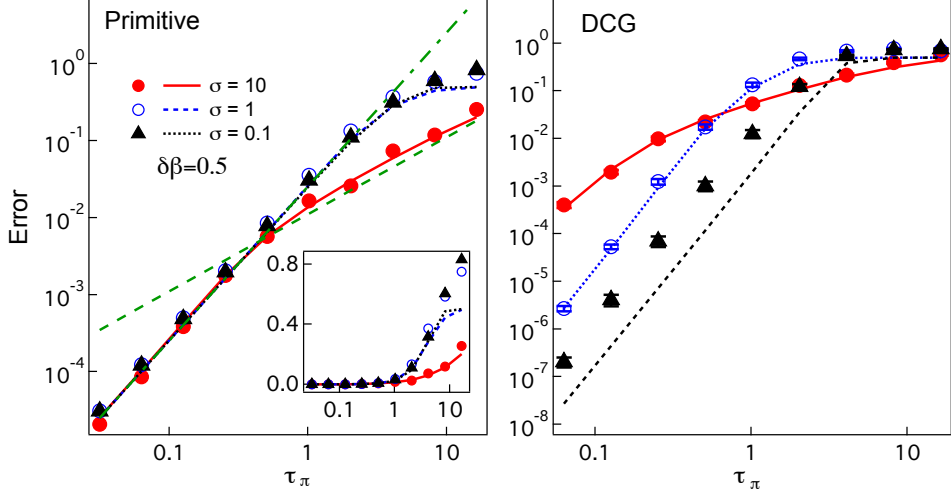


Figure 4.5: Comparison of operational error derived from numerical simulations of Bloch vector evolution (markers) with analytical filter functions (lines) under application of a NOT ( $\pi_X$ -pulse), showing good agreement. Left panel, Primitive gate, Right panel, Dynamically Corrected Gate. Straight green dashed lines illustrate the scaling behaviour in the limiting regimes: Green dash-dotted line represents the approximate analytical behavior for  $\tau_\pi/\tau_c \ll 1$ , green dashed line for  $\tau_c/\tau_\pi \ll 1$ . When conditions outlined in the text are not met, agreement between analytic and numeric results break down, as shown in the inset which plots the same data on a semilog scale. In this case, the origin of the breakdown is the growth of higher order terms in the expansion that are not accounted for in the lowest order expressions for the filter-function.

For concreteness we pick a Gaussian noise power spectrum,

$$S_z(\omega) = \sqrt{2\pi} \frac{\delta\beta^2}{4\sigma} e^{-\omega^2/(2\sigma^2)}. \quad (4.74)$$

Here  $\delta\beta \equiv \delta\beta_z$ ,  $\sigma$  is the bandwidth of the noise field, and the spectrum is properly normalized so that it is connected to the auto-correlation  $C(t)$  of the noise through a Fourier transform:

$$C(t) = \frac{1}{2\pi} \int_{-\infty}^{\infty} S_z(\omega) e^{i\omega t} d\omega = \frac{\delta\beta^2}{4} e^{-t^2/(2\tau_c^2)}, \quad (4.75)$$

where  $\tau_c = 1/\sigma$ . For our simulations we vary the spectral bandwidth of the Gaussian spectrum. The noise strength is parametrized by its root-mean-square deviation which we choose as  $\delta\beta = 0.5$  in each case.

To simulate the noise, we generate random classical noise trajectories by summing noise Fourier frequency components, each weighed by a random, normally distributed amplitude multiplied by the square root of the noise power at that frequency (as given by the power spectrum), and with a random phase. The gate fidelity is found by averaging over 100 realizations of the noise, and compared to the analytical results including only first-order terms in the Magnus expansion.

Analytic and numeric results are plotted in figure 4.5. We observe excellent agreement between the first-order-filter-function analytical prediction and detailed numerical simulation. We also find that there appear to be two different regimes of behavior in relation to dependence

on noise bandwidth (or identically the correlation time). The calculated gate fidelity appears to be independent of noise bandwidth in the short time regime  $\tau_\pi \ll 1$  and deviates from this behaviour only for the large bandwidth case  $\sigma = 10$ . We can understand this behaviour by analyzing in different temporal regimes, the behaviour of the first-order term in the fidelity expansion (4.32) which is simply

$$\langle a_1^2 \rangle = \frac{1}{4} \int_0^{\tau_\pi} dt_2 \int_0^{\tau_\pi} dt_1 \delta \beta^2 e^{-(t_1-t_2)^2/(2\tau_c^2)} \cos(\Omega_R t_1) \cos(\Omega_R t_2) \quad (4.76)$$

$$+ \frac{1}{4} \int_0^{\tau_\pi} dt_2 \int_0^{\tau_\pi} dt_1 \delta \beta^2 e^{-(t_1-t_2)^2/(2\tau_c^2)} \sin(\Omega_R t_1) \sin(\Omega_R t_2) \quad (4.77)$$

$$= \frac{1}{4} \int_0^{\tau_\pi} dt_2 \int_0^{\tau_\pi} dt_1 \delta \beta^2 e^{-(t_1-t_2)^2/(2\tau_c^2)} \cos[\Omega_R(t_1 - t_2)] \quad (4.78)$$

For short control times, i.e.  $\tau_\pi/\tau_c \ll 1$ , this integral reduces to

$$\langle a_1^2 \rangle = \delta \beta^2 \tau_\pi^2 \left[ \frac{1}{\pi^2} - \left( \frac{12 - \pi^2}{4\pi^2} \right) \left( \frac{\tau_\pi}{\tau_c} \right)^2 + \dots \right] \quad (4.79)$$

The lowest order term in equation (4.79) is plotted as the green dash-dotted line in figure 4.5. As demonstrated by both the analytical and the numerical results, one finds that the short-time behaviour is independent of bandwidth to lowest order.

Bandwidth dependent effects should only appear when the control time becomes of the same order as the correlation time, reached for the case when  $\sigma = 10$ . To elucidate the behaviour in that regime we evaluate equation (4.78) approximately when  $\tau_c/\tau_\pi \ll 1$ . To lowest order this gives

$$\langle a_1^2 \rangle \approx \sqrt{\pi} \frac{\delta \beta^2}{4} \tau_c \tau_\pi. \quad (4.80)$$

This approximate solution is plotted as the green dashed line in the left panel of figure 4.5, illustrating that the full numerics and first-order analytics obey the expected scaling with control time, and that the error magnitude is set by the noise correlation time. For a fixed root-mean-square noise strength, and long control times, a primitive NOT gate is more robust under wide-bandwidth noise conditions.

Since  $\xi^2 = \delta \beta^2 \tau_\pi^2 \ll 1$  over most of the regime we investigated, higher order terms in the Magnus expansion are expected to be negligible since they scale as  $\xi^4$  to lowest order (see Appendix). This expectation is confirmed by the numerics. The numerical results therefore support the scaling argument that  $\xi^2 \ll 1$  determines the bounds of validity of the first-order filter-function approximation. The inset to figure 4.5 shows that the analytical result becomes a poor approximation to the numerics when the condition  $\xi^2 \ll 1$  is violated in the vicinity of  $\tau_\pi \approx 10$ . Note that growth in higher-order terms does not necessarily coincide with divergence of the Magnus expansion, but rather a breakdown of the first-order approximation; higher-order filter functions may be incorporated to account for residual error.

Finally, we note that the same arguments we've applied to the primitive NOT gate may also be applied to more general control operations, including those designed to compensate for noise, such as DCGs. First order error correcting gates like the DCG will reduce the effect of the first order term in the Taylor expansion of the noise correlation function relative to the higher-order bandwidth-dependent terms. As a consequence, bandwidth effects are expected to be more pronounced for corrected gates, which we have confirmed via numerics. Despite this issue we still obtain good agreement between numerics and analytic filter functions to within factors of order unity, as demonstrated in previous work [100], and in the right panel of figure 4.5.

## 4.7 Conclusion

Understanding, predicting, and mitigating decoherence remain significant challenges for the development of quantum technologies. In particular, in order to effectively develop novel quantum control protocols that suppress error or evaluate the performance of a complex quantum error correction procedure, we require methods permitting a system designer to estimate error probabilities using real inputs about the environment. This capability is vital as the quantum science community moves from proof-of-principle concepts towards engineering of real quantum coherent technologies where rigid performance bounds are required.

In this chapter, we have presented a novel method for determining the fidelity of arbitrary quantum control operations in a universal time-dependent noise environment. Building on past work employing spectral overlap functions, our method provides a straightforward, easily automated approach to producing analytic functions capturing the effect of the control in the Fourier domain – generalized filter functions. Using these we are able to evaluate control fidelities to arbitrary order, for arbitrary time-dependent control operations in terms of experimentally relevant characteristics of the noise. While the error model we study is constrained to ignore, e.g., leakage errors from the qubit subspace or system-bath entanglement, the selected semiclassical model of universal, Non-Markovian, time-varying noise is far more realistic than earlier approximations based on uncorrelated errors.

We have exploited the capabilities provided by this technique to address the key challenge of accounting for nonidealities in control operations used to implement error-suppressing dynamical decoupling sequences. By generating filter functions incorporating pulse errors and even the effect of complex intrapulse modulation schemes in a single compact formalism, we have provided a simple, physically intuitive means to evaluate sequence performance and inform the development of new dynamical error suppression protocols.

Our approach permits an experimentalist or system designer to analytically study the efficacy and error-susceptibility of customized control protocols involving complex temporal modulation schemes (e.g. control-field phase and amplitude). For instance, it is possible to accurately account for error accumulation due to *control imperfections* arising from realistic constraints such as pulse overshoot, bandwidth limitations, or simple noise in the control field itself. Further, for quantum information one may consider applying this approach at an algorithmic level, permitting ‘echo’ type effects to be exploited in minimizing the error not just of a single operation, but of a complex chain in a computation. With validation for the utility of our method from our study of dynamical decoupling, we believe that this approach will prove invaluable for future experiments in which it is vital to accurately and efficiently estimate the effects of real experimental noise on the achievable fidelity of control operation.

*Acknowledgements:* The authors thank A.C Doherty, K. Khodjasteh, and L. Viola for useful discussions. This work partially supported by the US Army Research Office under Contract Number W911NF-11-1-0068, the Australian Research Council Centre of Excellence for Engineered Quantum Systems CE110001013, and the Office of the Director of National Intelligence (ODNI), Intelligence Advanced Research Projects Activity (IARPA), through the Army Research Office. All statements of fact, opinion or conclusions contained herein are those of the authors and should not be construed as representing the official views or policies of IARPA, the ODNI, or the U.S. Government.

## 4.8 Appendix

In this appendix we look more closely at the series expansion of the fidelity (4.32)

$$\mathcal{F}_{av} = 1 - \langle a_1^2 \rangle - 2\langle \mathbf{a}_1 \mathbf{a}_2^T \rangle - \left[ \langle a_2^2 \rangle + 2\langle \mathbf{a}_1 \mathbf{a}_3^T \rangle - \frac{\langle a_1^4 \rangle}{3} \right] + \dots \quad (4.81)$$

derived in section 4.3 above. By calculating the maximum magnitude of the higher-order terms we can determine the conditions under which they can be neglected. We also show how, by converting to the frequency domain, the fidelity maybe expressed in terms of the noise power spectral density and a series of generalized filter functions.

### Maximum magnitude of terms in the fidelity expansion

In order to determine their relative contributions to the fidelity, we examine the terms in (4.32), beginning with

$$\langle a_1^2 \rangle = \sum_{i,j=x,y,z} \int_0^\tau dt_2 \int_0^\tau dt_1 \langle \beta_i(t_1) \beta_j(t_2) \rangle \mathbf{R}_i(t_1) \mathbf{R}_j^T(t_2). \quad (4.82)$$

We consider only the case in which the three noise components are independent Gaussian random processes, so that  $\langle \beta_i(t_1) \beta_j(t_2) \rangle = \delta_{ij} \langle \beta_i(t_1) \beta_i(t_2) \rangle$  and

$$\langle a_1^2 \rangle = \sum_{i=x,y,z} \int_0^\tau dt_2 \int_0^\tau dt_1 \langle \beta_i(t_1) \beta_i(t_2) \rangle \mathbf{R}_i(t_1) \mathbf{R}_i^T(t_2). \quad (4.83)$$

Letting  $\langle \beta_i(t_1) \beta_i(t_2) \rangle = \langle \beta_i^2(0) \rangle \overline{\langle \beta_i(t_1) \beta_i(t_2) \rangle}$ , where  $\langle \beta_i^2(0) \rangle$  is the mean square value of the  $i$ -th component of the noise and  $|\overline{\langle \beta_i(t_1) \beta_i(t_2) \rangle}| \leq 1$ , we have

$$\begin{aligned} |\langle a_1^2 \rangle| &= \left| \sum_{i=x,y,z} \langle \beta_i^2(0) \rangle \int_0^\tau dt_2 \int_0^\tau dt_1 \overline{\langle \beta_i(t_1) \beta_i(t_2) \rangle} \mathbf{R}_i(t_1) \mathbf{R}_i^T(t_2) \right| \\ &\leq \sum_{i=x,y,z} \langle \beta_i^2(0) \rangle \left| \int_0^\tau dt_2 \int_0^\tau dt_1 \overline{\langle \beta_i(t_1) \beta_i(t_2) \rangle} \mathbf{R}_i(t_1) \mathbf{R}_i^T(t_2) \right| \\ &\leq \xi^2 \end{aligned} \quad (4.84)$$

where we've introduced the smallness parameter

$$\xi^2 \equiv \sum_{i=x,y,z} \langle \beta_i^2(0) \rangle \tau^2 = \langle \boldsymbol{\beta}(0) \boldsymbol{\beta}^T(0) \rangle \tau^2. \quad (4.85)$$

For Gaussian noise, correlation functions evaluated at an odd numbers of time points vanish, so  $\langle \mathbf{a}_1 \mathbf{a}_2^T \rangle = 0$ .

Moving on to the first of the three terms that involve four-point noise correlation functions:

$$\begin{aligned} \langle a_2^2 \rangle &= \sum_{i,j,i',j'} \int_0^\tau dt_1 \int_0^{t_1} dt_2 \int_0^\tau dt_3 \int_0^{t_3} dt_4 \langle \beta_i(t_1) \beta_j(t_2) \beta_{i'}(t_3) \beta_{j'}(t_4) \rangle \\ &\quad \times \tilde{\mathbf{R}}_{ij}(t_1, t_2) \tilde{\mathbf{R}}_{i'j'}^T(t_3, t_4). \end{aligned} \quad (4.86)$$

Here we can apply the Gaussian moment theorem to write

$$\begin{aligned} \langle \beta_i(t_1) \beta_j(t_2) \beta_{i'}(t_3) \beta_{j'}(t_4) \rangle &= \langle \beta_i(t_1) \beta_j(t_2) \rangle \langle \beta_{i'}(t_3) \beta_{j'}(t_4) \rangle \\ &\quad + \langle \beta_i(t_1) \beta_{i'}(t_3) \rangle \langle \beta_j(t_2) \beta_{j'}(t_4) \rangle + \langle \beta_i(t_1) \beta_{j'}(t_4) \rangle \langle \beta_{i'}(t_3) \beta_j(t_2) \rangle. \end{aligned} \quad (4.87)$$

Using the independence of the noise components, this becomes

$$\begin{aligned} \langle \beta_i(t_1) \beta_j(t_2) \beta_{i'}(t_3) \beta_{j'}(t_4) \rangle &= \delta_{ij} \delta_{i'j'} \langle \beta_i(t_1) \beta_i(t_2) \rangle \langle \beta_{i'}(t_3) \beta_{i'}(t_4) \rangle \\ &+ \delta_{ii'} \delta_{jj'} \langle \beta_i(t_1) \beta_i(t_3) \rangle \langle \beta_j(t_2) \beta_j(t_4) \rangle + \delta_{ij'} \delta_{i'j} \langle \beta_i(t_1) \beta_i(t_4) \rangle \langle \beta_{i'}(t_3) \beta_{i'}(t_2) \rangle \end{aligned} \quad (4.88)$$

so that

$$\begin{aligned} \langle a_2^2 \rangle &= \sum_{ij} \int_0^\tau dt_1 \int_0^{t_1} dt_2 \int_0^\tau dt_3 \int_0^{t_3} dt_4 \left\{ \langle \beta_i(t_1) \beta_i(t_2) \rangle \langle \beta_j(t_3) \beta_j(t_4) \rangle \tilde{\mathbf{R}}_{ii}(t_1, t_2) \tilde{\mathbf{R}}_{jj}^T(t_3, t_4) \right. \\ &\quad + \langle \beta_i(t_1) \beta_i(t_3) \rangle \langle \beta_j(t_2) \beta_j(t_4) \rangle \tilde{\mathbf{R}}_{ij}(t_1, t_2) \tilde{\mathbf{R}}_{ij}^T(t_3, t_4) \\ &\quad \left. + \langle \beta_i(t_1) \beta_i(t_4) \rangle \langle \beta_j(t_3) \beta_j(t_2) \rangle \tilde{\mathbf{R}}_{ij}(t_1, t_2) \tilde{\mathbf{R}}_{ji}^T(t_3, t_4) \right\} \end{aligned} \quad (4.89)$$

and

$$\begin{aligned} |\langle a_2^2 \rangle| &\leq \sum_{ij} \langle \beta_i^2(0) \rangle \langle \beta_j^2(0) \rangle \left| \int_0^\tau dt_1 \int_0^{t_1} dt_2 \int_0^\tau dt_3 \int_0^{t_3} dt_4 \right. \\ &\quad \left\{ \overline{\langle \beta_i(t_1) \beta_i(t_2) \rangle \langle \beta_j(t_3) \beta_j(t_4) \rangle} \tilde{\mathbf{R}}_{ii}(t_1, t_2) \tilde{\mathbf{R}}_{jj}^T(t_3, t_4) \right. \\ &\quad + \overline{\langle \beta_i(t_1) \beta_i(t_3) \rangle \langle \beta_j(t_2) \beta_j(t_4) \rangle} \tilde{\mathbf{R}}_{ij}(t_1, t_2) \tilde{\mathbf{R}}_{ij}^T(t_3, t_4) \\ &\quad \left. \left. + \overline{\langle \beta_i(t_1) \beta_i(t_4) \rangle \langle \beta_j(t_3) \beta_j(t_2) \rangle} \tilde{\mathbf{R}}_{ij}(t_1, t_2) \tilde{\mathbf{R}}_{ji}^T(t_3, t_4) \right\} \right|. \end{aligned} \quad (4.90)$$

Each of the three integrands in (4.90) has a magnitude less than or equal to unity, so

$$|\langle a_2^2 \rangle| \leq 3 \sum_{ij} \langle \beta_i^2(0) \rangle \langle \beta_j^2(0) \rangle \tau^4 / 4 = 3\xi^4 / 4. \quad (4.91)$$

Now

$$\langle \mathbf{a}_1 \mathbf{a}_3^T \rangle = \frac{2}{3} \sum_{i'ijk} \int_0^\tau dt_1 \int_0^\tau dt_2 \int_0^{t_2} dt_3 \int_0^{t_3} dt_4 \langle \beta_{i'}(t_1) \beta_i(t_2) \beta_j(t_3) \beta_k(t_4) \rangle \quad (4.92)$$

which, using the Gaussian moment theorem and the independence of the noise components, gives

$$\begin{aligned} \langle \mathbf{a}_1 \mathbf{a}_3^T \rangle &= \frac{2}{3} \sum_{ij} \int_0^\tau dt_1 \int_0^\tau dt_2 \int_0^{t_2} dt_3 \int_0^{t_3} dt_4 \\ &\quad \left\{ \langle \beta_i(t_1) \beta_i(t_2) \rangle \langle \beta_j(t_3) \beta_j(t_4) \rangle \mathbf{R}_i(t_1) \tilde{\mathbf{R}}_{ijj}^T(t_2, t_3, t_4) \right. \\ &\quad + \langle \beta_i(t_1) \beta_i(t_3) \rangle \langle \beta_j(t_2) \beta_j(t_4) \rangle \mathbf{R}_i(t_1) \tilde{\mathbf{R}}_{ijj}^T(t_2, t_3, t_4) \\ &\quad \left. + \langle \beta_i(t_1) \beta_i(t_4) \rangle \langle \beta_j(t_3) \beta_j(t_2) \rangle \mathbf{R}_i(t_1) \tilde{\mathbf{R}}_{jji}^T(t_2, t_3, t_4) \right\}. \end{aligned} \quad (4.93)$$

Following the same procedure used to derive (4.91), we find that

$$|\langle \mathbf{a}_1 \mathbf{a}_3^T \rangle| \leq \xi^4 / 3. \quad (4.94)$$

Finally,

$$\begin{aligned} \langle a_1^4 \rangle &= \sum_{i,j,i',j'} \int_0^\tau dt_1 \int_0^\tau dt_2 \int_0^\tau dt_3 \int_0^\tau dt_4 \langle \beta_i(t_1) \beta_j(t_2) \beta_{i'}(t_3) \beta_{j'}(t_4) \rangle \\ &\quad (\mathbf{R}_i(t_1) \mathbf{R}_j^T(t_2)) (\mathbf{R}_{i'}(t_3) \mathbf{R}_{j'}^T(t_4)) \end{aligned} \quad (4.95)$$

which becomes

$$\begin{aligned} \langle a_1^4 \rangle &= \sum_{ij} \int_0^\tau dt_1 \int_0^\tau dt_2 \int_0^\tau dt_3 \int_0^\tau dt_4 \\ &\quad \left\{ \langle \beta_i(t_1) \beta_i(t_2) \rangle \langle \beta_j(t_3) \beta_j(t_4) \rangle (\mathbf{R}_i(t_1) \mathbf{R}_i^T(t_2)) (\mathbf{R}_j(t_3) \mathbf{R}_j^T(t_4)) \right. \\ &\quad + \langle \beta_i(t_1) \beta_i(t_3) \rangle \langle \beta_j(t_2) \beta_j(t_4) \rangle (\mathbf{R}_i(t_1) \mathbf{R}_j^T(t_2)) (\mathbf{R}_i(t_3) \mathbf{R}_j^T(t_4)) \\ &\quad \left. + \langle \beta_i(t_1) \beta_i(t_4) \rangle \langle \beta_j(t_3) \beta_j(t_2) \rangle (\mathbf{R}_i(t_1) \mathbf{R}_j^T(t_2)) (\mathbf{R}_j(t_3) \mathbf{R}_i^T(t_4)) \right\}. \end{aligned} \quad (4.96)$$

We can then show that

$$|\langle a_1^4 \rangle| \leq 3\xi^4. \quad (4.97)$$

Obviously, for Gaussian noise, the overall trend here is that those terms containing  $n$ -point correlation functions make a maximum contribution of the order of  $\xi^n$  to the fidelity. If we limit our attention to a regime in which  $\xi^2 \ll 1$ , then higher order terms will have little effect and the fidelity may be expressed in terms of the first order error vector only.

## Spectral representation

The noise power spectral density  $S_i(\omega)$  of the  $i$ -th noise component may be defined by

$$\langle \beta_i(t_1) \beta_i(t_2) \rangle = \frac{1}{2\pi} \int_{-\infty}^{\infty} d\omega S_i(\omega) e^{i\omega(t_2-t_1)}. \quad (4.98)$$

Noting that

$$\langle \beta_i^2(0) \rangle = \frac{1}{2\pi} \int_{-\infty}^{\infty} d\omega S_i(\omega) = \frac{1}{\pi} \int_0^{\infty} d\omega S_i(\omega) \quad (4.99)$$

the smallness parameter  $\xi$  may be expressed in terms of the noise spectrum. In particular, if the  $i$ -th noise component has a cutoff frequency  $\omega_{ci}$ , then

$$\langle \beta_i^2(0) \rangle = \frac{1}{\pi} \int_0^{\omega_{ci}} d\omega S_i(\omega) \quad (4.100)$$

and

$$\xi^2 \equiv \frac{\tau^2}{\pi} \sum_{i=x,y,z} \int_0^{\omega_{ci}} d\omega S_i(\omega). \quad (4.101)$$

The dependence of the fidelity on the spectral properties of the noise and of the control can also be made explicit using (4.98). Substituting (4.98) into (4.83), we have

$$\langle a_1^2 \rangle = \frac{1}{2\pi} \sum_{i=x,y,z} \int_{-\infty}^{\infty} \frac{d\omega}{\omega^2} S_i(\omega) F_i^1(\omega) \quad (4.102)$$

where

$$F_i^{(1)}(\omega) \equiv \mathbf{R}_i(\omega) \mathbf{R}_i^{T*}(\omega) \quad (4.103)$$

is the first order generalized filter function for the  $i$ -th noise component, defined in terms of the  $i$ -th row of the frequency domain control matrix

$$\mathbf{R}_i(\omega) \equiv -i\omega \int_0^\tau dt e^{i\omega t} \mathbf{R}_i(t). \quad (4.104)$$

Similarly, from (4.89)

$$\begin{aligned} \langle a_2^2 \rangle &= \frac{1}{(2\pi)^2} \sum_{ij} \int_{-\infty}^{\infty} d\omega S_i(\omega) \int_{-\infty}^{\infty} d\omega' S_j(\omega') \int_0^{\tau} dt_1 \int_0^{t_1} dt_2 \int_0^{\tau} dt_3 \int_0^{t_3} dt_4 \\ &\left\{ e^{i\omega(t_2-t_1)} e^{i\omega'(t_4-t_3)} \tilde{\mathbf{R}}_{ii}(t_1, t_2) \tilde{\mathbf{R}}_{jj}^T(t_3, t_4) + e^{i\omega(t_3-t_1)} e^{i\omega'(t_4-t_2)} \tilde{\mathbf{R}}_{ij}(t_1, t_2) \tilde{\mathbf{R}}_{ij}^T(t_3, t_4) \right. \\ &\quad \left. + e^{i\omega(t_4-t_1)} e^{i\omega'(t_3-t_2)} \tilde{\mathbf{R}}_{ij}(t_1, t_2) \tilde{\mathbf{R}}_{ji}^T(t_3, t_4) \right\} \end{aligned} \quad (4.105)$$

while, from (4.93)

$$\begin{aligned} \langle \mathbf{a}_1 \mathbf{a}_3^T \rangle &= \frac{1}{(2\pi)^2} \sum_{ij} \int_{-\infty}^{\infty} d\omega S_i(\omega) \int_{-\infty}^{\infty} d\omega' S_j(\omega') \int_0^{\tau} dt_1 \int_0^{\tau} dt_2 \int_0^{t_2} dt_3 \int_0^{t_3} dt_4 \\ &\left\{ e^{i\omega(t_2-t_1)} e^{i\omega'(t_4-t_3)} \mathbf{R}_i(t_1) \tilde{\mathbf{R}}_{ijj}^T(t_2, t_3, t_4) + e^{i\omega(t_3-t_1)} e^{i\omega'(t_4-t_2)} \mathbf{R}_i(t_1) \tilde{\mathbf{R}}_{jij}^T(t_2, t_3, t_4) \right. \\ &\quad \left. + e^{i\omega(t_4-t_1)} e^{i\omega'(t_3-t_2)} \mathbf{R}_i(t_1) \tilde{\mathbf{R}}_{jji}^T(t_2, t_3, t_4) \right\} \end{aligned} \quad (4.106)$$

and from (4.96)

$$\begin{aligned} \langle a_1^4 \rangle &= \frac{1}{(2\pi)^2} \sum_{ij} \int_{-\infty}^{\infty} d\omega S_i(\omega) \int_{-\infty}^{\infty} d\omega' S_j(\omega') \int_0^{\tau} dt_1 \int_0^{\tau} dt_2 \int_0^{\tau} dt_3 \int_0^{\tau} dt_4 \\ &\left\{ e^{i\omega(t_2-t_1)} e^{i\omega'(t_4-t_3)} (\mathbf{R}_i(t_1) \mathbf{R}_i^T(t_2)) (\mathbf{R}_j(t_3) \mathbf{R}_j^T(t_4)) \right. \\ &\quad + e^{i\omega(t_3-t_1)} e^{i\omega'(t_4-t_2)} (\mathbf{R}_i(t_1) \mathbf{R}_j^T(t_2)) (\mathbf{R}_i(t_3) \mathbf{R}_j^T(t_4)) \\ &\quad \left. + e^{i\omega(t_4-t_1)} e^{i\omega'(t_3-t_2)} (\mathbf{R}_i(t_1) \mathbf{R}_j^T(t_2)) (\mathbf{R}_j(t_3) \mathbf{R}_i^T(t_4)) \right\}. \end{aligned} \quad (4.107)$$

Extrapolating these results, we find the following alternative form for the series expansion of the fidelity

$$\begin{aligned} \mathcal{F}_{av} &= 1 - \left[ \frac{1}{2\pi} \sum_i \int_{-\infty}^{\infty} \frac{d\omega}{\omega^2} S_i(\omega) F_i^{(1)}(\omega) \right. \\ &\quad \left. + \frac{1}{(2\pi)^2} \sum_{ij} \int_{-\infty}^{\infty} \frac{d\omega}{\omega^2} S_i(\omega) \int_{-\infty}^{\infty} \frac{d\omega'}{\omega'^2} S_j(\omega') F_{ij}^{(2)}(\omega, \omega') + \dots \right] \end{aligned} \quad (4.108)$$

where the generalized filter functions  $F_{i_1 i_2 \dots}^{(p)}(\omega, \omega' \dots)$  are derived solely from the control matrix.

## 4.9 Addendum

Following the publication of the work on which this chapter is based [108], Paz-Silva and Viola formalized and extended the concept of *generalized filter functions* (GFFs) beyond single-qubit systems, and beyond classical Gaussian noise environments [43]. In the *Supplemental material* section of their paper, the authors explain how their formalism relates to the work presented here and, indeed, can be used to rederive some of our key conclusions. In this addendum, we highlight some of these connections.

In [43], the basic interaction Hamiltonian (defined in the interaction picture with respect to the quantum bath  $\mathcal{B}$ ) is generalized from the single-qubit form given in equation (4.5) to

$$H_0(t) = \sum_u O_u \otimes B_u(t), \quad (4.109)$$

where  $\{O_u\}$  is a set of traceless Hermitian operators acting on the target system  $\mathcal{S}$ . As discussed in section 2.3.2, a semiclassical environment can be accounted for by letting  $B_u(t) = \beta_u(t)I_{\mathcal{B}}$ . The toggling frame Hamiltonian (assuming perfect control  $H_c(t)$ ) is then

$$\begin{aligned} \tilde{H}_0(t) &= \sum_u U_c^\dagger(t) O_u U_c(t) \otimes B_u(t) \\ &= \sum_{u,v} y_{uv}(t) O_v \otimes B_u(t), \end{aligned} \quad (4.110)$$

where  $y_{uv}(t)$  is the generalization of the control matrix  $R_{uv}(t)$ , defined in equation (4.14) of this work.

This Hamiltonian generates a toggling/control frame propagator which may be expressed in terms of a Magnus expansion of the error action operator

$$\Phi(\tau) = \sum_\alpha \Phi_\alpha(\tau), \quad (4.111)$$

evaluated at the conclusion of the total operation time  $\tau$ . Substituting (4.110) into this expansion gives a generalized form for each of the terms in the Magnus expansion in section 4.2.4:

$$\Phi_\alpha(\tau) = -i \sum_{\vec{u}, \vec{v}} \int_{V_\alpha} d^\alpha \vec{t} f(\{y_{[\alpha]}\}) O_{v_1} \dots O_{v_\alpha} \otimes B_{u_1}(t_1) \dots B_{u_\alpha}(t_\alpha), \quad (4.112)$$

where  $\vec{u} \equiv (u_1, \dots, u_\alpha)$ ,  $\vec{t} \equiv (t_1, \dots, t_\alpha)$ ,  $V_\alpha$  is a ‘volume’ in multi-dimensional time space, and  $f$  depends only on products of the control matrix elements  $y_{[\alpha]} \equiv y_{u_1 v_1} \dots y_{u_\alpha v_\alpha}$ .

Importantly, rather than calculate the relevant ‘figure of merit’ (in this chapter, it is the ensemble average gate fidelity  $\mathcal{F}_{av}$ ) in the time domain and then proceed to a frequency space analysis, as we do in section 4.3.1, the authors of [43] first rewrite (4.112) using the frequency space representation of the bath variables

$$B_u(t) = \frac{1}{2\pi} \int_{-\infty}^{\infty} d\omega e^{i\omega t} B_u(\omega) \quad (4.113)$$

to obtain

$$\Phi_\alpha(\tau) = -i \sum_{\vec{u}, \vec{v}} \int \frac{d^\alpha \vec{\omega}}{(2\pi)^\alpha} \tilde{G}_{\vec{u} \vec{v}}^{(\alpha)}(\vec{\omega}, \tau) O_{v_1} \dots O_{v_\alpha} \otimes B_{u_1}(\omega_1) \dots B_{u_\alpha}(\omega_\alpha). \quad (4.114)$$

Here, the  $\alpha$ th order generalized filter function  $\tilde{G}_{\vec{u}\vec{v}}^{(\alpha)}(\vec{\omega}, \tau)$  captures the  $\alpha$ th order filtering effect of the control, at the level of the toggling frame propagator. A key result is that these GFFs are expressible in terms of a set of simpler *fundamental filter functions* FFF, of order at most  $\alpha$ , where the  $\alpha$ th order FFF is defined as

$$\tilde{F}_{\vec{u}\vec{v}}^{(\alpha)}(\vec{\omega}, \tau) \equiv (-i)^\alpha \int_{V_\alpha} d^\alpha \vec{t} \prod_{j=1}^{\alpha} y_{u_j v_j}(t_j) e^{i\omega_j t_j}. \quad (4.115)$$

The generalized filter functions  $F_{i_1 i_2 \dots}^{(p)}(\omega, \omega' \dots)$  we've described in this chapter are referred to as *effective* generalized filter functions (EGFFs) in [43] and can also be expressed in terms of FFFs.

In the case of a single-qubit system subject to classical noise, equation (4.114) can be written in terms of the *error vector*  $\mathbf{a}(\tau)$ , introduced in section 4.3.1, and its associated Magnus expansion. The  $\alpha$ th order term in this expansion, associated with the Pauli operator  $\sigma_v$ , is given by [43]

$$[\mathbf{a}_1(\tau)]_v \sigma_v = \sum_{\langle \langle \vec{u}, \vec{v} \rangle \rangle} \int \frac{d^\alpha \vec{\omega}}{(2\pi)^\alpha} \tilde{G}_{\vec{u}\vec{v}}^{(\alpha)}(\vec{\omega}, \tau) \sigma_{v_1} \dots \sigma_{v_\alpha} \beta_{u_1}(\omega_1) \dots \beta_{u_\alpha}(\omega_\alpha), \quad (4.116)$$

where  $\langle \langle \vec{u}, \vec{v} \rangle \rangle$  is the set of all  $\vec{u}, \vec{v}$  such that  $\sigma_{v_1} \dots \sigma_{v_\alpha} = \sigma_v$ , and  $\beta_u(\omega)$  is the Fourier transform of the classical noise process  $\beta_u(t)$ . These expressions can be substituted directly into equation (4.32) to obtain the ensemble average fidelity  $\mathcal{F}_{av}(\tau)$  in terms of GFFs  $\tilde{G}_{\vec{u}\vec{v}}^{(\alpha)}(\vec{\omega}, \tau)$ .

If the noise is purely dephasing and Gaussian, we can employ the Gaussian moment theorem to rederive equation (4.50), reproduced here:

$$\begin{aligned} \mathcal{F}_{av} = 1 - & \left[ \frac{1}{2\pi} \int_{-\infty}^{\infty} \frac{d\omega}{\omega^2} S_z(\omega) F_z^{(1)}(\omega) \right. \\ & \left. + \frac{1}{(2\pi)^2} \int_{-\infty}^{\infty} \frac{d\omega}{\omega^2} S_z(\omega) \int_{-\infty}^{\infty} \frac{d\omega'}{\omega'^2} S_z(\omega') F_{zz}^{(2)}(\omega, \omega') + \dots \right], \end{aligned} \quad (4.117)$$

where  $S_z(\omega)$  is the dephasing noise power spectral density, and the EGFFs in equation (4.117) are constructed from FFFs. For example

$$\frac{F_z^{(1)}(\omega)}{\omega^2} = \tilde{F}_x^{(\alpha=1)}(\omega) \tilde{F}_x^{(\alpha=1)}(-\omega) + \tilde{F}_y^{(\alpha=1)}(\omega) \tilde{F}_y^{(\alpha=1)}(-\omega) + \tilde{F}_z^{(\alpha=1)}(\omega) \tilde{F}_z^{(\alpha=1)}(-\omega). \quad (4.118)$$

In a similar way, the connection between FFFs and our EGFFs can be used to redefine all results in this chapter so that they fit easily into the more unified formalism of [43].

# Chapter 5

## Robustness of composite pulses to time-dependent control noise

We study the performance of composite pulses in the presence of time-varying control noise on a single qubit. These protocols, originally devised only to correct for static, systematic errors, are shown to be robust to time-dependent non-Markovian noise in the control field up to frequencies as high as  $\sim 10\%$  of the Rabi frequency. Our study combines a generalized filter-function approach with asymptotic dc-limit calculations to give a simple analytic framework for error analysis applied to a number of composite-pulse sequences relevant to nuclear magnetic resonance as well as quantum information experiments. Results include examination of recently introduced concatenated composite pulses and dynamically corrected gates, demonstrating equivalent first-order suppression of time-dependent fluctuations in amplitude and/or detuning, as appropriate for the sequence in question. Our analytic results agree well with numerical simulations for realistic  $1/f$  noise spectra with a roll-off to  $1/f^2$ , providing independent validation of our theoretical insights.

The contents of this chapter have been published as: C. Kabytayev, T. J. Green, K. Khodjasteh, M. J. Biercuk, L. Viola and K. R. Brown, ‘Robustness of composite pulses to time-dependent control noise’, Physical Review A **90**, 012316 (2014). As mentioned briefly in section 2.5, DQES is derived from a class of techniques first employed in NMR. These techniques include error-robust, nontrivial operations, in the form of ‘composite pulses’. Assessing the performance of these pulses (and the closely related dynamically corrected gates) in a time-dependent environment, from a filtering perspective, demonstrates the practical utility of the analytical methods introduced in the previous two chapters.

### 5.1 Introduction

High-fidelity control of quantum systems is limited by unwanted interactions with the environment and imperfections in the applied control fields. Composite pulse (CP) sequences have long been employed in nuclear magnetic resonance (NMR) to mitigate the effects of systematic errors in the control [109, 110, 111, 87]. Initially developed to tackle static but otherwise unknown errors in the amplitude or frequency of the driving field, CPs are expressed as the composition of rotations. CPs have been recently extended to handle multiple error sources using symmetry [102, 112] and concatenation [113, 114] and to provide high-order error suppression by optimized design [115]. These capabilities have made CPs broadly attractive in laboratory quantum

systems, including experiments employing atomic [116] and solid-state [117, 33] qubits.

Despite these advances, an outstanding challenge to the systematic incorporation of CPs into practical quantum information systems remains the limited understanding of CP performance in the presence of *time-dependent* noise. This is in contrast to optimal control approaches for gate synthesis, where the presence of time-dependent noise is typically assumed in the control design (see, e.g., [118, 119, 120]). Previous studies for CPs have examined a restricted set of time-dependent fluctuations in the control including the numeric characterization of decoherence due to random-telegraph noise in the qubit frequency [121], the effect of stochastic fluctuations in the phase of the control [122], and the effect of  $1/f^\alpha$  noise on singlet-triplet spin qubits [123].

Treating the influence of time-dependent noise processes on quantum control operations beyond these limited examples has been facilitated by recent advances in dynamical error suppression based on open-loop Hamiltonian engineering [48, 58, 124, 68, 55, 108]. These approaches provide a general framework for understanding and mitigating non-Markovian time-dependent noise in a finite-dimensional open quantum system due to either uncontrolled couplings to the environment or a variety of control errors. In particular, both dynamical decoupling [48, 58, 64] and dynamically corrected gates (DCGs) [119, 68, 55, 54] are able to perturbatively reduce the effects of classical as well as quantum noise sources, provided that the correlation time scale of the noise is sufficiently long compared to the control time scale at which the noise is ‘coherently averaged out.’ These characteristics may be captured quantitatively in filter-transfer functions (FFs) for arbitrary single-qubit control using methods of spectral overlap in the frequency domain [108, 49]. The resulting approach allows for prediction of the leading-order contribution to fidelity loss and has been applied to the study of both dynamically protected memory [32, 88, 125, 47, 105] and nontrivial quantum logic operations [108, 100], with results borne out through a variety of experiments [32, 88, 125, 126, 127].

In this work, we use a combination of analytic formulations based on FFs and numerical simulations to demonstrate that CPs are able to effectively suppress control errors caused by time-dependent processes possessing realistic noise power spectra. Specifically, we consider a variety of both standard and concatenated CP sequences on a single qubit, as well as simple DCG protocols, and compare their performance within a unified control framework. Remarkably, robust performance of CP sequences is found *up to fluctuations as fast as  $\sim 10\%$  of the Rabi frequency*, providing an explicit *quantitative* characterization of the sensitivity of these approaches to time-dependent control noise. Calculations show that even under such noise environments, which are beyond the static ones originally assumed for CPs, predicted fidelities are at least comparable to those for DCGs in scenarios where protocols of both kinds are applicable. We present a geometric interpretation of CP performance under time-dependent amplitude noise in order to provide insight into this behavior, further linking the FF formalism with known techniques in CP construction [87].

## 5.2 Theoretical framework

### 5.2.1 Control protocols

Both CP and DCG protocols consist of multiple elementary control operations, which are sequentially implemented in such a way that the desired target operation (quantum gate) is realized while simultaneously reducing the net sensitivity to error. The mathematical frameworks and error-model assumptions employed in arriving at these constructions vary considerably, leading to different control modalities. While we refer to the relevant literature for a more complete discussion [87, 119, 68, 55, 54], we focus here on the task of effecting a target rotation on a

Composite pulse	Error model	$(\theta_1, \phi_1)$	$(\theta_2, \phi_2)$	$(\theta_3, \phi_3)$	$(\theta_4, \phi_4)$	$(\theta_5, \phi_5)$	$(\theta_6, \phi_6)$
SK1	$a$	$(\theta, 0)$	$(2\pi, -\phi_1)$	$(2\pi, \phi_1)$	—	—	—
BB1	$a$	$(\theta, 0)$	$(\pi, \phi_1)$	$(2\pi, 3\phi_1)$	$(\pi, \phi_1)$	—	—
CORPSE	$d$	$(2\pi + \theta/2 - k, 0)$	$(2\pi - 2k, \pi)$	$(\theta/2 - k, 0)$	—	—	—
Reduced CinSK	$s$	$(2\pi + \theta/2 - k, 0)$	$(2\pi - 2k, \pi)$	$(\theta/2 - k, 0)$	$(2\pi, -\phi_1)$	$(2\pi, \phi_1)$	—
Reduced CinBB	$s$	$(2\pi + \theta/2 - k, 0)$	$(2\pi - 2k, \pi)$	$(\theta/2 - k, 0)$	$(\pi, \phi_1)$	$(2\pi, 3\phi_1)$	$(\pi, \phi_1)$

Table 5.1: CP sequences correcting the target rotation  $R(\theta, \phi)$  against different error models [87, 114]. Here,  $\phi_1 = \cos^{-1}(-\theta/4\pi)$ ,  $k = \arcsin[\sin(\theta/2)/2]$ ,  $a$ : amplitude noise,  $d$ : detuning noise and  $s$ : simultaneous noise sources. For the DCG sequence [68, 55, 108],  $\Omega_1 = \Omega$ ,  $0 \leq t < t_1 \equiv \tau/4$ ;  $\Omega_2 = \Omega/2$ ,  $t_1 \leq t < t_2 \equiv 3\tau/4$ ;  $\Omega_3 = \Omega$ ,  $t_2 \leq t < t_3 \equiv \tau$ .

single qubit, which, as usual, may be parametrized as

$$R(\theta, \phi) = \exp[-i\theta\boldsymbol{\rho}(\phi) \cdot \boldsymbol{\sigma}/2], \quad \boldsymbol{\sigma} \equiv (\sigma_x, \sigma_y, \sigma_z).$$

Ideally,  $R(\theta, \phi)$  rotates the qubit Bloch vector through an angle  $\theta$ , about an axis defined by the unit vector  $\boldsymbol{\rho}(\phi) \equiv (\cos \phi, \sin \phi, 0)$ . In practice, any environmental and/or control errors cause the actual effect of a control protocol to differ from the intended one. We are interested here in error models that may be pictured in terms of coupling to classical degrees of freedom, as arise from noisy control actions and/or a fluctuating background environment – in which case the net result is the implementation of a different operation on the target system, say,  $M(\theta, \phi) \neq R(\theta, \phi)$ .

The standard error model assumed in CP constructions involves a combination of *static* (dc) pulse-length and off-resonance control errors, which we may represent as

$$M(\theta, \phi) = \exp[-i\theta\{(1 + \epsilon_a)\boldsymbol{\rho}(\phi) \cdot \boldsymbol{\sigma} + \epsilon_d\sigma_z\}/2],$$

where  $\epsilon_a$  and  $\epsilon_d$  quantify the amplitude and detuning offsets, respectively. CPs rely on the application of constant-amplitude control fields segmented into rotations of different durations about different axes (phase modulation) to counter these errors, which, until recently [102, 112, 113, 114], have been addressed separately. If  $M_a(\theta, \phi)$  [respectively,  $M_d(\theta, \phi)$ ] denote the propagator for the special case in which only  $\epsilon_a$  [respectively,  $\epsilon_d$ ] is significant, an  $m$ -th order CP protocol  $M_\mu^{[m]}(\theta, \phi)$  is a sequence of elementary operations  $\{M_\mu(\theta, \phi)\}$  for which [87]

$$M_\mu^{[m]}(\theta, \phi) = R(\theta, \phi) + \mathcal{O}(\epsilon_\mu^{m+1}), \quad \mu \in \{a, d\}.$$

The representative CP sequences we consider are listed in table 5.1. For instance, SK1 and BB1 are first- and second-order CPs correcting for pure amplitude errors [110, 111], whereas CORPSE is a first-order compensating sequence for pure detuning errors [128]. Simultaneous errors can be systematically suppressed for arbitrary  $(\theta, \phi)$  by applying concatenated CPs [114], such as reduced CinSK (CORPSE in SK1) and reduced CinBB (CORPSE in BB1).

DCG protocols are constructed from general Hamiltonian models for finite-dimensional open quantum systems exposed to non-Markovian decoherence due to quantum or, as considered here, classical environments. This is to be contrasted with CP constructions, which are obtained without making reference to an underlying physical model for the intervening error dynamics. In the simplest case DCGs employ piecewise-constant amplitude and phase modulation of the applied control fields across a sequence of carefully designed elementary segments. Through this approach, the error sensitivity of the target operation is perturbatively minimized

to a given order [68, 55]. More general analytical DCG constructions are also possible, involving ‘stretching and scaling’ arbitrary control profiles. In the present setting, we take advantage of the formal similarity of the propagator  $M(\theta, \phi)$  under pure off-resonance errors ( $\epsilon_a = 0$ ) to the one arising from single-axis classical decoherence in the DCG context. Specifically, the representative DCG we study is a first-order three-segment sequence, obtained from general constructions in the special case  $\theta = \pi$  [68, 55, 108] (see also table 5.1).

### 5.2.2 Time-dependent error model

In order to both introduce and analyze the effect of time-dependent amplitude and detuning errors in CP sequences, and compare them to DCGs in a unified setting, it is necessary to formulate the control problem at the Hamiltonian (rather than propagator) level. While here we assume piecewise-constant control, more general control modulations may be included as discussed in the Appendix.

Let us consider a piecewise-constant chain of  $n$  discrete time segments, each indexed by  $l$  and spanning time  $t \in [t_{l-1}, t_l]$  such that, in units of  $\hbar = 1$  and in a suitable frame, we may write a total Hamiltonian of the form

$$H(t) = \sum_{l=1}^n G^{(l)}(t) \frac{[\Omega_l + \beta_a(t)]}{2} \boldsymbol{\rho}_a^{(l)} \cdot \boldsymbol{\sigma} + \frac{\beta_d(t)}{2} \sigma_z \quad (5.1)$$

$$\equiv H_0(t) + H_{\text{err}}(t). \quad (5.2)$$

Here, we have introduced a modulation function  $G^{(l)}(t) \equiv \Theta[t - t_{l-1}] \Theta[t_l - t]$ , which has unit value for  $t \in [t_{l-1}, t_l]$ , and is equal to zero otherwise, in order to capture the fact that the control is implemented in a piecewise-constant fashion. The ideal control-field amplitude for the  $l$ -th segment is denoted by  $\Omega_l$ , and its axis of rotation,  $\boldsymbol{\rho}_a^{(l)} \equiv \boldsymbol{\rho}(\phi_l) = (\cos \phi_l, \sin \phi_l, 0)$ . The two zero-mean Gaussian (stationary) stochastic processes  $\beta_a(t)$  and  $\beta_d(t)$  model amplitude and detuning noise, respectively. We assume that both these processes enter the dynamics additively and are independent of the ideal amplitude and phase of the control, while also being mutually independent; that is,  $\langle \beta_a(t) \beta_d(t') \rangle = 0$ .

The total Hamiltonian in equation (5.1) may be separated into ideal plus error Hamiltonians by isolating the noise terms proportional to  $\beta_\mu$ . That is, acting alone,  $H_0(t)$  generates the unitary propagator  $U_0(t, 0) = \sum_{l=1}^n G^{(l)}(t) U_0(t, t_{l-1}) R'_{l-1}$ , which describes a sequence of  $n$  consecutive elementary control operations  $R_l \equiv R(\theta_l, \phi_l)$ , for  $l = 1, \dots, n$ , executed over a total gating time  $\tau \equiv t_n$ . Here, the operator  $U_0(t, t_{l-1}) = \exp[-i\Omega_l(t - t_{l-1}) \boldsymbol{\rho}_a^{(l)} \cdot \boldsymbol{\sigma}/2]$  is the time-dependent propagator for the  $l$ -th elementary pulse, such that  $\theta_l = \Omega_l(t_l - t_{l-1})$  and  $U_0(t_l, t_{l-1}) = R_l$ . At the end of the sequence,  $U_0(\tau, 0) = R(\theta, \phi) = R'_n$  (the desired target operation), where  $R'_l \equiv R_l R_{l-1} \dots R_0$  and  $R_0 \equiv I$ .

Following [68, 55], the total evolution operator  $U(t, 0)$ , generated by the controlled Hamiltonian in equation (5.1), may then be written as  $U(\tau, 0) \equiv U_0(\tau, 0) \exp[-i\Phi(\tau)]$ , where the ‘error action operator’ encapsulates the effect of  $H_{\text{err}}(t)$  and, to the lowest order in a perturbative Magnus-series expansion, we may write

$$\Phi(\tau) \approx \Phi_1(\tau) = \int_0^\tau dt U_0^\dagger(t, 0) H_{\text{err}}(t) U_0(t, 0). \quad (5.3)$$

Calculating this quantity requires consideration of all (ideal) time-ordered control operations enacted during the sequence; let us therefore define ‘control vectors’ as [108]

$$\boldsymbol{\rho}_a(t) \equiv \frac{1}{2} \sum_{l=1}^n G^{(l)}(t) \boldsymbol{\rho}_a^{(l)} \boldsymbol{\Lambda}^{(l-1)}, \quad \boldsymbol{\rho}_d(t) \equiv \frac{1}{2} \sum_{l=1}^n G^{(l)}(t) \boldsymbol{\rho}_d^{(l)}(t - t_{l-1}) \boldsymbol{\Lambda}^{(l-1)},$$

where the matrices (vectors)  $\Lambda^{(l-1)}$  [ $\rho_d^{(l)}(t - t_{l-1})$ ] have components

$$\Lambda_{ij}^{(l-1)} = \text{Tr}[R'_{l-1}^\dagger \sigma_i R'_{l-1} \sigma_j]/2, \quad \rho_{d,j}^{(l)}(t - t_{l-1}) = \text{Tr}[U_0^\dagger(t, t_{l-1}) \sigma_z U_0(t, t_{l-1}) \sigma_j]/2,$$

for  $i, j \in \{x, y, z\}$ . Thus,  $\Phi_1(\tau) = \mathbf{a}(\tau) \cdot \boldsymbol{\sigma}$ , where the ‘error vector,’

$$\mathbf{a}(\tau) \equiv \int_0^\tau dt [\beta_a(t) \rho_a(t) + \beta_d(t) \rho_d(t)],$$

captures the difference between the actual and the target control operations, for each realization of the noise.

In order to gain useful information about the overall performance of a CP protocol, we must characterize performance across an ensemble of noise realizations. As a figure of merit, we consider the ensemble-averaged (denoted by  $\langle \cdot \rangle$ ) propagator fidelity which, in our qubit setting, reads

$$\mathcal{F} = \frac{1}{4} \langle |\text{Tr}[U_0^\dagger(\tau, 0) U(\tau, 0)]|^2 \rangle.$$

In the (weak noise or/and short time) limit where the first-order description of equation (5.3) is accurate, we may further write [108, 127]

$$\mathcal{F} \approx 1 - \langle a(\tau)^2 \rangle, \quad a(\tau) \equiv [\mathbf{a}(\tau) \cdot \mathbf{a}(\tau)]^{1/2}.$$

This quantity is most conveniently calculated in the Fourier domain; introducing the noise power spectral densities,

$$S_\mu(\omega) \equiv \int_{-\infty}^{\infty} dt e^{-i\omega t} \langle \beta_\mu(t_0) \beta_\mu(t_0 + t) \rangle,$$

for  $\mu \in \{a, d\}$ , and exploiting the stationarity and independence properties of the noise sources, we finally obtain the following expression for the (first-order) fidelity loss:

$$1 - \mathcal{F} \approx \frac{1}{2\pi} \int_{-\infty}^{\infty} \frac{d\omega}{\omega^2} \sum_{\mu=a,d} S_\mu(\omega) F_\mu(\omega). \quad (5.4)$$

Here,  $F_\mu(\omega) \equiv \rho_\mu^*(\omega) \cdot \rho_\mu(\omega)$  is the *generalized* FF for amplitude ( $\mu = a$ ) and detuning ( $\mu = d$ ), respectively, defined in terms of the frequency-domain control vectors  $\rho_\mu(\omega) = -i\omega \int_0^\tau dt \rho_\mu(t) e^{i\omega t}$ .

The FFs characterize the spectral properties of the applied control and thus provide a simple quantitative means to compare the control protocols of interest (see table 5.1) in the presence of time-dependent Gaussian noise [108, 47]. In general, one may interpret these functions by considering the transfer function of a high-pass filter, including pass band, stop band, and roll-off. The filter roll-off, captured by the slope of the FF near zero frequency, serves as a lower bound on the order of error suppression in the presence of time-dependent noise [43]. This approach has been validated for nontrivial control – including CP constructions – in recent experiments [127]. We next proceed to calculate and present independently the FFs for both amplitude and detuning quadratures.

## 5.3 Results

### 5.3.1 Analytical results and geometric picture

We begin by analyzing the effect of a single noise source, as described by the appropriate generalized FF introduced in the previous section. Results are summarized in figures 5.1(a) and

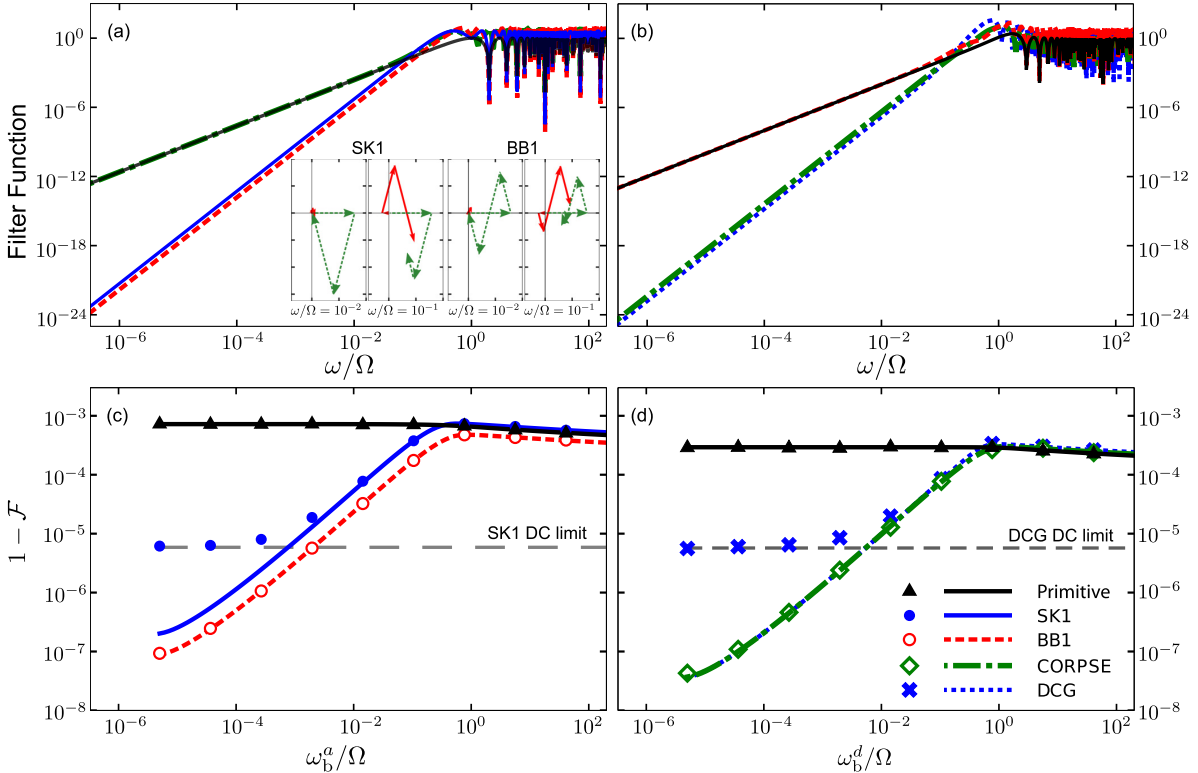


Figure 5.1: (a, b) FFs as a function of dimensionless frequency for amplitude (a) and detuning noise (b). A target rotation angle  $\theta = \pi$  is used for all sequences. Inset: Geometric picture of first- vs second-order amplitude-error CPs. Axes represent Cartesian  $x$  and  $y$ , indicating the rotation axes of the different segments (see text). The initial rotation is effected about the  $x$  axis, indicated by the horizontal line, with corrections about different axes conducted subsequently. Returning to the origin indicates suppression of error, with two time-domain elements of the FF being indicated by color (dashed green and solid red). (c, d) Performance of CP sequences in the presence of a constant power amplitude (c) and detuning noise (d) with a  $1/f$  Gaussian noise spectrum and  $1/f^2$  roll-off, equation (5.7). Spectrum parameters:  $A_a = A_d = A = 2.07 \times 10^9 / [\ln(\omega_b/\omega_{min}) + 1 - (\omega_b/\omega_{max})]$  (rad/s) $^3$ /Hz, where  $\omega_b$  is the knee of the roll-off;  $\omega_{min} = 2\pi$  rad/s,  $\omega_{max} = 4.5 \times 10^9$  rad/s. Control amplitude:  $\Omega = 1.5 \times 10^6$  rad/s. Numerical simulation involves discretizing the continuous noise functions  $\beta_\mu(t)$ , calculating a single instance of  $U(\tau, 0)$  and a single value for fidelity, and averaging over  $N$  noise realizations. We employ the Karhunen-Loeve filter [129] to simulate discrete noise in the Gaussian limit [130]. Analytical lines representing the fidelity loss calculated by the FF approach [equation (5.4); colored] and by the dc-limit approach [equation (5.6); gray] are plotted. The dc limits for BB1 and CORPSE are below the bounds of the plot at  $1 - \mathcal{F} = 3.9 \times 10^{-9}$  and  $1 - \mathcal{F} = 3.0 \times 10^{-9}$ , respectively.

5.1(b), where we also show, for comparison, FFs for an uncorrected (elementary or ‘primitive’)  $\pi$  rotation. As the latter is expected to have no error-suppressing properties, a comparison of the FFs for CP protocols against the primitive rotation reveals their relative performance advantages; a steeper slope indicates improved (higher-order) error suppression. All compensating sequences show the expected first-order suppression of errors against which they are designed to be effective, in the low-frequency limit. At the same time, they show no improvement over the primitive for the uncompensated error quadrature. Remarkably, our analysis reveals that the

crossover frequency at which the FF for CP protocols becomes larger than that for the primitive is as high as  $\sim 10\%$  of the driving frequency  $\Omega$ . Accordingly, in circumstances where the noise power spectral density is dominated by frequencies below this value, CP sequences are still expected to provide robust error-suppressing performance.

For amplitude noise, it is possible to make connections between the form of the amplitude FF and geometric models commonly used to describe CPs [87, 112, 115, 131]. One may represent a compensating sequence as an initial target rotation, followed by correction rotations, captured through a set of vectors in a multidimensional space. Direct calculation shows that a sequence correcting dc errors to the first order satisfies the condition

$$\sum_l \Omega(t_l - t_{l-1}) \tilde{\rho}_a^{(l)} = 0, \quad \tilde{\rho}_a^{(l)} \equiv \rho_a^{(l)} \Lambda^{(l-1)}. \quad (5.5)$$

If one treats each term in the above sum as a vector of length  $\Omega(t_l - t_{l-1})$  pointing in the direction  $\tilde{\rho}_a^{(l)}$ , then placing the vectors end to end forms a closed figure, demonstrating the effective dc error suppression. In this picture, SK1 yields a triangle, whereas BB1 corresponds to two triangles with opposite-signed area, indicating second-order correction, as expected [87].

Returning to the FF construction, we find that the amplitude-noise FF may be written as

$$F_a(\omega) = \frac{1}{4} \left\{ \left| \sum_l A_l(\omega) \tilde{\rho}_a^{(l)} \right|^2 + \left| \sum_l B_l(\omega) \tilde{\rho}_a^{(l)} \right|^2 \right\},$$

$$A_l(\omega) \equiv \cos(\omega t_l) - \cos(\omega t_{l-1}),$$

$$B_l(\omega) \equiv \sin(\omega t_l) - \sin(\omega t_{l-1}).$$

The above expression for  $F_a(\omega)$  may be interpreted in terms of the magnitudes of two three-dimensional real vectors  $\mathbf{A} \equiv \sum_l A_l(\omega) \tilde{\rho}_a^{(l)}$  and  $\mathbf{B} \equiv \sum_l B_l(\omega) \tilde{\rho}_a^{(l)}$ . When  $\omega$  is small compared to the relevant time scales, Taylor expansion of  $B_l$  shows that, to second order in  $\omega$ , we have  $\sum_l B_l(\omega) \tilde{\rho}_a^{(l)} \approx \frac{\omega}{\Omega} \sum_l \Omega(t_l - t_{l-1}) \tilde{\rho}_a^{(l)} = 0$  which corresponds to (a scaled version of) the closed-loop condition required for error suppression at dc, equation (5.5). To second order,  $A_l \approx \frac{\omega^2}{2}(t_l^2 - t_{l-1}^2)$ , which thus dominates the error. This implies that all CPs for amplitude noise should have FFs that scale at least as  $\omega^4$  in the limit of small  $\omega$ . These observations tie into previous knowledge about general FFs and associated error-suppressing properties [108, 47].

The inset in figure 5.1(a) shows the vectors  $\mathbf{A}$  and  $\mathbf{B}$  divided by  $\omega$  [dashed (green) arrows corresponding to  $B_l/\omega$  and solid (red) arrows corresponding to  $A_l/\omega$ ] and placed end to end for SK1 and BB1, for two values of the dimensionless frequency  $\omega/\Omega$ . At sufficiently small  $\omega$  the dashed (green) arrows trace an approximate closed path, whereas for higher frequencies,  $\omega \geq 0.1\Omega$ , higher-order terms become important. In this case, the resulting figure is no longer closed and the sequence will not be error suppressing, in agreement with the FF analysis presented above. Thus, this geometric picture reflects common observations for dc error analyses, but now lifted to a time-dependent error model, analyzed in the frequency domain.

We can also use the small- $\omega$  limit of  $\mathbf{A}$  and  $\mathbf{B}$  to estimate the crossover frequency at which the CP FF,  $F_a^{\text{CP}}(\omega)$ , will exceed the primitive pulse FF,  $F_a^{\text{P}}(\omega)$ . The primitive pulse FF is determined by the leading term in  $\mathbf{B}$ ,  $F_a^{\text{P}}(\omega) \approx \frac{1}{4}(\omega\tau_p)^2$ , where  $\tau_p$  is the pulse duration. The low-frequency CP FF is determined by the leading term in  $\mathbf{A}$ , which can be bounded from above by making the assumption that all  $\tilde{\rho}_a^{(l)}$  are the same. This results in  $F_a^{\text{CP}} \approx \frac{1}{16}(\omega\tau_{\text{CP}})^4$ , where  $\tau_{\text{CP}}$  is the length of the CP. For SK1 and BB1 with  $\theta = \pi$ ,  $\tau_{\text{CP}} = (4\pi + \theta)/\Omega$  and this bound predicts that the CP will reduce the error,  $F_a^{\text{CP}}(\omega) < F_a^{\text{P}}(\omega)$ , when  $\omega < 0.025\Omega$ . This is an approximate lower bound; the actual crossover frequencies are  $\omega = 0.069\Omega$  for SK1 and  $\omega = 0.127\Omega$  for BB1.

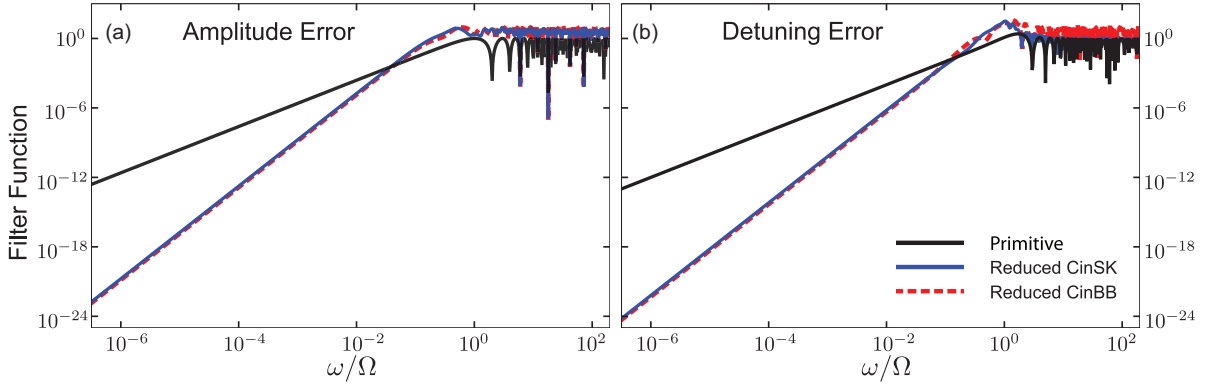


Figure 5.2: FFs as a function of dimensionless frequency for amplitude error (a) and detuning error (b) for concatenated CP sequences Reduced CinSK and Reduced CinBB. Unlike SK1, BB1, CORPSE, and DCG (see figure 5.1), these FFs scale as  $\omega^4$  for both errors.

While these approaches capture the effects of dynamic control noise well, the first-order FF formalism underestimates error in the region  $\omega/\Omega \ll 1$ , corresponding to noise processes fluctuating slowly on the scale of operation time. This may be understood by treating very slow noise as a constant error term equal to the strength of  $H_{\text{err}}$  at the start of the sequence,  $\beta_\mu(0)$ . For small, constant noise an  $m$ th-order CP (or DCG) sequence is well approximated by  $U^{[m]}(\tau, 0) \approx U_0(\tau, 0) \exp[-i\Phi_{m+1}(\tau)]$ , where  $\Phi_{m+1}(\tau)$  is the  $(m+1)$ th order term in the perturbative Magnus expansion [87, 68, 55]. For a qubit like we consider,  $\Phi_{m+1}(\tau)$  is traceless with eigenvalues  $\pm\lambda_{m+1}$  and the magnitude of  $\lambda_{m+1}$  is proportional to  $\beta_\mu(0)^{m+1}$ . The fidelity of the sequence is then  $\mathcal{F} \approx \langle \cos(\lambda_{m+1})^2 \rangle$ . In this limit, the leading-order error term can thus be written as

$$1 - \mathcal{F} \approx \langle \lambda_{m+1}^2 \rangle = c_{m+1} \langle \beta_\mu(0)^{2(m+1)} \rangle, \quad (5.6)$$

where the proportionality constant  $c_{m+1}$ , like  $F_\mu(\omega)$ , depends on the sequence and the noise axis but not the noise strength.

As an example, consider SK1 with constant noise  $\beta_a(0)$ . The leading-order Magnus term is

$$\begin{aligned} \Phi_2(\tau) &= i \frac{\beta_a(0)^2}{2} \int_0^\tau dt \int_0^t dt' [\rho_a(t), \rho_a(t')] \\ &= \beta_a(0)^2 \pi^2 \sin(2\phi_1) \sigma_z, \end{aligned}$$

where  $\phi_1 = \cos^{-1}(-1/4)$  (table 5.1). The eigenvalues of  $\Phi_2$  are  $\pm\lambda_2 = \pm\beta_a(0)^2 \pi^2 \sin(2\phi_1)$ , and as a result,  $1 - \mathcal{F} \approx (\pi^2 \sin(2\phi_1))^2 \langle \beta_a(0)^4 \rangle$ . The term  $c_2 = (\pi^2 \sin(2\phi_1))^2$  depends only on the pulse sequence and  $\langle \beta_a(0)^4 \rangle$  is averaged over the ensemble of initial noise strengths.

The error of the first-order fidelity approximation in the FF formalism [equation (5.4)] depends only on the first-order Magnus term [equation (5.3)], so the slow-noise (dc) limit contains fidelity loss contributions from higher-order FF terms that are ignored in the first-order approximation (see also [108] for additional details). For a zero-mean Gaussian noise described by a spectral density  $S(\omega)$ , by definition,  $\langle \beta_\mu(0)^2 \rangle = \int_{-\infty}^{\infty} d\omega S_\mu(\omega)$ . All odd orders of the expectation value are 0 and all even orders are proportional to powers of the second-order expectation value,

$$\langle \beta_\mu(0)^{2(m+1)} \rangle = (2m+1)!! \left( \int_{-\infty}^{\infty} d\omega S_\mu(\omega) \right)^{m+1}.$$

We may therefore estimate the analytical fidelity loss over the entire frequency range by combining the contributions from equation (5.4) and equation (5.6).

### 5.3.2 Comparison with numerical results

Quantifying the fidelity loss [equation (5.4)] for control protocols implemented in a real (classical) noise environment requires one to choose a specific noise spectrum. As a practical example, we consider  $1/f$  Gaussian noise with a roll-off to  $1/f^2$  noise at high frequency with spectrum

$$S_\mu(\omega) = \begin{cases} A_\mu/\omega, & \omega_{min}^\mu < \omega < \omega_b^\mu, \\ \omega_b^\mu \cdot A_\mu/\omega^2, & \omega_b^\mu < \omega < \omega_{max}^\mu, \\ 0 & \text{otherwise,} \end{cases} \quad (5.7)$$

where  $A_\mu$  is a constant amplitude for the two error quadratures  $\mu \in \{a, d\}$ . This type of noise is frequently encountered in experimental qubit systems over a wide frequency range [33, 132, 133] and naturally arises from independent bistable fluctuators [134]. The generality of this power spectrum in various noise processes allows us to reasonably assume the same power spectrum for both amplitude and detuning noise, despite the fact that these two noise sources have different physical origins in general and, as remarked, we take them to be independent. Nonetheless, we emphasize that our methods are independent of the specific form of the power spectrum assumed in our numerical calculations.

We analytically compute the fidelity loss according to equation (5.4) in combination with the asymptotic error floor, equation (5.6). These analytic results are compared to numerical data obtained from simulation of the Bloch vector evolution under the noisy Hamiltonian in equation (5.1). Provided that the number of noise realizations,  $N$ , over which we average is large enough (typically  $N \geq 10^4$ ), this numeric simulation can be considered a reliable direct method for calculating the fidelity. For the three first-order protocols studied (SK1, CORPSE, and DCG), figures 5.1(c) and 5.1(d) show that, as the roll-off frequency is reduced, the fidelity loss is well approximated by the combination of the FF estimate and dc limit (lines). Vitally, both the analytic and the numerical approach directly reveal the robustness of CP protocols against noise fluctuations up to  $\sim 0.1\Omega$ . Detailed performance variation in the slow-noise limit stems from differences in construction of the selected gate protocols. The DCG and CORPSE sequences both correct dc detuning noise to the first order and have first-order FFs for time-dependent errors. While for frequencies below  $\sim 10\%$  of the Rabi frequency the DCG has an FF of lower magnitude than CORPSE, the specific CORPSE sequence used is designed to additionally minimize the residual second-order dc prefactor [87] [namely,  $c_2$  in equation (5.6)], which results in a dc limit of  $X$  well below the plotted fidelities. The resulting relative performance between the DCG and the CORPSE protocols further depends on the specifics of the noise power spectral density. Similarly, the effective second-order dc error cancellation associated with BB1 means that the dc limit does not provide a substantial contribution relative to the FF calculation for the example noise spectrum.

Finally, we extend our analysis to include representative concatenated CP sequences (table 5.1). We see that the FFs of the concatenated CP sequences depicted in figure 5.2 exhibit error suppression for both forms of error at low frequencies relative to a primitive pulse, in contrast to the standard CP sequences. In the presence of simultaneous noise, this leads to substantially improved performance when both noises are slow. Figure 5.3 presents a quantitative comparison of analytical and numerical fidelity-loss calculations for the primitive  $\pi$  pulse and for reduced CinBB, showing good agreement between the two approaches. For this two-parameter compensating sequence, the constant-error dc fidelity limit may be seen to arise due to a cross-term of the two noise sources, namely,

$$1 - \mathcal{F} = c_{1,1} \langle \beta_a(0)^2 \beta_d(0)^2 \rangle, \quad (5.8)$$

where  $c_{m+1,n+1}$  is the cross-term equivalent of  $c_{m+1}$  for single noise sources in equation 5.6. As

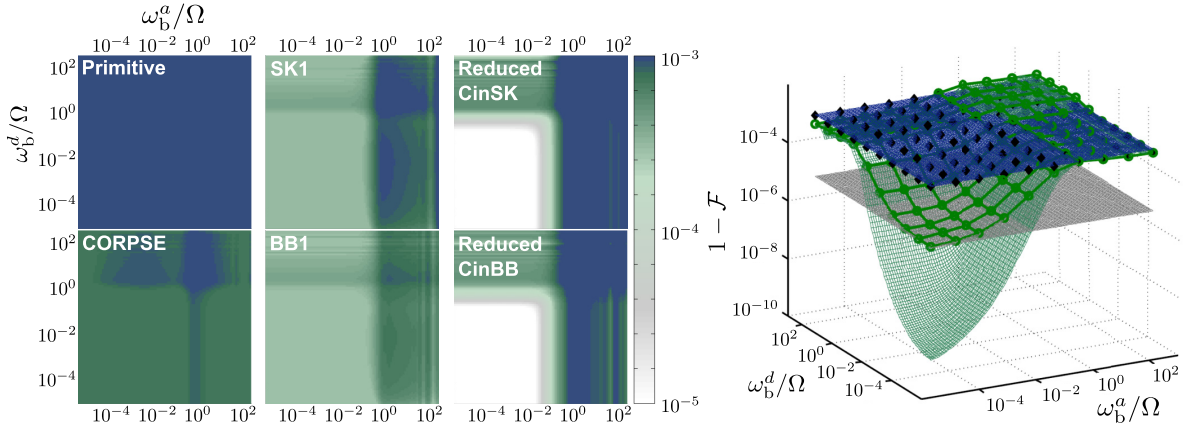


Figure 5.3: *Performance of CPs under simultaneous amplitude and detuning noise, as a function of dimensionless frequency roll-off from  $1/f$  to a  $1/f^2$  spectral density,  $\omega_b^a$  and  $\omega_b^d$ , respectively. Spectrum and control parameters as in figure 5.1.* Left: Analytical results for fidelity loss. For each point the FF and dc-limit calculations are compared and the larger fidelity loss value is plotted. Right: Analytical (FF, green surface; dc limit, gray surface) and numerical results (green circles and mesh) for Reduced CinBB vs analytical (dc limit, blue surface) and numerical (black diamonds) results for a primitive pulse.

the data show, the resulting dc limit matches the fidelity loss in the very-low-frequency regime for the reduced CinBB sequence

Our numerical calculations validate the insights provided by the analytic FF formalism and demonstrate that, in combination with the calculated dc error floor, the first-order FF is an effective tool for predicting single-qubit control performance in the presence of time-dependent noise. The analytic approach comes with an additional benefit, however, in terms of computational efficiency; the numerical calculations of fidelity loss under time-dependent noise are in fact significantly more computationally intensive than the FF approach.<sup>1</sup> While this is beyond our current purpose, this advantage is likely to become even more dramatic in more complex control scenarios, in particular, including multiple qubits.

## 5.4 Conclusion

We have shown that CP sequences originally designed to compensate only for static control errors may be successfully employed for non-Markovian time-dependent control and/or environmental errors as well. Our numeric and analytic results demonstrate that these sequences are robust against noise fluctuations up to  $\sim 10\%$  of the control frequency, a surprisingly high value. In addition to substantially expanding the practical significance of open-loop quantum control protocols, our analysis further establishes the utility of FFs as a unifying and computationally efficient framework for estimating and understanding the performance of coherent control protocols under realistic noise spectra. Furthermore, we have shown that, at least for the single-qubit setting under consideration, slow noise can be accurately modeled by a dc-limit approximation that can be combined with the FF approach to accurately estimate control performance over a broader frequency range. Altogether, our results show that, in combination,

<sup>1</sup>For our current analysis, numerical calculation of the fidelity numerically requires the generation of  $N \geq 10^4$  noise trajectories for each spectral density. The FF and dc-limit calculations of fidelity require only two numerical integrals per spectral density.

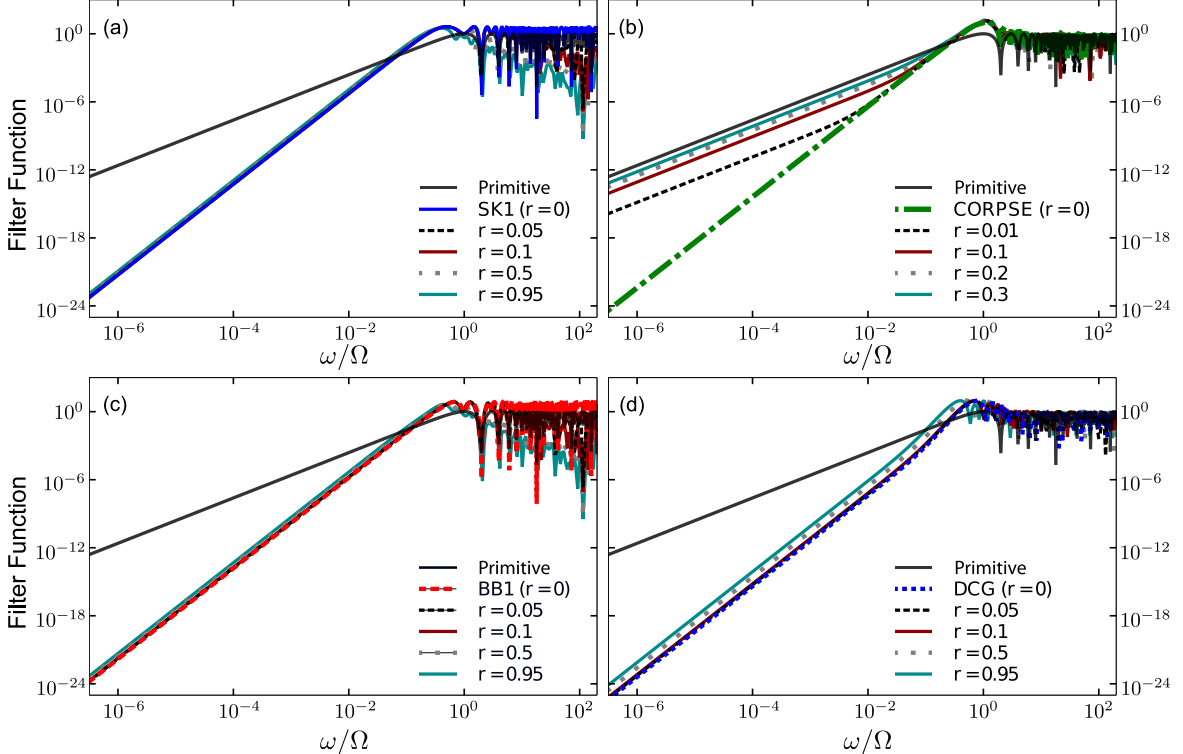


Figure 5.4: FFs as a function of dimensionless frequency for SK1 (a) and BB1 (c) in the presence of multiplicative amplitude noise and for CORPSE (b) and DCG (d) in the presence of detuning noise. The CPs are constructed from trapezoidal pulses with ramp time  $r$  in units of  $\pi/\Omega$ .

CP and DCG protocols provide experimentalists with a viable toolkit capable of meeting a variety of constraints, including the presence of colored time-dependent control noise. We further expect that the geometric picture we have developed, in conjunction with the FF approach, may prove instrumental for finding new CPs which are resilient to specific noise spectra.

*Acknowledgements:* It is a pleasure to thank Harrison Ball, J. True Merrill, and Alexander Soare for helpful comments. This work was supported by the Office of the Director of National Intelligence/IARPA through ARO Contract No. W911NF-10-1-0231 and Department of Interior Contract No. D11PC20167, ARC Centre for Engineered Quantum Systems Grant No. CE110001013, the US ARO under Contract No. W911NF-11-1-0068, and Lockheed Martin Corporation.

The views and conclusions contained herein are those of the authors and should not be interpreted as necessarily representing the official policies or endorsements, either expressed or implied, of IARPA, DoI/NBC, or the US Government.

## 5.5 Appendix

In actual experiments, the pulse shape deviates from the ideal square pulses under which CPs are derived. This is often done on purpose when, for example, Gaussian pulses or Blackman pulses are used to limit the spectral bandwidth of the control [135]. This also occurs accidentally due to bandwidth limitations of the instrument resulting in fast amplitude fluctuations or slow turn-off times. Although the FF formalism as described in section 5.2.2 assumes piecewise-constant control, continuous pulse-modulation profiles can be analyzed by a discrete time-step

approximation. We apply this approximation to examine the effect of pulse shape on CP FFs for amplitude and detuning noise. We expect that the FF of amplitude noise CPs will be weakly dependent on the pulse shape since amplitude noise, unlike detuning noise, commutes with the control pulse. In fact, using the error model of equation (5.1), the FF is pulse shape independent if the total pulse time is the same as the square pulse it replaces. CPs for amplitude noise were developed assuming that the error is proportional to the control (multiplicative noise). This noise can be modeled in our formalism by replacing  $\beta_a(t)$  in equation (5.1) with  $\Omega_l/\Omega_{max}\beta_a(t)$ . We note that additive and multiplicative error models are equivalent for the constant  $\Omega$  pulses considered in the main text. In the case of multiplicative noise, static error correction only requires that the rotation angle be constant. On the other hand, detuning noise does not commute with the control, and as a result the pulse shape can have a significant effect.

As an example, we examine trapezoidal pulses where the  $k$ th pulse is ramped up to  $\Omega_k$  in a time  $r$ , held for a time  $w$ , and then ramped down in a time  $r$ . The total pulse time is  $w + 2r$ , and  $w + r$  is held constant to preserve the rotation angle. For the CPs studied here,  $\Omega_k = \Omega$ . BB1 and SK1 are designed assuming a systematic and proportional error in the rotation angle. This is preserved for multiplicative amplitude noise, and we see that the FF form is maintained (figure 5.4). There is an increase in the magnitude of the FF in the small- $\omega$  region due to the increase in the overall sequence length in time.

CORPSE is designed under the assumption of square pulses and the detuning is additive. Consequently, trapezoidal pulses do not perfectly remove the first-order error using the rotation angles of CORPSE. This changes the asymptotic behavior of the FF and we see a bend corresponding to the residual  $\omega^2$  term due to imperfect error cancellation [figure 5.4(b)]. The bend occurs at lower frequencies as the control approaches a square profile. In contrast, the design of  $\pi$  DCG does not assume square pulses [68, 55]. The static error cancellation will occur if the first and the third pulses have the same time-dependent control profile applied for a total time  $T$  and the second pulse has the stretched and scaled control profile applied for time  $2T$ . The parameters for the first and second trapezoidal pulses are related as follows:  $2r_1 - r_2$ ,  $2w_1 - w_2$ , and  $\Omega_1/2 = \Omega_2$ . The FF form at small  $\omega$  remains unchanged and the magnitude again increases with overall sequence length [figure 5.4(d)]. In practice, if square pulses are not an adequate approximation, then CORPSE should not be used. Instead a DCG should be chosen or one can derive a CORPSE-like sequence using soft pulses to achieve similar slow-noise cancellation [136].

# Chapter 6

## Experimental noise filtering by quantum control

Extrinsic interference is routinely faced in systems engineering, and a common solution is to rely on a broad class of *filtering* techniques in order to afford stability to intrinsically unstable systems or isolate particular signals from a noisy background. Experimentalists leading the development of a new generation of quantum enabled technologies similarly encounter time-varying noise in realistic laboratory settings. They face substantial challenges in either suppressing such noise for high-fidelity quantum operations [137] or controllably exploiting it in quantum-enhanced sensing [138, 139, 140] or system identification tasks [141, 93], due to a lack of efficient, validated approaches to understanding and predicting quantum dynamics in the presence of realistic time-varying noise. In this work we use the theory of quantum control engineering [79, 80] and experiments with trapped  $^{171}\text{Yb}^+$  ions to study the dynamics of controlled quantum systems. Our results provide the first experimental validation of generalized filter-transfer functions casting arbitrary quantum control operations on qubits as *noise spectral filters* [100, 108]. We demonstrate the utility of these constructs for directly predicting the evolution of a quantum state in a realistic noisy environment as well as for developing novel robust control and sensing protocols. These experiments provide a significant advance in our understanding of the physics underlying controlled quantum dynamics, and unlock new capabilities for the emerging field of quantum systems engineering.

The contents of this chapter have been published as: A. Soare, H. Ball, D. Hayes, J. Sastrawan, M. C. Jarratt, J. J. McLoughlin, X. Zhen, T. J. Green and M. J. Biercuk, “Experimental noise filtering by quantum control”, *Nature Physics* **10**, 825 (2014). Here, we demonstrate the utility of the filtering perspective (section 2.4.2) in an experimental context.

### 6.1 Introduction

Time-varying noise coupled to quantum systems – typically qubits – generically results in decoherence, or a loss of ‘quantumness’ of the system. Broadly, one may think of the state of the quantum system becoming randomized through uncontrolled (and often uncontrollable) interactions with the environment during both idle periods and active control operations (figure 6.1a). Despite the ubiquity of this phenomenon, it is a challenging problem to predict the average evolution of a qubit state undergoing a specific, but arbitrary operation in the presence of realistic time-dependent noise – how much randomization does one expect and how well can one per-

form the target operation? Making such predictions accurately is precisely the capability that experimentalists require in realistic laboratory settings. Moreover, this capability is fundamental to the development of novel control techniques designed to modify or suppress decoherence as researchers attempt to build quantum-enabled technologies for applications such as quantum information and quantum sensing.

These considerations motivate the development of novel engineering-inspired analytic tools enabling a user to accurately predict the behavior of a controlled quantum system in realistic laboratory environments. Recent work has demonstrated that the average dynamics of a controlled qubit state evolution may be captured using *filter transfer functions* (FFs) characterizing the control. The fidelity of an arbitrary operation over duration  $\tau$ ,  $\mathcal{F}_\chi(\tau) \propto e^{-\int_0^\infty d\omega S(\omega)F(\omega)}$ , is degraded due to frequency-domain spectral overlap between noise in the environment given by a power spectrum  $S(\omega)$ , and the filter transfer functions denoted  $F(\omega)$  (see Appendix A) [49, 67, 53, 47].

The FF description of ensemble-average quantum dynamics tremendously simplifies the task of analyzing the expected performance of a control protocol in a noisy environment as it permits consideration of control as *noise spectral filtering*. The FFs themselves may be described using familiar concepts such as frequency passbands, stopbands, and filter order, enabling a simple graphical representation of otherwise complex concepts in the dynamics of controlled quantum systems (figure 6.1b). Noise filtering, in practice, is achieved through construction of a control protocol (figure 6.1a) which modifies the *controllability* of the quantum system by the noisy environment *over a defined frequency band*. Adjusting  $F(\omega)$  and changing its overlap with the noise spectrum thus allows a user to change the average dynamics of the system in a predictable way.

To see the importance of this capability we may consider the various tasks that might be of interest in experimental quantum engineering and the role of noise spectral filtering in these applications. In quantum information an experimentalist may aim to suppress broadband low-frequency noise in order to maximize the fidelity of a bounded-strength quantum logic operation (figure 6.1b, upper trace), and then calculate the residual error. Alternatively, in quantum enabled sensing or system identification he or she may perform narrowband spectral characterization of a given operation (figure 6.1b, lower trace), where any change in the measured fidelity under filter application represents the signal of interest [93, 140].

The intuitive nature of this framework is belied by the challenge of calculating FFs for arbitrary control protocols, generally involving time-domain modulation of control parameters such as the frequency and amplitude of a driving field. The nature of quantum dynamics means that the implemented control framework is generally nonlinear; for instance, one finds complex dynamics in circumstances where the noise and control operations do not commute such as a driven operation ( $\propto \sigma_x$ ) in the presence of dephasing noise ( $\propto \sigma_z$ ). Recent theoretical effort has allowed calculation of FFs for arbitrary single-qubit control and arbitrary universal classical noise [100, 108], expanding significantly beyond previous demonstrations restricted to the identity operator in pure-dephasing environments [32]. It is this more general case where the impact of noise filtering and the FFs may have the most significant impact on the quantum engineering community, and where experimental tests are vital.

## 6.2 Results

In our experimental system, based on the 12.6 GHz qubit transition in  $^{171}\text{Yb}^+$  (Appendix B), we are able to perform quantitative tests of operational fidelity for arbitrary control operations; these may then be compared against calculations of  $\mathcal{F}_\chi(\tau)$  as a fundamental test of FF validity. A key tool in our studies is bath engineering [127], in which we add noise with user-defined

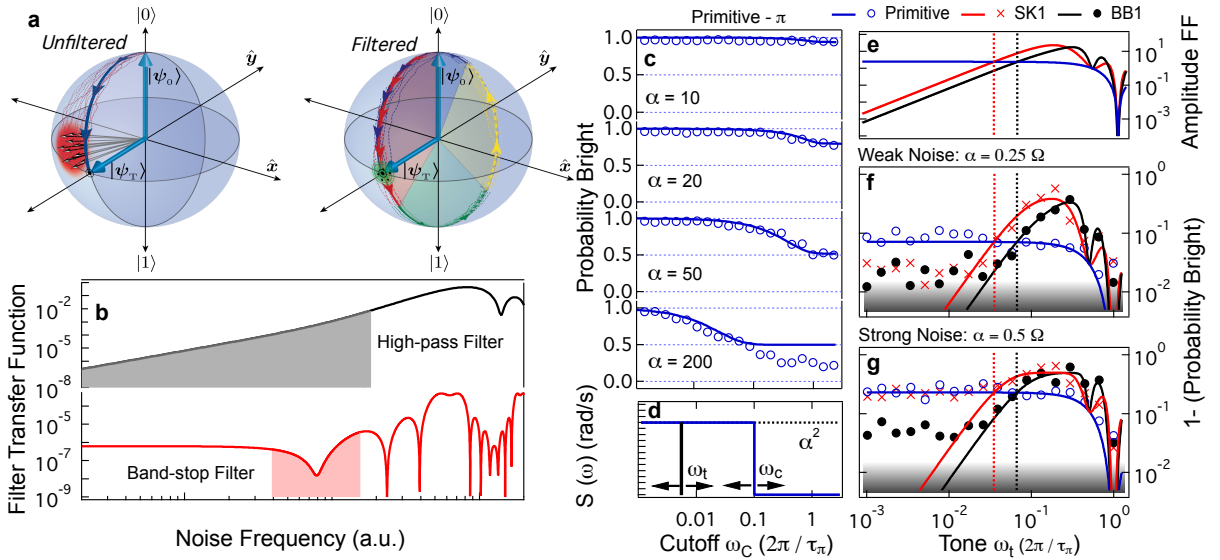


**Figure 6.1:** *Noise filters and experimental validation of the predictive power of the filter transfer function.* a) Time-varying noise during an operation (a rotation on the Bloch sphere, here  $\theta = \pi/2$ ,  $\phi = 0$ ) produces a broad range of outcomes (red uncertainty cone, left) and may yield an offset of the average final state from the target state, measured as operational infidelity. Schematic filtered state evolution, depicted as a user-defined modulation pattern on the control (colored segments), changes the measured fidelity by reducing the uncertainty due to noise in a specified band. b) Schematic representation of noise filters of interest - shaded areas represent filter stop-bands - crafted by control modulation as indicated above. c) Measurements of operational fidelity with engineered dephasing noise for primitive  $\pi$  rotation,  $|0\rangle \rightarrow |1\rangle$ , as a function of dimensionless noise cutoff frequency overlaid with FF-based calculations of  $\mathcal{F}_\chi(\tau)$ . Decay to value 0.5 corresponds to full decoherence. Each data point is the result of averaging over 50 different noise realizations. (d) Schematic representation of the quasi-white noise power spectrum employed in (c) and single-tone power spectrum employed in (f-g). Noise strength parameterized by  $\alpha$ . e) Calculated  $F_\Omega(\omega)$ , for primitive and compensating  $\pi$  pulses (see [87]). Vertical lines indicate frequencies where  $F_\Omega(\omega)$  for SK1 (red) and BB1 (black) cross primitive (blue), indicating an expected inversion of performance. f)-g) Swept-tone multiplicative amplitude noise measurements,  $S_\Omega(\omega) \propto \delta(\omega_t - \omega)$ , for various  $\pi$  rotations (averaged over 20 noise realizations). Vertical axis is a proxy for measured operational infidelity. Solid lines indicate  $1 - \mathcal{F}_\chi(\tau)$ , revealing good agreement in the weak noise limit (f) across three decades of frequency, down to measurement fidelity limit,  $\sim 98.5\%$ , indicated by grey shading. Measured gate-error crossover points correspond well with crossovers in the FFs for these gates (vertical dashed lines). Detailed performance differences between protocols in the low-error limit can be revealed through randomized benchmarking, as performed later (figure 6.3). g) Strong-error limit, first-order approximations are violated and contributions from higher-order Magnus terms contribute to the measured error in the low-frequency limit, yielding (expected) differences between SK1 and BB1 due to Magnus order cancellation and not captured by the FF.

spectral characteristics to the control system, producing well controlled unitary dephasing or depolarization.

As a first example, experimental measurements of operational fidelity for a  $\pi_x$ -pulse driving qubit population from the dark state to the bright state,  $|0\rangle \rightarrow |1\rangle$ , in the presence of engineered time-dependent dephasing noise give good agreement with analytic calculation of  $\mathcal{F}_x(\tau)$  using the noise power spectrum and analytic FFs [108] with *no free parameters* (see *Appendix A*). This approach therefore immediately demonstrates the predictive power of the FF formalism.

The FFs for much more complex control such as compensating composite pulses [142, 87] can be calculated and experimentally validated as well (figure 6.1e). These protocols are commonly used in nuclear magnetic resonance and electron spin resonance in attempting to suppress static offsets in control parameters such as the frequency of the drive inducing spin rotations. Calculating the FFs for these protocols now reveals their sensitivity to *time-dependent* noise - an important characteristic for deployment in realistic quantum information settings [143]. We experimentally demonstrate a form of quantum system identification (see *Appendix A*), effectively reconstructing the amplitude-noise filter functions,  $F_\Omega(\omega)$ , for two well known compensating pulse sequences known by the shorthand designations SK1 and BB1 (Appendix B). Again, calculations of  $\mathcal{F}_x(\tau)$  match data well over the entire band in the weak noise limit (figure 6.1f) with *no free parameters*.

Our choice of characterizing these compensating pulse sequences highlights an important issue in the prediction of ensemble-average dynamics of controlled quantum systems. Ultimately, the underlying physical principles giving rise to the analytic form of  $F(\omega)$  are based on the well tested average Hamiltonian theory [20] exploited in crafting these pulses. Despite this shared theoretical foundation, the calculation of spectral filtering properties is quite distinct from calculation of quasi-static error terms in a Magnus expansion, with important consequences for average quantum dynamics in realistic time-varying noise environments [108].

Accordingly, our tests of the FF formalism reveal that compensating pulses designed to suppress errors to high order in a Magnus-expansion framework *need not* be efficient noise spectral filters (Appendix B and reference [143]). Despite significant differences in their construction – the BB1 protocol is designed to provide higher-order cancellation of Magnus terms than SK1 – both of the selected composite pulses provide similar filtering of time-dependent noise, given by the *filter order* (slope of the FF in figure 6.1e). In the weak-noise limit frequency-domain characteristics are captured accurately through the FF across frequencies ranging from quasi-static to rapidly fluctuating on the timescale of the pulse (figure 6.1f). Performance deviations between the pulses arise and the FF approximation breaks down as the noise strength is increased and higher order terms in the Magnus series become important, but *only at low frequencies* (figure 6.1g). At frequencies fast relative to the control the FF again accurately predicts the relevant quantum dynamics even in the strong-noise limit. This is the first direct manifestation of the difference between studying quantum dynamics in terms of frequency-domain noise filtering and calculation of error contributions in a Magnus expansion as is appropriate in the quasi-static limit.

These simple but powerful validations of the predictive power of the generalized FF formalism now open the possibility of demonstrating the *construction* of noise filters with a specified spectral response, employing the filter transfer functions as key analytic tools. Filters may take a wide variety of forms as needed by users - including high-pass filters for broadband noise suppression and band-stop filters useful for narrowband noise characterization (figure 6.1b).

In the discussion that follows, we focus on a common setting in which we aim to improve operational fidelity by reducing the influence of broadband non-Markovian noise on a target state transformation. Filters are realized as  $n$ -step sequences of time-domain control operations with tunable pulse amplitude and phase, similar in spirit to compensating composite pulses in NMR [142, 87, 143], dynamically corrected gates (DCGs) in quantum information [68, 144],

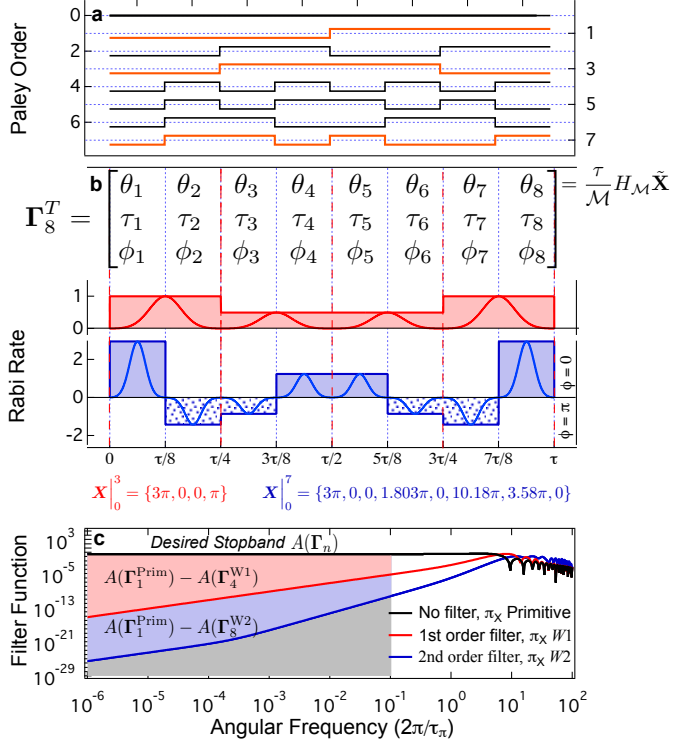


Figure 6.2: Synthesis of high-pass amplitude-modulated filters from the Walsh functions. a) The first eight Walsh functions used in filter synthesis,  $\{PAL_0, PAL_7\}$ , with maximum-Hamming-weight-indexed functions highlighted. b) Representative amplitude profiles for filter constructions found via numerical search over the Walsh basis with four (red, denoted  $W1$ ) and eight (blue, denoted  $W2$ ) time steps. Vertical axis represents  $\Omega$ , the Rabi rate per time step; negative values indicate  $\pi$ -phase shifts. Synthesis may be performed over square (flat-top) pulse-segments or Gaussian-shaped pulse segments with results differing only in the resulting Walsh coefficients. The matrix representing filter characteristics over eight segments is superimposed on the amplitude profiles (for  $n = 4$ , neighboring segments between red dashed lines are combined). The first row (the angles of rotation in each segment of the filter) is determined via Walsh synthesis, indicated by the vectors  $X|_0^n$ , containing the spectral weights over  $PAL_0 \rightarrow PAL_n$ . In the case of Gaussian pulse envelopes Walsh synthesis sets the first line,  $\theta_l$ . The symbol  $\tilde{X}$  indicates reordering for Hadamard synthesis, with listed coefficients appropriate for square pulse envelopes. c) The filter transfer function for a primitive  $\pi_x$  rotation and for synthesized noise filters. Performance improvement over the desired stopband of the filter captured in cost function  $A(\Gamma_4^{W1(W2)})$  and its difference relative to that for the primitive operation,  $A(\Gamma_1^{Prim})$ . Filter  $W1$  gives improvement indicated by the red shading, with additional improvement in the cost function given by  $W2$  indicated by blue shading.

and open-loop modulated pulses in quantum control [97, 145]. However, recalling the difference between Magnus cancellation order and filtering order described above, in this setting we wish to synthesize a filter with arbitrary, user-defined spectral characteristics captured by a cost-function,  $A(\Gamma_n)$ , to be minimized for a filter represented by  $\Gamma_n(\theta_l, \tau_l, \phi_l)$  (figure 6.2b-c, *Appendix A*).

To provide *efficient* solutions to filter design we restrict our control space and focus on constructions synthesized using concepts from functional analysis in the basis set of *Walsh functions* - square-wave analogues of the sines and cosines [146, 75, 140] (figure 6.2a). This approach provides significant benefits for our problem [75], but is by no means the only basis set for composite filter construction [147, 148].

As an example we synthesize filters via weighted linear combination of Paley-ordered Walsh functions,  $PAL_k(x)$ , designed to suppress time-varying dephasing noise over a low-frequency stopband while implementing a bounded-strength driven rotation about the  $x$ -axis on the Bloch sphere (*Appendix B*). In this case the Walsh-synthesized waveform dictates an amplitude modulation pattern for the control field over discrete time-segments. Importantly, Walsh filter synthesis is compatible with pulse segments possessing *arbitrary pulse envelope*, including sequences of *e.g.* square (used here) or Gaussian pulse segments (figure 6.2b).

Analytic design rules provide simple insights into how one may craft effective modulation protocols, and a Nelder-Mead simplex optimization is used to find high-performing operations as defined by our cost function. Relative to an unfiltered primitive gate,  $F_z(\omega)$  for the simplest four-pulse construction  $W1$  shows increased steepness in the stopband (figure 6.2c, red), reducing  $A(\Gamma_4)$  (here the gate performs  $\theta = \pi$ ). This measure of filter order may be further increased via construction  $W2$ , in turn reducing the cost function for optimization (blue shaded area in figure 6.2c). Relating back to earlier demonstrations of filter order in compensating pulses,  $W2$  presents an interesting case of a high-order noise filter over the target band which provides only first-order Magnus cancellation.

Filters  $W1$  and  $W2$  are representative, rather than unique solutions. In figure 6.3b we show the calculated cost function,  $A(\Gamma_4)$ , as a function of the Walsh coefficients used in constructing  $W1$ ,  $X_0$  and  $X_3$ . Blue areas meet our minimized target indicating useful filters, revealing a wide variety of possible constructions with favorable characteristics. Experimental tests of these protocols reveal that Walsh-modulated waveforms minimizing  $A(\Gamma_4)$  effectively suppress noise in the designated stop-band for arbitrary rotation angles (figure 6.3c-e), and outperform standard pulses in the small-error limit germane to quantum information (figure 6.3f). See *Appendix A*.

## 6.3 Conclusion

Our focus has been on providing a validated framework for the vital task of predicting quantum dynamics in realistic environments and demonstrating the relevant physics through construction of noise spectral filters. The Walsh modulated filters presented here - based on the achievable frequency-domain filter order - complement existing techniques rather than attempting to provide optimal-performance error-robust gates. Our results on high-pass noise filters, for instance, add to existing compensating pulse sequences designed for quasi-static noise, as well as gate constructions with interleaved dynamical decoupling that seek to periodically ‘refocus’ quantum evolution [149, 150, 151, 152].

Importantly, recent work has demonstrated that the filter transfer function formalism is applicable to multi-qubit settings where dynamics may be considerably more complex than the single-qubit case [153, 43, 154]. In addition, ongoing efforts suggest there exists a path towards further extension of the generalized filter transfer function and noise filtering formalisms to ar-

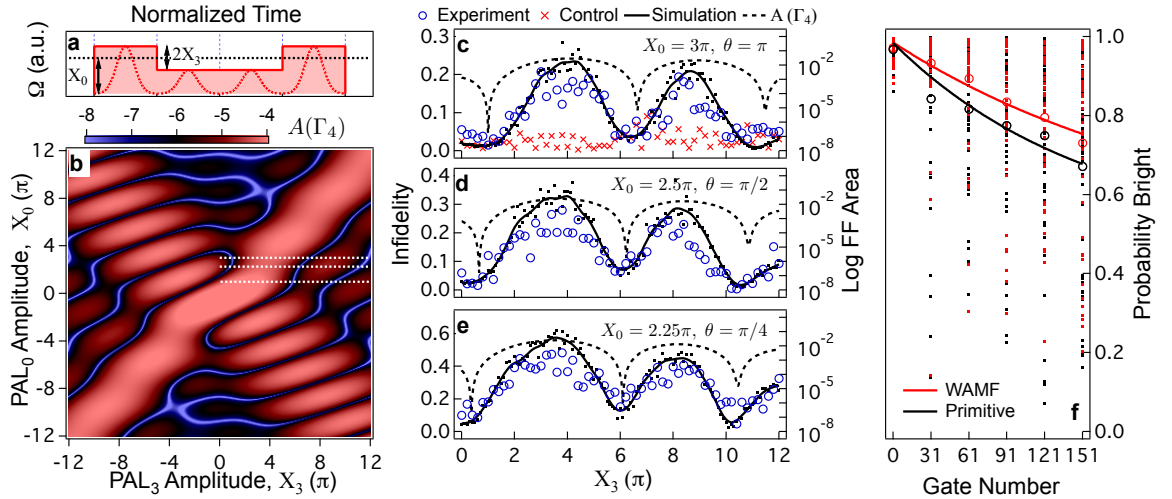


**Figure 6.3: Construction of the first-order Walsh amplitude modulated dephasing-suppressing filter.**

a) Schematic representation of Walsh synthesis for a four-segment amplitude-modulated filter (WAMF). Walsh synthesis can be used to determine either the modulating envelope of square pulse segments, or the net area of discrete Gaussian pulses with differing amplitudes. b) Two-dimensional representation of the integral metric defining our target cost function,  $A(\Gamma_4)$  integrated over the stopband  $\omega \in [10^{-9}, 10^{-1}]\tau^{-1}$ . Areas in blue minimize  $A(\Gamma_4)$ , representing effective filter constructions. The  $X_0$  determines the net rotation enacted in a gate while  $X_3$  determines the modulation depth, as represented in a). White lines indicate possible constructions for filters implementing rotations of  $\theta = \pi$ ,  $\theta = \pi/2$ , and  $\theta = \pi/4$  from top to bottom. c)-e) Experimental measurement of gate infidelity (left axis) for rotations constructed from various Walsh coefficients in the presence of engineered noise ( $\omega_c/2\pi = 20$  Hz). Black dots and line represented calculated fidelity by Schrödinger equation integration (raw and smoothed respectively). All values of  $X_3$  for a given  $X_0$  implement the same net rotation, indicated by control experiment with no noise. Total rotation time is scaled with  $X_3$  to preserve a maximum Rabi rate. Black dashed line (right axis) corresponds to  $A(\Gamma_4)$  from panel (a). In experiments we always perform a net  $\pi$  rotation  $|0\rangle \rightarrow |1\rangle$  by sequentially performing identical copies of rotations for  $\theta < \pi$ . f) Randomized benchmarking results (50 randomizations) demonstrating superior performance of modulated gate in the small-error limit (infidelity  $< 0.5\%$  per gate), see Appendix B.

bitrary control settings involving multiple qubits subject to general noise from non-Markovian classical and/or quantum mechanical environments. We believe that with the validations provided here, this simple extensible framework with precise predictive power will provide a path for experimentalists to characterize and suppress the effects of noise in generic quantum coherent technologies, ultimately enabling a new generation of engineered quantum systems.

*Acknowledgements:* We thank P. Fisk, M. Lawn, M. Wouters, and B. Warrington for technical assistance and K. Brown, J.T. Merrill and L. Viola for useful discussions. This work partially supported by the US Army Research Office under Contract Number W911NF-11-1-0068, and the Australian Research Council Centre of Excellence for Engineered Quantum Systems CE110001013, the Office of the Director of National Intelligence (ODNI), Intelligence Advanced Research Projects Activity (IARPA), through the Army Research Office, and the Lockheed Martin Corporation.

## 6.4 Appendix A

The fidelity of a control operation for a single qubit in the presence of a time-dependent environment is reduced as  $\mathcal{F}_\chi(\tau) = \frac{1}{2}(1 + e^{-\chi(\tau)})$ , where  $\chi(\tau) = \frac{1}{\pi} \sum_i \int_0^\infty d\omega S_i(\omega) F_i(\omega)$ , and  $\tau$  is the total duration of the operation. In this expression for fidelity, the integral considers contributions from independent noise processes through their frequency-domain power spectra  $S_i(\omega)$ ,  $i \in \{z, \Omega\}$ , capturing dephasing along  $\hat{z}$  and amplitude noise co-rotating with a resonant drive field (Appendix B). We employ here the so-called modified filter transfer function, which subsumes a factor of  $\omega^{-2}$  into the definition of  $F_i(\omega)$ . See [47, 93] for details.

Experimental measurements involve state initialization in  $|0\rangle$  followed by a control operation - or series of control operations - designed to drive qubit population from the dark state to the bright state,  $|0\rangle \rightarrow |1\rangle$ . For instance, tests of filters used for rotations  $\theta < \pi$  are repeated sequentially such that the net rotation enacts  $|0\rangle \rightarrow |1\rangle$  (see figure 6.3d-e). The operational fidelity is measured as the probability that the qubit is in the bright state over an ensemble of measurements. In general, a non-Markovian noise bath is engineered with specific properties of interest (see Appendix B for full details).

Measurements in figure 6.1c are conducted for a simple  $\pi_x$  enacted while varying the high-frequency cutoff,  $\omega_c$ , of a flat-top engineered non-Markovian dephasing bath (figure 6.1d). As the high-frequency cutoff of the noise is increased and fluctuations fast compared to the control ( $\tau_\pi$ ) are added to the noise power spectrum,  $S_z(\omega)$ , errors accumulate reducing the measured fidelity. For  $\omega_c/2\pi = 1$  the highest frequency contribution to  $S_z(\omega)$  undergoes a complete cycle of oscillation over  $\tau_\pi$ , indicating that the noise is time-dependent on the scale of a single experiment even for  $\omega_c/2\pi \ll 1$ . We calculate  $\mathcal{F}_\chi(\tau)$  using the form of the noise and the analytic FF for a driven primitive gate under dephasing [108], finding good agreement with experimental measurements using *no free parameters*.

Measurements in figure 6.1f-g employ a narrowband ‘delta-function’ noise power spectrum swept as an experimental variable,  $\omega_t$ . The form of  $\mathcal{F}_\chi(\tau)$  demonstrates that the calculated fidelity involves an exponentiated value of the FF at frequency  $\omega_t$ , meaning that fidelity measurements effectively reconstruct the filter functions. Key features in the data such as performance-crossover frequencies between primitive and compensating gates and deep notches in the filter at high frequency are quantitatively reproduced in experimental measurements.

Filter construction presented in figures 6.2 and 6.3 is parametrized as a function of controllable properties of a near-resonant carrier frequency enacting driven operations. An arbitrary  $n$ -segment filter is represented over successive timesteps through the matrix quantity  $\Gamma_n(\theta_l, \tau_l, \phi_l)$  (figure 6.2b; in each segment of duration  $\tau_l$  we perform a driven operation generating a rotation

through an angle  $\theta_l = \int_{t_{l-1}}^{t_l} \Omega_l(t) dt$  about the axis  $\vec{r}_l = (\cos(\phi_l), \sin(\phi_l), 0)$ , with  $\Omega_l(t)$  the Rabi rate over the  $l$ th pulse segment.

The value of  $n$  is chosen to be a power of two, compatible with synthesis over discrete-time Walsh functions. The Walsh functions are piecewise-constant over segments which are all integer multiples of base period  $\tau_l$ . This approach brings benefits for the current setting [75]; for instance, their piecewise-constant construction builds intrinsic compatibility with discrete clocking and classical digital logic, while the well characterized mathematical properties of the Walsh functions provide a basis for establishing simple *analytic* filter-design rules, and flexibility in realizing a wide variety of filter forms.

For the filters  $W1$  and  $W2$  presented in the main text, Walsh-synthesis design rules dictate that we implement our filtered rotation by  $\theta_x$  over a minimum of four discrete steps, permitting synthesis over  $\text{PAL}_0$  to  $\text{PAL}_3$ . Within this small set, the coefficient of  $\text{PAL}_0$ , denoted  $X_0$ , sets the total rotation angle  $\theta \bmod 2\pi$  for the modulated driven evolution, and only nonzero  $X_3$  preserves symmetry. We experimentally test the performance of four-segment amplitude-modulated filters by scanning over  $X_3$  for fixed  $X_0$  (denoted by white dotted lines in figure 6.3b). Values of  $X_3$  minimizing  $A(\Gamma_4)$  (dips in the dashed trace, right axis) also minimize the experimentally measured infidelity in the presence of engineered low-frequency noise (open circles, left axis). This behavior is observed for various target rotation angles of interest (figure 6.3c-e), with predicted shifts in the optimal values of  $X_3$  with changes in  $X_0$  borne out through experiment. Filter  $W2$  is constructed over  $\text{PAL}_0$  to  $\text{PAL}_7$ , and has twice as many timesteps as  $W1$ . Interestingly,  $W1$  is a special case of an analytically constructed dynamically corrected NOT gate (a  $\pi$ -rotation) [68]. For details of the Walsh functions, Walsh synthesis, and Walsh-basis analytic design rules see Appendix B.

## 6.5 Appendix B

### Theoretical model

We consider a model quantum system consisting of an ensemble of identically prepared noninteracting qubits immersed in a weakly interacting noise bath and driven by an external control device. Working in the interaction picture with respect to the qubit splitting  $\omega_a$  state transformations are represented as unitary rotations of the Bloch vector. The generalized time-dependent Hamiltonian is then written

$$H(t) = H_c(t) + H_0(t) \quad (6.1)$$

where  $H_c(t)$  describes perfect control of the qubit state, e.g. via an ideal external driving field, and the noise Hamiltonian  $H_0(t)$  captures undesirable interactions with a (universal) noise bath.

The specific forms taken by  $H_c(t)$  and  $H_0(t)$  in this work are given in the sections below, where we treat both dephasing (detuning) and amplitude-damping (coherent relaxation) noise processes. We will begin with this model to craft time-dependent noise filters, and detail this method in the following sections.

### Defining the control space

Representing the qubit state on the Bloch sphere, state manipulation maps to a rotation of the Bloch vector in  $\mathbb{R}^3$  and described by the unitary  $U(\theta, \hat{\sigma}_{\vec{r}}) := \exp\left(\frac{-i\vec{\sigma}\cdot\vec{r}\theta}{2}\right)$ , reflecting the homeomorphism between  $SU(2)$  and  $SO(3)$ . In effect, the spin operator  $\hat{\sigma}_{\vec{r}} := \vec{r} \cdot \boldsymbol{\sigma}$  generates a rotation through an angle  $\theta$  about an axis defined by the unit vector  $\vec{r} \in \mathbb{R}^3$ . For our purpose

control takes the form of a composite pulse sequence consisting of  $n$  such unitaries executed over a time period  $[0, \tau]$ , with the  $l$ th pulse in the sequence written

$$P_l := U(\theta_l, \hat{\sigma}_{\phi_l}) = \exp \left[ -i \frac{\hat{\sigma}_{\phi_l}}{2} \int_{t_{l-1}}^{t_l} \Omega_l(t) dt \right] \quad (6.2)$$

$$\hat{\sigma}_{\phi_l} := \cos(\phi_l) \hat{\sigma}_x + \sin(\phi_l) \hat{\sigma}_y. \quad (6.3)$$

Here  $\Omega_l(t)$  is the Rabi rate with arbitrary amplitude envelope in a single pulse,  $\tau_l = t_l - t_{l-1}$  is the pulse duration, and the spin operator  $\hat{\sigma}_{\phi_l}$ , parametrized by  $\phi_l \in [0, 2\pi]$ , generates a rotation  $\theta_l = \int_{t_{l-1}}^{t_l} \Omega_l(t) dt$  of the Bloch vector about an axis  $\vec{r}_l \equiv (\cos(\phi_l), \sin(\phi_l), 0)$  in the  $xy$ -plane<sup>1</sup>. This sequence of control unitaries implies a natural partition of the total sequence duration  $\tau$  into  $n$  subintervals  $I_l = [t_{l-1}, t_l]$ ,  $l \in \{1, n\}$ , such that the  $l$ th pulse has duration  $\tau_l = t_l - t_{l-1}$  with  $t_{l-1}$  and  $t_l$  the start and end times respectively. Here  $t_0 \equiv 0$  and  $t_n \equiv \tau$ .

The control Hamiltonian associated with this composite pulse sequence takes the form

$$H_c(t) = \sum_{l=1}^n G^{(l)}(t) \frac{\Omega_l(t)}{2} \hat{\sigma}_{\phi_l} \quad (6.4)$$

where the function  $G^{(l)}(t)$  is 1 if  $t \in I_l$  and zero otherwise. The sequence of  $n$  triples  $\{(\theta_l, \tau_l, \phi_l)\}_{l=1}^n$  completely characterizes the net effect of the applied control ( $P_l = P_l(\theta_l, \Omega_l(t), \tau_l, \phi_l)$ ) at the end of successive pulse applications. We define the  $n \times 3$  *composite pulse sequence matrix*

$$\Gamma_n = \begin{bmatrix} \theta_1 & \tau_1 & \phi_1 \\ \theta_2 & \tau_2 & \phi_2 \\ \vdots & \vdots & \vdots \\ \theta_n & \tau_n & \phi_n \end{bmatrix} \quad (6.5)$$

to compactly describe any arbitrary  $n$ -pulse control sequence. The entire space of such control forms therefore corresponds to an infinite set of  $\Gamma_n$  matrices ranging continuously over all possible values taken by the control parameters. We denote this set by  $\mathfrak{C}_n$  and refer to it as the  *$n$ -pulse control space*. Written formally

$$\mathfrak{C}_n := \left\{ \Gamma_n \mid \theta_l, \tau_l > 0, \phi_l \in [0, 2\pi], l \in \{1, \dots, n\}, \sum_l^n \tau_l = \tau \right\}.$$

## Noise bath model

We consider semi-classical time-dependent dephasing (detuning) and amplitude damping (relaxation) processes, captured respectively through the appearance of stochastic rotations about  $\hat{\sigma}_z$  and  $\hat{\sigma}_\phi := \cos(\phi) \hat{\sigma}_x + \sin(\phi) \hat{\sigma}_y$ . The universal noise Hamiltonian then takes the form  $H_0(t) = H_0^{(z)}(t) + H_0^{(\Omega)}(t)$  where  $H_0^{(z)}(t)$  and  $H_0^{(\Omega)}(t)$  denote noise interactions associated with the dephasing and amplitude noise quadratures respectively. The dephasing noise Hamiltonian is then given by

$$H_0^{(z)}(t) = \beta_z(t) \hat{\sigma}_z \quad (6.6)$$

---

<sup>1</sup>For a resonantly driven qubit  $\phi_l$  is the phase of the driving field and  $\Omega_l$  is linearly proportional to the driving amplitude.

where  $\beta_z(t)$  is a classical stochastic process. During each pulse we also make the substitution  $\Omega_l(t) \longrightarrow (\Omega_l(t) + \beta_\Omega(t)\Omega_l^{(\max)})$  where  $\beta_\Omega(t)$  describes captures a (multiplicative) stochastic noise scaled by the maximum Rabi rate in a pulse segment in the amplitude of the driving field. Thus the amplitude noise Hamiltonian takes the form

$$H_0^{(\Omega)} = \beta_\Omega(t) \sum_{l=1}^n G^{(l)}(t) \frac{\Omega_l^{(\max)}}{2} \hat{\sigma}_{\phi_l} \quad (6.7)$$

and generates errors in intended rotation angle coaxial with the target rotation axis  $\hat{\sigma}_{\phi_l}$ .

## Calculating operational fidelity & the first-order approximation

In the absence of noise, state evolution is determined by  $i\dot{U}_c(t) = H_c(t)U_c(t)$  with  $U_c(t)$  describing a target operation. Including the effects of noise, however, the actual evolution operator  $U(t)$  satisfies  $i\dot{U}(t) = (H_c(t) + H_0(t))U(t)$ . A measure of the average gate fidelity  $\mathcal{F}_{av}(\tau) = \frac{1}{4}\langle|\text{Tr}(U_c^\dagger(\tau)U(\tau))|^2\rangle$  is then obtained using the Hilber-Schmidt inner product, effectively measuring the overlap between the intended and realized operators. These evolution dynamics however are challenging to compute due to sequential application of noncommuting, time-dependent operations giving rise to both dephasing and depolarization errors. Our approach follows the method developed by Green *et al.* [108], using average Hamiltonian theory and the generalized filter-transfer function formalism to obtain a first order approximation for gate infidelity.

### Magnus Expansion

We write the total evolution operator  $U(t) = U_c(t)\tilde{U}(t)$ , where the *error propagator*  $\tilde{U}(t)$  satisfies the Schrodinger equation  $i\dot{\tilde{U}}(t) = \tilde{H}_0(t)\tilde{U}(t)$  in a frame co-rotating with the control defined by the *Toggling frame Hamiltonian*  $\tilde{H}_0(t) := U_c^\dagger(t)H_0(t)U_c(t)$ . Thus, in the event that  $\tilde{U}(\tau) = \mathbf{I}$ , the realized evolution operator  $U(\tau)$  approaches the target operation  $U_c(\tau)$  and errors do not affect the gate. This can be systematized by writing  $\tilde{U}(\tau) = \exp[-i\Phi(\tau)]$  in terms of a time-independent effective error operator  $\Phi(\tau) = \sum_{\mu=1}^{\infty} \Phi_\mu(\tau)$  with Magnus expansion terms

$$\begin{aligned} \Phi_1(\tau) &= \int_0^\tau dt \tilde{H}_0(t) \\ \Phi_2(\tau) &= -\frac{i}{2} \int_0^\tau dt_1 \int_0^{t_1} dt_2 [\tilde{H}_0(t_1), \tilde{H}_0(t_2)] \\ \Phi_3(\tau) &= \frac{1}{6} \int_0^\tau dt_1 \int_0^{t_1} dt_2 \int_0^{t_2} dt_3 \left\{ [\tilde{H}_0(t_1), [\tilde{H}_0(t_2), \tilde{H}_0(t_3)]] \right. \\ &\quad \left. + [\tilde{H}_0(t_3), [\tilde{H}_0(t_2), \tilde{H}_0(t_1)]] \right\} \dots \end{aligned}$$

generally taking the form of time-ordered integrals over nested commutators in  $\tilde{H}_0(t)$ .

One may then use vector identities to re-express the so-called *error vector* in the toggling frame, again in an infinite power-series expansion

$$\mathbf{a}(\tau) = \sum_{\mu}^{\infty} \mathbf{a}_\mu(\tau). \quad (6.8)$$

This is a reexpression of the Magnus expansion error terms in the language of our control Hamiltonian. For details of this derivation and the definition of all terms see [108].

Our theoretical predictions based on the filter-transfer function formalism involve an approximation to the *trace* or *gate fidelity* defined by

$$\mathcal{F}_{av}(\tau) = \frac{1}{4} \langle |\text{Tr}(\tilde{U}(\tau))|^2 \rangle = \frac{1}{4} \langle |\text{Tr}(e^{-i\mathbf{a}(\tau)\boldsymbol{\sigma}})|^2 \rangle \quad (6.9)$$

where  $\mathbf{a}(\tau) = \sum_{\mu}^{\infty} \mathbf{a}_{\mu}(\tau)$  is the error vector given in terms of the Magnus expansion. Following the method developed in reference [108] and expanding the exponential in equation (6.9) we obtain

$$\mathcal{F}_{av}(\tau) = \frac{1}{2} [\langle \cos(2a) \rangle + 1] \quad (6.10)$$

$$= \frac{1}{2} \left[ 1 + \sum_{m=0}^{\infty} (-1)^m \frac{2^{2m}}{(2m)!} \langle a^2 \rangle^m \right] \quad (6.11)$$

$$\langle a^2 \rangle = \sum_{\mu\nu} [\langle a_1^2 \rangle + \langle a_2^2 \rangle + \dots] \quad (6.12)$$

$$+ 2(\langle \mathbf{a}_1 \mathbf{a}_2^T \rangle + \langle \mathbf{a}_1 \mathbf{a}_3^T \rangle + \langle \mathbf{a}_2 \mathbf{a}_3^T \rangle + \dots) \quad (6.13)$$

with  $a^2 \equiv \mathbf{a}(\tau) \mathbf{a}(\tau)^T$  the norm square of the error vector. The full expansion rapidly becomes too complex to write explicitly, however it is convenient to write  $\mathcal{F}_{av} = \sum_{k=0}^{\infty} \mathcal{O}(\xi^{2k})$  where  $\xi$  is the *smallness parameter* quantifying the RMS deviation of the noise integrated over the sequence duration,  $\xi \equiv \Delta\beta\tau/2$  [100]. For this series to formally converge we require  $\xi^2 < 1$  (see main text and figure 6.4).

Here odd powers of  $\xi$  are omitted since these involve ensemble averages over odd powers of the noise strength and vanish under our assumption of zero-mean, Gaussian-distributed random variables. Writing the  $\mathcal{O}(\xi^0), \mathcal{O}(\xi^2), \mathcal{O}(\xi^4)$  classes explicitly we have

$$\mathcal{F}_{av} = 1 - \langle a_1^2 \rangle - \left[ \langle a_2^2 \rangle + 2\langle \mathbf{a}_1 \mathbf{a}_3^T \rangle - \frac{\langle a_1^4 \rangle}{3} \right] + \sum_{k=3}^{\infty} \mathcal{O}(\xi^{2k}) \quad (6.14)$$

Immediately we see that there is a collection of terms with equal magnitude arising from *different orders* of the Magnus expansion (e.g.  $a_2^2$  vs  $a_1^4$ ). The individual terms in the series expansion of the fidelity rely on time-domain correlation and cross-correlation functions and convolution with a multidimensional control matrix capturing the effect of the control operations.

The fidelity is thus expressed explicitly in terms of noise correlations and the control matrix. For instance,

$$\begin{aligned} \langle a_1^2 \rangle &= \sum_{i,j=x,y,z} \int_0^{\tau} dt_2 \int_0^{\tau} dt_1 \langle \beta_i(t_1) \beta_j(t_2) \rangle \mathbf{R}_i(t_1) \mathbf{R}_j^T(t_2) \\ &= \sum_{i,j,k=x,y,z} \int_0^{\tau} dt_2 \int_0^{\tau} dt_1 \langle \beta_i(t_1) \beta_j(t_2) \rangle R_{ik}(t_1) R_{jk}(t_2) \end{aligned} \quad (6.15)$$

contains all two-point noise cross-correlation functions  $\langle \beta_i(t_1) \beta_j(t_2) \rangle$ , for  $i, j \in \{x, y, z\}$ . Higher-order terms contain multipoint correlation functions (this is determined by the sum of subscript indices, as they indicate the expansion-order of the error vector).

We rewrite these terms in the frequency domain, defining the Fourier transform  $\mathcal{S}_{i_1 \dots i_n}(\omega_1, \dots, \omega_n)$  of an  $n$ -point cross-correlation function via

$$\langle \beta_{i_1}(t_1) \beta_{i_2}(t_2) \dots \beta_{i_n}(t_n) \rangle \equiv \frac{1}{(2\pi)^n} \int d\omega_1 \dots \int d\omega_n \mathcal{S}_{i_1 \dots i_n}(\omega_1, \dots, \omega_n) e^{i(\omega_1 t_1 + \dots + \omega_n t_n)} \quad (6.16)$$

The fidelity above can then be rewritten as

$$\mathcal{F}_{av} = 1 - \sum_{n=2}^{\infty} \left\{ \frac{1}{(2\pi)^n} \sum_{i_1 \dots i_n} \int d\omega_1 \dots \int d\omega_n \mathcal{S}_{i_1 \dots i_n}(\omega_1, \dots, \omega_n) \mathcal{R}i_1 \dots i_n(\omega_1, \dots, \omega_n) \right\} \quad (6.17)$$

where  $\mathcal{R}_{i_1 \dots i_n}(\omega_1, \dots, \omega_n)$  is determined solely by the control matrix and increases in complexity at higher order. Explicit expressions for terms to arbitrary order are found in [108].

### First-order fidelity approximation

Here we briefly explain the choice of fidelity metric used in the figures of the main text to produce the theory curves against which our experimental data is compared. Experimental fidelities are determined by measuring the brightness of the ion cloud after completing the control sequence, effectively yielding a projective measurement onto the  $| \uparrow \rangle$  state. We denote this metric by  $P_{\uparrow}(\tau) \in [\frac{1}{2}, 1]$  and refer to it as the *state fidelity*, with lower and upper bounds corresponding to complete decoherence and perfect fidelity respectively.

If the noise is sufficiently weak ( $\xi^2 \ll 1$ ) we may truncate the series expansion for fidelity after the  $\mathcal{O}(\xi^2)$  term yielding the approximation

$$\mathcal{F}_{\mathcal{O}(1)} = 1 - \langle a_1^2 \rangle. \quad (6.18)$$

Here the term which dominates the measured infidelity is  $\langle a_1^2 \rangle := \langle \mathbf{a}_1(\tau) \mathbf{a}_1^T(\tau) \rangle$ , defined as the ensemble averaged modulus square of the first order error vector  $\mathbf{a}_1(\tau)$ . Assuming wide sense stationarity, independence and zero mean of both noise fields  $\beta_z(t)$  and  $\beta_{\Omega}(t)$  we may derive a spectral representation of  $\langle a_1^2 \rangle$  of the form

$$\langle a_1^2 \rangle = \frac{1}{2\pi} \int_{-\infty}^{\infty} \frac{d\omega}{\omega^2} S_z(\omega) F_z(\omega) + \frac{1}{2\pi} \int_{-\infty}^{\infty} \frac{d\omega'}{\omega'^2} S_{\Omega}(\omega') F_{\Omega}(\omega'). \quad (6.19)$$

Here  $S_z(\omega)$  and  $S_{\Omega}(\omega)$  denote the dephasing and amplitude noise PSDs. The dephasing  $F_z(\omega)$  and amplitude  $F_{\Omega}(\omega)$  filter functions, on the other hand, capture the spectral response of the control sequence and are completely defined as functions of the control sequence.

As the integrated noise content increases, however, higher-order error contributions must be included; neglecting to do leads to the unphysical result that  $\mathcal{F}_{\mathcal{O}(1)} \leq 0$  when  $\xi^2 \geq 1$ . Although computation of all higher-order contributions is challenging we may gain some insight into the full expansion by considering terms of the form  $\langle a_1^{2m} \rangle \equiv \langle a_1^2 \rangle^m$  in each class  $\mathcal{O}(\xi^{2m})$ . This collection of terms is obtained by setting  $a^2 \rightarrow a_1^2$  in equation (6.10), effectively including only the first-order *Magnus* expansion term in the expansion for *Fidelity*, yielding

$$\mathcal{F}'_{\mathcal{O}(1)}(\tau) = \frac{1}{2} \left[ 1 + \sum_{m=0}^{\infty} (-1)^m \frac{2^{2m}}{(2m)!} \langle a_1^2 \rangle^m \right] \quad (6.20)$$

$$= 1 - \langle a_1^2 \rangle + \frac{\langle a_1^4 \rangle}{3} - \frac{2\langle a_1^6 \rangle}{45} + \dots \quad (6.21)$$

The oscillating sign of these terms is characteristic of the higher-order classes in converging to the true expression. To overcome the unphysicality of  $\mathcal{F}_{\mathcal{O}(1)}$  as the noise content increases we employ a metric  $\mathcal{F}_{\chi}$  with the physically reasonable properties that

$$\mathcal{F}_{av} \approx \mathcal{F}_{\mathcal{O}(1)} \approx \mathcal{F}_{\chi}, \quad \langle a_1^2 \rangle \ll 1 \quad (6.22)$$

$$\mathcal{F}_{\mathcal{O}(1)} \leq \mathcal{F}'_{\mathcal{O}(1)} \leq \mathcal{F}_{av}, \mathcal{F}_{\chi}, \quad \langle a_1^2 \rangle \approx 1 \quad (6.23)$$

$$\mathcal{F}_{\chi} \rightarrow 1/2 \rightarrow P_{\uparrow}(\tau), \quad \langle a_1^2 \rangle \gg 1 \quad (6.24)$$

We may satisfy these conditions by noticing the qualitative resemblance between equations (6.20) and (6.21) and the expansion for a simple exponential

$$1 - \langle a_1^2 \rangle + \langle a_1^4 \rangle - \frac{2\langle a_1^6 \rangle}{3} + \dots = \frac{1}{2} \left[ 1 + \sum_{m=0}^{\infty} (-1)^m \frac{2^m}{m!} \langle a_1^2 \rangle^m \right] \quad (6.25)$$

$$= \frac{1}{2} \left[ 1 + \sum_{k=0}^{\infty} \frac{(-\chi(\tau))^m}{m!} \right] \quad (6.26)$$

where we have defined  $\chi(\tau) \equiv 2\langle a_1^2 \rangle$ . Hence we use the following metric in calculating fidelities to be compared with experimental data

$$\mathcal{F}_x = \frac{1}{2} \left\{ 1 + \exp[-\chi(\tau)] \right\} \quad (6.27)$$

This approximation represents the *first-order fidelity approximation*: it ignores higher-order cross correlations in the noise arising from higher-order Magnus contributions to the error vector, with diminishing overall magnitude (as given by the smallness parameter), but incorporates an approximation to higher-order terms important as the total noise-induced infidelity grows. We work in this limit throughout this manuscript.

### Breakdown of the first-order fidelity approximation

As described above, the first-order fidelity ignores higher-order terms expressed as nested-integrals over cross-correlations between noise along different directions, assuming weak noise. As these contributions to gate infidelity grow in importance (for instance with  $\alpha$ ) we expect the filter-transfer-function fidelity calculations to underestimate measured error in cases where the control has filtered the noise to leading order.

We measure the probability that a  $\pi_x$ -pulse drives qubit population from the dark state to the bright state,  $|0\rangle \rightarrow |1\rangle$ , as a function of the high-frequency cutoff,  $\omega_c$ , of a white dephasing bath (figure 6.4b). As the high-frequency cutoff of the noise is increased and fluctuations fast compared to the control are added to the noise power spectrum,  $S_z(\omega)$ , errors accumulate reducing the measured fidelity. The value of  $\omega_c$  at which the fidelity drops from near unity decreases as a function of the noise strength, parametrized by  $\alpha$ . In all cases for the primitive  $\pi$  pulse the fidelity calculated using the filter transfer function matches the measured data well with *no free parameters*.

Performance is notably different when studying the four-segment WAMF  $\pi$ -pulse,  $W1$ , indicated in figure 6.2b-c of the main text. The WAMF construction provides *first-order* filtering of time-dependent noise (red line in figure 6.2c) (effectively cancelling terms proportional to  $\langle a_1^2 \rangle$ ), but does not provide suppression of higher-order terms in the Magnus expansion for fidelity which grow in importance with noise strength. Unlike data for the primitive gate, as the noise strength increases we observe a growing divergence between the measured fidelity and the fidelity calculated using the filter-transfer functions introduced above assuming a first order approximation (figure 6.4b).

This phenomenon is not a function of total error magnitude, but instead occurs for  $\xi^2 \geq 1$  (red lines, right axis), a proxy measure indicating that we are not formally able to truncate the series expansion for fidelity at first order and must consider higher-order error contributions [108], including Magnus terms above  $\langle a_1^2 \rangle$ . These measurements therefore reveal the efficacy of noise filtering and quantitatively demonstrate the bounds of the first-order fidelity approximation as breakdown routinely occurs near the predicted value  $\xi^2 \geq 1$ . Notably, while formal convergence of this series requires  $\xi^2 \ll 1$ , we find reasonable agreement between experiment and theory up to  $\xi^2 \sim 5$  (figure 6.4c).

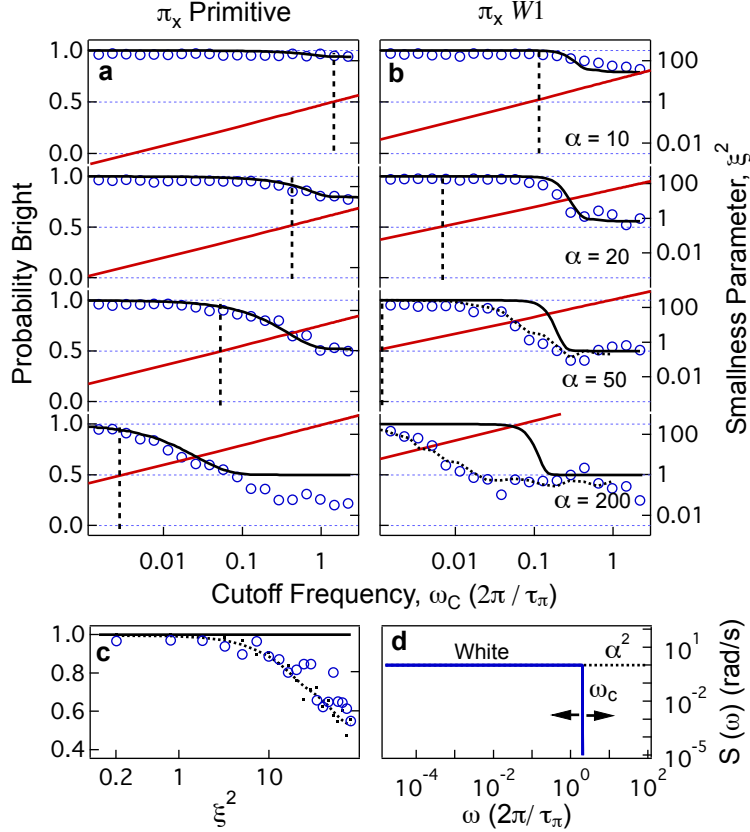


Figure 6.4: *Experimental validation of the breakdown of the first-order approximation to fidelity. a)-b) Measurements of operational fidelity with engineered noise for rotation  $|0\rangle \rightarrow |1\rangle$  as a function of dimensionless noise cutoff frequency. Primitive rotation (a) and four-segment WAMF modulated rotation, W1, (b). Decay to value 0.5 corresponds to full decoherence. Each data point is the result of averaging over 50 different noise realizations. Maximum Rabi rate is fixed; filter W1 is conducted over time  $4\tau_\pi$ . Black dotted lines indicate the (smoothed) results of numerical integration of the Schroedinger equation, indicating that divergence between data and filter-function calculation is not due to experimental artefacts. Red lines (right axis) give  $\xi^2$  employed in making the first-order filter-transfer function approximation. Vertical dashed lines indicate values of  $\omega_c$  beyond which  $\xi^2 \geq 1$ . c) Measurements of W1 fidelity revealing a growing breakdown in agreement between filter-transfer function fidelity prediction and experimental data beyond  $\xi^2 \gtrsim 1$ , taken for  $\omega_c/2\pi = 1.7\%\tau_\pi^{-1}$ . d) Schematic representation of the white noise power spectrum employed.*

## Time-domain filter order vs. Magnus order

We may formally indicate the functional dependence of the filter function on the control sequence by writing  $F(\tau\omega) = F(\tau\omega; \Gamma_n)$ . Noise filtering (and hence error suppression) corresponds to minimizing the area under the filter transfer function in the spectral region where the noise PSD is non-negligible. We therefore define a cost function over a user-defined frequency band which may take the form

$$A(\Gamma_n) := \int_{\omega_L}^{\omega_c} d\omega F(\tau\omega; \Gamma_n) \quad (6.28)$$

to diagnose the filtering effectiveness achieved by the control sequence  $\Gamma_n$ ; the smaller the integral  $A(\Gamma_n)$ , the more effective the noise filtering in this band. Having defined control sequences as continuous elements of the corresponding control space, for a given  $n$  we may in principle construct a variational procedure on  $\mathfrak{C}_n$  to derive ‘values’ of  $\Gamma_n$  satisfying a given cost function.

The filter transfer function may be approximated by a polynomial expression  $F(\omega\tau) \propto (\omega\tau)^{2p}$  for some  $p$  near  $\omega \approx 0$ . As  $p$  increases the integral in (6.28), and hence the infidelity, decreases: the noise in the time domain is then said to be filtered to order  $p - 1$ .

Equivalently stated, a control sequence  $\Gamma_n \in \mathfrak{C}_n$  filters time-dependent noise to order  $p - 1$  if  $\Gamma_n$  is a *concurrent zero* of the first  $p - 1$  coefficients in the Taylor expansion<sup>2</sup> of the filter transfer function about  $\omega = 0$ .

$$F(\omega\tau; \Gamma_n) = \sum_{k=1}^{\infty} C_{2k}(\Gamma_n) (\omega\tau)^{2k}. \quad (6.29)$$

The dependence of the expansion coefficients on our control parameters  $\Gamma_n$  has been made explicit, and we include only even powers of  $\omega\tau$  due to the evenness of the filter transfer function. In this case  $A(\Gamma_n) \approx C_{2p}(\Gamma_n) \frac{(\tau\omega_c)^{2p+1}}{2p+1}$  and the condition that

$$\frac{A(\Gamma_n)}{C_{2p}(\Gamma_n)} = \mathcal{O}\left(\frac{(\tau\omega_c)^{2p+1}}{2p+1}\right) \quad (6.30)$$

therefore implies the control sequence  $\Gamma_n$  filters noise to order  $p - 1$ . This effect is visualized through the slope of the filter transfer function in the stopband on a log-log plot (figure 6.2c, main text). A high-order filter has a higher slope in this region, indicating improved suppression of time-dependent noise.

General filter design focuses on a band of interest, permitting spectral response to diverge outside of the spectral region of interest - for instance electrical filters in the microwave may appear transparent in the THz or Hz. Therefore, in addition to the asymptotic, zero-frequency filter order ( $p - 1$ ), we introduce a more general metric capable of describing filter performance *over an arbitrary spectral band*. The *local filter order* ( $p^* - 1$ ) establishes that the filter-transfer function is well approximated by  $F_i \propto (\omega\tau)^{2p^*}$  over the band  $[\omega_L, \omega_c]$ . It is this more narrowly defined metric that is used in most practical filter-design tasks, including those undertaken above.

The performance of filter-order ( $p - 1$ ) or local filter order ( $p^* - 1$ ) for time-dependent noise described above must be distinguished from the order of error suppression for quasistatic errors in the Magnus expansion. The latter measure is typically used in NMR literature to the pulse sequences designed to compensate for quasistatic errors. In this regime the time dependence of the dephasing (amplitude) noise fields reduces to constants  $\beta_z$  ( $\beta_\Omega$ ) and the Magnus expansion terms  $\Phi_\mu^{(DC)}$  are evaluated strictly as time integrals over *ideal* control operations scaled by powers

---

<sup>2</sup>This procedure is valid for frequencies sufficiently lower than  $1/\tau$  (the inverse of the total sequence duration).

	Amplitude Errors		Dephasing Errors	
	$\mu - 1$	$p - 1$	$\mu - 1$	$p - 1$
SK1	1	1	0	0
P2	2	1	0	0
B2	2	1	0	0
C1	0	0	1	1
C2 ( $\pi$ )	0	0	2	0
W1	0	0	1	1
W2	0	0	1	2
UWMG <sub>1,SK1</sub>	1	1	1	1

Table 6.1: *Comparision between suppressing stochastic errors to order  $p - 1$  (filter order) and compensating for static offset errors to order  $\mu - 1$  (Magnus order). Naming conventions for NMR sequences in top panel are consistent with the review article by Merrill and Brown [87]. The final entry corresponds to a concatenated construction described below.*

of the offset magnitude  $\beta_z^\mu$  ( $\beta_\Omega^\mu$ ). A pulse sequence for which  $\Phi_1^{(\text{DC})} = \dots = \Phi_{\mu-1}^{(\text{DC})} = 0$  is then said to compensate offset errors to order  $\mu - 1$ . In this case the total error operator satisfies  $\Phi^{(\text{DC})}(\tau) = \mathcal{O}(\Phi_\mu^{(\text{DC})})$  and is dominated by the residual error proportional to the  $\mu$ th power in the offset magnitude.

*High-order error suppression in the Magnus expansion does not imply high-order time-domain noise filtering.* Table 6.1 reveals the importance of not conflating these two measures when assessing the performance of a control sequence against static vs stochastic errors. The upper panel compares the two performance measures for some well-known phase-modulated NMR sequences, the naming conventions for which are consistent with the review by Merrill and Brown [87]. For completeness, in the lower panel we also make the comparison for the novel control sequences derived in this paper.

Later we will return to the question of time-domain filter order and introduce a set of analytic design rules for filter construction based on the characteristics of our selected basis functions - the Walsh functions.

## Walsh basis functions

We impose physically motivated constraints on the form of  $\Gamma_n$  in order to reduce the search to a manageable subspace of  $\mathfrak{C}_n$ , and elect to synthesize control sequences from the Walsh basis functions. The set of Walsh functions  $w_k : [0, 1] \rightarrow \{\pm 1\}$ ,  $k \in \mathbb{N}$  form an orthonormal-complete family of binary-valued square waves defined on the unit interval and are the *digital analogues* of the sines and cosines in Fourier analysis. Since their formulation in the first half of the twentieth century, Walsh functions have played an important role in scientific and engineering applications. Their development and utilization has been strongly influenced by parallel developments in digital electronics and computer science since the 1960s, with Walsh-type transforms replacing Fourier transforms in a range of engineering applications such as communication, signal processing, image processing, pattern recognition, noise filtering and so forth [146].

We summarize the relevant mathematical details of the Walsh basis, outlining two equivalent

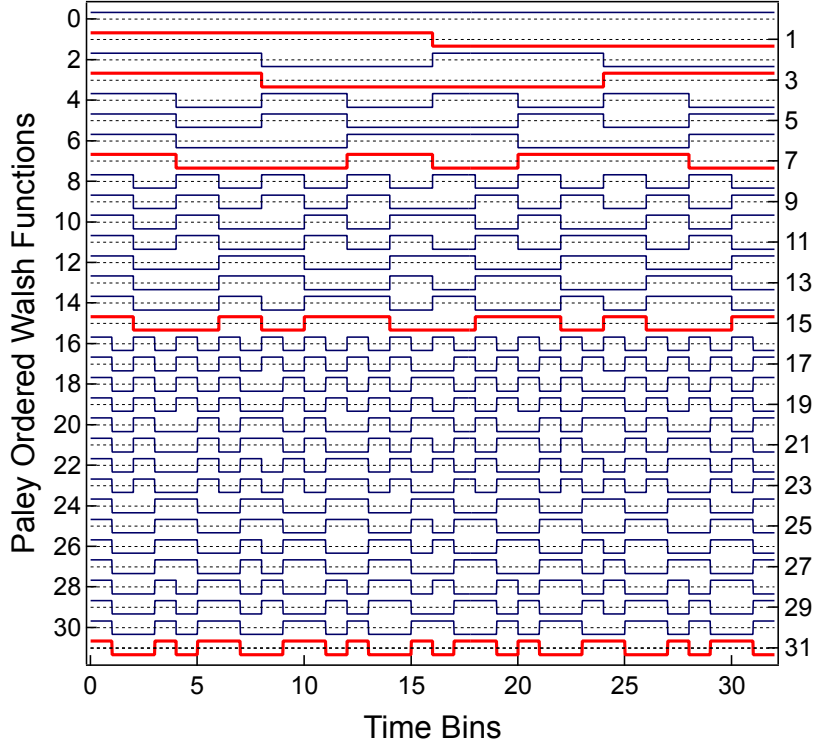


Figure 6.5: The first 32 Walsh functions in Paley ordering.

representations, *Paley ordering* and the *Hadamard representation*, both of which are useful to understand the Walsh control space.

### Paley ordering

The Walsh functions are aperiodic and hence do not admit to the unique ordering according to increasing *frequency* characteristic of the sinusoids in the Fourier basis. A number of different orderings exist with associated definitions of the basis elements. We employ the *Paley ordering* in which basis functions are generated from products of *Rademacher functions*, a family of square waves defined by

$$R_j(x) := \text{sgn}[\sin(2^j \pi x)], \quad x \in [0, 1], \quad j \geq 0, \quad (6.31)$$

switching between  $\pm 1$  at rate  $2^j$ . The Walsh function of Paley order  $k$ , denoted  $\text{PAL}_k(x)$ , is then defined by

$$\text{PAL}_k(x) = \prod_{j=1}^m R_j(x)^{b_j} \quad (6.32)$$

where  $(b_m, b_{m-1}, \dots, b_1)_2$  is the binary representation of  $k$ . That is,  $k = b_m 2^{m-1} + b_{m-1} 2^{m-2} + \dots + b_1 2^0$ , where  $b_m \equiv 1$  defines the most significant binary digit. Hence  $R_j(x)$  is a factor of  $\text{PAL}_k(x)$  whenever  $b_j$  is a nonzero binary digits of  $k$ . The total number of nonzero  $b_j$ 's in  $k$  define the *Hamming wieght*, denoted by  $r$ . We write  $m(k)$  and  $r(k)$  when it is desirable to emphasize that both  $m$  and  $r$  are functions of  $k$ . For illustration, the first 32 Walsh functions in the Paley ordering are shown in figure 6.5.

## Hadamard representation

For our purposes we require an expression for the piecewise-constant structure of an arbitrary superposition of Walsh functions, and therefore desire *a priori* knowledge of the locations of their various zero crossings. A general expression, however, is difficult due to the aperiodicity of the Walsh functions. It is convenient instead to use the Hadamard representation in which any continuously defined basis member  $\text{PAL}_k(x)$  projects completely onto a digital vector in  $\mathbb{R}^{2^n}$  provided  $m(k) \leq n$ , which is true for the  $2^n$  Paley orders in the set  $k \in \{0, 1, \dots, 2^n - 1\}$ . Since these vectors have dimension  $2^n$  and inherit the orthogonality of the  $\text{PAL}_k(x)$  they therefore form a *discrete* Walsh basis spanning  $\mathbb{R}^{2^n}$ . Such a projection is clearly possible since the fastest modulation rate in  $\text{PAL}_k(x)$  derives from the periodicity of  $R_{m(k)}(x)$ , which switches sign  $2^{m(k)}$  times over  $x \in [0, 1]$ . The projection then involves partitioning the domain into  $2^n$  bins and associating the value of  $\text{PAL}_k(x)$  in the  $j$ th bin to the  $j$ th element  $P_j^{(k)} \in \{\pm 1\}$  of the discrete digital vector

$$\mathbf{P}_{2^n}^{(k)} = \left[ P_1^{(k)}, P_2^{(k)}, \dots, P_{2^n}^{(k)} \right]. \quad (6.33)$$

Using the so-called *Sylvester construction* [155], the  $2^n$ -dimensional Hadamard matrix  $H_{2^n}$  is generated recursively by

$$H_{2^n} = \begin{bmatrix} H_{2^{n-1}} & H_{2^{n-1}} \\ H_{2^{n-1}} & -H_{2^{n-1}} \end{bmatrix} = S^{\otimes n} \quad (6.34)$$

$$S = \begin{bmatrix} 1 & 1 \\ 1 & -1 \end{bmatrix}, \quad H_1 = 1 \quad (6.35)$$

where  $S$  is the Sylvester matrix, and  $\otimes n$  denotes  $n \geq 1$  applications of the Kronecker product. In this construction  $\mathbf{P}_{2^n}^{(k)}$  defines the  $i(k) = 1 + \sum_{j=1}^{m(k)} b_j 2^{n-j}$  column (row) of  $H_{2^n}$ . The orthogonality of the Walsh basis is thereby reflected in the property that  $H_{2^n} H_{2^n}^T = 2^n I$ , implying the orthogonality of the Hadamard matrices.

This representation is particularly useful for efficiently constructing Walsh-synthesized waveforms. Consider an arbitrary function  $f(x) = \sum_{k=0}^N X_k \text{PAL}_k(x)$  synthesized in the Walsh basis where  $N$  sets the highest (Paley) ordered function in the construction. Then, from the above discussion, all Walsh functions in this synthesis projected onto a Hadamard matrix of dimension  $\geq 2^{m(N)}$ , with  $\mathcal{M} = 2^{m(N)}$  giving the minimal sufficient dimension. A discrete representation of the function  $f(x)$  therefore exists as a projection onto the column space of  $H_{\mathcal{M}}$  by writing

$$\mathbf{f} = H_{\mathcal{M}} \tilde{\mathbf{X}}. \quad (6.36)$$

The column vector  $\tilde{\mathbf{X}} = [\tilde{X}_1, \tilde{X}_2, \dots, \tilde{X}_{\mathcal{M}}]^T$  contains the reordered Paley amplitudes  $X_k$  reordered under the change of basis map  $i(k)$  specified by

$$\tilde{X}_{i(k)} = \begin{cases} X_k & \text{for } 0 \leq k \leq N \\ 0 & \text{for } N < k < \mathcal{M} \end{cases}. \quad (6.37)$$

The vector  $\mathbf{f} = [f_1, f_2, \dots, f_{\mathcal{M}}]^T$  so generated then represents the piecewise constant structure of  $f(x)$ , with  $f_j$  giving the value taken by  $f(x)$  on the  $j$ th of  $\mathcal{M}$  equal subintervals partitioning  $x \in [0, 1]$ .

## Walsh synthesis for amplitude modulated filters

Any square integrable function  $f(x)$  on the interval  $[0, 1]$  has a unique *spectral decomposition* in the *Walsh basis*

$$f(x) = \sum_{k=0}^{\infty} X_k w_k(x) \iff X_k := \int_0^1 f(x) w_k(x) dx.$$

We consider a control regime referred to as *single-axis amplitude-modulation* defined by

$$\Gamma_n \cong \{(\tau_l, \theta_l)\}_{l=1}^n, \quad \phi_l = \phi_0 \quad \forall l \in \{1, \dots, n\} \quad (6.38)$$

where the waveform structuring the total angle swept out in each pulse segment,  $\theta_l$ , is based on a linear superposition of well-defined square waves known as Walsh functions. We refer to these sequences as *Walsh amplitude modulated filters* (WAMFs), and speak of searching over the *Walsh-modulated control subspace*.

Using the above framework, we may efficiently construct arbitrary WAMFs for arbitrary pulse-segment envelopes. We define a time-varying Rabi rate  $\Omega_l(t)$ ,  $l \in \{1, \dots, \mathcal{M}\}$  over the time period  $t \in [t_{l-1}, t_l]$  of each segment,  $l \in \{1, \dots, \mathcal{M}\}$ ,  $t \in [t_{l-1}, t_l]$ . Each segment has duration  $\tau_l = \tau/\mathcal{M}$  and generates a *total rotation angle* for each segment,  $\theta_l$  given by the integral

$$\theta_l = \int_{t_{l-1}}^{t_l} \Omega_l(t) dt \quad (6.39)$$

We now treat the rotation angles  $\theta_l$  as parameters by which to optimize filter performance. For efficient filter construction, however, it is convenient to instead transform this optimization over  $\theta_l$  to an optimization over a Walsh spectrum. This is achieved by writing  $\theta_l = \theta_l(X_0, X_1, \dots, X_N)$  with the dependence on the Walsh spectra defined by the Hadamard-matrix equation

$$\vec{\theta} = (\theta_1, \theta_2, \dots, \theta_{\mathcal{M}})^T = (\tau/\mathcal{M}) H_{\mathcal{M}} \tilde{X}. \quad (6.40)$$

Defined in this way, the  $\mathcal{M}$ -segment arbitrary-envelope construction achieves total gate-rotation angle  $\Theta = \sum_{l=1}^n \theta_l = X_0 \tau$ , completely determined by the spectral amplitude of  $\text{PAL}_0$ . All symmetry-based design rules carry over, regardless of the modulation envelope for an individual pulse segment.

## Square pulses

The special case of square pulse segments is treated here as it allows a reduction in synthesis complexity and is compatible with many experimental systems. We may replace the time-dependent Rabi rate  $\Omega(t)$  over a single segment with a piecewise-constant (over a single-segment) construction used in Walsh synthesis over a complete pulse sequence

$$\Omega(t) = \sum_{k=0}^N X_k \text{PAL}_k(t/\tau), \quad t \in [0, \tau]. \quad (6.41)$$

This permits synthesis over the Rabi rate per segment rather than the total rotation angle, which is often simpler in experimental settings. Substituting  $\Omega(t/\tau)$  for  $f(x)$  in equation (6.36) we

obtain  $\Omega = H_{\mathcal{M}} \tilde{\mathbf{X}}$ . The vector  $\Omega = [\Omega_1, \Omega_2, \dots, \Omega_{\mathcal{M}}]^T$  thus defines a sequence of modulated Rabi rates each functionally dependent on the Walsh amplitudes

$$\Omega_l = \Omega_l(X_0, X_1, \dots, X_N), \quad l \in \{1, \dots, \mathcal{M}\}. \quad (6.42)$$

The WAMF is then defined by explicitly writing  $\Omega$  as an additional column leading the representation of equation (6.5), yielding the form

$$\Gamma_{\mathcal{M}} = \begin{bmatrix} P_1 & \begin{array}{cccc} \Omega_l & \theta_l & \tau_l & \phi_l \\ \Omega_1 & \frac{\Omega_1 \tau}{\mathcal{M}} & \frac{\tau}{\mathcal{M}} & \phi_0 \\ \Omega_2 & \frac{\Omega_2 \tau}{\mathcal{M}} & \frac{\tau}{\mathcal{M}} & \phi_0 \\ \vdots & \vdots & \vdots & \vdots \\ \Omega_{\mathcal{M}} & \frac{\Omega_{\mathcal{M}} \tau}{\mathcal{M}} & \frac{\tau}{\mathcal{M}} & \phi_0 \end{array} \\ P_2 \\ \vdots \\ P_{\mathcal{M}} \end{bmatrix} \quad (6.43)$$

Here the degree of freedom associated with  $\tau_l$  has apparently been removed. This reflects the fact that the choice of  $\tau_l$  has been transformed into the choice of Walsh basis functions in the synthesis, each contributing its characteristic temporal profile. The remaining degrees of freedom reside in functional dependence of  $\Omega_l$  on the Walsh spectrum and our variational search is thus limited to the subspace of  $\mathfrak{C}_{\mathcal{M}}$  effectively spanned by  $\mathbf{X}$ .

Negative Walsh spectral amplitudes may produce negative valued Rabi rates under a linear superposition. For a pulse of the form  $P_l = \exp[-i\Omega_l \tau_l \hat{\sigma}_{\phi_l}/2]$  the negative sign of  $\Omega_l$  may be absorbed into the spin operator  $\phi_l$  corresponds physically to the application of a  $\pi$  phase shift int he diriving field. This follows from the fact that  $\hat{\sigma}_{\phi+\pi} = -\hat{\sigma}_{\phi}$ , which is clear from the definition of our spin operator in equation (6.3). Thus including negative-valued Walsh spectral amplitudes generally produces single axis control only up to a sign change.

## Gaussian pulse envelopes

The square-envelope pulses studied experimentally in the main text are easy to generate in our experimental system but may prove difficult in other settings where abrupt amplitude shifts at timestep-edges produce significant pulse distortion. Here we show that achieving Walsh synthesized filters using a common Gaussian pulse envelope yields comparable results with a simple re-optimization of Walsh-synthesis coefficients.

The square amplitude-modulated waveform is here replaced with a smoothly varying pulse envelope in each segment, each associated with a specific rotation angle  $\theta_l$  subject to optimization. We assume a Gaussian profile  $G_l(t; \mu_l, \sigma_l)$  defined on  $t \in [t_{l-1}, t_l]$  with mean  $\mu_l$  and standard deviation  $\sigma_l$ . Specifically, we construct

$$G_l(t; \mu_l, \sigma_l) = \frac{\theta_l}{C_l \sigma_l \sqrt{2\pi}} \exp\left[-\frac{(t - \mu_l)^2}{2\sigma_l^2}\right] \quad (6.44)$$

$$\mu_l = \frac{t_{l-1} + t_l}{2} \quad (6.45)$$

$$\sigma_l = g\tau/\mathcal{M} \quad (6.46)$$

with  $\mu_l$  the segment midpoint and  $\sigma_l$  expressed as a multiple  $g$  of the segment duration. The normalizing factor

$$C_l := \int_{t_{l-1}}^{t_l} \frac{1}{\sigma_l \sqrt{2\pi}} \exp\left[-\frac{(t - \mu_l)^2}{2\sigma_l^2}\right] dt \quad (6.47)$$

is included to ensure the total rotation implemented by the Gaussian pulse in the  $l$ th segment is given by  $\int_{t_l}^{t_{l-1}} G_l(t; \mu_l, \sigma_l) dt = \theta_l$ . We now impose the same structure on the segment rotations  $\theta_l$  as presented above in equation (6.40). Defined in this way, the  $M$ -segment Gaussian-pulse sequence shares with the square WAMF construction the property that the total gate rotation angle  $\Theta = \sum_{l=1}^n \theta_l = X_0\tau$  is completely determined by the spectral amplitude of  $\text{PAL}_0$ .

We may therefore construct a Gaussian-pulse variation on any candidate WAMF such that, having set  $g$  to some value relevant to the control hardware, the smooth pulse sequence remains strictly parametrized in the Walsh spectrum  $\mathbf{X}$ . In particular, filter optimization proceeds in the same manner as for ordinary Walsh-modulated control by minimizing the cost function with respect to the Walsh spectrum.

## Analytic design rules

An advantage of Walsh synthesis is that the well-defined spectral properties and symmetries of the Walsh functions may be employed to further restrict the search space available for filter construction.

First, in practice the achievable filter order *over the entire stopband* is limited by the number of constituent control operations; one may achieve higher  $p$  at the cost of higher  $n$ . The maximum achievable value of  $p$  for a given filter is set by the power-law expansion of the filter for the single Walsh function with the highest Paley order for a given  $n$ . As has been shown previously, all Walsh functions with given Hamming weight of the Paley order have the same power-law expansion near zero frequency [75]. Therefore, in principle, every doubling of  $n$  increases the maximum achievable time-domain filter order by one. The Walsh functions highlighted in red in figure 6.5 represent those with the highest Paley-order Hamming weight for a given  $n$ . Nonetheless we find that in general we are able to construct filters with higher order than prescribed *over narrow regions in the stopband*, as a result of Walsh synthesis (see the multiple slopes for the blue line in figure 6.2c).

In filter construction we may further constrain the form of a candidate pulse sequence by imposing required physical properties on the sequence, such as fixing the total rotation angle of the Bloch vector in order to implement a target logic operation. In order to proceed we then partition the Walsh spectrum  $\mathbf{X} \equiv (\mathbf{X}_\nu, \mathbf{X}_\rho)$  into spectral amplitude classes  $\mathbf{X}_\nu$  and  $\mathbf{X}_\rho$  to be treated as *variational* and *fixed* parameters respectively. Fixed parameters set the physical state transformation of interest while the remaining unconstrained components in  $\mathbf{X}_\nu$  serve as tuning parameters by which to minimize  $A(\mathbf{X}_\nu; \mathbf{X}_\rho)$ .

The primary constraint in WAMF constructions is that the total rotation angle executed depends only on the value of  $X_0$ , the zeroth order spectral component; it sets the effective average Rabi rate for the WAMF. This can be seen as follows. First observe all Walsh functions of higher than zeroth order are *balanced* in the sense that  $\int_0^1 \text{PAL}_k(x) dx = \delta_{0k}$ . For the control field defined by equation (6.41) the total gate rotation angle  $\Theta = \int_0^\tau \Omega(t) dt$  then takes the form

$$\begin{aligned}\Theta &= \int_0^\tau \sum_{k=1}^N X_k \text{PAL}_k(t/\tau) dt \\ &= \tau \sum_{k=1}^N X_k \int_0^1 \text{PAL}_k(x) dx \\ &= \tau \sum_{k=1}^N X_k \delta_{0k} = X_0\tau.\end{aligned}$$

In this case the net gate rotation  $\theta = \Theta \bmod 2\pi$  is given by

$$\theta = X_0\tau \bmod 2\pi \quad (6.48)$$

implying the necessary constraint on  $X_0$  in order to achieve a desired  $\theta$ .

Next, we observe that the Walsh functions have distinct parity, but that filter constructions mandate symmetric constructions in order to enact a target operation and provide effective noise cancellation. The result is that odd-parity Walsh functions may generally be excluded from the variational search. While this is not necessarily strictly required (multiple odd parity Walsh functions may in principle be added with opposite signs to produce net symmetric constructions), it is convenient and effective to restrict the synthesis space to the so-called CAL subset of the Walsh functions.

Our reduced search problem may then be represented formally by replacing  $\Gamma_{\mathcal{M}} \rightarrow (\mathbf{X}_{\nu}, \mathbf{X}_{\rho})$  in equation (6.28) to obtain

$$A(\mathbf{X}_{\nu}; \mathbf{X}_{\rho}) := \int_0^{\omega_c} d\omega F(\tau\omega; \mathbf{X}_{\nu}, \mathbf{X}_{\rho}) \quad (6.49)$$

with the variational search now restricted to the subspace spanned by  $\mathbf{X}_{\nu}$  with the  $\mathbf{X}_{\rho}$  held constant.

## First order WAMFs

As a first application of the above result, we derive a family of nontrivial gates decoupled to first order against dephasing noise by constructing a pulse sequence from the synthesis  $\theta(t) = \frac{\tau}{4}(X_0 \text{PAL}_0(t/\tau) + X_3 \text{PAL}_3(t/\tau))$ . Note that  $\theta(t)$  is only formally defined at the end of pulse segments. That is, we set  $\mathbf{X}_{\rho} \equiv X_0$  and  $\mathbf{X}_{\nu} \equiv X_3$ . In this case  $N = 3$  and  $\mathcal{M} = 4$ , so the minimal pulse duration is  $\tau/4$ . Using equation (6.37) we obtain  $\tilde{\mathbf{X}} = [\tilde{X}_1, \tilde{X}_2, \tilde{X}_3, \tilde{X}_4]^T = [X_0, 0, 0, X_3]^T$ , yielding the minimal Hadamard representation

$$\boldsymbol{\theta} = \frac{\tau}{4} \begin{bmatrix} 1 & 1 & 1 & 1 \\ 1 & -1 & 1 & -1 \\ 1 & 1 & -1 & -1 \\ 1 & -1 & -1 & 1 \end{bmatrix} \begin{bmatrix} X_0 \\ 0 \\ 0 \\ X_3 \end{bmatrix} = \frac{\tau}{4} \begin{bmatrix} X_0 + X_3 \\ X_0 - X_3 \\ X_0 - X_3 \\ X_0 + X_3 \end{bmatrix} \quad (6.50)$$

These sequences therefore span the control subspace parametrized by ( $\tau = 1$ )

$$\text{WAMF } \mathcal{O}(1) = \begin{array}{c} \Omega_l \quad \theta_l \quad \tau_l \quad \phi_l \\ \hline P_1 \left[ \begin{array}{l} X_+ \\ X_- \end{array} \right] \left[ \begin{array}{l} \frac{X_+}{4} \\ \frac{X_-}{4} \end{array} \right] \left[ \begin{array}{l} \frac{1}{4} \\ \frac{1}{4} \end{array} \right] \left[ \begin{array}{l} 0 \\ 0 \end{array} \right] \\ P_2 \left[ \begin{array}{l} X_- \\ X_- \end{array} \right] \left[ \begin{array}{l} \frac{X_-}{4} \\ \frac{X_-}{4} \end{array} \right] \left[ \begin{array}{l} \frac{1}{4} \\ \frac{1}{4} \end{array} \right] \left[ \begin{array}{l} 0 \\ 0 \end{array} \right] \\ P_3 \left[ \begin{array}{l} X_- \\ X_+ \end{array} \right] \left[ \begin{array}{l} \frac{X_-}{4} \\ \frac{X_+}{4} \end{array} \right] \left[ \begin{array}{l} \frac{1}{4} \\ \frac{1}{4} \end{array} \right] \left[ \begin{array}{l} 0 \\ 0 \end{array} \right] \\ P_4 \left[ \begin{array}{l} X_+ \\ X_+ \end{array} \right] \left[ \begin{array}{l} \frac{X_+}{4} \\ \frac{X_+}{4} \end{array} \right] \left[ \begin{array}{l} \frac{1}{4} \\ \frac{1}{4} \end{array} \right] \left[ \begin{array}{l} 0 \\ 0 \end{array} \right] \end{array} \quad (6.51)$$

where we have defined  $X_{\pm} = X_0 \pm X_3$ . This choice is motivated by the fact that Paley order  $k = 3$  corresponds to the lowest order non-constant Walsh function with even symmetry about  $\tau/2$  (figure 6.5). Hence (6.50) is the simplest Walsh modulated form which includes the zeroth order Walsh function in the synthesis and which possesses time-reversal symmetry about the sequence midpoint. The former property ensures a nontrivial gate angle is executed. The latter

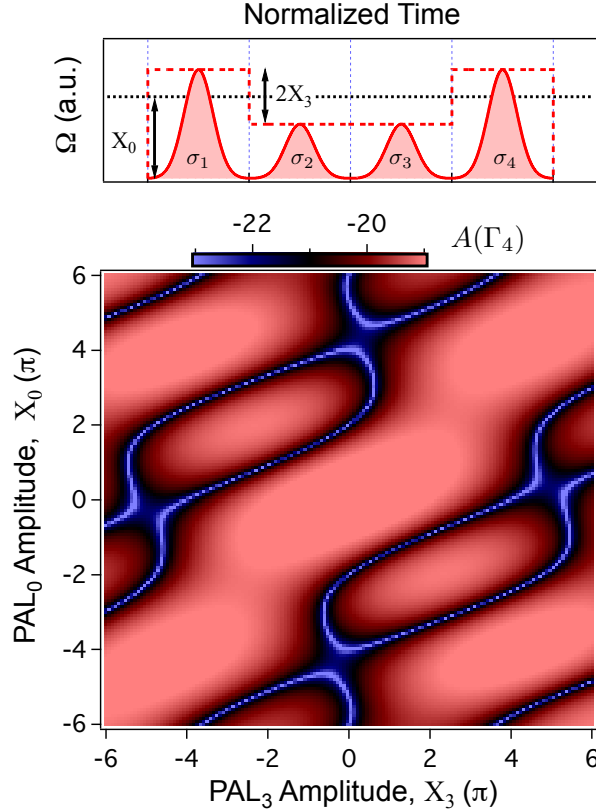


Figure 6.6: *Construction of the first-order Walsh amplitude modulated dephasing-suppressing filter using Gaussian-shaped pulse segments.* a) Schematic representation of Walsh synthesis for a four segment gate of discrete Gaussian segments. Walsh synthesis determines the overall amplitude of Gaussian pulses with fixed duration and standard deviation, setting the effective pulse area in each segment. b) Two-dimensional representation of the integral metric defining our target cost function,  $A(\Gamma_4)$  integrated over the stopband  $\omega \in [10^{-9}, 10^{-6}]\tau^{-1}$ . Areas in blue minimize  $A(\Gamma_4)$ , representing effective filter constructions. The  $X_0$  determines the net rotation enacted in a gate while  $X_3$  determines the modulation depth, as represented in a).

is chosen due to the observation in dynamic decoupling literature that using time-symmetric building blocks often improves the performance of the sequence compared to sequences formed by time-asymmetric building blocks [156, 151]. In this construction we have maintained a leading column of rabi rates,  $\Omega_l$ , as would be appropriate for the square-pulse forms used in the main text.

### Gaussian pulse construction

Adding to the results presented in the main text, constructing the 4-segment filter  $W1$  using square pulse segments, we examine the Gaussian-pulse variation here. The cost function  $A_z(X_3; X_0) = \int_{\omega_L}^{\omega_c} d\omega F_z(\omega\tau; X_3; X_0)$  may be computed by partitioning the time domain into a large number  $N_s$  of subintervals on which the continuous Gaussian envelope is treated as approximately constant. Figure 6.6 shows a two-dimensional representation of  $A_z(X_3; X_0)$  integrated over the interval  $\omega \in [10^{-9}, 10^{-6}]\tau^{-1}$ , with  $g = 1/6$  and  $N_s = 100$ . The value of  $\text{Log}_{10}[A_z(X_3; X_0)]$  is indicated by the color scale. Total sequence length is normalized to

$\tau = 1$  in this data, so the total gate rotation angle  $\Theta \equiv X_0$  is given directly by the  $X_0$ -axis. Regions in blue represent effective (first-order) filter constructions, where the cost function is minimized.

We conclude useful filter construction using Gaussian pulses is a simple matter of re-optimization in the Walsh-synthesis framework. This is readily achieved using a Nelder-Mead optimization of  $A_z(X_3; X_0)$  for any particular choice of  $g, \omega_L, \omega_c, X_0$  or  $N_s$ , in a manner precisely the same as for square envelopes.

## Universal Filters by Concatenation

Phase-modulated sequences robust against amplitude noise may also be found in the Walsh basis, yielding *Walsh phase-modulated filters* (WPMFs) analogous to WAMFs, and implementing arbitrary target rotations  $\theta$ . There are a variety of techniques to construct such WPMFs, but we use analytic design rules in which a target rotation is performed (with some error due to noise), and phase-modulated segments are added in order to produce the net filtering effect. The simplest WPMF adds two segments phase modulated according to Walsh function  $\text{PAL}_1$  with coefficient  $X_1$ , subject to the constraint that one enacts the desired driven rotation by  $\theta$ .

The result of this approach yields a WPMF that is identical to the NMR sequence SK1, with value  $X_1 = \cos^{-1}(-\theta/4\pi) \equiv \phi_{\text{SK1}}(\theta)$  [87], as represented

$$\boldsymbol{\Gamma}_3^{(\text{SK1})} = \begin{matrix} & \Omega_l & \theta_l & \tau_l & \phi_l \\ P_1 & \left[ \begin{array}{cccc} \Omega_0 & \theta & \tau_\theta & 0 \\ \Omega_0 & 2\pi & \tau_{2\pi} & \phi_{\text{SK1}} \\ \Omega_0 & 2\pi & \tau_{2\pi} & -\phi_{\text{SK1}} \end{array} \right] \\ P_2 & & & & \\ P_3 & & & & \end{matrix} \quad (6.52)$$

$$\Omega_0 = \frac{\theta + 4\pi}{\tau}, \quad \tau_\theta = \frac{\theta}{\Omega_0}, \quad \phi_{\text{SK1}}(\theta) := \cos^{-1}\left(-\frac{\theta}{4\pi}\right). \quad (6.53)$$

Note that the Walsh timing construction only holds in the two correction steps represented above. Following a similar route allows one to construct a sequence with modulation given by  $\text{PAL}_3$  which is formally identical to the three-segment (four-timestep) phase modulation given by gate  $P_2$  [87].

These WPMF sequences perform as first-order time-dependent noise filters, captured in the form of  $F_\Omega(\tau\omega)$ , and noted in table 6.1 (column 2). For example, filter functions for the WPMF that is equivalent to SK1 are shown in figure 6.7b, revealing first-order filtering of amplitude noise, but not dephasing noise.

We may now concatenate WAMFs and WPMFs in order to simultaneously filter universal noise. We focus on an explicit example providing first-order amplitude and dephasing noise filtering. The basic procedure is to implement each constant-amplitude segment of a four-segment WAMF,  $W_1$ , using a constant-amplitude phase-modulated sequence robust against amplitude noise. As a reminder, the noise-filtering performance of  $W_1$  is shown in figure 6.7c. Here we use the  $\text{WPMF} \equiv \text{SK1}$  sequence for the phase modulation. We refer to the concatenated gate as a Universal Walsh Modulated Gate,  $\text{UWMF}_{1,\text{SK1}}$ .

Referring to equation 6.51, the WAMF filter is similarly written

$$P_3(X_+/4, 0)P_2(X_-/2, 0)P_1(X_+/4, 0).$$

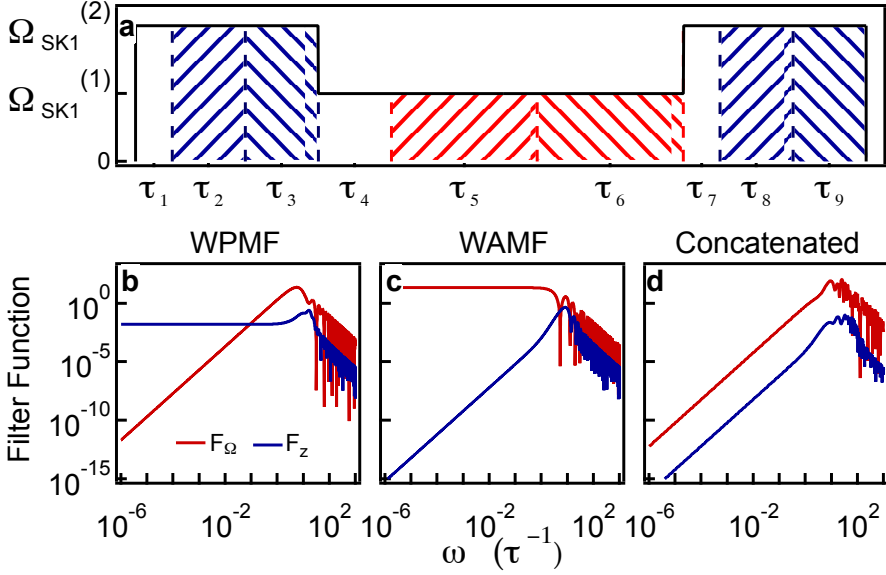


Figure 6.7: Concatenation scheme for universal noise suppression. a) Concatenation of  $WPMF \equiv SK1$  within first order WAMF sequence yielding  $UWMF_{1,SK1}$ . White fill indicates rotations enacted with  $\phi = 0$ ; orientation of hatching denotes  $SK1$  phase flips  $\phi = \pm\phi_{SK1}$ . b) Filter functions for  $WPMF \equiv SK1$  sequence. c) Filter functions for four-segment WAMF sequence,  $W1$ . d) Filter functions for concatenated sequence.

Concatenation then involves the operator substitutions

$$P_1(X_+/4, 0) \rightarrow SK1^{(1)}(X_+/4) \quad (6.54)$$

$$P_2(X_-/2, 0) \rightarrow SK1^{(2)}(X_-/2) \quad (6.55)$$

$$P_3(X_+/4, 0) \rightarrow SK1^{(3)}(X_+/4). \quad (6.56)$$

The composite structure for  $UWMF_{1,SK1}$  is shown in figure 6.7a. Here the  $SK1$  phase flips  $\phi = \pm\phi_{SK1}$  within each segment of the WAMF profile are indicated by the oppositely oriented hatching;  $\phi = 0$  is indicated by white fill. The dephasing and amplitude filter functions for the concatenated sequence are shown in figure 6.7d, indicating effective filtering of both amplitude and dephasing noise.

## Ytterbium Ion Trapping

We use trapped  $^{171}\text{Yb}^+$  ions as our experimental platform; a detailed description of related experimental approaches appears in [157, 127]. A linear Paul trap enclosed in an ultra-high vacuum (UHV) chamber is used to trap several hundred  $^{171}\text{Yb}^+$  ions as a small homogeneous ensemble (in magnetic field and microwave field amplitude). Doppler cooling of the ions is achieved using 369 nm laser light, slightly red-detuned from the  $^2\text{S}_{1/2}$  to  $^2\text{P}_{1/2}$  transition. Additional lasers near 935 nm and 638 nm are employed to depopulate metastable states.

Our qubit is the 12.6 GHz hyperfine splitting between the two states  $^2\text{S}_{1/2} |F = 0, m_f = 0\rangle$  and  $^2\text{S}_{1/2} |F = 1, m_f = 0\rangle$  states. For notational simplicity we will designate  $|0\rangle$  and  $|1\rangle$  to these states respectively. Addition of a 2.1 GHz sideband to the 369nm laser using an electro-optic modulator permits high-fidelity state preparation in  $|0\rangle$ . For details of ion loading, laser cooling, state preparation, and state detection see [127]. While we typically employ a small ensemble of ions, the system behaves similarly to single-ion experiments in our lab, and benefits

from both high-fidelity state initialization and projective measurement - the system does not bear similarity to NMR-style ensembles.

State detection is achieved by counting 369 nm photons scattered from the ions and converting to a probability that the Bloch vector lies at a particular location along a meridian of the Bloch sphere. This measurement is susceptible ion loss in the ensemble and both laser amplitude and frequency drifts over long timescales, resulting in variable maximum and dark count rates over time. We therefore employ a normalization and Bayesian estimation procedure for state detection, see [127].

An important advantage of this system is that the selected qubit transition is first order insensitive to magnetic field fluctuations; the measured free-evolution in our setup is  $T_2 \approx 4$  s, limited by coherence between the qubit and the master oscillator [127]. Coherent rotations between the measurement basis states are driven by using the magnetic field component of resonant microwave radiation. The Rabi rate for driven oscillations reaches  $\sim 14 \mu\text{s}$  in our system, with typical operation near  $\sim 50 \mu\text{s}$ . Rotations are implemented about an axis  $\vec{r}$  lying on the  $xy$ -plane of the Bloch sphere and set by the phase of the microwaves as  $\vec{r} = (\cos \phi(t), \sin \phi(t), 0)$ . Driven operations, characterized by randomized benchmarking, exhibit a mean fidelity in excess of 99.99%.

## Noise Engineering

In the laboratory we rely on engineering noise in our control system to provide a method to accurately reproduce decoherence processes of interest. We begin with a desired noise power spectral density in either the amplitude or detuning quadrature (or both), assuming they are statistically independent. From this power spectrum, defined by the noise strength  $\alpha$ , the exponent of the power-law scaling  $p$ , the comb spacing  $\omega_0$ , and the high-frequency cutoff  $\omega_c \geq J\omega_0$ , we numerically generate time-domain vectors for amplitude and frequency errors. Noise is injected into the system by adding these modulation patterns on top of the control sequence being implemented (e.g. a pulse of radiation for implementing a  $\pi$ -pulse) using  $IQ$  modulation in our vector signal generator [127].

## Randomized Benchmarking

We use randomized benchmarking as a tool for resolving small gate errors which cannot be resolved in the application of a single gate. Our randomized benchmarking sequence consists of interleaved  $\pi/2$  and  $\pi$  pulses each applied along axes randomly selected from  $\pm x$  and  $\pm y$ . Each sequential pair of  $\pi/2$  and  $\pi$  rotations is referred to a computational gate. A given randomized benchmarking sequence consists of  $l$  computational gates followed by a final correcting gate which is selected such that the aggregate Unitary operation applied is a  $\pi$  rotation. For each  $l$  we measure 50 randomizations (dots in Fig. 3f of the main text), and in each randomization average over 20 different realizations of a white dephasing noise bath. Each realization, in turn, employs 20 measurements in our Bayesian state-detection algorithm, in addition to associated normalization experiments.

Comparisons of  $W1$  to primitive  $\pi$  rotation performance in randomized benchmarking is conducted via replacement of all  $\pi$  pulses with  $W1$  constructions, again about randomly selected axes. In either case the  $\pi/2$  rotation is achieved using a primitive gate, although we have also validated that replacement of the  $\pi/2$  gates with WAMF constructions yields net improvement in gate fidelity.

# Chapter 7

## Designing a practical high-fidelity long-time quantum memory

Quantum memory is a central component for quantum information processing devices, and will be required to provide high-fidelity storage of arbitrary states, long storage times and small access latencies. Despite growing interest in applying physical-layer error-suppression strategies to boost fidelities, it has not previously been possible to meet such competing demands with a single approach. Here we use an experimentally validated theoretical framework to identify periodic repetition of a high-order dynamical decoupling sequence as a systematic strategy to meet these challenges. We provide analytic bounds – validated by numerical calculations – on the characteristics of the relevant control sequences and show that a stroboscopic saturation of coherence, or coherence plateau, can be engineered, even in the presence of experimental imperfection. This permits high-fidelity storage for times that can be exceptionally long, meaning that our device-independent results should prove instrumental in producing practically useful quantum technologies.

The contents of this chapter have been published as: K. Khodjasteh, J. Sastrawan, D. Hayes, T. J. Green, M. J. Biercuk and L. Viola, “Designing a practical high-fidelity long-time quantum memory”, *Nature Communications* **4**, 2045 (2013). The ‘bang bang’ dynamical decoupling sequences described in section 2.5.3 are designed, primarily, for the purposes of short-time state preservation. In this work, we take up the challenge of adapting these protocols to the task of long-time state preservation, or quantum memory. It is the perspective of spectral filtering that gives us the insight on which we base our response to this challenge.

### 7.1 Introduction

Developing techniques for the preservation of arbitrary quantum states – that is, quantum memory – in realistic, noisy physical systems is vital if we are to bring quantum-enabled applications, including secure communications and quantum computation, to reality. While numerous techniques relying on both open- and closed-loop control have been devised to address this challenge, *dynamical error suppression* strategies based on dynamical decoupling (DD) [48, 58, 64, 67], dynamically corrected gates (DCGs) [68, 54], and composite pulsing [87] are emerging as a method of choice for *physical-layer* decoherence control in realistic settings described by non-Markovian open-quantum-system dynamics. Theoretical and experimental studies in a variety of platforms [32, 125, 158, 159, 160, 90, 161, 149, 91, 162, 163, 89, 164, 165, 166, 167]

have consistently pointed to dynamical error suppression as a resource-efficient approach to substantially reducing physical error rates.

Despite these impressive advances, investigations to date have largely failed to capture the typical operating conditions of any true quantum memory; namely, high-fidelity storage of quantum information for *arbitrarily long storage times*, with on-demand access. This would be required, for instance, in a quantum repeater, or in a quantum computer where some quantum information must be maintained with error rates deep below fault-tolerant thresholds while large blocks of an algorithm are carried out on other qubits. Instead, both experiment and theory have primarily focused on two control regimes [47]: the ‘coherence-time regime,’ where the goal is to extend the characteristic ( $1/e$ ’ or  $T_2$ ) decay time for coherence as long as possible, and the ‘high-fidelity regime,’ where the goal is to suppress errors as low as possible for storage times short compared to  $T_2$  (for instance, during a single gating period). Similarly, practical constraints on control timing and access latency – of key importance to laboratory applications – have yet to be considered in a systematic way.

In this chapter, we demonstrate how to realize a practically useful quantum memory via dynamical error suppression. Specifically, our studies identify the *periodic repetition of a high-order DD sequence* as an effective strategy for memory applications, considering realistic noise models, incorporating essential experimental limitations on available controls, and addressing the key architectural constraint of maintaining short access latencies to stored quantum information. We consider a scenario where independent qubits couple to a noisy environment, and both dephasing and depolarization errors introduced by realistic DD sequences of bounded-strength  $\pi$ -pulses are fully accounted for. We analytically and numerically characterize the achievable long-time coherence for repeated sequences and identify conditions under which a stroboscopic ‘coherence plateau’ can be engineered, and fidelity *guaranteed* to a desired level at long storage times – even in the presence of experimentally realistic constraints and imperfections. We expect that our approach will provide a practical avenue to high-fidelity low-latency quantum storage in realistic devices.

## 7.2 Results

### 7.2.1 Model

The salient features of our approach may be appreciated by first focusing on a single qubit subject to dephasing. In the absence of control, we consider a model Hamiltonian of the form  $H \equiv \sigma_z \otimes (\epsilon_0 + B_z) + H_B$ , where the Pauli matrix  $\sigma_z$  and  $\epsilon_0$  define the qubit quantization axis and internal energy, respectively (we can set  $\epsilon_0 = 0$  henceforth), and  $B_z$ ,  $H_B$  are operators acting on the environment Hilbert space. An *exact* analysis of both the free and the controlled dynamics is possible if the environment can be described in terms of either a quantum bosonic bath in thermal equilibrium (spin-boson model), a weakly-coupled quantum spin bath (spin-bath model), or a stationary Gaussian stochastic process (classical-noise model) [168, 48, 67, 53, 169, 72, 75, 170, 171]. Such dephasing models provide an accurate physical description whenever relaxation processes associated with energy exchange occur over a characteristic time scale ( $T_1$ ) substantially longer than any typical time scale associated with the dephasing dynamics. As a result, our analysis is directly relevant to a wide range of experimentally relevant qubit systems, from trapped ions and atomic ensembles [32, 158] to spin qubits in nuclear and electron magnetic resonance and quantum dots [102, 171, 162, 160, 90, 161].

We shall proceed by considering the effects of DD within a filter-design framework which generalizes the transfer-function approach widely used across the engineering community [172]

and provides a transparent and experimentally relevant picture of the controlled dynamics in the frequency domain [49, 53, 32, 125, 47, 100]. In order to more easily introduce key concepts and clearly reveal our underlying strategy, we first consider an idealized ‘bang-bang’ DD setting in which perfect instantaneous  $\pi$  rotations are effected by using unbounded control amplitudes. As we move forward, we will relax these unphysical constraints, and demonstrate how similar results may be obtained with experimentally realistic controls.

In such an idealized control scenario, a DD sequence may be specified in terms of the pulse-timing pattern  $p \equiv \{t_j\}_{j=1}^n$ , where we also define  $t_0 \equiv 0$ ,  $t_{n+1} \equiv T_p$  as the sequence duration, and we take all the interpulse intervals  $(t_{j+1} - t_j)$  to be lower-bounded by a *minimum interval*  $\tau$  [72]. The control propagator reads  $U_c(t) = \sigma_x^{[y_p(t)+1]/2}$ , with  $y_p(t)$  being a piecewise-constant function that switches between  $\pm 1$  whenever a pulse is applied. The effect of DD on qubit dephasing may be evaluated exactly in terms of a spectral overlap of the control modulation and the noise power spectral density,  $S(\omega)$  [49, 53], which is determined by the Fourier transform of the two-time noise correlation function [170]. Typically,  $S(\omega)$  has a power-law behavior at low frequencies, and decays to zero beyond an upper cutoff  $\omega_c$ , that is,  $S(\omega) \propto \omega^s f(\omega, \omega_c)$ , and the ‘rolloff function’  $f$  specifies the high-frequency behavior,  $f = \Theta(\omega - \omega_c)$  corresponding to a ‘hard’ cutoff. Let  $\tilde{y}_p(\omega)$  denote the Fourier transform of  $y_p(t)$ , which is given by [67, 53]

$$\tilde{y}_p(\omega) = \omega^{-1} \sum_{j=0}^n (-1)^j [\exp(it_j\omega) - \exp(it_{j+1}\omega)].$$

The *filter function* (FF) of the sequence  $p$  is given by  $F_p(\omega) = \omega^2 |\tilde{y}_p(\omega)|^2$ , and the bang-bang-controlled qubit coherence decays as  $e^{-\chi_p}$ , where the *decoupling error*  $\chi_p = \int_0^\infty \frac{S(\omega)}{2\pi\omega^2} F_p(\omega) d\omega$  at time  $t = T_p$ , and the case  $n = 0$  recovers free evolution over  $[0, T_p]$ .

In this framework, the applied DD sequence behaves like a ‘high-pass’ filter, suppressing errors arising from slowly fluctuating (low-frequency) noise. Appropriate construction of the sequence then permits the bulk of the noise power spectrum to be efficiently suppressed, and coherence preserved. For a given sequence  $p$ , this effect is captured quantitatively through the *order of error suppression*  $\alpha_p$ , determined by the scaling of the FF near  $\omega = 0$ , that is,  $F_p(\omega) \equiv |A_{bb}|^2 \omega^{2(\alpha_p+1)} \propto (\omega\tau)^{2(\alpha_p+1)}$ , for a sequence-dependent pre-factor  $A_{bb}$ . A high multiplicity of the zero at  $\omega = 0$  leads to a perturbatively small value of  $\chi_p$  as long as  $\omega_c\tau \ll 1$ . In principle, one may thus achieve low error probabilities over a desired storage time  $T_s$  simply by using a high-order DD sequence, such as Concatenated DD (CDD, [64]) or Uhrig DD (UDD, [67]), with the desired storage time  $T_s \equiv T_p$ .

### 7.2.2 Quantum memory requirements

Once we attempt to move beyond this idealized scenario in order to meet the needs of a practically useful, long-time quantum memory, several linked issues arise. First, perturbative DD sequences are *not* generally viable for high-fidelity long-time storage as they require arbitrarily fast control ( $\tau \rightarrow 0$ ). Real systems face systematic constraints mandating  $\tau > 0$ , and as a result, increasing  $\alpha_p$  necessitates extension of  $T_p$ , placing an upper bound on high-fidelity storage times [169, 173, 72]. (For instance, a UDD <sub>$n$</sub>  sequence achieves  $\alpha_p = n$  with  $n$  pulses, applied at  $t_j = T_p \sin^2[\pi j/(2n+2)]$ . For fixed  $T_p$ , increasing  $\alpha_p$  implies increasing  $n$ , at the expense of shrinking  $\tau$  as  $\tau \equiv t_1 = \mathcal{O}(T_p/n^2)$ . If  $\tau > 0$  is fixed, and  $\alpha_p$  is increased by lengthening  $T_p$ , eventually the perturbative corrections catch up, preventing further error reduction.) Second, potentially useful numerical DD approaches, such as randomized DD [174, 175] or optimized ‘bandwidth-adapted’ DD [72], become impractical as the configuration space of *all* possible DD sequences over which to search grows exponentially with  $T_s$ . Third, DD exploits inter-

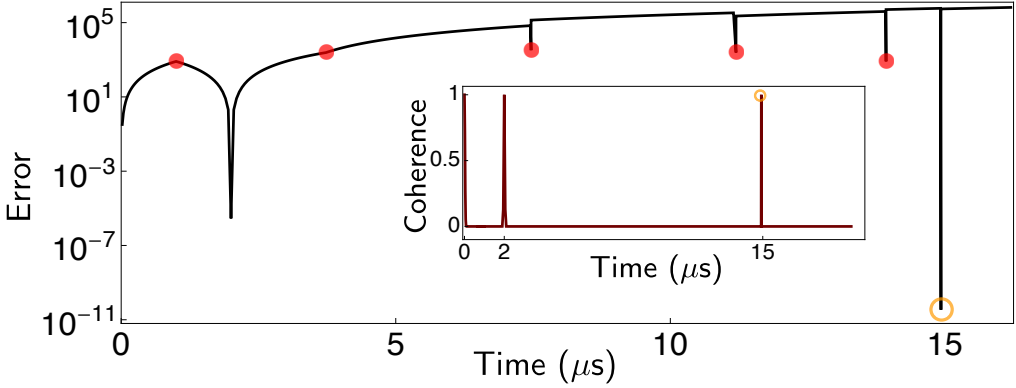


Figure 7.1: **Access-latency in high-order DD sequences.** DD error and coherence (inset) during a  $UDD_5$  sequence with minimum interpulse time  $\tau = 1 \mu\text{s}$ . Pulse times are marked with filled circles while the open circle indicates the readout time  $T_p$ . Minimal error (maximal coherence) is reached only at the conclusion of the sequence, with the coherence spike near  $2 \mu\text{s}$  resulting from a spin-echo effect. For illustration purposes, in all figures we assume a phenomenological noise model appropriate for nuclear-spin induced decoherence in a spin qubit in GaAs,  $S(\omega) = g(\omega/\omega_c)^{-2}e^{-\omega^2/\omega_c^2}$ , with  $\omega \in [\omega_{\min}, \omega_{\max}]$ . We set  $g = 0.207\omega_c$ ,  $\omega_c/2\pi = 10\text{kHz}$ ,  $\omega_{\min}/2\pi = 0.01 \text{ Hz}$ , and  $\omega_{\max}/2\pi = 10^8 \text{ Hz}$  to maximize agreement with the measured  $T_2$  ( $\approx 35 \text{ ns}$ ) [90, 76]. We chose  $\tau$  well above technological constraints ( $\sim \text{ns}$ ) in order to reduce  $n$ .

ference pathways between control-modulated trajectories, meaning that mid-sequence interruption ( $t < T_p$ ) typically result in significantly sub-optimal performance (figure 7.1). However, a stored quantum state in a practical quantum memory must be accessible not just at a designated final retrieval time but at intermediate times also, at which it may serve as an input to a quantum protocol.

Addressing all such issues requires a systematic approach to DD sequence construction. Here, we identify a ‘modular’ approach to generate low-error, low-latency DD sequences for long-time storage out of shorter blocks: *periodic repetition* of a base, high-order DD cycle.

### 7.2.3 Quantum memory via periodic repetition

The effect of repetition for an *arbitrary* sequence is revealed by considering the transformation properties of the FF under sequence combination. Consider two sequences,  $p_1$  and  $p_2$ , joined to form a longer one, denoted  $p_1 + p_2$ , with propagator  $y_{p_1+p_2}(t)$ . In the Fourier space we have  $\tilde{y}_{p_1+p_2}(\omega) = \tilde{y}_{p_1}(\omega) + e^{i\omega T_{p_1}} \tilde{y}_{p_2}(\omega)$ . Let now  $[p]^m$  denote the sequence resulting from repeating  $p$ , of duration  $T_p$ ,  $m$  times, with  $T_s = mT_p$ . Computing  $\tilde{y}_{[p]^m}(\omega)$  by iteration, the following exact expression is found:

$$\chi_{[p]^m} = \int_0^\infty \frac{S(\omega)}{2\pi\omega^2} \frac{\sin^2(m\omega T_p/2)}{\sin^2(\omega T_p/2)} F_p(\omega) d\omega. \quad (7.1)$$

Equation (7.1) describes dephasing dynamics under *arbitrary* multipulse control, generalizing special cases in which this strategy is implicitly used for simple base sequences (periodic DD,  $p = \{\tau, \tau\}$  [169] and Carr-Purcell,  $p = \{\tau, 2\tau, \tau\}$ ), and showing similarities with the intensity pattern due to an  $m$ -line diffraction grating [171]. The single-cycle FF,  $F_p(\omega)$ , is multiplied by a factor which is rapidly oscillating for large  $m$  and develops peaks scaling with  $\mathcal{O}(m^2)$  at

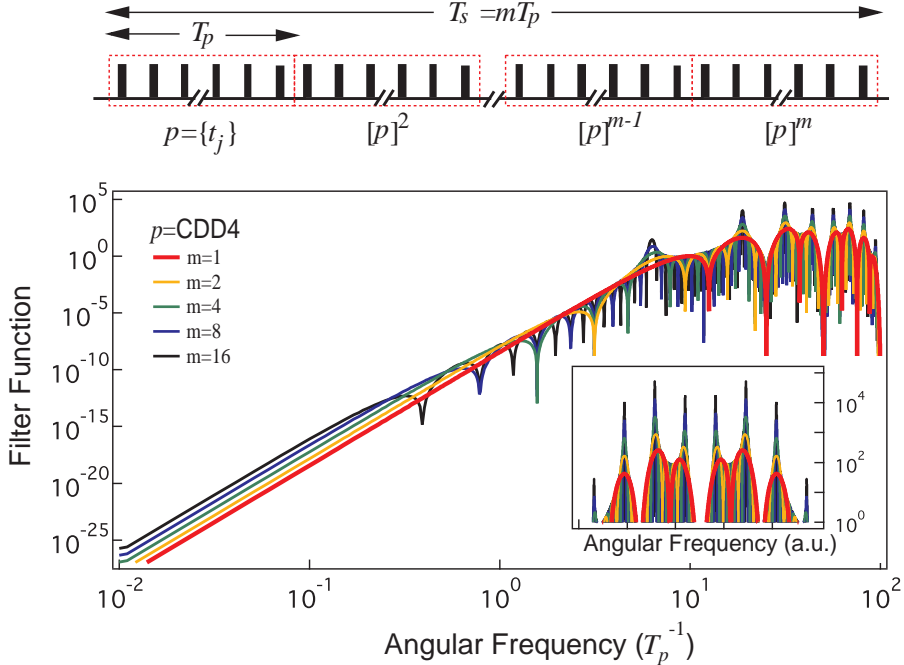


**Figure 7.2: Schematic representation of base sequence repetition and the effect on the filter function.** Top: The base sequence  $p$  is indicated in red dashed boxes, and repeated  $m$  times up to a total storage time  $T_s$ . Bottom: FF for repetition of a  $CDD_4$  cycle. The FF on a log-log plot grows with frequency with slope set by  $\alpha_p$  until it reaches the passband, where noise is passed largely unimpeded (red thick line). Noise dominated by spectral components in this region is efficiently suppressed by DD. As  $m$  grows, the sinusoidal terms in equation (7.1) lead to the emergence of ‘resonance’ frequencies that modify the single-cycle FF and produce sharp peaks in the passband. These must be considered when accounting for the effects of noise at long storage time due to ‘resonance’ effects. Inset: FF passband on a log-linear plot.

multiples of the ‘resonance frequency,’  $\omega_{\text{res}} = 2\pi/T_p$ , introduced by the periodic modulation (see figure 7.2 for an illustration).

After many repeats, the DD error is determined by the interplay between the order of error suppression of the base sequence, the noise power behavior at low frequencies, and the size of noise contributions at the resonance frequencies. The case of a hard upper frequency cutoff at  $\omega_c$  is the simplest to analyze. Applying the Riemann-Lebesgue lemma removes the oscillating factor, resulting in the following asymptotic expression:

$$\lim_{m \rightarrow \infty} \chi_{[p]^m} \equiv \chi_{[p]^\infty} = \int_0^{\omega_c} \frac{S(\omega)}{4\pi\omega^2} \frac{F_p(\omega)}{\sin^2(\omega T_p/2)} d\omega, \quad (7.2)$$

provided that  $\chi_{[p]^\infty}$  is finite. The meaning of this exact result is remarkable: for small  $m$ , the DD error initially increases as  $(m^2 \chi_p)$ , until coherence stroboscopically saturates to a non-zero *residual plateau* value ( $e^{-\chi_{[p]^\infty}}$ ), and *no further decoherence occurs*. Mathematically, the emergence of this coherence plateau requires that simple conditions be obeyed by the chosen base sequence relative to the characteristics of the noise:

$$s + 2\alpha_p > 1, \quad T_p \omega_c < 2\pi, \quad (7.3)$$

which correspond to removing the singularity of the integrand in equation (7.2) at 0 and  $\omega_{\text{res}}$ , respectively. Thus, judicious selection of a base sequence, fixing  $\alpha_p$  and  $T_p$ , can guarantee

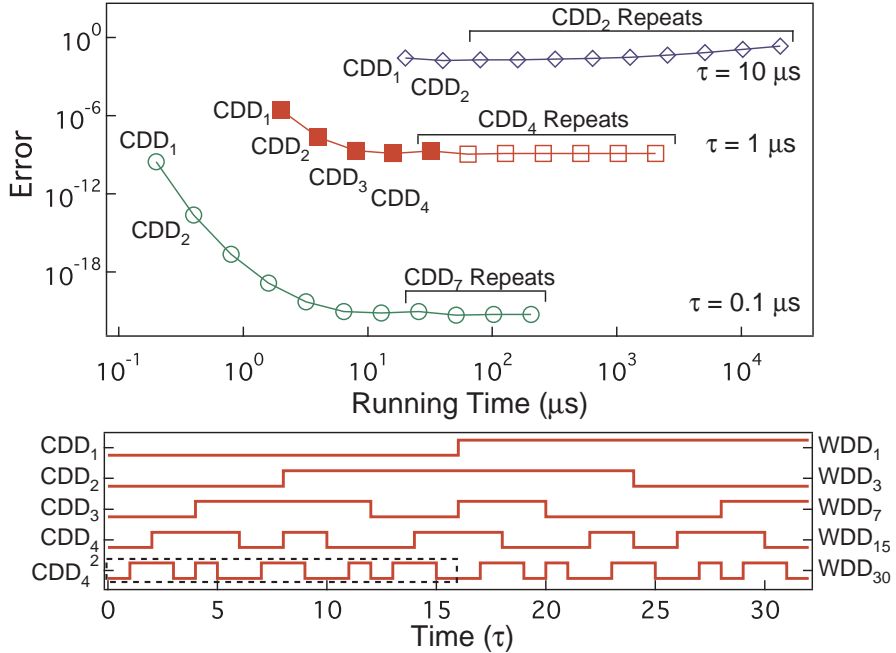


**Figure 7.3: Emergence of coherence plateau and sequence structure.** *Top:* Minimal-error DD sequences from numerical search over Walsh DD, for  $\tau = 0.1, 1, 10 \mu\text{s}$ . In each series, the minimal-error sequences systematically access higher orders of error cancellation (via concatenation) over increasing running times, until an optimal concatenated sequence is found which is then repeated in the longer minimal-error sequences. The gradual increase in error (loss of plateau) for the series with  $\tau = 10 \mu\text{s}$  is due to the softness of the high-frequency cutoff and the constraints placed on  $T_p$  by fixing  $\tau$ . For the case of  $\tau = 1 \mu\text{s}$ , we have calculated the error out to  $m \approx 10^8$  repeats ( $T_s \approx 10^3 \text{ s}$ , data not shown) without an observable effect from the soft cutoff. *Bottom:* Control propagators corresponding to the solid markers in the middle data series ( $\tau = 1 \mu\text{s}$ ), showing the emergence of a periodic structure for sufficiently long storage time. Labels indicate the corresponding sequence designations in either the CDD or Walsh basis. Control propagators scaled to same length for ease of comparison. Dashed box highlights base sequence  $CDD_4$  that is repeated for long times.

indefinite saturation of coherence in principle. Moreover, since  $\chi_{[p]^m} \leq 2\chi_{[p]^\infty}$  for all  $m$ , the emergence of coherence saturation in the infinite-time limit stroboscopically guarantees high fidelity throughout long storage times. By construction, this approach also guarantees that *access latency is capped* at the duration of the base sequence, with  $t_\ell = T_p \ll T_s$ ; sequence interrupts at intermediate times that are multiples of  $T_p$  are thus permitted in the plateau regime *without degradation of error suppression*.

Additional insight into the above phenomenon may be gained by recalling that for free dephasing dynamics ( $\alpha_p = 0$ ), the possibility of non-zero asymptotic coherence is known to occur for supra-Ohmic ( $s > 1$ ) bosonic environments [168, 169], consistent with equation (7.3). The onset of a plateau regime in the controlled dynamics may then be given an intuitive interpretation by generalizing the analysis carried out in [169] for periodic DD: if the conditions in equation (7.3) are obeyed, the low-frequency (long-time) behavior becomes effectively supra-ohmic by action of the applied DD sequence and, after a short-time transient, the dephasing dynamics ‘oscillate in phase’ with the periodically repeated blocks. For sufficiently small  $T_p$ , the ‘differential’ DD error accumulated over each cycle in this steady state is very small, leading

to the stroboscopic plateau. Interestingly, that phase noise of a local oscillator can saturate at long times under suitable spectral conditions has also long been appreciated in the precision oscillator community [172].

In light of the above considerations, the occurrence of a coherence plateau may be observed even for sub-Ohmic noise spectra ( $s < 1$ ), as typically encountered, for instance, in both spin qubits ( $s = -2$ , as in figure 7.1) and trapped ions ( $s = -1$ , [176]). Numerical calculations of the DD error using such realistic noise spectra demonstrate both the plateau phenomenon and the *natural* emergence of periodically repeated sequences as an efficient solution for long-time storage, also confirming the intuitive picture given above. In these calculations, we employ a direct bandwidth-adapted DD search up to time  $T_s$ , by enforcing additional *sequencing constraints*. Specifically, we turn to Walsh DD, wherein pulse patterns are given by the Walsh functions, to provide solutions that are efficient in the complexity of sequencing [75]. Walsh DD comprises familiar DD protocols, such as spin echo, Carr-Purcell, and CDD, along with more general protocols, including repetitions of shorter sequences.

Starting with a free evolution of duration  $\tau$ , all possible Walsh DD sequences can be recursively built out of simpler ones within Walsh DD, doubling in length with each step. Further, since all interpulse intervals in Walsh DD protocols are constrained to be integer multiples of  $\tau$ , there are  $\frac{1}{2}(T_s/\tau)$  Walsh DD sequences that stop at time  $T_s$ , a very small subset of all  $2^{T_s/\tau}$  possible digital sequences, enabling an otherwise intractable bandwidth-adapted DD numerical minimization of the spectral overlap integral  $\chi_p$ .

Representative results are shown in figure 7.3, where for each  $T_s$  all Walsh DD sequences with given  $\tau$  are evaluated and those with the lowest error are selected. The choice of  $\tau$  sets the minimum achievable error and also determines whether a plateau is achievable, as, for a given  $T_s$ , it influences the available values of  $T_p$  and  $\alpha_p$ . As  $T_s$  grows, the best performing sequences (shown) are found to consist of a few concatenation steps (increasing  $\alpha_p$  of the base sequence to obey equation. (7.3)), followed by successive repetitions of that fixed cycle. Once the plateau is reached, increasing the number of repetitions does not affect the calculated error, indicating that stroboscopic sequence interrupts would be permitted without performance degradation. Beside providing a direct means of finding high-fidelity long-time DD schemes, these numerical results support our key analytic insights as to use of periodic sequence design.

## 7.2.4 Realistic effects

For clarity, we have thus far relied on a variety of simplifications, including an assumption of pure phase decoherence and perfect  $\pi$  rotations. However, as we next show, our results hold in much less idealized scenarios of interest to experimentalists. We begin by considering realistic control limitations. Of greatest importance is the inclusion of errors due to finite pulse duration, as they will grow with  $T_s$  if not appropriately compensated. Even starting from the dephasing-dominated scenario we consider, applying real DD pulses with duration  $\tau_\pi > 0$  introduces both dephasing and depolarization errors, the latter along, say, the  $y$ -axis if control along  $x$  is used for pulsing. As a result, the conditions given in equation (7.3) can no longer guarantee a coherence plateau in general: simply incorporating ‘primitive’ uncorrected  $\pi$ -pulses into a high-order DD sequence may contribute a net depolarizing error substantial enough to make a plateau regime inaccessible. This intuition may be formalized, and new conditions for the emergence of a coherence plateau determined, by exploiting a *generalized multi-axis FF formalism* [100, 108], in which both environmental and finite-width errors may be accounted for, to the leading order, by adding in quadrature the  $z$  and  $y$  components of the ‘control vector’ that are generated in the non-ideal setting (see Appendix).

The end result of this procedure may be summarized in a transparent way: to the leading

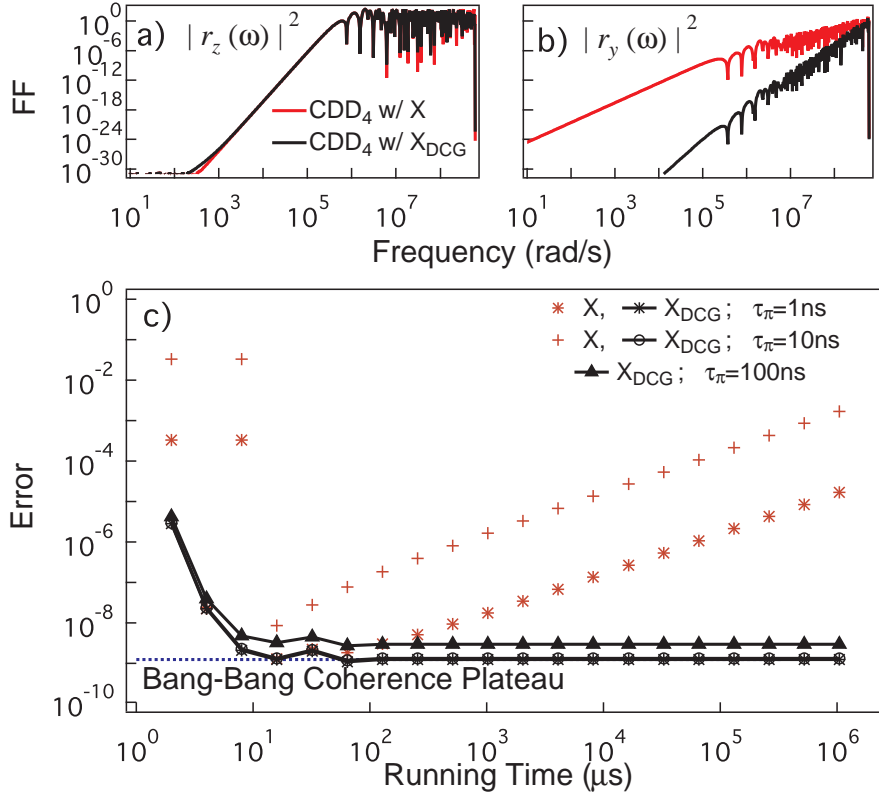


**Figure 7.4: Realistic filter functions and effect of finite-width errors and soft cutoff.** *a)*  $z$  (dephasing) and *b)*  $y$  (depolarization) quadrature components of the total FF for  $CDD_4$ ,  $F(\omega) = F_p(\omega) + F_{pul}(\omega) \equiv |r_y(\omega)|^2 + |r_z(\omega)|^2$ , incorporating non-zero duration uncorrected  $\pi_x$  pulses (red), and first-order DCGs [68, 108],  $\tau_\pi = 1$  ns (see Appendix). In the ideal case, the depolarizing contribution  $|r_y(\omega)|^2 \equiv 0$ , and  $F(\omega) \equiv F_p(\omega)$ . The improvement of  $\alpha_{pul}$  for  $CDD_4$  with DCGs is demonstrated by the increased slope of  $|r_y(\omega)|^2$  in panel *b*). *c)* DD error for the  $\tau = 1$  μs data set of figure 7.3, using finite-duration pulses. Sub-Ohmic noise spectrum with  $s = -2$  and soft Gaussian cutoff as in figure 7.1 are assumed. The low-value of  $\alpha_{pul}$  for primitive pulses leads to unbounded error growth, terminating the plateau after a small number of repeats, determined by the ratio of  $\tau_\pi/\tau$ . Sequences incorporating DCGs meet the conditions for plateau out to at least 1 s storage time, with error increased by a factor of order unity compared with the bang-bang coherence plateau value, using  $\tau_\pi$  up to 100 ns. Outlier data points for  $CDD_3$  arise because of even-odd effects in the FF when including pulse effects.

order, the total FF can be written as  $F(\omega) \equiv F_p(\omega) + F_{pul}(\omega) \approx |A_{bb}|^2 \omega^{2(\alpha_p+1)} + |A_{pul}|^2 \omega^{2(\alpha_{pul}+1)}$ , where  $F_p(\omega)$  is the FF for the bang-bang DD sequence previously defined and  $F_{pul}(\omega)$  depends on the details of the pulse implementation. Corrections in the pre-factors  $A_{bb}, A_{pul}$  arise from higher-order contributions. The parameter  $\alpha_{pul}$  captures the error suppression properties of the pulses themselves, similar to the sequence order of error suppression  $\alpha_p$ . A primitive pulse results in  $\alpha_{pul} = 1$  due to the dominant uncorrected  $y$ -depolarization. An expression for the asymptotic DD error may then be obtained starting from equation (7.1) and separating  $\chi_{[p]\infty} \equiv \chi_{[p]\infty}^{bb} + \chi_{[p]\infty}^{pul}$ . An additional constraint thus arises by requiring that *both* the original contribution  $\chi_{[p]\infty}^{bb}$  of equation (7.2) and  $\chi_{[p]\infty}^{pul}$  be finite. Thus, in order to maintain a coherence plateau in the

long-time limit we now require

$$s + 2\alpha_p > 1, \quad s + 2\alpha_{\text{pul}} > 1, \quad T_p\omega_c < 2\pi. \quad (7.4)$$

We demonstrate the effects of pulse-width errors in figure 7.4c). When using primitive  $\pi_x$ -pulses ( $\alpha_{\text{pul}} = 1$ ), the depolarizing contribution due to  $F_{\text{pul}}(\omega)$  dominates the total value of  $\chi_{[p]^m}$ . For the dephasing spectrum we consider,  $s = -2$ , the condition for maintenance of a plateau using primitive pulses is not met, and the total error grows unboundedly with  $m$  after a maximum plateau duration  $T_{\max} \equiv m_{\max}T_p$  ( $m_{\max}$  may be estimated by requiring that  $\chi_{[p]^m}^{\text{pul}} > \chi_{[p]^m}^{\text{bb}}$ , along lines similar to those discussed in the Appendix). The unwanted depolarizing contribution can, however, be suppressed by appropriate choice of a higher-order ‘corrected’ pulse, such as a DCG [68, 54], already shown to provide efficient error suppression in the presence of non-Markovian time-dependent noise [100]. For a first-order DCG, the dominant error contribution is canceled, resulting in  $\alpha_{\text{pul}} = 2$ , as illustrated in figures 7.4a)-b); incorporating DCGs into the base DD sequence thus allows the coherence plateau to be restored. For small values of  $\tau_\pi$ , the error contribution  $\chi_{[p]^m}^{\text{pul}}$  remains small and the plateau error is very close to that obtained in the bang-bang limit. Increasing  $\tau_\pi$  leads this error contribution to grow, and the plateau saturates at a new higher value.

‘Hardware-adapted’ DCGs additionally provide a means to ensure robustness against control imperfections (including rotation-angle and/or off-resonance errors) while incorporating realistic control constraints. For instance, sequences developed for singlet-triplet spin qubits [119] can simultaneously achieve insensitivity against nuclear-spin decoherence and charge noise in the exchange control fields, with inclusion of finite timing resolution and pulse rise times. A quantitative performance analysis may be carried out in principle through appropriate generalization of the FF formalism introduced above. Thus, the replacement of low-order primitive pulses with higher-order corrected pulses provides a straightforward path toward meeting the conditions for a coherence plateau with realistic DD sequences. These insights are also supported by recent DD nuclear magnetic resonance experiments [102, 171], that have demonstrated the ability to largely eliminate the effects of pulse imperfections in long pulse trains.

Another experimentally realistic and important control imperfection is limited timing precision. The result of this form of error is either premature or delayed memory access at time  $T'_s = mT_p \pm \delta t$ , offset relative to the intended one. Qualitatively, the performance degradation resulting from such access-timing errors may be expected to be similar to the one suffered by a high-order DD sequence under pulse-timing errors, analyzed in [47]. A rough sensitivity estimate may be obtained by adding an uncompensated ‘free-evolution’ period of duration  $\delta t$  following the  $m$ th repeat of the sequence, with the resulting FF being determined accordingly. In this case the effective order of suppression transitions  $\alpha_p \rightarrow 0$ , appropriate for free evolution, at a crossover frequency determined by the magnitude of the timing jitter. In order to guarantee the desired (plateau) fidelity level, it is necessary that the total FF – including timing errors – still meets the requirements set in equation (7.4). In general, this is achievable for supra-Ohmic spectra with  $s > 1$ . When these conditions are not met, the resulting error can be much larger than the plateau value if the jitter is appreciable. Access timing therefore places a constraint on a system designer to ensure that quantum memories are clocked with low-jitter, high-resolution systems. Considering the situation analyzed in figure 7.3 with  $\tau = 1 \mu\text{s}$  and  $\chi_{[p]^\infty} \sim 1.3 \times 10^{-9}$ , we estimate that access jitter of order 1.5 ps may be tolerated before the total measured error exceeds the bound of  $2\chi_{[p]^\infty}$ . Since current digital delay generators allow for sub-ps timing resolution and ps jitter, the requisite timing accuracy is nevertheless within reach with existing technologies.

We next address different aspects of the assumed noise model. Consider first the assumption of a hard spectral cutoff in bounding the long-storage-time error. If such an assumption is not obeyed (hence residual noise persists beyond  $\omega_c$ ), it is impossible to fully avoid the singular

behavior introduced by the periodic modulation as  $m \rightarrow \infty$ . Contributions from the resonating region  $\omega \approx \omega_{\text{res}}$  are amplified with  $m$ , and, similar to pulse-errors, cause  $\chi_{[p]^m}$  to increase unboundedly with time and coherence to ultimately decay to zero. Nonetheless, a very large number of repetitions,  $m_{\text{max}}$ , may still be applied before such contributions become important (note that this is the case in the previous figures, where we assume a *soft Gaussian cutoff*). We lower-bound  $m_{\text{max}}$  by considering a scenario in which a plateau is preserved with a hard cutoff and estimating when contributions to error for frequencies  $\omega > \omega_c$  become comparable to the plateau error. For simplicity, we assume that noise for  $\omega > \omega_c$  falls in the passband of the FF and that at  $\omega = \omega_c$  the noise power law changes from  $\omega^s \rightarrow \omega^{-r}$ , with  $r > 0$ . Treating such a case with  $s = -2$  and using again repeated CDD<sub>4</sub> with  $\tau = 1 \mu\text{s}$  as in figure 7.3, we find that as long as  $r$  is sufficiently large, the plateau error  $\chi_{[p]^\infty} \sim 10^{-9}$  can persist for  $m_{\text{max}} \gtrsim 10^4$ - $10^6$  repetitions (that is, up to a storage time of over 10 s), before the accumulated error due to high-frequency contributions exceeds the plateau coherence (see Appendix). This makes it possible to engineer a coherence plateau over an intermediate range of  $T_s$  which can still be exceptionally long from a *practical* standpoint, depending on the specific rolloff behavior of  $S(\omega)$  at frequencies beyond  $\omega_c$ .

Lastly, we turn to consideration of more general open-system models. For instance, consider a system-bath interaction which includes both a dominant dephasing component and an ‘off-axis’ perturbation, resulting in energy relaxation with a characteristic timescale  $T_1$ . Then the initial dephasing dynamics, *including the onset of a coherence plateau*, will not be appreciably modified so long as these two noise sources are uncorrelated and there is a sufficient separation of time scales. If  $T_1 \gg T_2$ , and the maximum error *per cycle* is kept sufficiently small, the plateau will persist until uncorrected  $T_1$  errors dominate  $\chi_{[p]^m}$ . We reiterate that in many experimentally relevant settings - notably, both trapped-ion and spin qubits -  $T_1$  effects may indeed be neglected up to very long storage times. Ultimately, stochastic error sources due, for instance, to spontaneous emission processes and/or Markovian noise (including white control noise) may form a limiting mechanism. In such circumstances, the unfavorable exponential scaling of Markovian errors with storage time poses a problem for high-fidelity storage through DD alone. Given a simple exponential decay with time-constant  $T_M$  and assuming that equation (7.4) is met, we may estimate a maximum allowed plateau duration as  $T_{\text{max}} \approx T_M \chi_{[p]^\infty}$ . Thus, even with  $T_M = 100$  s, a plateau at  $\chi_{[p]^\infty} = 10^{-5}$  would terminate after  $T_{\text{max}} = 1$  ms. Our results thus confirm that guaranteeing high-fidelity quantum memory through DD alone requires Markovian noise sources to be minimized, or else motivates the combination of our approach with quantum error correction protocols.

## 7.3 Discussion

The potential performance provided by our approach is quite remarkable. Besides the illustrative error calculations we have already presented, we find that many other interesting scenarios arise where extremely low error rates can be achieved in realistic noise environments for leading quantum technologies. For instance, Ytterbium ion qubits, of direct relevance to applications in quantum repeaters, allow long-time, low-error coherence plateaus at the timescale of *hours*, based on bare free-induction-decay (1/e) times of order seconds [176]. Calculations using a common  $1/\omega$  noise power spectrum with CDD<sub>2</sub>, a Gaussian high-frequency cutoff near 100 Hz,  $\tau = 1\text{ms}$ , and DCG operations with  $\tau_\pi = 10 \mu\text{s}$ , give an estimate of the plateau error rate of  $2.5 \times 10^{-9}$ . This kind of error rate – and the corresponding access latency of just 4 ms – has the potential to truly enable viable quantum memories for repeater applications. Similarly, the calculations shown throughout the manuscript rely on the well-characterized noise power spectrum associated with nuclear spin fluctuations in spin qubits. Appropriate sequence con-

struction and timing selection [119] permits the analytical criteria set out in equation (7.3) to be met, and similar error rates to be achieved, subject to the limits of Markovian noise processes as described above.

In summary, we have addressed a fundamental and timely problem in quantum information processing – determining a means to effectively produce a practically useful high-fidelity quantum memory, by using dynamical error suppression techniques. We have identified the key requirements towards this end, and developed a strategy for sequence construction based on repetition of high-order DD base sequences. Our results allow analytical bounding of the long-time error rates and identify conditions in which a *maximum error rate can be stroboscopically guaranteed for long times* with small access latencies, even in the presence of limited control. We have validated these insights and analytic calculations using an efficient search over Walsh DD sequences assuming realistic noise spectra. The results of our numerical search bear similarity to an analytically defined strategy established in [169] for optimizing long-time storage in a supra-Ohmic excitonic qubit.

From a practical perspective, our analyses help set technological targets on parameters such as error-per-pulse, timing resolution, and Markovian noise strengths required to achieve the full benefits of our approach to quantum memory. This work also clearly shows how a system designer may calculate the impact of such imperfections for a specific platform, bound performance, and examine technological trade-offs in attempting to reach a target memory fidelity and storage time. As the role of optimization in any particular setting is limited to finding a low-error sequence of duration  $T_p$  to be repeated up to  $T_s$ , our framework dramatically reduces the complexity of finding high-performance DD protocols.

Future work will characterize the extent to which similar strategies may be employed to tackle more generic quantum memory scenarios. For instance, recent theoretical methods permit consideration of noise correlations across different spatial directions [108] in general non-Markovian single-qubit environments for which  $T_2$  and  $T_1$  may be comparable. In such cases, multi-axis DD sequences such as XY4 [58] may be considered from the outset in order to suppress phase and energy relaxation, as experimentally demonstrated recently [177]. Likewise, we remark that our approach naturally applies to multiple qubits subject to dephasing from *independent* environments. Since expressions similar to the spectral overlap integral still determine the decay rates of different coherence elements [178], exact DD can be achieved by simply replacing individual with *collective*  $\pi$  pulses, and conditions similar to equation (7.2) may then be separately envisioned to ensure that each coherence element saturates, again resulting in a guaranteed high storage fidelity. Addressing the role of correlated dephasing noise and/or other realistic effects in multi-qubit long-time storage represents another important extension of this work.

## 7.4 Appendix

### Inclusion of pulse errors

Consider a base sequence  $p$  of total duration  $T_p$ , including both free evolution periods and control pulses with non-zero duration  $\tau_\pi$ , where the center of the  $j$ th pulse occurs at time  $t_j \equiv \delta_j T_p$ , with  $\delta_j \in [0, 1]$ . FFs that incorporate, to leading order in  $T_p$ , errors due to both dephasing dynamics and non-ideal pulses are derived following [108]. The total FF,  $F(\omega) = F_p(\omega) + F_{\text{pul}}(\omega)$ , may be expressed as

$$F(\omega) \equiv |r_y(\omega)|^2 + |r_z(\omega)|^2, \quad (7.5)$$

where  $r_{z(y)}$  are, respectively, the total  $z(y)$  components of the control vector for pure dephasing in the relevant quadrature, determined by the toggling-frame Hamiltonian associated with the control sequence. In the ideal bang-bang limit,  $r_y(\omega) \equiv 0$  and  $r_z(\omega) = A_{\text{bb}}\omega^{\alpha_p+1}$ , where e.g.  $\alpha_p = 4$ ,  $A_{\text{bb}} = -iT_p^5/2^{14}$  for CDD<sub>4</sub>. In general, the total contributions to the FF are

$$\begin{aligned} r_z(\omega) &= 1 - e^{i\omega T_p} + [2 \cos(\omega\tau_\pi/2) - e^{-i\omega\tau_\pi/2} r_z^{\text{pul}}(\omega)] u_p, \\ r_y(\omega) &= -e^{-i\omega\tau_p/2} r_y^{\text{pul}}(\omega) u_p, \end{aligned} \quad (7.6)$$

where  $u_p \equiv \sum_{\ell=1}^n (-1)^\ell e^{i\omega\delta_\ell T_p}$  and we incorporate pulse contributions through  $r_{z(y)}^{\text{pul}}$ .

For primitive pulses with a rectangular profile, and  $\Omega \equiv \pi/\tau_\pi$ , direct calculation yields [100]:

$$\begin{aligned} r_z^{\text{pul}}(\omega) &= \frac{\omega^2}{(\omega^2 - \Omega^2)} (e^{i\omega\tau_\pi} + 1), \\ r_y^{\text{pul}}(\omega) &= \frac{i\omega\Omega}{(\omega^2 - \Omega^2)} (e^{i\omega\tau_\pi} + 1). \end{aligned} \quad (7.7)$$

For the 3-segment first-order DCG we employ, one finds instead [100, 108]:

$$\begin{aligned} r_z^{\text{pul}}(\omega) &= \omega^2 \left[ \frac{c_1(\omega)}{(\omega^2 - \Omega^2)} - \frac{c_2(\omega)}{(\omega^2 - (\Omega/2)^2)} \right], \\ r_y^{\text{pul}}(\omega) &= i\omega\Omega \left[ \frac{c_1(\omega)}{(\omega^2 - \Omega^2)} - \frac{c_2(\omega)}{2(\omega^2 - (\Omega/2)^2)} \right], \end{aligned} \quad (7.8)$$

where  $c_1(\omega) \equiv e^{4i\omega\tau_\pi} + e^{3i\omega\tau_\pi} + e^{i\omega\tau_\pi} + 1$  and  $c_2(\omega) \equiv e^{3i\omega\tau_\pi} + e^{i\omega\tau_\pi}$ . Starting from these expressions and suitably Taylor-expanding around  $\omega = 0$ , one may then show that the dominant pulse contributions arise from  $r_y(\omega)$  in the uncorrected case, with  $\alpha_{\text{pul}} = 1$  and  $A_{\text{pul}} = -T_p\tau_\pi/\pi$ , whereas they arise from  $r_z(\omega)$  in the DCG case, with  $\alpha_{\text{pul}} = 2$  and  $A_{\text{pul}} = -2iT_p\tau_\pi^2/(1 + 1/\pi^2)$ .

Assuming a noise power spectrum with a hard cutoff,  $S(\omega) = g(\omega/\omega_c)^s \Theta(\omega - \omega_c)$ , the following expression for the (leading-order) total asymptotic DD error,  $\chi_{[p]^\infty} \equiv \chi_{[p]^\infty}^{\text{bb}} + \chi_{[p]^\infty}^{\text{pul}}$ , is obtained:

$$\chi_{[p]^\infty} = \frac{g|A_{\text{bb}}|^2 \omega_c^{2\alpha_p-1}}{\pi T_p^2(s + 2\alpha_p - 1)} + \frac{g|A_{\text{pul}}|^2 \omega_c^{2\alpha_{\text{pul}}-1}}{\pi T_p^2(s + 2\alpha_{\text{pul}} - 1)}, \quad (7.9)$$

leading to the plateau conditions quoted in equation (7.4).

## Effect of a soft spectral cutoff

Consider, again, a high-order DD sequence which is implemented with realistic pulses and is repeated  $m$  times. Then the leading contribution to the DD is given by

$$\chi_{[p]^m} = \int_0^\infty \frac{S(\omega)}{2\pi\omega^2} \frac{\sin^2(m\omega T_p/2)}{\sin^2(\omega T_p/2)} F(\omega) d\omega, \quad (7.10)$$

where the FF  $F(\omega)$  is computed as described above and  $S(\omega) = g(\omega/\omega_c)^s f(\omega, \omega_c)$ . While this integral converges nicely if we assume a sharp high-frequency cutoff, this is rarely encountered in reality. For a soft spectral cutoff, we can break the error integral up into two (low- vs. high-frequency) contributions, say,  $\chi_{[p]^m} \equiv \chi_{[p]^m}^{\text{low}} + \chi_{[p]^m}^{\text{high}}$ . We wish to estimate how many repeats of the base sequence are permitted *under conditions otherwise leading to a plateau*, before corrections due to the high-frequency tail dominate the error behavior and destroy the plateau. Assume that the conditions given in equation (7.4) are obeyed, and let the maximum number of allowed repetitions be denoted by  $m_{\max}$ . Then  $m_{\max}$  may be determined by requiring that  $\chi_{[p]^{m_{\max}}}^{\text{low}} = \chi_{[p]^{m_{\max}}}^{\text{high}}$ .

Since, for every  $m$ , we have  $\chi_{[p]^m}^{\text{low}} \leq 2\chi_{[p]^\infty}^{\text{low}}$ , a lower bound for  $m_{\max}$  may be obtained by estimating  $m_*$  such that  $\chi_{[p]^{m_*}}^{\text{high}} = 2\chi_{[p]^\infty}^{\text{low}}$ . We may therefore simply identify  $\chi_{[p]^\infty}^{\text{low}}$  with the hard-cutoff asymptotic value given in equation (7.9). In order to obtain an explicit expression for the high-frequency contribution, we assume that the noise power above  $\omega_c$  also takes a power-law form,  $S(\omega) = g(\omega/\omega_c)^r$ , formally corresponding to a rolloff  $f = (\omega/\omega_c)^{r-s}$ , with power  $r > 0$ . (Note that other possible choices of  $f$ , such as exponential or Gaussian rolloffs, may be treated along similar lines, at the expense of more complicated integrals). Thus, we may write

$$\chi_{[p]^{m_*}}^{\text{high}} \leq \int_{\omega_c}^{\infty} \frac{g(\omega/\omega_c)^{-r}}{2\pi\omega^2} \frac{\sin^2(m\omega T_p/2)}{\sin^2(\omega T_p/2)} F_{[p]}^{\max} d\omega, \quad (7.11)$$

where we have set the FF to the maximum value  $F_{[p]}^{\max} \equiv F_{[p]}^{\max}(n, \alpha)$  of the peaks in the passband. This value increases with pulse number and sequence order and must be calculated explicitly for a particular base sequence.

For sufficiently large  $m$ , the oscillatory factor in the integrand may be approximated in terms of a Dirac comb,

$$\frac{\sin^2(m\omega T_p/2)}{\sin^2(\omega T_p/2)} \approx \frac{2\pi m}{T_p} \sum_{n=-\infty}^{\infty} \delta\left(\omega - \frac{2\pi n}{T_p}\right). \quad (7.12)$$

This allows us to write

$$\begin{aligned} \chi_{[p]^{m_*}}^{\text{high}} &\lesssim F_{[p]}^{\max}(n, \alpha_p) \frac{g\omega_c^r}{T_p} \sum_{n=1}^{\infty} \left(\frac{2\pi n}{T_p}\right)^{-(r+2)} \\ &= \frac{mgT_p F_{[p]}^{\max}(n, \alpha_p)}{4\pi^2} \left(\frac{\omega_c T_p}{2\pi}\right)^r \zeta(r+2), \end{aligned} \quad (7.13)$$

where we have exploited the fact that  $0 < \omega_c < 2\pi/T_p$  and  $\zeta(s)$  denotes the Riemann zeta function.

The error due to the soft rolloff at high frequencies thus increases linearly with  $m$  (hence  $T_s = mT_p$ ), as intuition suggests. Since the zeta function is decreasing with  $r$  and attains its maximum value at  $r = 0$ , corresponding to an infinite white noise floor, we obtain the following upper bound (recall that  $\zeta(2) = \pi^2/6$ ):

$$\chi_{[p]^{m_*}}^{\text{high}} \lesssim \frac{1}{24} mgT_p F_{[p]}^{\max}(n, \alpha_p) \left(\frac{\omega_c T_p}{2\pi}\right)^r. \quad (7.14)$$

By equating  $\chi_{[p]^{m_*}}^{\text{high}} = 2\chi_{[p]^\infty}^{\text{low}}$  and using equations (7.9)-(7.14), we finally arrive at the desired lower-bound:

$$m_{\max} \gtrsim \frac{48}{F_{[p]}^{\max}(n, \alpha_p)} \left(\frac{2\pi}{\omega_c T_p}\right)^r \left(\frac{\chi_{[p]^\infty}^{\text{low}}}{gT_p}\right). \quad (7.15)$$

The above estimate can be applied, in particular, to the specific situation analyzed in the main text: base sequence CDD<sub>4</sub> with  $\tau = 1\mu\text{s}$ , DCG implementations with  $\tau_\pi \leq 10\text{ ns}$ , and  $s = -2$ . In this case  $T_p \approx 16\mu\text{s}$ ,  $\alpha_p = 4$ ,  $F_{[p]}^{\max}(n, \alpha_p) = 256$ ,  $A_{\text{bb}} = -iT_p^5/2^{14}$ , and one can effectively neglect the contribution to  $m_{\max}$  due to pulse errors to within the accuracy of this lower bound. Let  $x \equiv T_p\omega_c/2\pi$  which, by the assumed plateau condition, ranges within  $[0, 1]$ . Then we may rewrite

$$m_{\max} \gtrsim \frac{3\pi^6}{5 \times 2^{25}} x^{-r+7}, \quad (7.16)$$

implying that, for instance, at least  $10^5$  repetitions are allowed at  $x = 0.001$  if  $r \geq 6$ , and at least  $10^4$  at  $x = 0.01$  if  $r \geq 8$ . At the value  $x = 0.16$ , corresponding to  $\omega_c/2\pi$  as used

in the main text,  $r \gtrsim 18$  ensures  $m_{\max} \gtrsim 10^4$  hence a storage time of about  $T_s \approx 0.1$  s *with error as low as  $10^{-9}$* . As demonstrated by the data in figure 7.4,  $T_s$  is in fact in excess of 1 s under the assumed Gaussian cutoff, which is realistic for this system. In general, we have verified by direct numerical evaluation of the error integral in equation (7.10) that, although qualitatively correct, the lower bound in equation (7.16) can significantly under-estimate the achievable plateau length (*e.g.*, at  $x = 0.16$ , a storage time  $T_s \approx 0.1$  s is reached already at  $r \gtrsim 15$ ). Altogether, this analysis thus indicates that high-frequency tails do not pose a practically significant limitation provided that the noise falls off sufficiently fast, as anticipated.

# Chapter 8

## Dynamical decoupling sequences for multi-qubit dephasing suppression

We consider a class of multi-qubit dephasing models that combine classical noise sources and linear coupling to a bosonic environment, and that are controlled by arbitrary sequences of dynamical decoupling pulses. Building on a general transfer filter-function framework for open-loop control, we provide an exact representation of the controlled dynamics for arbitrary stationary *non-Gaussian* classical and quantum noise statistics, with analytical expressions emerging when all dephasing sources are Gaussian. This exact characterization is used to establish two main results. First, we construct multi-qubit sequences that ensure maximum high-order error suppression in *both* the time and frequency domain and that can be *exponentially more efficient* than existing ones in terms of total pulse number. Next, we show how long-time multi-qubit storage may be achieved by meeting appropriate conditions for the emergence of a *fidelity plateau* under sequence repetition, thereby generalizing recent results for single-qubit memory under Gaussian dephasing. In both scenarios, the key step is to endow multi-qubit sequences with a suitable *displacement anti-symmetry* property, which is of independent interest for applications ranging from environment-assisted entanglement generation to multi-qubit noise spectroscopy protocols.

The contents of this chapter have been published as: G. A. Paz-Silva, S.-W. Lee, T. J. Green and L. Viola, “Dynamical decoupling sequences for multi-qubit dephasing suppression and long-time quantum memory”, New Journal of Physics **18**, 073020 (2016). Realizing the full potential of QIP technology mandates the capacity to store and manipulate multi-qubit states (section 2.2.2). In this publication/chapter we address the first of these tasks – multi-qubit state preservation.

### 8.1 Introduction

Characterizing and counteracting decoherence generated by noise environments which may exhibit both *temporal and spatial correlations* is a significant challenge to the realization of high-fidelity quantum information processing (QIP) and fault-tolerant quantum computation [156, 179]. Of particular interest are purely dephasing environments, which provide an accurate physical description whenever relaxation processes associated with energy exchange occur over a characteristic time scale that is substantially longer than that associated with dephasing dynamics. Provided that the noise arises predominantly from low-frequency components, and

that external control is available over time scales that are short compared to the resulting temporal correlations, open-loop techniques based on dynamical decoupling and dynamically error-corrected gates [156, 48, 58, 64, 67, 68, 54] provide a powerful tool for boosting operational fidelities – potentially eliminating ‘coherent’ (highly ‘non-Markovian’) errors that dominate worst-case error estimates in rigorous threshold analyses [180, 181].

Our focus in this work is dynamical decoupling (DD) for a class of purely dephasing models that describe the effects of *stationary but not necessarily Gaussian correlated noise*, from combined classical and quantum sources, on a multi-qubit system. More precisely, as detailed in section 8.2.1, we consider arbitrary single- and two-qubit classical time-dependent phase noise, along with quantum noise from a dephasing ‘free field’ Hamiltonian – namely, a linear diagonal spin-boson model where non-Gaussian statistics may arise solely from the bath initial state [182, 183, 184, 185]. Our motivation is twofold: on the one hand, while general-purpose multi-qubit DD sequences based on concatenation and nesting are known, and may in principle ensure the desired error suppression up to arbitrarily high order [64, 186, 187] (section 8.2.2), it may be possible to design less resource-intensive DD protocols by tailoring construction to dephasing models with particular characteristics; on the other hand, while an approach to practical long-time high-fidelity quantum memory has been recently proposed based on the idea of engineering a ‘coherent plateau’ [105] by sequence repetition, the existing analysis is only applicable to a single qubit exposed to Gaussian phase noise.

We tackle the above issues under the simplifying assumptions that the required DD pulses may be instantaneously and perfectly effected on selected (subsets of) qubits – subject, however, to a realistic constraint on their minimum separation, or ‘switching time’ [105, 72]. We leverage a general filter-transfer function formalism for characterizing open-loop error-suppression capabilities in both the time and the frequency domain using *fundamental filter functions* (FFs) as building blocks [43]. Our first result, and starting point for subsequent analysis, is an exact analytical characterization for the multi-qubit controlled dynamics in terms of a suitably defined time-ordered cumulant expansion, given in section 8.2.3. While it is known that an exact solution exists for the free evolution of a system subject to Gaussian bosonic phase noise [168, 178, 188], and is in fact equivalent to the one resulting from a second-order Magnus perturbative treatment [183], our analysis extends this equivalence to DD-controlled evolution. In the process, we recover a number of partial results that have appeared in the literature, limited to two qubits under special symmetry assumptions [189, 190, 191, 192, 193]. For generic *non-Gaussian* dephasing noise, our representation shows how arbitrary high-order cumulants may still be expressed in terms of *only two* FFs associated with the control modulation of single- and two-qubit terms.

Sections 8.3 and 8.4 contain our core results on two control tasks of increasing complexity: (i) suppressing errors as effectively as possible, so that quantum information is preserved over a short-time regime of interest (e.g., a single gating period); (ii) ensuring that quantum information is preserved with high fidelity for long storage times, with on-demand access. Provided that selective control over individual qubits is available, we show that new multi-qubit DD sequences may be constructed, so that a *displacement anti-symmetry* property is obeyed by the control switching functions, both in the simplest case of  $N = 2$  qubits (sections 8.3.2) and, by appropriately orchestrating the sign pattern for every qubit pair, for general  $N$  (sections 8.3.3). Such sequences ensure the same order of error suppression as the best known nested or concatenated protocols, while *also* maximizing their ‘filtering order’ in the frequency domain [43]. Further, for a fixed system size  $N$ , DD sequences incorporating displacement anti-symmetry are *exponentially more efficient* in terms of total pulse number, as long as any direct coupling between qubits is time-independent. The possibility of achieving multi-qubit long-time storage by meeting appropriate conditions for the emergence of a *fidelity plateau* under sequence repetition is first established for the important case of non-Gaussian classical stationary phase noise

in section 8.4.1. Generalization of this result to dephasing scenarios that also include bosonic noise sources again relies crucially on incorporating displacement anti-symmetry in the DD sequences used for repetition (section 8.4.2).

Provided that the relevant conditions for the emergence of a fidelity plateau can be satisfied, we argue in section 8.5.1 that the combined use of multi-qubit DD sequences that do not (or, respectively, do) obey displacement anti-symmetry provides a systematic method for controlled generation and storage of *multi-partite entanglement* mediated by a common quantum environment, extending known schemes for bipartite entanglement generation [194, 195]. Section 8.5.2 briefly addresses aspects related to the practical significance and main anticipated limitations of our findings in the light of realistic considerations, whereas a summary and outlook to future research conclude the main text in section 8.6. By way of concrete illustration of our general FF formalism, we provide in appendix A additional technical detail on the simplest yet practically important case of a DD-controlled two-qubit system under Gaussian dephasing from combined classical and quantum bosonic sources. Lastly, we include in appendix B a discussion of the impact of timing errors on the ideal fidelity plateau, based on a simple error model that breaks the required underlying displacement anti-symmetry in a two-qubit system.

## 8.2 Multi-qubit controlled dephasing dynamics

### 8.2.1 Gaussian versus non-Gaussian dephasing models

We consider a class of purely-dephasing noise models on  $N$  qubits in which no energy exchange takes place between the system and an environment ('bath') modeled by a continuum of classical and/or quantum modes – see section 8.5.2 for further discussion on their physical relevance. The general form of the relevant open-system Hamiltonian reads

$$H(t) = H_S(t) \otimes I_B + I_S \otimes H_B + H_{SB}, \quad (8.1)$$

where  $H_S(t)$  and  $H_B$  denote, respectively, the internal Hamiltonian for the system and bath, and  $H_{SB}$  describes their interaction. For a purely dephasing model,  $[H_{SB}, H_S] = 0$ , implying the existence of a preferred (energy or computational) basis [156]. Without loss of generality, we take this to be the  $z$ -basis, and use  $Z_\ell$  to denote the Pauli operator  $\sigma_z$  acting on qubit  $\ell$ . A general multi-qubit dephasing Hamiltonian that includes up to two-body noisy qubit interactions and linear system-bath coupling may then be written as

$$H_S(t) = \sum_{\ell=1}^N Z_\ell (d_\ell + \zeta_\ell(t)) + \sum_{\ell \neq \ell'=1}^N Z_\ell \otimes Z_{\ell'} (d_{\ell,\ell'} + \eta_{\ell,\ell'}(t)), \quad (8.2)$$

$$H_{SB} = \sum_{\ell=1}^N Z_\ell \otimes B_\ell, \quad (8.3)$$

where we allow for dephasing due to both *classical and quantum noise sources*, as represented by the fluctuating system Hamiltonian  $H_S(t)$  and the system-bath interaction Hamiltonian  $H_{SB}$ , for suitable (Hermitian) operators  $B_\ell$  acting on  $B$ . Specifically,  $\zeta_\ell(t)$  and  $\eta_{\ell,\ell'}(t)$  are classical stochastic processes describing random fluctuations of the local energy splittings and two-local (Ising) coupling strengths,  $d_\ell$  and  $d_{\ell,\ell'}$ .

A formally similar treatment of classical and quantum noise sources is possible upon moving to the interaction picture associated with the bath Hamiltonian  $H_B$ . The total Hamiltonian becomes  $H(t) \mapsto \tilde{H}(t) = \tilde{H}_S(t) \otimes I_B + \tilde{H}_{SB}(t)$ , with  $\tilde{H}_S(t) \equiv H_S(t)$ ,  $\tilde{H}_{SB}(t) \equiv \sum_{\ell=1}^N Z_\ell \otimes B_\ell(t)$ ,

and where, for notational convenience, we simply use  $B_\ell(t)$  to denote the interaction-picture representation of  $B_\ell$ . For the purpose of achieving decoherence suppression and arbitrary state preservation, the dynamics generated by  $\tilde{H}(t)$  corresponds to unwanted ('error') evolution, thus  $\tilde{H}(t) \equiv H_e(t)$  in the framework of dynamical error suppression [54, 43]. In a multi-qubit setting, the noise acting on different (subsets of) qubits may exhibit different kinds of *temporal as well as spatial correlations*. In particular, two limiting situations may be envisioned for the coupling of the quantum bath to different qubits:

- A *common* bath, in which case  $[B_\ell(t), B_{\ell'}(t')] \neq 0, \forall \ell \neq \ell'$  for at least some  $t, t'$ .
- A *private* (or independent) bath, in which case  $[B_\ell(t), B_{\ell'}(t')] = 0, \forall \ell \neq \ell', \forall t, t'$ .

While intermediate situations are clearly possible, an additional distinction is relevant for the common-bath scenario depending on whether qubit-permutation symmetry is present. Specifically, *collective* dephasing corresponds to  $B_\ell(t) = B(t), \forall \ell$ , as extensively studied in the context of decoherence-free subspaces [156, 196]. Noise processes and their correlations can be further characterized by their spectral properties in the frequency domain.

**Spectral properties of classical phase noise** – Classical noise processes may be compactly characterized by their statistical moments [197], obtained via the ensemble average over noise realizations, henceforth denoted by  $\langle \cdot \rangle_c$ . Given the fluctuating Hamiltonian  $H_S(t)$  in equation (8.2), we are most generally interested in cross-correlations of the form

$$\langle \zeta_{\ell_1}(t_1) \cdots \zeta_{\ell_j}(t_j) \eta_{p_{j+1}}(t_{j+1}) \cdots \eta_{p_k}(t_k) \rangle_c \quad (8.4)$$

for all  $j, k$ , where  $p \equiv \{\ell, \ell'\}$  labels qubit pairs, and we include joint moments of a single noise source,  $\zeta_\ell(t)$  or  $\eta_p(t)$ , as a particular case. A simpler description is obtained by using *cumulants*, which we denote  $C^{(k)}(\zeta_{\ell_1}(t_1) \cdots \zeta_{\ell_j}(t_j) \eta_{p_{j+1}}(t_{j+1}) \cdots \eta_{p_k}(t_k))$  and define via general moment-cumulant relations [197]. If  $\{A_i\}$  denotes a set of random variables, then

$$\langle A_1 \rangle_c = C^{(1)}(A_1), \quad \langle A_1 \cdots A_n \rangle_c = \sum_{\pi \in \Pi(n)} \prod_i C^{(V_i)}(A_1 \cdots A_n), \quad (8.5)$$

where  $\Pi(n)$  is the set of partitions of  $n$  elements,  $\pi = \{V_1, \dots, V_r\}$ , and each block  $V_i$  contains the elements  $\{v_i(s)\}_{s=1}^{|V_i|}$  ordered according to  $A_1, \dots, A_n$ , with

$$C^{(V_i)}(A_1 \cdots A_n) \equiv C^{(|V_i|)}(A_{v_i(1)} \cdots A_{v_i(|V_i|)}). \quad (8.6)$$

For example:

$$\begin{aligned} \langle A_3 A_1 A_2 \rangle_c &= C^{(3)}(A_3 A_1 A_2) + C^{(1)}(A_3) C^{(1)}(A_1) C^{(1)}(A_2) + \\ &\quad C^{(2)}(A_3 A_1) C^{(1)}(A_2) + C^{(2)}(A_3 A_2) C^{(1)}(A_1) + C^{(2)}(A_1 A_2) C^{(1)}(A_3), \end{aligned}$$

and so on. The above definition of cumulant, which respects the order of the arguments, is equivalent to the traditional one when the random variables commute, but solves the ambiguity that arises when ordering becomes important, as it does for non-commuting operator-variables in the quantum case. The expressions in equation (8.5) can be inverted as usual in probability theory and statistics, allowing one to write the cumulants in terms of the moments [197].

A description of the noise process in frequency space may be given by considering the Fourier transform of cumulants. Specifically, the Fourier transform of a  $k$ -th order (cross-) cumulant defines the *k-th order polyspectrum* [198, 185],  $S_{\ell_1, \dots, \ell_j, p_{j+1}, \dots, p_k}^{\zeta, \eta}(\omega_1, \dots, \omega_k)$ , via

$$S_{\ell_1, \dots, \ell_j, p_{j+1}, \dots, p_k}^{\zeta, \eta}(\vec{\omega}_{[k]}) \equiv C^{(k)}(\tilde{\zeta}_{\ell_1}(\omega_1) \cdots \tilde{\zeta}_{\ell_j}(\omega_j) \tilde{\eta}_{p_{j+1}}(\omega_{j+1}) \cdots \tilde{\eta}_{p_k}(\omega_k)),$$

where  $\tilde{\zeta}_\ell(\omega)$ ,  $\tilde{\eta}_p(\omega)$  are random variables obtained from  $\zeta_\ell(t)$ ,  $\eta_p(t)$  via Fourier transform, and we have introduced the notation  $\vec{\omega}_{[k]} \equiv (\omega_1, \dots, \omega_k)$  to denote a vector of length  $k$ .<sup>1</sup> The noise process is *stationary* if arbitrary cumulants,  $C^{(k)}(\zeta_{\ell_1}(t_1) \cdots \zeta_{\ell_j}(t_j) \eta_{p_{j+1}}(t_{j+1}) \cdots \eta_{p_k}(t_k))$ , depend solely on time differences, say,  $\tau_j \equiv t_{j+1} - t_1$  for  $j = 1, \dots, k-1$ , rather than absolute time values. Thus, the stationarity assumption translates into

$$S_{\ell_1, \dots, \ell_j, p_{j+1}, \dots, p_k}^{\zeta, \eta}(\vec{\omega}_{[k]}) = 2\pi\delta(\omega_1 + \cdots + \omega_k) S_{\ell_1, \dots, \ell_j, p_{j+1}, \dots, p_k}^{\zeta, \eta}(\vec{\omega}_{[k-1]}), \quad (8.7)$$

where, by letting  $d\vec{\tau}_{[k-1]} \equiv \prod_{i=1}^{k-1} d\tau_i$  and  $\vec{\omega} \cdot \vec{\tau} \equiv \omega_1\tau_1 + \dots + \omega_{k-1}\tau_{k-1}$ , we may write

$$S_{\ell_1, \dots, \ell_j, p_{j+1}, \dots, p_k}^{\zeta, \eta}(\vec{\omega}_{[k-1]}) = \int_{-\infty}^{\infty} d\vec{\tau}_{[k-1]} e^{-i\vec{\omega} \cdot \vec{\tau}} C^{(k)}(\zeta_{\ell_1}(t)\zeta_{\ell+2}(t+\tau_1) \cdots \eta_{p_k}(t+\tau_{k-1})), \quad \forall t.$$

Of particular interest are *stationary zero-mean classical Gaussian noise processes*, whose statistical properties are completely characterized by the second-order cumulants. That is,

$$C^{(k)}(\zeta_{\ell_1}(t)\zeta_{\ell+2}(t+\tau_1) \cdots \eta_{p_k}(t+\tau_{k-1})) = 0, \quad \forall k \neq 2, \quad \forall t, \tau_j. \quad (8.8)$$

Accordingly, for Gaussian noise all relevant statistical properties are formally encapsulated by  $S_{\ell_1, \dots, \ell_j, p_{j+1}, \dots, p_k}^{\zeta, \eta}(\omega)$  for  $k = 2$  and  $j = 0, 1, 2$ ; that is, physically, the noise power spectra associated to two-point correlations in the single-qubit and two-qubit energy fluctuations,  $S_{\ell_1, \ell_2}^{\zeta}(\omega)$  ( $j = 2$ ),  $S_{p_1, p_2}^{\eta}(\omega)$  ( $j = 0$ ), and the cross-power spectrum  $S_{\ell_1, p_1}^{\zeta, \eta}(\omega)$  ( $j = 1$ ). If, additionally, the local and two-local classical noise sources,  $\zeta_\ell(t)$  and  $\eta_p(t)$ , are statistically independent, one may further simplify to  $S_{\ell_1, \dots, \ell_j, p_{j+1}, \dots, p_k}^{\zeta, \eta}(\omega) = 0$  for  $0 < j < k$ .

**Spectral properties of quantum phase noise** – The spectral properties of a quantum dephasing environment may likewise be characterized in terms of statistical moments and cumulants. The starting point is to define statistical averages with respect to the initial state of the bath, say,  $\rho_B$ , by using  $\text{Tr}_B(\cdot\rho_B)$  instead of  $\langle \cdot \rangle_c$ . While in the most general case initial system-bath correlations may be present (hence  $\rho_B = \text{Tr}_S[\rho_{SB}(0)]$ ), throughout the present analysis we shall work under the standard assumption of an *initial factorized state* of the form  $\rho_{SB}(0) \equiv \rho_S(0) \otimes \rho_B$ . Thus, we are interested in the time-domain  $k$ -th order moments,

$$\text{Tr}_B[B_{\ell_1}(t_1) \cdots B_{\ell_k}(t_k)\rho_B] \equiv \langle B_{\ell_1}(t_1) \cdots B_{\ell_k}(t_k) \rangle_q,$$

or in the frequency Fourier transform of the corresponding cumulant,

$$S_{\ell_1, \dots, \ell_k}^B(\vec{\omega}_{[k]}) = C^{(k)}(\tilde{B}_{\ell_1}(\omega_1) \cdots \tilde{B}_{\ell_k}(\omega_k)), \quad (8.9)$$

where  $\tilde{B}_\ell(\omega)$  is the Fourier transform of  $B_\ell(t)$ . Operator cumulants are defined recursively via the moment-cumulant relations given earlier, equation (8.5), upon replacing  $\langle \cdot \rangle_c$  with  $\langle \cdot \rangle_q$ , e.g.,

$$\begin{aligned} \langle B_{\ell_1}(t_1)B_{\ell_2}(t_2) \rangle_q &= C^{(2)}(B_{\ell_1}(t_1)B_{\ell_2}(t_2)) + C^{(1)}(B_{\ell_1}(t_1))C^{(1)}(B_{\ell_2}(t_2)), \\ \langle B_{\ell_2}(t_2)B_{\ell_1}(t_1) \rangle_q &= C^{(2)}(B_{\ell_2}(t_2)B_{\ell_1}(t_1)) + C^{(1)}(B_{\ell_2}(t_2))C^{(1)}(B_{\ell_1}(t_1)). \end{aligned}$$

In the generic case where  $[B_\ell, H_B] \neq 0$ , one can see that a necessary and sufficient condition for stationarity is that  $[\rho_B, H_B] = 0$ . In particular, a *stationary zero-mean quantum Gaussian noise process* may be defined by requiring that, for all  $t$ ,  $\langle B_\ell(t) \rangle_q = 0$ , and, in analogy to equation

---

<sup>1</sup>Noise cross-power spectra may be also defined in terms of the Fourier transform of the moments (and related high-order time-correlation functions) [197]. Following standard practice in classical signal processing theory [198] and our previous analysis [43], we employ cumulants in what follows. In addition, we will assume sufficient regularity for all the relevant Fourier transforms to be mathematically well-defined.

(8.8), that arbitrary cumulants vanish for  $k > 2$ . The corresponding  $k = 2$  quantum power spectrum then obeys the relation  $S_{\ell,\ell'}^B(\omega_1, \omega_2) = 2\pi\delta(\omega_1 + \omega_2)S_{\ell,\ell'}^B(\omega_2)$ , where

$$S_{\ell,\ell'}^B(\omega_2) = \int_{-\infty}^{\infty} d\tau e^{-i\omega_2\tau} \langle B_\ell(t + \tau)B_{\ell'}(t) \rangle_q, \quad \forall t.$$

In what follows, we focus on dephasing noise originating from bosonic sources, representing for instance phonon or photon modes. In this context, a paradigmatic example is the *linear spin-boson model* [182, 168, 48, 178, 188, 184, 169, 199], defined by the following bath Hamiltonian and interaction operators in equations (8.1) and (8.3) (in units where  $\hbar = 1$ ):

$$H_B = \sum_k \Omega_k a_k^\dagger a_k, \quad \Omega_k \geq 0, \quad B_\ell = \sum_k (g_k^\ell a_k^\dagger + g_k^{\ell*} a_k), \quad (8.10)$$

where  $[a_k, a_{k'}^\dagger] = \delta_{k,k'}$ ,  $[a_k, a_{k'}] = 0 = [a_k^\dagger, a_{k'}^\dagger]$ , and  $g_k^\ell$  describes the coupling strength between qubit  $\ell$  and bath mode  $k$ . If the initial bath state  $\rho_B$  is thermal, with inverse temperature  $\beta = 1/k_B T$ ,  $\rho_B \propto e^{-\beta H_B}$ , the family of operators  $B_\ell(t) = \sum_k (g_k^\ell e^{i\Omega_k t} a_k^\dagger + g_k^{\ell*} e^{-i\Omega_k t} a_k)$  describes a stationary noise process which also obeys free-field Gaussian statistics [184]. The above quantum power spectrum is explicitly given by

$$S_{\ell,\ell'}^B(\omega) = 2\pi \sum_k \left( g_k^\ell g_k^{\ell*} \delta(\omega + \Omega_k) \langle a_k^\dagger a_k \rangle_q + g_k^{\ell*} g_k^\ell \delta(\omega - \Omega_k) \langle a_k a_k^\dagger \rangle_q \right), \quad (8.11)$$

where  $\langle a_k^\dagger a_k \rangle_q = (\coth(\beta\Omega_k/2) - 1)/2 = \langle a_k a_k^\dagger \rangle_q - 1$  are equilibrium expectation values. Assuming that the couplings are position-dependent as  $g_k^\ell = |g_k| e^{i\vec{k} \cdot \vec{r}_\ell}$  [182], where  $\vec{k}$  is the momentum associated with the  $k$ -th mode and  $\vec{r}_\ell$  the position of the  $\ell$ -th qubit, one gets

$$g_k^\ell g_k^{\ell*} = |g_k|^2 e^{i\vec{k} \cdot (\vec{r}_\ell - \vec{r}_{\ell'})} \equiv |g_k|^2 e^{i\Omega_k t_{\ell,\ell'}}, \quad (8.12)$$

where we have further expressed the exponent in terms of the mode frequency and the *transit time* [188] via the (linear) dispersion relation  $\Omega_k t_{\ell,\ell'} = \vec{k} \cdot (\vec{r}_\ell - \vec{r}_{\ell'})$ . Under these assumptions,

$$S_{\ell,\ell'}^B(\omega) = 2\pi J(\omega) \begin{cases} e^{-i\omega t_{\ell,\ell'}} (\coth(\beta\omega/2) + 1)/2, & \omega > 0, \\ e^{-i\omega t_{\ell,\ell'}} (\coth(-\beta\omega/2) - 1)/2, & \omega < 0, \end{cases} \quad (8.13)$$

where  $J(\omega) = \sum_k |g_k|^2 [\delta(\omega - \Omega_k) + \delta(\omega + \Omega_k)] = J(-\omega)$  is the *spectral density function* of the oscillator bath in the continuum limit.<sup>2</sup>

Since, by definition,  $S_{\ell,\ell'}^B(\omega_1, \omega_2)$  is the second-order cumulant of the Fourier-transformed bath operators, we may write  $S_{\ell,\ell'}^B(\omega) \equiv S_{\ell,\ell'}^{B,+}(\omega) + S_{\ell,\ell'}^{B,-}(\omega)$  upon separating operator products into anti-commutators and commutators. If the latter are, respectively, denoted by  $[\cdot, \cdot]_\pm$ , direct calculation yields

$$\text{Tr} \left[ [\tilde{B}_\ell(\omega_1), \tilde{B}_{\ell'}(\omega_2)]_\pm \rho_B \right] \equiv S_{\ell,\ell'}^{B,\pm}(\omega_1, \omega_2) = 2\pi\delta(\omega_1 + \omega_2)S_{\ell,\ell'}^{B,\pm}(\omega_2), \quad (8.14)$$

$$S_{\ell,\ell'}^{B,+}(\omega) = \pi J(\omega) \begin{cases} e^{-i\omega t_{\ell,\ell'}} \coth(\beta\omega/2), & \omega > 0, \\ -e^{-i\omega t_{\ell,\ell'}} \coth(\beta\omega/2), & \omega < 0, \end{cases} \quad S_{\ell,\ell'}^{B,-}(\omega) = \pi J(\omega) \begin{cases} e^{-i\omega t_{\ell,\ell'}}, & \omega > 0, \\ -e^{-i\omega t_{\ell,\ell'}}, & \omega < 0. \end{cases} \quad (8.15)$$

<sup>2</sup>Note that, unlike classical noise, quantum noise is *spectrally asymmetric* in general, with the ratio  $S_{\ell,\ell'}^B(\omega)/S_{\ell',\ell}^B(-\omega) = e^{\beta\omega}$  enforcing detailed balance at thermal equilibrium.

Thus,  $S_{\ell,\ell'}^{B,+}(\omega)$  ( $S_{\ell,\ell'}^{B,-}(\omega)$ ) have symmetric (anti-symmetric) character in the sense that

$$S_{\ell,\ell'}^{B,+}(-\omega) = [S_{\ell,\ell'}^{B,+}(\omega)]^*, \quad S_{\ell,\ell'}^{B,-}(-\omega) = -[S_{\ell,\ell'}^{B,-}(\omega)]^*, \quad \forall \ell, \ell', \quad (8.16)$$

a feature that will be useful in understanding their contribution to different dynamical aspects.

While the free dynamics under multi-qubit classical plus bosonic dephasing will be recovered as a special case of the DD-controlled dynamics, two remarks are in order. First, our approach may be applied to a wider class of quantum noise scenarios, for instance environments consisting of multiple interacting types of bosons, as long as the relevant Hamiltonian can be mapped to equation (8.10) via an appropriate Bogoliubov transformation [200]. Second, for all the noise sources considered, a finite norm of the error dynamics to be filtered out will be assumed – or, in more physical terms, a *finite correlation time* ('non-Markovian' behavior in the sense of [58, 184]) relative to which *fast control* regimes may be accessed. This is a crucial requirement for DD methods to be effective [156, 58, 43, 72, 99], which will translate into assuming that all relevant noise spectra decay sufficiently rapidly at high frequencies.

## 8.2.2 Control protocols

To facilitate presentation of the essential new results, we assume access to perfect instantaneous  $\pi$  rotations, and postpone discussion of realistic effects to section 8.5.2. This ideal ‘bang-bang’ DD setting has been extensively investigated in both single-qubit [48, 64, 67, 199, 169] and multi-qubit systems [58, 201, 186, 187] (see [156] for a review). For the sake of completeness and consistency, we summarize the basic ingredients in this section, building in particular on references [187, 202]. In the process, we introduce a new *composition rule* which unifies existing high-order sequence constructions and may be of independent interest within DD theory.

For the dephasing noise models under consideration, control implemented via instantaneous rotations along a fixed axis (say,  $x$ ), suffices. Let a DD sequence, labeled by an integer index  $s$ , be specified in terms of a control operation  $X (\equiv \sigma_x)$ , and a number  $n(s)$  of control intervals  $\{\tau_j^{(s)} \equiv r_j^{(s)} T\}$ , where  $T$  is the total evolution time and  $\{r_j^{(s)}\}_{j=0}^{n(s)-1}$  are positive numbers, that satisfy  $\sum_j r_j^{(s)} = 1$  and describe the relative pulse timings. If  $U_0(\tau_j^{(s)})$  denotes free evolution over  $\tau_j^{(s)}$ , the controlled propagator induced by such a sequence reads

$$U_s^{(X)}(T) = X^s U_0(\tau_{n(s)-1}^{(s)}) X \cdots X U_0(\tau_1^{(s)}) X U_0(\tau_0^{(s)}), \quad (8.17)$$

where operators are applied from right to left and a final pulse is included at time  $t = T$  depending on the parity of  $s$  in order to ensure a cyclic control propagator. Following [43, 202], we say that the DD sequence achieves *cancellation order* (CO)  $\alpha$ , with respect to the control operation  $X$ , if the norm of unwanted (non-commuting) error terms is suppressed up to order  $\alpha$  in time, that is,  $\| [X, U_\alpha^{(X)}(T)] \| \sim \mathcal{O}(T^{\alpha+1})$ . With this in mind, we shall henceforth identify  $s \equiv \alpha$ . Consider two DD sequences, each acting on qubit  $\ell, \ell'$  via control operations  $X_\ell, X_{\ell'}$ , and specified in terms of intervals  $\{\tau_j^{(s)}\}, \{\tau_{j'}^{(s')}\}$  respectively. We can build a new sequence over time  $T$  by using the following composition rule:

$$U_{s'}^{(X_{\ell'})} \circ U_s^{(X_\ell)}(T) \equiv X_{\ell'}^{s'} U_s^{(X_\ell)}(\tau_{n(s')-1}^{(s')}) X_{\ell'} \cdots X_{\ell'} U_s^{(X_\ell)}(\tau_1^{(s')}) X_{\ell'} U_s^{(X_\ell)}(\tau_0^{(s')}). \quad (8.18)$$

That is, each free evolution period in the original ‘outer sequence’  $U_{s'}^{(X_{\ell'})}(T)$  is replaced by an ‘inner sequence’  $U_s^{(X_\ell)}$  of duration determined by the corresponding outer interval  $\tau_{j'}^{(s')}$ . We are now ready to define the specific high-order sequences we will be using.

**Single-qubit DD sequences –** The two relevant sequences are single-axis CDD [64] and Uhrig DD (UDD) [67]. The former may be defined recursively via

$$\text{CDD}_\alpha^{(X)}(T) = \text{CDD}_1^{(X)} \circ \text{CDD}_{\alpha-1}^{(X)}(T),$$

with relative pulse timings  $\{r_j^{(1)}\} = \{1/2, 1/2\}$ , so that, for example,

$$\begin{aligned}\text{CDD}_1^{(X)}(T) &= XU_0(T/2)XU_0(T/2), \\ \text{CDD}_2^{(X)}(T) &= XCDD_1^{(X)}(T/2)XCDD_1^{(X)}(T/2) = U_0(T/4)XU_0(T/2)XU_0(T/4),\end{aligned}$$

and so on. On the other hand, the  $\alpha$ -th order UDD protocol is defined by the pulse timings  $t_j^{(\alpha)} = T \sin^2[\pi j/(2\alpha + 2)]$ , with  $\tau_j^{(\alpha)} = t_{j+1}^{(\alpha)} - t_j^{(\alpha)}$  for  $j = 0, \dots, \alpha$ .

**Multi-qubit DD sequences** – Both single-qubit CDD and UDD sequences admit extensions to multiple qubits via the composition rule given in equation (8.18). In particular, by letting  $\vec{X} \equiv (X_1, \dots, X_N)$ , one can define the following  $N$ -qubit sequences:

$$\mathring{U}_{(\alpha_1, \dots, \alpha_N)}^{(\vec{X})}(T) \equiv U_{\alpha_1}^{(X_1)} \circ \left( U_{\alpha_2}^{(X_2)} \circ \left( \dots \left( U_{\alpha_{N-1}}^{(X_{N-1})} \circ U_{\alpha_N}^{(X_N)} \right) \dots \right) \right)(T), \quad (8.19)$$

$$\mathring{U}'_{(\alpha, \dots, \alpha)}^{(\vec{X})}(T) \equiv \underbrace{\mathring{U}_{(1, \dots, 1)}^{(\vec{X})} \circ \left( \mathring{U}_{(1, \dots, 1)}^{(\vec{X})} \circ \left( \dots \circ \mathring{U}_{(1, \dots, 1)}^{(\vec{X})} \right) \dots \right)}_{\alpha \text{ times}}(T). \quad (8.20)$$

By construction, both achieve CO equal to  $\alpha = \min\{\alpha_1, \dots, \alpha_N\}$  with respect to  $\{X_\ell\}$ . However, if the single-qubit sequence  $U_{\alpha_\ell}^{(X_\ell)}$  uses  $n_P = n(\alpha_\ell)$  pulses,  $\mathring{U}_{(\alpha_1, \dots, \alpha_N)}^{(\vec{X})}(T)$  in equation (8.19) uses a total number of pulses

$$n_P^{\text{tot}}(N) = \prod_{\ell=1}^N n(\alpha_\ell) \geq [n(\alpha)]^N, \quad (8.21)$$

whereas  $\mathring{U}'_{(\alpha, \dots, \alpha)}^{(\vec{X})}(T)$  in equation (8.20) uses  $n_P^{\text{tot}}(N) = [n(1)]^{\alpha N}$ , with  $n_P^{\text{tot}}(N)$  growing exponentially with  $N$  in either case. Depending on the sequences used as building blocks, all known high-order DD sequences may be recovered. Specifically, we shall consider the following  $\alpha$ -th order  $N$ -qubit sequences:

(i) Multi-qubit CDD [64]:

$$\mathring{\text{CDD}}_{(\alpha, \dots, \alpha)}^{(\vec{X})}(T) = \underbrace{\text{CDD}_{(1, \dots, 1)}^{(\vec{X})} \circ \left( \text{CDD}_{(1, \dots, 1)}^{(\vec{X})} \circ \left( \dots \circ \text{CDD}_{(1, \dots, 1)}^{(\vec{X})} \right) \dots \right)}_{\alpha \text{ times}}(T).$$

(ii) Nested UDD (NUDD) [186]:

$$\text{NUDD}_{(\alpha_1, \dots, \alpha_N)}^{(\vec{X})}(T) = \text{UDD}_{\alpha_1}^{(X_1)} \circ \left( \text{UDD}_{\alpha_2}^{(X_2)} \circ \left( \dots \left( \text{UDD}_{\alpha_{N-1}}^{(X_{N-1})} \circ \text{UDD}_{\alpha_N}^{(X_N)} \right) \dots \right) \right)(T).$$

(iii) Nested CDD (NCDD):<sup>3</sup>

$$\text{NCDD}_{(\alpha_1, \dots, \alpha_N)}^{(\vec{X})}(T) = \text{CDD}_{\alpha_1}^{(X_1)} \circ \left( \text{CDD}_{\alpha_2}^{(X_2)} \circ \left( \dots \left( \text{CDD}_{\alpha_{N-1}}^{(X_{N-1})} \circ \text{CDD}_{\alpha_N}^{(X_N)} \right) \dots \right) \right)(T).$$

To date, NUDD is the most efficient known sequence, in terms of the required number of pulses capable of ensuring CO  $\alpha$  for general multi-qubit dephasing noise as in equations (8.2)-(8.3), at least for sufficiently hard noise spectral cutoffs [203].

<sup>3</sup>Note that the sequences given in (ii) and (iii) are two extremes of the possible range of sequences that may be built using the composition rule of equation (8.18) and CDD as building blocks. The composition rule may be naturally extended to *multi-axis* DD sequences, recovering for instance concatenated UDD or quadratic DD [156].

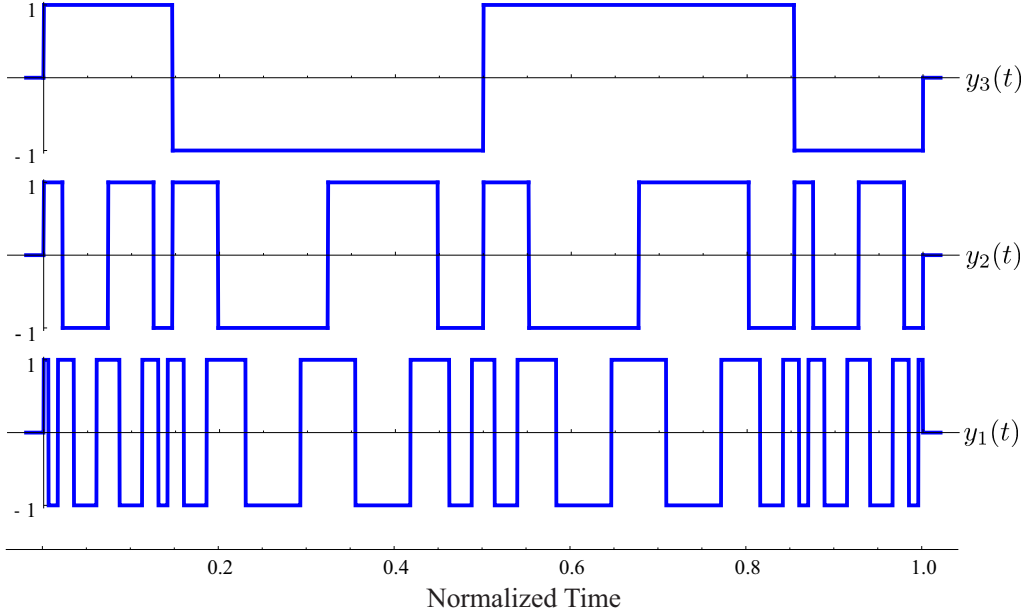


Figure 8.1: *Control switching functions vs. normalized time for NUDD on  $N = 3$  qubits,  $\text{NUDD}_{(\alpha_1, \alpha_2, \alpha_3)}^{(X_1, X_2, X_3)} = \text{UDD}_{\alpha_3}^{(X_3)} \circ (\text{UDD}_{\alpha_2}^{(X_2)} \circ \text{UDD}_{\alpha_1}^{(X_1)})$ , resulting in  $\text{CO } \alpha = 2$ . Each crossing of the switching function with the time axis is associated with a control pulse on the corresponding qubit (for a total of  $n_P^{\text{tot}} = 4 \times 4 \times 2 = 32$  pulses).*

Once a multi-qubit DD sequence is chosen, the effect of the control is most simply described in the interaction picture associated to the control propagator  $U_c(t)$ , which in the present setting simply leads to time-dependent ‘error generators,’ namely,

$$Z_\ell \mapsto Z_\ell(t) \equiv U_c^\dagger(t) Z_\ell U_c(t) = y_\ell(t) Z_\ell, \quad \forall \ell,$$

$$Z_\ell Z_{\ell'} \mapsto Z_\ell Z_{\ell'}(t) \equiv U_c^\dagger(t) Z_\ell Z_{\ell'} U_c(t) = y_\ell(t) y_{\ell'}(t) Z_\ell Z_{\ell'}, \quad \forall \ell \neq \ell',$$

where the *control switching function* for the  $\ell$ -th qubit has the form

$$y_\ell(t) = \sum_{j=0}^{n_P^{(\ell)}} (-1)^j \Theta(t - t_j^{(\ell)}) \Theta(t_{j+1}^{(\ell)} - t). \quad (8.22)$$

Here,  $n_P^{(\ell)}$  denotes the total number of pulses applied on qubit  $\ell$  and  $\Theta$  is, as usual, the step function. We say that the control is (qubit) *non-selective* (or global) if  $y_\ell(t) = y(t) \forall \ell$ , and that it is *selective* otherwise. Note that nested multi-qubit sequences necessarily require qubit-selective control. A simple illustrative example is depicted in figure 8.1.

### 8.2.3 Exact representation of the controlled dynamics and fundamental filter functions

In order to determine the reduced dynamics of the controlled multi-qubit system, the first step is to obtain an expression for the unitary ‘error propagator’ resulting from equation (8.1) under DD, evaluated in the combined interaction picture associated with the control and bath evolution. Thanks to the fact that the bosonic algebra guarantees simple commutation relationships between noise operators, namely,  $[B_\ell(t), B_{\ell'}(t')] \propto I_B$  for all  $t \neq t'$ , the Magnus expansion [156] truncates exactly at the second order. Accordingly, the desired propagator, which we

denote henceforth  $\tilde{U}_e(T)$ , may be compactly expressed as follows (up to an irrelevant global phase factor):

$$\begin{aligned}\tilde{U}_e(T) &= \mathcal{T}_+ \exp \left[ -i \int_0^T U_c^\dagger(t) \left( \tilde{H}_S(t) + \tilde{H}_{SB}(t) \right) U_c(t) dt \right] \equiv \exp[-i H_{\text{eff}} T] \\ &= \exp \left[ \sum_\ell Z_\ell \left( \bar{\zeta}'_\ell(T) + \bar{B}_\ell(T) \right) + \sum_{\ell \neq \ell'} Z_\ell Z_{\ell'} \left( \bar{\eta}'_{\ell, \ell'}(T) + \bar{R}_{\ell, \ell'}(T) \right) \right],\end{aligned}\quad (8.23)$$

where equation (8.23) explicitly defines the relevant effective Hamiltonian  $H_{\text{eff}}$ , and we have introduced new random variables as well as time-averaged quantities by letting

$$\zeta'_\ell(t) \equiv d_\ell + \zeta_\ell(t), \quad \eta'_{\ell, \ell'}(t) \equiv d_{\ell, \ell'} + \eta_{\ell, \ell'}(t), \quad (8.24)$$

$$\bar{A}_\ell(T) \equiv -i \int_0^T dt y_\ell(t) A_\ell(t), \quad A_\ell \in \{\zeta'_\ell, B_\ell\}, \quad \bar{\eta}_{\ell, \ell'}(T) \equiv -i \int_0^T dt y_\ell(t) y_{\ell'}(t) \eta_{\ell(t), \ell'}(t) \quad (8.25)$$

$$\bar{R}_{\ell, \ell'}(T) \equiv -\frac{1}{2} \int_0^T dt_1 \int_0^{t_1} dt_2 y_\ell(t_1) y_{\ell'}(t_2) [B_\ell(t_1), B_{\ell'}(t_2)]. \quad (8.26)$$

It is instructive to examine the propagator in the frequency domain, by exploiting the *fundamental FF* formalism introduced in [43]. Substituting the explicit forms of the Magnus terms in equations (8.25)-(8.26) in the expression for  $\tilde{U}_e(T)$  in equation (8.23) and taking the Fourier transform, one may rewrite (up to irrelevant global phase factors):

$$\begin{aligned}\tilde{U}_e(T) = \exp \left[ -i \sum_\ell Z_\ell \int_{-\infty}^{\infty} \frac{d\omega}{2\pi} G_{Z_\ell}^{(1)}(\omega, T) (\tilde{\zeta}'_\ell(\omega) + \tilde{B}_\ell(\omega)) \right. \\ \left. - i \sum_{\ell < \ell'} Z_\ell Z_{\ell'} \left( \int_{-\infty}^{\infty} \frac{d\omega}{2\pi} G_{Z_\ell Z_{\ell'}}^{(1)}(\omega, T) \tilde{\eta}'_{\ell, \ell'}(\omega) \right. \right. \\ \left. \left. + \int_{-\infty}^{\infty} \frac{d\omega_1}{2\pi} \int_{-\infty}^{\infty} \frac{d\omega_2}{2\pi} G_{Z_\ell, Z_{\ell'}}^{(2)}(\omega_1, \omega_2, T) [\tilde{B}_\ell(\omega_1), \tilde{B}_{\ell'}(\omega_2)] \right) \right],\end{aligned}\quad (8.27)$$

where the relevant first- and second-order generalized FFs,  $G^{(1)}(\omega, T)$  and  $G^{(2)}(\omega_1, \omega_2, T)$ , may in turn be expressed in terms of fundamental FFs:

$$\begin{aligned}-iG_{Z_\ell}^{(1)}(\omega, T) &= F_{Z_\ell}^{(1)}(\omega, T), \quad \ell = 1, \dots, N, \\ -iG_{Z_\ell Z_{\ell'}}^{(1)}(\omega, T) &= F_{Z_\ell Z_{\ell'}}^{(1)}(\omega, T) + F_{Z_{\ell'} Z_\ell}^{(1)}(\omega, T), \quad \ell \neq \ell', \\ -iG_{Z_\ell, Z_{\ell'}}^{(2)}(\omega_1, \omega_2, T) &= \frac{1}{2} \left( F_{Z_\ell, Z_{\ell'}}^{(2)}(\omega_1, \omega_2, T) - F_{Z_{\ell'}, Z_\ell}^{(2)}(\omega_2, \omega_1, T) \right), \quad \ell \neq \ell',\end{aligned}$$

and the corresponding *first- and second-order fundamental FFs* are given by

$$F_{Z_\ell}^{(1)}(\omega, T) \equiv -i \int_0^T dt y_\ell(t) e^{i\omega t} = -[F_{Z_\ell}^{(1)}(-\omega, T)]^*, \quad (8.28)$$

$$F_{Z_\ell Z_{\ell'}}^{(1)}(\omega, T) \equiv -i \int_0^T dt y_\ell(t) y_{\ell'}(t) e^{i\omega t} = -[F_{Z_\ell Z_{\ell'}}^{(1)}(-\omega, T)]^*, \quad (8.29)$$

$$F_{Z_\ell, Z_{\ell'}}^{(2)}(\omega_1, \omega_2, T) \equiv - \int_0^T dt_1 \int_0^{t_1} dt_2 y_\ell(t_1) y_{\ell'}(t_2) e^{i\vec{\omega} \cdot \vec{t}} = [F_{Z_\ell, Z_{\ell'}}^{(2)}(-\omega_1, -\omega_2, T)]^*. \quad (8.30)$$

We recall that this general filtering formalism allows one to determine the CO of a control protocol as well as its *filtering order* (FO) – in particular, around  $\vec{\omega} = 0$ , as relevant to DD. If

$$G_{O_{a_1}, \dots, O_{a_j}}^{(j)}(\omega_1, \dots, \omega_j, T) = \mathcal{O}(m^{\Phi_{a_1, \dots, a_j}^{(j)}}(\vec{\omega}) T^{\alpha_{a_1, \dots, a_j}^{(j)} + 1}), \quad (8.31)$$

where  $m^{\Phi_{a_1, \dots, a_j}^{(j)}}(\vec{\omega})$  is a degree- $\Phi_{a_1, \dots, a_j}^{(j)}$  monomial in the components of  $\vec{\omega}$ , then the CO  $\alpha = \min\{\alpha_{a_1, \dots, a_j}^{(j)}\}$  and the (level-2-Magnus) FO  $\Phi^{[2]} \equiv \Phi = \min\{\Phi_{a_1, \dots, a_j}^{(j)}\}$ , respectively. In general, it is crucial to analyze the suppression capabilities of a protocol in *both* the frequency and time domain to fully characterize the control performance [43]. As defined in equation (8.31), the FO contains information about how ‘flat’ the filter implemented by  $G_{O_{a_1}, \dots, O_{a_j}}^{(j)}(\vec{\omega}, T)$  is around  $\vec{\omega} = 0$ , and hence how well it attenuates low-frequency noise. The CO, on the other hand, quantifies the way in which uncorrected error contributions are expected to scale with the total sequence time, irrespective of frequency. In this sense, the CO can be thought of as providing information about the overall magnitude of the filtered signal. Notice that dimensional analysis establishes a relation between the CO and FO of any generalized FF. Since  $G_{O_{a_1}, \dots, O_{a_j}}^{(j)}(\vec{\omega}, T)$  is a  $j$ -nested time integral, it has dimensions of [time] $^j$ , which yields

$$\alpha_{a_1, \dots, a_j}^{(j)} - \Phi_{a_1, \dots, a_j}^{(j)} = j - 1 \geq 0, \quad \forall j. \quad (8.32)$$

Minimization of the left hand-side also implies that the overall CO and FO of a protocol obey the simple relationship<sup>4</sup>  $\Phi \leq \alpha$ . In the light of these considerations, the high-order sequences described in the previous section have interesting filtering properties: because only FFs of order  $\alpha = 1, 2$  are relevant to the analysis, one may verify that CDD and NUDD sequences have CO equal to  $\alpha$  and FO  $\in \{\alpha - 1, \alpha\}$ .

The effective Hamiltonian  $H_{\text{eff}}$  defined in equation (8.23) [or equation (8.27) in Fourier space] comprises different physical contributions. One-body terms, proportional to  $Z_\ell$ , are present for qubits coupled to arbitrary classical or private quantum baths. Two-body terms, proportional to  $Z_\ell Z_{\ell'}$  and capable of inducing quantum correlations between different qubits, may have two distinct origins within our model:

- They may result from the ‘direct’ Ising coupling in the free Hamiltonian, corresponding to the term  $\tilde{\zeta}'_\ell(T)$  in equation (8.23) and filtered by  $G_{Z_\ell Z_{\ell'}}^{(1)}(\omega, T)$  in equation (8.27);
- They may result from the ‘induced’ coupling mediated by the quantum bath via its non-commuting character, corresponding to the term  $\tilde{R}_{\ell, \ell'}(T)$  in equation (8.23) and filtered by  $G_{Z_\ell, Z_{\ell'}}^{(2)}(\omega_1, \omega_2, T)$  in equation (8.27).

Even in the absence of direct coupling ( $\eta'_{\ell, \ell'}(t) \equiv 0$ ), the bath-mediated interaction poses a main obstacle to designing less resource-intensive DD sequences, as we will see in the following section. Notwithstanding, it is important to reiterate that, thanks to the bosonic algebra, the frequency-domain commutator  $[\tilde{B}_\ell(\omega_1), \tilde{B}_{\ell'}(\omega_2)] \propto I_B$  depends *only* on one frequency variable, and thus only  $G_{Z_\ell, Z_{\ell'}}^{(2)}(\omega, -\omega, T)$  will be relevant to our analysis.

Depending on the initial state of the system and/or bath, the cancellation or filtering order of a DD sequence may be *higher* [43] than they are at the propagator level. In order to proceed to the exact solution for the reduced system dynamics under the initial factorization assumption  $\rho_{S\mathcal{B}}(0) = \rho(0) \otimes \rho_{\mathcal{B}}$ , let the initial  $N$ -qubit state be

$$\rho(0) = \sum_{a,b} |a_1 \cdots a_N\rangle \langle b_1 \cdots b_N| \rho_{a,b}(0) \equiv \sum_{a,b} |a\rangle \langle b| \rho_{a,b}(0), \quad (8.33)$$

where the sum ranges over all possible binary strings  $a \equiv a_1 \cdots a_N$  and  $b \equiv b_1 \cdots b_N$  of length  $N$ . The interaction-picture reduced density matrix at time  $T$  may then be expressed as

$$\langle \rho(T) \rangle_{c,q} = \langle \text{Tr}_{\mathcal{B}} \left[ \tilde{U}_e(T) \rho(0) \otimes \rho_{\mathcal{B}} \tilde{U}_e(T)^\dagger \right] \rangle_c \equiv \sum_{a,b} e^{-Z_{a,b}(T)} \rho_{a,b}(0) |a\rangle \langle b|, \quad (8.34)$$

---

<sup>4</sup>We stress that for noise models more general than dephasing, as considered here,  $\Phi$  and  $\alpha$  need *not* be tightly related, and one can only guarantee that the (infinite-level-Magnus)  $\Phi^{[\infty]} \leq \alpha$  [43].

where in general the complex factor  $Z_{a,b}(T) \equiv \chi_{a,b}(T) + i\phi_{a,b}(T)$  allows for both non-trivial decay and phase evolution of each coherence element. Specifically, direct calculation yields:

$$e^{-Z_{a,b}(T)} = \langle e^{\sum_{\ell < \ell'} \Delta[a_\ell + a_{\ell'}, b_\ell + b_{\ell'}] \bar{\eta}'_{\ell, \ell'}(T)} e^{\sum_{\ell} \Delta[a_\ell, b_\ell] \bar{\zeta}'_{\ell}(T)} \rangle_c \quad (8.35)$$

$$\cdot \langle e^{\sum_{\ell} \Delta[a_\ell, b_\ell] \bar{B}_{\ell}(T)} \rangle_q \langle e^{\sum_{\ell < \ell'} \Delta[a_\ell + a_{\ell'}, b_\ell + b_{\ell'}] (\bar{R}_{\ell, \ell'}(T) + \bar{R}_{\ell', \ell}(T))} \rangle_q \quad (8.36)$$

$$\cdot \langle e^{\sum_{\ell, \ell'} \frac{(-1)^{|a_\ell| + |b_{\ell'}|}}{2} [\bar{B}_{\ell}(T), \bar{B}_{\ell'}(T)]} \rangle_q, \quad (8.37)$$

where  $\Delta[u, v] \equiv (-1)^u - (-1)^v$  and  $a_\ell$  is the  $\ell$ -th entry of the string  $a$ . Formally, irrespective of whether we consider the classical ensemble average or the quantum statistical average with respect to  $\rho_B$ , the following cumulant expansion holds for a random variable or operator  $Q$ :

$$\langle e^Q \rangle = \left\langle \sum_{s=0}^{\infty} \frac{Q^s}{s!} \right\rangle = e^{\sum_{k=1}^{\infty} C^{(k)}(Q, \dots, Q)/k!}, \quad (8.38)$$

where  $\langle \cdot \rangle$  stands for either  $\langle \cdot \rangle_q$  or  $\langle \cdot \rangle_c$ . If  $Q$  has stationary zero-mean Gaussian statistics, the only non-vanishing cumulant is  $C^{(2)}(Q, Q) = \langle QQ \rangle$ , hence  $\langle e^Q \rangle = e^{\langle QQ \rangle/2}$ . Note that all the quantities in the exponents that define  $Z_{a,b}(T)$ , which involve sums over single (classical or quantum) noise sources, inherit the properties of the corresponding noise processes: e.g., if  $\zeta_\ell(t)$  is zero-mean Gaussian, the same holds for  $Q = \sum_{\ell} \Delta[a_\ell, b_\ell] \bar{\zeta}'_{\ell}(T)$  in equation (8.35). Furthermore, in view of the bosonic algebra, [equation (8.14)], the two contributions  $\langle e^{\sum_{\ell < \ell'} \Delta[a_\ell + a_{\ell'}, b_\ell + b_{\ell'}] (\bar{R}_{\ell, \ell'}(T) + \bar{R}_{\ell', \ell}(T))} \rangle_q$  [equation (8.36)] and  $\langle e^{\sum_{\ell, \ell'} \frac{(-1)^{|a_\ell| + |b_{\ell'}|}}{2} [\bar{B}_{\ell}(T), \bar{B}_{\ell'}(T)]} \rangle_q$  [equation (8.37)] are *independent of  $\rho_B$*  and thus constants with respect to  $\langle \cdot \rangle_q$ . This allows us to obtain exact analytical expressions for the controlled dynamics when all noise sources are Gaussian.

For non-Gaussian dephasing models in which the cumulant series does not truncate to the second order (including non-linear spin-boson models [204]), one needs to consider, in principle, all the infinite multiple-point correlations which, in the Fourier domain, implies dealing with an infinite hierarchy of FFs. Remarkably, however, for the family of classical plus linear bosonic noise models studied in this paper, arbitrary high-order cumulants can still be written in a compact way in terms of *only two generalized FFs, regardless of stationarity*:

$$\begin{aligned} C^{(k)}(\bar{\zeta}_{\ell_1}(T) \cdots \bar{\eta}_{p_{j+1}}(T) \cdots \bar{\eta}_{p_k}(T)) &= \int_{-\infty}^{\infty} \frac{d\vec{\omega}_{[k]}}{(2\pi)^k} S_{\ell_1, \dots, p_k}^{\zeta, \eta}(\vec{\omega}_{[k]}) G_{Z_{\ell_1}}^{(1)}(\omega_1, T) \cdots G_{Z_{\ell_j}}^{(1)}(\omega_j, T) \\ &\quad \cdot G_{Z_{\ell_{j+1}} Z_{\ell'_{j+1}}}^{(1)}(\omega_{j+1}, T) \cdots G_{Z_{\ell_k} Z_{\ell'_k}}^{(1)}(\omega_k, T), \\ C^{(k)}(\bar{B}_{\ell_1}(T) \cdots \bar{B}_{\ell_k}(T)) &= \int_{-\infty}^{\infty} \frac{d\vec{\omega}_{[k]}}{(2\pi)^k} S_{\ell_1, \dots, \ell_k}^B(\vec{\omega}_{[k]}) G_{Z_{\ell_1}}^{(1)}(\omega_1, T) \cdots G_{Z_{\ell_k}}^{(1)}(\omega_k, T), \end{aligned}$$

and

$$\bar{R}_{\ell, \ell'}(T) + \bar{R}_{\ell', \ell}(T) = \int_{-\infty}^{\infty} \frac{d\vec{\omega}_{[2]}}{(2\pi)^2} G_{Z_{\ell}, Z_{\ell'}}^{(2)}(\omega_1, \omega_2, T) S_{\ell, \ell'}^{B, -}(\omega_1, \omega_2),$$

where now both  $G_{Z_{\ell}, Z_{\ell'}}^{(2)}$  and  $S_{\ell, \ell'}^{B, -}$  are functions of two independent frequency variables. Similarly the  $k$ -th order polyspectra depend on the full set of  $k$  frequency variables. Together with the exact expressions in equations (8.35)–(8.37), the above still provide a closed-form representation of the reduced multi-qubit dynamics, which may be used to infer general results or serve as a basis to build approximations via truncation of the cumulant expansion.

## 8.3 Dynamical decoupling vs. multi-qubit dephasing noise: short-time memory

Having introduced the necessary tools, we are now poised to address the first of the two control problems we set out to explore, namely, efficient short-term memory using DD. Different DD protocols will be contrasted, and in each case we will characterize their decoherence suppression capabilities and extract their CO and FO directly from the relevant generalized FFs. While certain control strategies will only allow a fixed, small CO, we will see how, as sufficient structure is added to the control in terms of selectivity and symmetry, arbitrarily high CO is possible in principle. Beside re-establishing CDD and NUDD sequences as capable of arbitrary CO against general dephasing noise [156, 67, 64, 187, 186], a major goal is to construct more efficient DD sequences tailored to dephasing noise with particular features. We will present a new family of multi-qubit sequences that, by satisfying a particular *displacement anti-symmetry* condition, can achieve arbitrary CO *using exponentially less resources*, so long as no direct Ising coupling is present. The symmetry that these new sequences possess will also prove fundamental in the context of building long-term multi-qubit memories [see section 8.4].

### 8.3.1 Non-selective multi-qubit control sequences

The most naive, yet often readily available, strategy to decouple multiple qubits from their environment is to rely on non-selective control. In the formalism of section 8.2.2, this means applying global control operations of the form  $X_1 \otimes \dots \otimes X_N \equiv X_1 \cdots X_N$ , with a corresponding controlled propagator  $U_\alpha^{(X_1 \cdots X_N)}(T)$ . If  $y_\ell(t)$  is the control switching function for qubit  $\ell$ , requiring that the CO  $\alpha \geq 1$  implies that  $G_{Z_\ell}^{(1)}(\omega, T) \sim \mathcal{O}(m^\alpha(\vec{\omega})T^{\alpha+1})$  [43]. Since, however, the same pulse is applied synchronously to each qubit,  $y_\ell(t) = y(t)$  for all  $\ell$ , hence  $y_\ell(t)y_{\ell'}(t) = 1$  for all  $t$ . This affects the ability of non-selective DD to suppress time-independent noise: while  $G_{Z_\ell}^{(1)}(0, T) = 0$ , it follows from equation (8.29) that  $G_{Z_\ell Z_{\ell'}}^{(1)}(0, T) = 2T \neq 0$ , i.e., the noise induced by any constant two-qubit direct coupling [ $d_{\ell, \ell'} \neq 0$  in equation (8.2)] *cannot* be suppressed by non-selective DD. This is expected, as global pulses commute with the direct (system-only) coupling term and thus cannot affect it.

Interestingly, the bath-induced two-qubit coupling and the phase evolution ensuing from the second-order Magnus term *can* nevertheless be suppressed, albeit not according to an arbitrarily high power-law behavior. If either a CDD $_\alpha$  or UDD $_\alpha$  non-selective protocol is applied, the FF suppressing the induced coupling term,  $G_{Z_\ell Z_{\ell'}}^{(2)}(\omega, -\omega, T)$ , is found to scale as  $\mathcal{O}(m^1(\vec{\omega})T^3)$ , similar to free evolution (note that, using equation (8.30),  $G_{Z_\ell Z_{\ell'}}^{(2)}(\omega, -\omega, T)$  is a real function). Thus, non-selective DD cannot suppress the induced coupling term any better than free evolution, namely, only up to a fixed order independent of  $\alpha$ . While at first it would then seem that increasing  $\alpha$  would not improve error suppression, as claimed in some two-qubit analysis [192, 189], numerical exploration clearly demonstrates that as  $\alpha$  increases, the absolute value  $|G_{Z_\ell Z_{\ell'}}^{(2)}(\omega_1, \omega_2, T)|$  *does* decrease, i.e., better suppression is achieved (see figure 8.2).

This behavior may be understood in terms of a formal analogy between DD and a Zeno effect resulting from the increasingly more frequent pulses within  $[0, T]$ , as suggested in [48] for a single qubit. Consider implementing  $M$  repetitions of a given non-selective DD sequence  $U_1^{(X_1 \cdots X_N)}(\tau_M = T/M)$ , that is, an overall sequence  $[U_1^{(X_1 \cdots X_N)}(T/M)]^M$  over a fixed time  $T$ , in the continuous limit where  $M \rightarrow \infty$ . While the CO is fixed, the number of pulses grows as  $2M$ . In the simplest case of  $U_1^{(X_1 \cdots X_N)} = \text{CDD}_1$ , direct calculation yields

$$|G_{Z_\ell Z_{\ell'}}^{(2)}(\omega, -\omega, T)| = \frac{2 \left| \omega T - \tan\left(\frac{\omega T}{4M}\right) [\sin(\omega T) \tan\left(\frac{\omega T}{4M}\right) + 4M] \right|}{\omega^2} \sim \mathcal{O}\left(\frac{\omega T^3}{M^2}\right).$$

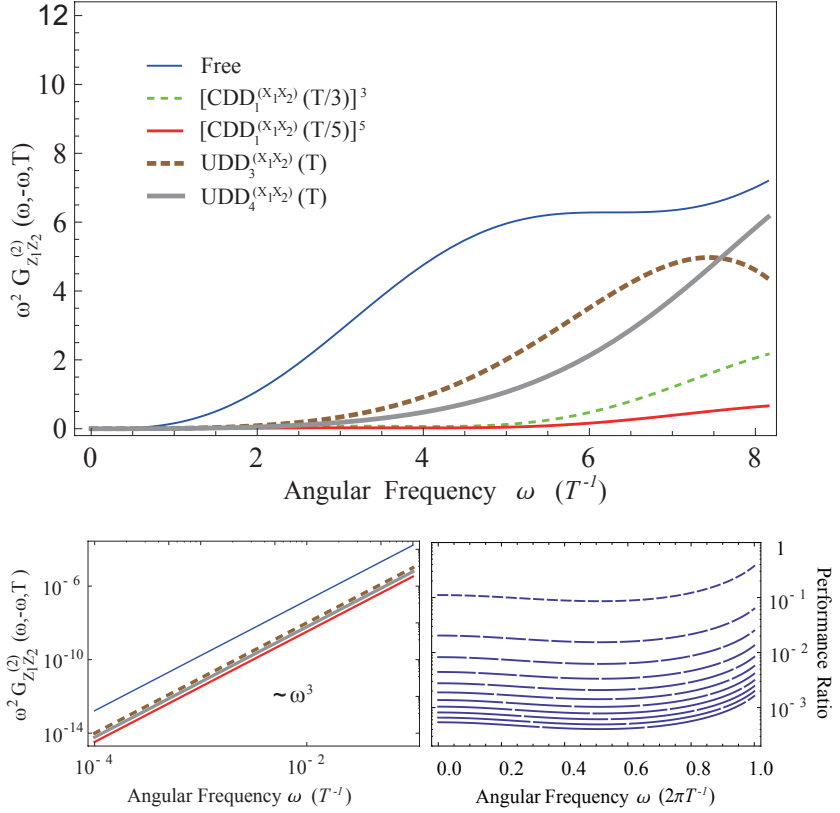


Figure 8.2: *Effect of non-selective DD sequences on two-qubit bath-induced phase evolution.* Top: FFs for sequences with comparable minimum interpulse separation,  $\tau$ :  $\tau \sim 0.14T$  for  $UDD_3^{(X_1 X_2)}(T)$  and  $[CDD_1^{(X_1 X_2)}(T/3)]^3$ , while  $\tau \sim 0.09T$  for  $UDD_4^{(X_1 X_2)}(T)$  and  $[CDD_1^{(X_1 X_2)}(T/5)]^5$ . In all cases the CO and FO are the same as for free evolution (lower left panel), but the value of the FF decreases as the number of pulses within a fixed time  $T$  grows. This is verified by studying  $M$  repetitions of  $CDD_1$  ( $2\tau_M = 2T/M$ ) within  $T$ . Lower right panel: Log-plot of the ratio  $|G_{Z_\ell, Z_{\ell'}}^{(2)}(\omega, -\omega, T = 2M\tau_M)|/|G_{Z_\ell, Z_{\ell'}}^{(2)}(\omega, -\omega, T = 2\tau_1)|$  for  $M = 3 + 4s'$  and  $s' \in [0, 10]$ . Plots with longer dashes correspond to larger values of  $M$  and exhibit smaller ratios, hence better suppression, of the bath-induced coupling.

Thus, while increasing  $M$  does not change the power law of  $\omega$  or  $T$ , a suppression effect still takes place, stemming from the increasing number of pulses within the storage time.

Assuming that no significant direct Ising couplings are present, simple non-selective control sequences may still offer adequate short-time suppression in practical scenarios, depending upon specific system and noise features. Given their inability to access high CO, however, the benefits of such sequences become increasingly limited as technological limitations prevent access to sufficiently short minimum switching times, making qubit-selective sequences essential to achieve high-fidelity control.

### 8.3.2 Selective two-qubit control sequences

When qubit-selective control is available, multi-qubit DD protocols with arbitrarily high CO may be devised, using the composition rule in equation (8.18). Both for clarity and relevance to near-term implementations, we first consider two-qubit systems, however, we will do so using

notation that may be easily adapted to the multi-qubit case (section 8.3.3). Let the DD sequences being composed have CO  $\alpha_1, \alpha_2$ , and require  $n(\alpha_1), n(\alpha_2)$  pulses. The composition guarantees a high CO,  $\alpha = \min\{\alpha_1, \alpha_2\}$ , hence all the generalized FFs are  $\mathcal{O}(T^{\alpha+1})$ . We seek strategies that achieve the same CO, but that also ensure high FO and require *less* than  $n_P^{\text{tot}} = n(\alpha_1)n(\alpha_2)$  pulses.

### Vanishing direct qubit-qubit coupling

Assume that no direct inter-qubit coupling is present, i.e.,  $d_{\ell,\ell'} = 0 = \eta_{\ell,\ell'}(t)$  for all  $t$  (hence, no contribution to decay due to  $\bar{\eta}'_{\ell,\ell}(T)$  in equation (8.35)). Similar to the non-selective protocols  $U_{\alpha}^{(X_{\ell} X_{\ell'})}$  considered above, one can see that simply executing the single-qubit sequences  $U_{\alpha_{\ell}}^{(X_{\ell})}(T)$  and  $U_{\alpha_{\ell'}}^{(X_{\ell'})}(T)$  *independently* on the two qubits achieves the desired power-law dependence for the local (one-body) terms but *not* for the induced (two-body) coupling terms: that is,  $G_{Z_{\ell}}^{(1)}(\omega, T) \sim \mathcal{O}(\omega^{\alpha} T^{\alpha+1})$ , whereas  $G_{Z_{\ell}, Z_{\ell'}}^{(2)}(\omega_1, \omega_2, T) \neq \mathcal{O}(m^{\alpha}(\vec{\omega}) T^{\alpha+1})$  in general. However, adding more structure to the control design can overcome the issue, yielding arbitrarily high FO and CO for all the generalized FFs relevant to the problem, as we show next.

• **Mirror anti-symmetry** – While, as remarked, the commutator spectrum  $S_{\ell,\ell'}^{B,-}(\omega_1, \omega_2)$  that enters the error integrals for two-body terms, equation (8.27), is in general complex, albeit anti-symmetric in the sense of equation (8.16), a simplified solution is possible if the noise is known to obey additional symmetry properties. Suppose that

$$S_{\ell,\ell'}^{B,-}(\omega) = -S_{\ell,\ell'}^{B,-}(-\omega), \quad \forall \omega, \quad (8.39)$$

and consider any DD protocol that satisfies the following *mirror anti-symmetry* condition (see also top panel in figure 8.3 for a pictorial illustration):

$$y_{\ell}(T/2 + t_1)y_{\ell'}(T/2 + t_2) = -y_{\ell}(T/2 - t_1)y_{\ell'}(T/2 - t_2), \quad \forall t_1, t_2 \in [0, T/2], \quad (8.40)$$

with *mirror symmetry*, corresponding to a reflection about  $t = T/2$ , being correspondingly described by a + sign in the right hand-side of equation (8.40). Then it is easy to verify that

$$\begin{aligned} & -2i \int_{-\infty}^{\infty} d\omega_1 \int_{-\infty}^{\infty} d\omega_2 G_{Z_{\ell}, Z_{\ell'}}^{(2)}(\omega_1, \omega_2, T) S_{\ell,\ell'}^{B,-}(\omega_1, \omega_2) \\ &= \int_{-\infty}^{\infty} d\omega \left[ \int_0^T dt_1 \int_0^{t_1} dt_2 y_{\ell}(t_1)y_{\ell'}(t_2) - \int_T^0 dt_2 \int_T^{t_2} dt_1 y_{\ell}(t_1)y_{\ell'}(t_2) \right] e^{i\omega(t_1-t_2)} S_{\ell,\ell'}^{B,-}(\omega) = 0. \end{aligned}$$

Thus, mirror anti-symmetry guarantees that no contribution to the propagator in equation (8.27) arises from the above integral. A simple recipe to generate a control protocol with the required anti-symmetry is to execute independent CDD or UDD sequences with CO  $\alpha_{\ell}$  and  $\alpha_{\ell'}$  obeying the ‘odd-parity condition’ that  $\alpha_{\ell} + \alpha_{\ell'}$  is odd. If so,  $y_{\ell}(t)$  has mirror symmetry,  $y_{\ell}(T/2 + t) = y_{\ell}(T/2 - t)$ , whereas  $y_{\ell'}(t)$ , has mirror anti-symmetry,  $y_{\ell'}(T/2 + t) = -y_{\ell'}(T/2 - t)$ , their product then obeying equation (8.40). Let us denote this type of independent sequence combination by  $U_{\alpha_{\ell}}^{X_{\ell}} \times U_{\alpha_{\ell'}}^{X_{\ell'}}(T)$ . The only contributing generalized FF,  $G_{Z_{\ell}}^{(1)}(\omega, T) \sim \mathcal{O}(\omega^{\alpha} T^{\alpha+1})$ , implies then that the sequence achieves CO = FO =  $\alpha = \min\{\alpha_{\ell}, \alpha_{\ell'}\}$  by using *only*  $n(\alpha_{\ell}) + n(\alpha_{\ell'})$  pulses, as opposed to the  $n(\alpha_{\ell})n(\alpha_{\ell'})$  for a sequence built via composition. For example, using the UDD sequences as building blocks, NUDD would require  $(\alpha_1 + 1)(\alpha_2 + 1)$  pulses, in contrast to  $(\alpha_1 + \alpha_2 + 2)$  pulses for mirror anti-symmetric DD.

The symmetry condition imposed on the noise spectra by equation (8.39) corresponds to requiring that  $g_k^{\ell} g_k^{\ell'*} \in \mathbb{R}$ . In view of equation (8.12), this in turn implies *real coupling strengths*,  $\text{Im}[g_k^{\ell}] = 0$  for all  $\ell$ , with collective dephasing as a special case. Interestingly, it had already been shown [192] that enhanced DD protocols obeying the above-mentioned odd-parity condition

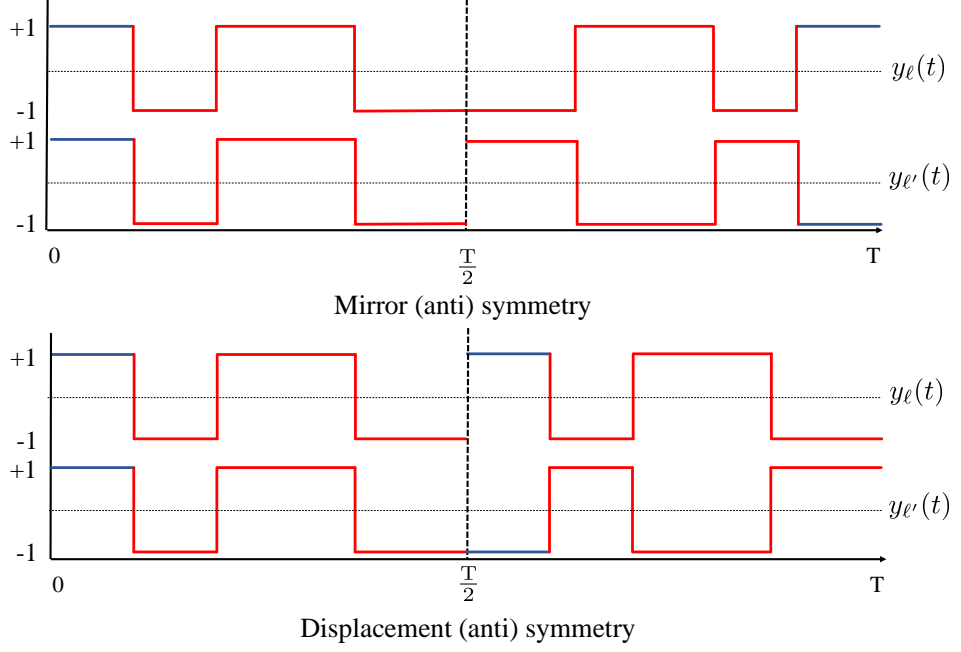


Figure 8.3: Mirror- (or displacement-) symmetric patterns (top row in each diagram) vs. mirror- (or displacement-) anti-symmetric pattern (bottom rows). Mirror symmetry [equation (8.40)] entails a reflection of the pattern with respect to  $T/2$ , whereas displacement symmetry [equation (8.41)] is achieved via a translation in  $[0, T/2]$ . Anti-symmetry requires an extra inversion operation – effectively multiplying the pattern by  $-1$ . The segment highlighted in blue is a visual aid.

guarantee high CO for two qubits exposed to collective spin-boson dephasing from a Gaussian (thermal) bath state. Beside shedding light on the underlying symmetry enabling this result, our analysis at the propagator level shows something stronger: as long as equation (8.39) is obeyed, mirror anti-symmetric sequences achieve arbitrary CO irrespective of the initial state  $\rho_B$ , hence including arbitrary *non-Gaussian* bath states.

**• Displacement anti-symmetry** – Since the environmental couplings may not be precisely characterized in realistic scenarios, or need not comply with equation (8.39), we proceed to design *model-robust* efficient high-order sequences without any further symmetry assumptions beyond those stemming from the bosonic algebra. Demanding a suitable symmetry on the control switching functions will still be crucial to achieve this goal. Building on the explicit form of the second-order fundamental FF relevant to the problem,  $F_{Z_\ell, Z_{\ell'}}^{(2)}(\omega_1, \omega_2, T)$  in equation (8.30), we propose the use of a *displacement anti-symmetry*, defined as follows (see also bottom panels in figure 8.3):

$$y_\ell(T/2 + t_1)y_{\ell'}(T/2 + t_2) = -y_\ell(t_1)y_{\ell'}(t_2), \quad \forall t_1, t_2 \in [0, T/2], \quad (8.41)$$

with displacement symmetry being instead associated with the + sign in the right hand-side of the above equation. Direct calculation shows that the second-order fundamental FF obeys

$$\begin{aligned} F_{Z_\ell, Z_{\ell'}}^{(2)}(\omega_1, \omega_2, T) &= - \left[ \int_0^{T/2} dt_1 \int_0^{t_1} dt_2 + \int_{T/2}^T dt_1 \int_0^{T/2} dt_2 + \int_{T/2}^T dt_1 \int_{T/2}^{t_1} dt_2 \right] y_\ell(t_1)y_{\ell'}(t_2)e^{i\vec{\omega}\cdot\vec{t}} \\ &= F_{Z_\ell, Z_{\ell'}}^{(2)}(\omega_1, \omega_2, T/2) - \int_0^{T/2} dt'_1 \int_0^{T/2} dt_2 y_\ell(T/2 + t'_1)y_{\ell'}(t_2)e^{i\vec{\omega}\cdot\vec{t}}e^{i\frac{\omega_1 T}{2}} \\ &\quad - \int_0^{T/2} dt'_1 \int_0^{t'_1} dt'_2 y_\ell(T/2 + t'_1)y_{\ell'}(T/2 + t'_2)e^{i\vec{\omega}\cdot\vec{t}}e^{i\frac{(\omega_1 + \omega_2)T}{2}}, \end{aligned}$$

where  $t'_j = t_j - T/2$  for  $j = 1, 2$ . Thus, the anti-symmetry requirement implies that

$$\begin{aligned} F_{Z_\ell, Z_{\ell'}}^{(2)}(\omega_1, \omega_2, T) &= (1 - e^{i\frac{(\omega_1 + \omega_2)T}{2}}) F_{Z_\ell, Z_{\ell'}}^{(2)}(\omega_1, \omega_2, T/2) - e^{i\frac{\omega_1 T}{2}} F_{Z_\ell}^{(1)}(\omega_1, T/2) F_{Z_{\ell'}}^{(1)}(\omega_2, T/2), \\ F_{Z_{\ell'}, Z_\ell}^{(2)}(\omega_2, \omega_1, T) &= (1 - e^{i\frac{(\omega_1 + \omega_2)T}{2}}) F_{Z_{\ell'}, Z_\ell}^{(2)}(\omega_2, \omega_1, T/2) + e^{i\frac{\omega_2 T}{2}} F_{Z_{\ell'}}^{(1)}(\omega_2, T/2) F_{Z_\ell}^{(1)}(\omega_1, T/2), \end{aligned}$$

with each fundamental FF appearing in an integral over  $(\omega_1, \omega_2)$  and being multiplied by  $S_{\ell, \ell'}^B(\omega_1, \omega_2) \propto \delta(\omega_1 + \omega_2)$ . Accordingly,  $1 - e^{i\frac{(\omega_1 - \omega_2)T}{2}} = 0$  and the first term in each of the above expressions never contributes. It follows that the relevant second-order generalized FF factorizes into a product of first-order fundamental FFs:

$$-iG_{Z_\ell, Z_{\ell'}}^{(2)}(\omega, -\omega, T) = -\cos(\omega T/2) F_{Z_\ell}^{(1)}(\omega, T/2) F_{Z_{\ell'}}^{(1)}(-\omega, T/2). \quad (8.42)$$

Let the two basic single-qubit DD sequences correspond to CO (FO) equal to  $\alpha_\ell (\Phi_\ell)$  and  $\alpha_{\ell'} (\Phi_{\ell'})$  in the intervals  $[0, T/2]$  and  $[T/2, T]$ , respectively. Equation (8.42) then implies that

$$G_{Z_\ell, Z_{\ell'}}^{(2)}(\omega, -\omega, T) \sim \mathcal{O}(\omega^{\Phi_\ell + \Phi_{\ell'}} T^{\alpha_\ell + \alpha_{\ell'} + 2}),$$

and thus the resulting two-qubit sequence achieves  $\text{CO} = \min\{\alpha_1, \alpha_2\}$  and  $\text{FO} = \min\{\Phi_1, \Phi_2\}$ , using *only*  $2[n(\alpha_1) + n(\alpha_2)]$  pulses. Notice that it is straightforward to build a control sequence possessing the required displacement anti-symmetry: given a DD sequence over an interval of duration  $T/2$ , say  $U_{\alpha_\ell}^{(X_\ell)} \times U_{\alpha_{\ell'}}^{(X_{\ell'})}(T/2)$  or  $U_\alpha^{(X_\ell X_{\ell'})}(T/2)$ , define

$$U_{\alpha_\ell, \alpha_{\ell'}}^{d, (X_\ell, X_{\ell'})(T)} \equiv X_\ell \left( U_{\alpha_\ell}^{(X_\ell)} \times U_{\alpha_{\ell'}}^{(X_{\ell'})}(T/2) \right) X_\ell^\dagger \left( U_{\alpha_\ell}^{(X_\ell)} \times U_{\alpha_{\ell'}}^{(X_{\ell'})}(T/2) \right), \quad (8.43)$$

$$U_\alpha^{d, (X_\ell X_{\ell'})(T)} \equiv X_\ell \left( U_\alpha^{(X_1 X_2)}(T/2) \right) X_\ell^\dagger \left( U_\alpha^{(X_1 X_2)}(T/2) \right), \quad (8.44)$$

where the conjugation of the second half of the sequence, over time  $[T/2, T]$ , by  $X_{\ell'}$  guarantees that  $y_\ell(T/2 + t_1) = -y_\ell(t_1)$  while  $y_{\ell'}(T/2 + t_2) = y_{\ell'}(t_2)$ , altogether ensuring that the product  $y_\ell(T/2 + t_1)y_{\ell'}(T/2 + t_2) = -y_\ell(t_1)y_{\ell'}(t_2)$  in agreement with equation (8.41).

While the relevant first- and second-order generalized FFs give us information on the worst-case filtering and cancellation capabilities that a DD protocol can ensure under minimal knowledge about the noise process, higher *effective* CO and FO can be achieved if additional assumptions hold [43]. Recall, in particular, the pure spin-boson stationary Gaussian noise model on two qubits discussed in the appendix. As remarked there,  $G_{Z_\ell}^{(1)}(\omega, T)$  never appears alone in the reduced dynamics and thus, assuming e.g. that qubit 1 corresponds to an anti-symmetric switching function, we have the *effective* generalized FFs

$$\begin{aligned} G_{Z_1}^{(1)}(\omega, T) G_{Z_1}^{(1)}(-\omega, T) &\sim \omega^{2(\alpha_1 + 1)} T^{2(\alpha_1 + 1) + 2}, \\ G_{Z_2}^{(1)}(\omega, T) G_{Z_2}^{(1)}(-\omega, T) &\sim \omega^{2\alpha_2} T^{2\alpha_2 + 2}, \\ G_{Z_1}^{(1)}(\omega, T) G_{Z_2}^{(1)}(-\omega, T) &\sim \omega^{(\alpha_1 + 1) + \alpha_2} T^{(\alpha_1 + 1) + \alpha_2 + 2}, \\ G_{Z_1, Z_2}^{(2)}(\omega, -\omega, T) &\sim \omega^{\alpha_1 + \alpha_2} T^{\alpha_1 + \alpha_2 + 2}. \end{aligned}$$

Thus, the extra symmetry associated with the zero-mean Gaussian nature of the initial bath state has effectively increased the CO and FO of the sequence. The above predicted power-law behaviors are demonstrated in figure 8.4.

- **Sequence comparison –** In order to gain quantitative insight, it is useful to compare the more efficient displacement-anti-symmetric DD sequences we have just built with other DD sequences applicable to our noise model. The term which is most relevant to such a comparison is the induced coupling term, since guaranteeing a high CO for this term is the whole point

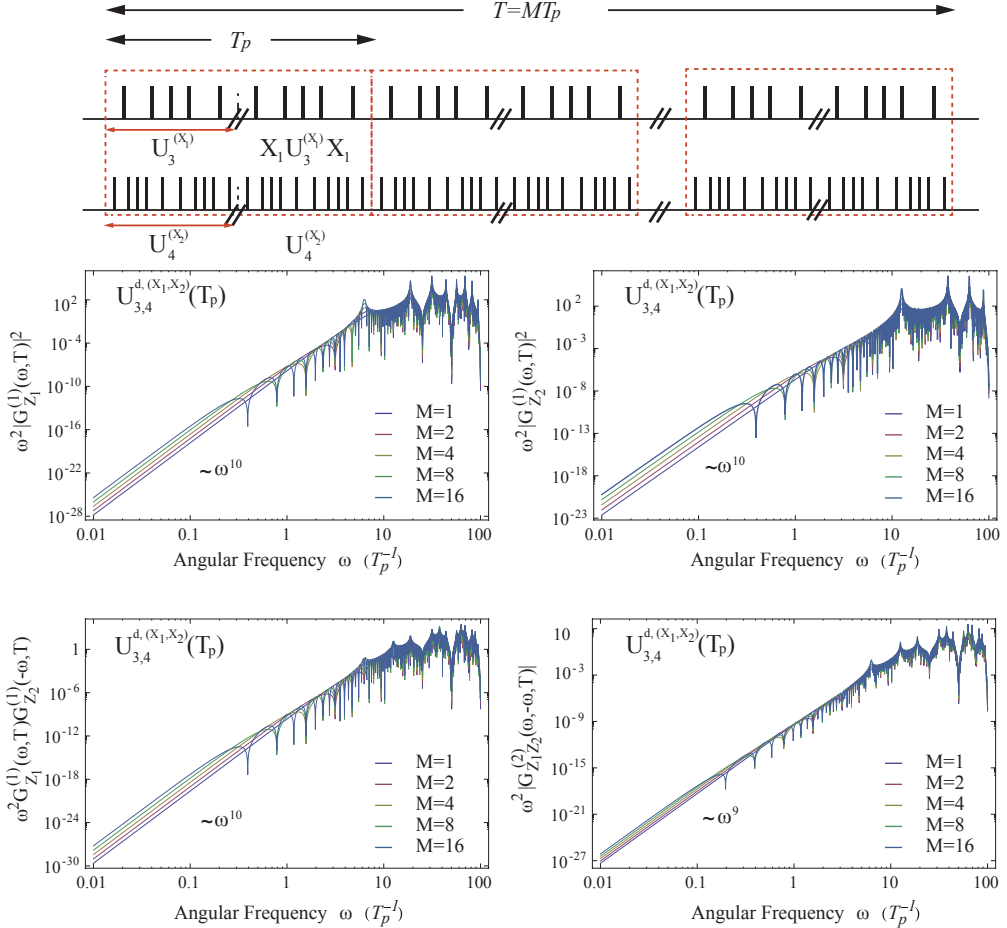


Figure 8.4: Top: Pulse structure for  $M$  repetitions of a  $U_{3,4}^{d,(X_1,X_2)}$  sequence with displacement anti-symmetry, equation (8.43), and CDD $_{\alpha_\ell}$ ,  $\alpha_1 = 3, \alpha_2 = 4$ , as building blocks. Bottom: Effective FFs entering the two-qubit reduced dynamics vs. frequency, for a different  $M$ .  $G_{Z_1,Z_2}^{(2)}(\omega, -\omega, T)$  is purely imaginary whenever displacement anti-symmetry is imposed, whereas  $G_{Z_1}^{(1)}(\omega, T)G_{Z_2}^{(1)}(-\omega, T)$  is purely real, due to the fact that  $\alpha^{(1)} + \alpha^{(2)} = 7$  is odd.

of introducing anti-symmetry or using the composition rule. Specifically, let us focus on the noise-induced phase evolution  $i\phi^0(T)$  over time  $T$ , namely, from equation (8.72),

$$2\pi i\phi^0(T) = -i \int_{-\infty}^{\infty} d\omega G_{Z_1,Z_2}^{(2)}(\omega, -\omega, T) S_{1,2}^{B,-}(\omega) \equiv -i \int_{-\infty}^{\infty} d\omega I(\omega, T) \quad (8.45)$$

evaluated for a sub-Ohmic noise spectrum  $S_{1,2}^{B,-}(\omega)$ , inspired by phenomenological treatments of nuclear-spin-induced dephasing in semiconductor quantum-dot qubits [76, 105]. For fixed total time  $T$  and minimum switching time  $\tau$ , we construct sequences with the highest possible CO  $\alpha$  within these constraints, using CDD as building blocks and incorporating mirror anti-symmetry, displacement anti-symmetry, or using nesting – see table 8.1 for a summary.

Representative results are shown in figure 8.5. While absolute values of the unwanted contribution  $I(\omega, T)$  are quoted in the in-line table, we plot a small power of the integrand,  $I(\omega, T)^{1/p}$ ,  $p = 15$ , rather than using a logarithmic scale as in figure 8.4, in order to better visualize the full range of values while avoiding issues associated to the negative values of  $I(\omega, T)$  at large frequencies. As one may see, guaranteeing a high FO (hence a high CO) for  $G_{Z_1,Z_2}^{(2)}(\omega, -\omega, T)$  is key to effectively suppressing phase evolution, with similar conclusions holding for any spectrum  $S_{1,2}^{B,-}(\omega)$  that is heavily weighted around  $\omega = 0$ . Because displacement-anti-symmetric

Free evolution	CO = 2, FO = 1	No DD applied
$\text{CDD}_{\alpha_1}^{(X_1)} \times \text{CDD}_{\alpha_2}^{(X_2)}(T)$	CO = 1, FO = 0	Mirror anti-symmetric DD, $\alpha_1 = 3, 5, \alpha_2 = 2, 4$
$\text{CDD}_\alpha^{(X_1 X_2)}(T)$	CO = 2, FO = 1	Non-selective CDD, $\alpha = 3, 5$
$\text{CDD}_{2,1}^{d,(X_1,X_2)}(T)$	CO = 5, FO = 4	Displacement anti-symmetric DD, $T = T_1$
$\text{CDD}_{4,4}^{d,(X_1,X_2)}(T)$	CO = 9, FO = 8	Displacement anti-symmetric DD, $T = T_2$
$\text{NCDD}_{2,1}^{(X_1,X_2)}(T)$	CO = 1, FO = 0	Nested CDD, $T = T_1$
$\text{NCDD}_{3,2}^{(X_1,X_2)}(T)$	CO = 5, FO = 4	Nested CDD, $T = T_2$
$\text{CDD}_{1,1}^{(X_1,X_2)}(T)$	CO = 2, FO = 1	Multi-qubit CDD, $T = T_1$
$\text{CDD}_{2,2}^{(X_1,X_2)}(T)$	CO = 3, FO = 2	Multi-qubit CDD, $T = T_2$

Table 8.1: *DD sequences applied in figure 8.5, along with the corresponding CO and FO for the second-order FF  $G_{Z_1, Z_2}^{(2)}(\omega, -\omega, T)$  relevant for noise-induced phase evolution.*

DD achieves the highest CO and FO for the induced coupling term, it outperforms all other strategies. Interestingly, two suppression mechanisms are evident: the first, stemming from the FO and CO, is manifest in the relative amplitudes of the oscillating functions, especially at low frequency; the second is the oscillatory character of the integrand itself, with positive and negative contributions partially canceling each other.

The absolute values of  $I(\omega, T)$  quoted in figure 8.5 further show the importance of the FO: amongst all sequences, displacement anti-symmetry-enhanced DD yields substantially better suppression. While one might naively expect such a difference in performance to originate solely from the difference in CO, it has already been shown that sequences with the same CO can have very different performance because their FO differs [43]. Here, we observe a related behavior. Since  $G^{(2)}(\omega, -\omega, T) \sim \mathcal{O}(\omega^{\Phi^{(2)}} T^{\alpha^{(2)}+1})$ , it follows from equation (8.32) that  $-\Phi^{(2)} + \alpha^{(2)} = 1$ . The sequence with the highest value of  $\Phi^{(2)}$  will thus also have the largest  $\alpha^{(2)}$ . Accordingly, a higher FO does not only imply better protection around  $\omega = 0$ , but indeed a higher protection in the sense of the power law in  $T$ . Also notice that when the FO/CO of a sequence are below those of free evolution, DD may become a liability, effectively increasing the unwanted noise effect; e.g., this is the case for both the nested CDD sequence and for the mirror anti-symmetric sequences for  $T = 8\mu\text{s}$ .

### Non-vanishing direct coupling

In the presence of a direct Ising coupling in the system Hamiltonian, i.e.,  $d_{\ell,\ell'} \neq 0 \neq \eta_{\ell\ell'}(t)$ , DD sequences applied independently to each qubit will not suppress such terms to arbitrary order. Using the displacement anti-symmetry-enhanced sequences described earlier and recalling equation (8.27), one finds that for the static direct coupling, proportional to  $d_{\ell,\ell'}$ , the relevant generalized FF  $G_{Z_\ell Z_{\ell'}}^{(1)}(\omega = 0, T) = 2 \int_0^T dt y_\ell(t) y_{\ell'}(t) = 0$ , as desired. However, for the FF corresponding to the time-dependent noise component, proportional to  $\eta_{\ell,\ell'}(t)$ , we find that, in general,

$$G_{Z_\ell Z_{\ell'}}^{(1)}(\omega, T) = 2 \int_0^T dt y_\ell(t) y_{\ell'}(t) e^{i\omega t} \neq \mathcal{O}((\omega T)^{\alpha_\ell + \alpha'_{\ell'} + 1}).$$

Thus, displacement anti-symmetry alone guarantees a high FO and CO *only in the presence of a static Ising coupling*. In such a case,  $U_{\alpha_\ell, \alpha'_{\ell'}}^{d,(X_\ell, X_{\ell'})}$  achieves  $\text{CO} = \text{FO} = \alpha = \min\{\alpha_\ell, \alpha'_{\ell'}\}$ .

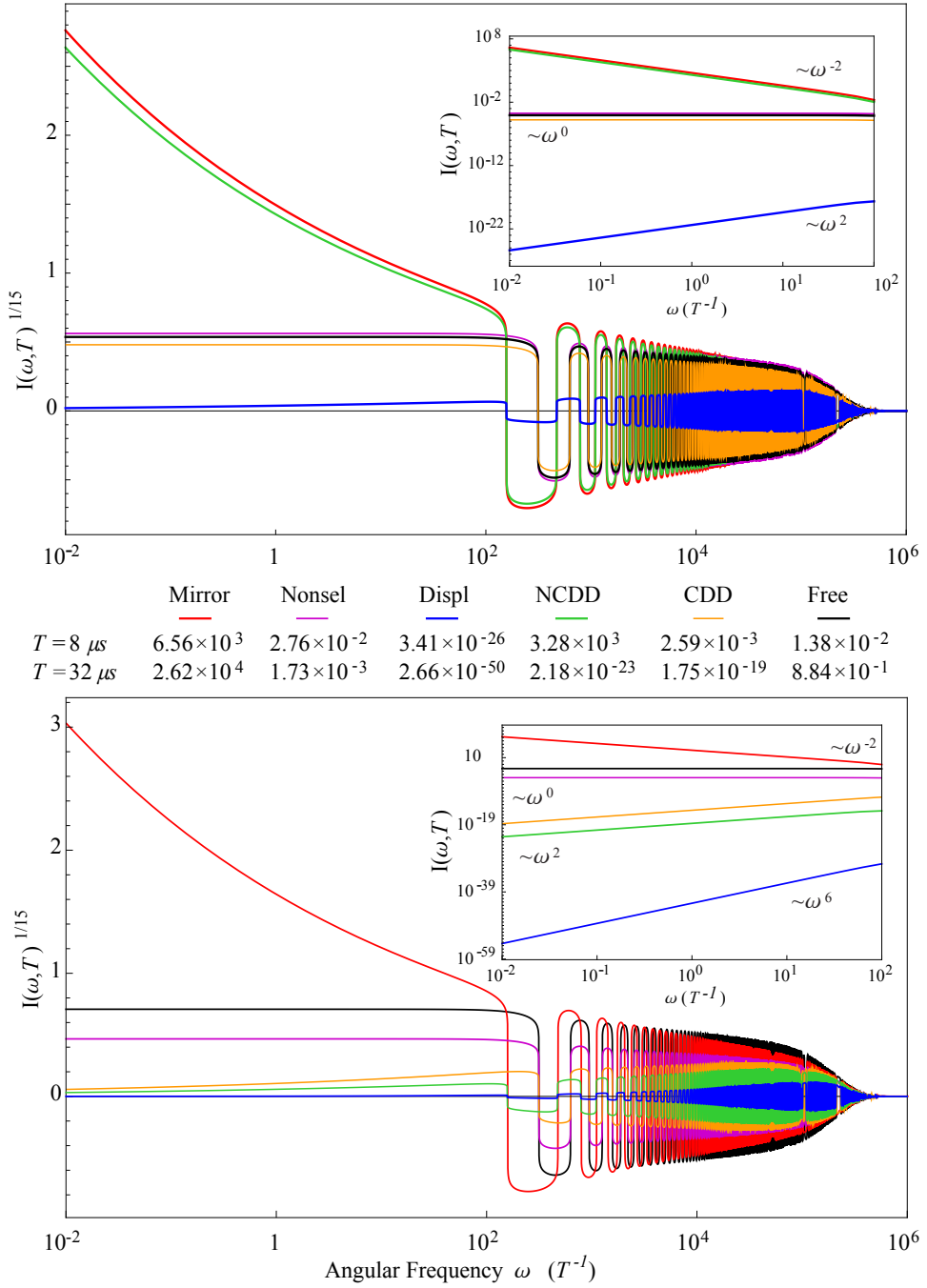


Figure 8.5: Comparison between different DD sequences capable of suppressing the induced coupling term vs. free evolution, for times  $T \equiv T_1 = 8\mu s$  (top) and  $T \equiv T_2 = 32\mu s$  (bottom), at same minimum switching time  $\tau = 1\mu s$ . A sub-Ohmic spectrum with Gaussian cutoff is used,  $S_{1,2}^{B,-}(\omega) \simeq e^{i\omega t_{1,2}} g(\omega/\omega_c)^{-2} e^{-\omega^2/\omega_c^2}$ , with  $g/\omega_c = 0.2078$ ,  $\omega_c = 2\pi 10^4 Hz$ , and  $t_{1,2} = 10^{-2} s$ . The main panels show  $I(\omega, T)^{1/15}$  [equation (8.45)]; insets are in log scale to facilitate the visualization of power-law behavior. The in-line table lists the value of  $|\int d\omega I(\omega, T)| = 2\pi\phi^0(T)$  for the corresponding sequence. Specifically, we compare (see also table 8.1):  $CDD_3^{(X_1)} \times CDD_2^{(X_2)}(T)$ ,  $CDD_3^{(X_1)} \times CDD_3^{(X_2)}(T)$ ,  $CDD_{2,1}^{d,(X_1, X_2)}(T)$ ,  $NCDD_{2,1}^{(X_1, X_2)}(T)$ , and  $\mathring{CDD}_{1,1}^{(X_1, X_2)}(T)$  for  $T = T_1$ ; and  $CDD_5^{(X_1)} \times CDD_4^{(X_2)}(T)$ ,  $CDD_5^{(X_1)} \times CDD_5^{(X_2)}(T)$ ,  $CDD_{4,4}^{d,(X_1, X_2)}(T)$ ,  $NCDD_{3,2}^{(X_1, X_2)}(T)$ , and  $\mathring{CDD}_{2,2}^{(X_1, X_2)}(T)$  for  $T \equiv T_2$ .

If a time-dependent noisy coupling is present, it is necessary to resort to nested two-qubit DD sequences built via composition, i.e.,  $\mathring{U}_{(\alpha_\ell, \alpha_{\ell'})}^{(\vec{X})}(T)$  or  $\mathring{U}'_{(\alpha, \alpha)}^{(\vec{X})}(T)$ . These sequences, which include NUDD and multi-qubit CDD, are the only known protocols capable of achieving arbitrary CO  $\alpha$ . However, their FO need not be maximum: direct calculation of  $G_{Z_\ell, Z_{\ell'}}^{(2)}(\omega, -\omega, T)$ , combined with dimensional analysis, shows that indeed  $\Phi = \alpha$  for  $\mathring{\text{CDD}}_{(\alpha, \alpha)}^{(\vec{X})}(T)$ , but  $\mathring{\text{NUDD}}_{(\alpha_\ell, \alpha_{\ell'})}^{(\vec{X})}(T)$  only achieves  $\Phi = \alpha - 1$  in general. As before, by further imposing a displacement anti-symmetry on NUDD, the FO can be maximized to  $\Phi = \alpha$ .

### 8.3.3 Selective multi-qubit control sequences

#### General construction

The above results may be extended beyond the  $N = 2$  qubit scenario. Doing so requires generalizing displacement anti-symmetry to multiple qubits. Since satisfying the requirement of pairwise displacement anti-symmetry, equation (8.41), for all pairs simultaneously is clearly impossible, we seek a control structure capable of satisfying an analogue to displacement anti-symmetry *at different timescales*. We start by subdividing the total evolution time  $T$  in  $2^{N-1}$  segments of length  $\tau_0$ , i.e.,  $T = 2^{N-1}\tau_0$ . One can then demand that for every  $\ell$  and  $\tau_s = 2^s\tau_0$ ,  $s = 0, \dots, N-2$ , and  $t \in [0, \tau_s]$ ,

$$y_\ell(T/2 - m\tau_s + t) = (-1)^{P^{(N)}(\ell, s)} y_\ell(T/2 + (m-1)\tau_s + t), \quad 1 \leq m \leq 2^{N-s-2},$$

where  $P^{(N)}(\ell, s)$  are the entries of a  $N \times (N-1)$  binary matrix. In this notation, the  $N = 2$  qubit displacement anti-symmetry is simply represented by  $P^{(2)} = \begin{pmatrix} 0 \\ 1 \end{pmatrix}$ , which yields

$$y_1(t) = (+1)y_1(T/2 + t), \quad y_2(t) = (-1)y_2(T/2 + t).$$

We can generalize to multiple qubits via an appropriate matrix

$$P^{(N)}(\ell, s) = \begin{pmatrix} 0 & 0 & 0 & \cdots & 0 \\ 1 & 0 & 0 & \cdots & 0 \\ 0 & 1 & 0 & \cdots & 0 \\ \vdots & & & & \\ 0 & 0 & \cdots & 0 & 1 \end{pmatrix}. \quad (8.46)$$

In this way, for every pair  $\ell, \ell'$  there exists an  $s$  such that, when  $t_1$  and  $t_2$  are in an interval  $[T/2 - m\tau_s, T/2 - (m-1)\tau_s]$ ,

$$\begin{aligned} y_\ell(t_1)y_{\ell'}(t_2) &= (-1)^{P^{(N)}(\ell, s) + P^{(N)}(\ell', s)} y_\ell((2m-1)\tau_s + t_1)y_{\ell'}((2m-1)\tau_s + t_2) \\ &= (-1)^{P^{(N)}(\ell, s)} y_\ell((2m-1)\tau_s + t_1)y_{\ell'}((2m-1)\tau_s + t_2), \end{aligned} \quad (8.47)$$

for all  $1 \leq m \leq 2^{N-s-2}$ , resulting in what we call *generalized displacement anti-symmetry*.

The next step is to give a systematic procedure to build  $N$ -qubit DD sequences that incorporate the above symmetry constraint. We do so by introducing an auxiliary  $N \times 2^{N-1}$  matrix  $Q^{(N)}$  associated to  $P^{(N)}$ , with the  $\ell$ -th row,  $Q_\ell$ , defined as follows. Let the  $2^{N-2}$  entry of the row  $Q_\ell$ ,  $[Q_\ell]_{2^{N-2}}$ , be set to 0. First,  $[Q_\ell]_{2^{N-2}+1}$  is chosen such that  $[Q_\ell]_{2^{N-2}} = [Q_\ell]_{2^{N-2}+1} \oplus P(\ell, 1)$ , where  $\oplus$  denotes addition modulo two. Next,  $[Q_\ell]_{2^{N-2}-1}$  and  $[Q_\ell]_{2^{N-2}+2}$  are chosen such that  $\{[Q_\ell]_{2^{N-2}-1}, [Q_\ell]_{2^{N-2}}\} = \{[Q_\ell]_{2^{N-2}-1} \oplus P(\ell, 2), [Q_\ell]_{2^{N-2}} \oplus P(\ell, 2)\}$ . We then proceed recursively: given  $\{[Q_\ell]_{2^{N-2}-(2^{y-1}-1)}, \dots, [Q_\ell]_{2^{N-2}+2^{y-1}}\}$ , we may build a *unique* string  $\{[Q_\ell]_{2^{N-2}-(2^y-1)} \dots [Q_\ell]_{2^{N-2}}, [Q_\ell]_{2^{N-2}+1}, \dots, [Q_\ell]_{2^{N-2}+2^y}\}$  such that

$$\{[Q_\ell]_{2^{N-2}-(2^y-1)}, \dots, [Q_\ell]_{2^{N-2}}\} = \{[Q_\ell]_{2^{N-2}} \oplus P(\ell, y), \dots, [Q_\ell]_{2^{N-2}+2^y} \oplus P(\ell, y)\}.$$

The resulting matrix  $Q^{(N)}$  gives us a way to build-in the symmetries and anti-symmetries of the switching functions  $y_\ell(t)$  at different timescales; e.g., in the two qubit case described earlier,

$$Q^{(2)} = \left( \begin{array}{c|c} 0 & 0 \\ 0 & 1 \end{array} \right).$$

Given a base DD sequence on an interval  $T_0 \equiv T/2$ , say  $U_{\alpha_\ell}^{(X_\ell)} \times U_{\alpha_{\ell'}}^{(X_{\ell'})}(T/2)$ , the displacement anti-symmetry-enhanced version is then given by

$$\left( X_1^{Q_{1,1}} X_2^{Q_{2,1}} U_{\alpha_\ell}^{(X_\ell)} \times U_{\alpha_{\ell'}}^{(X_{\ell'})}(T/2) X_1^{Q_{1,1}} X_2^{Q_{2,1}} \right) \left( X_1^{Q_{1,2}} X_2^{Q_{2,2}} U_{\alpha_\ell}^{(X_\ell)} \times U_{\alpha_{\ell'}}^{(X_{\ell'})}(T/2) X_1^{Q_{1,2}} X_2^{Q_{2,2}} \right),$$

in agreement with our construction in equation (8.43). For  $N$  qubits, the generalized-displacement anti-symmetry-enhanced sequence  $U_{\vec{\alpha}}^{d,(\vec{X})}(T) \equiv U_{\alpha_1, \dots, \alpha_N}^{d,(X_1, \dots, X_N)}(T = 2^{N-1}T_0)$  of a base DD sequence  $U_{\vec{\alpha}}^{(\vec{X})}(T_0)$  is similarly given by

$$U_{\vec{\alpha}}^{d,(\vec{X})}(T = 2^{N-1}T_0) = \prod_{s=1}^{2^{N-1}} \left( \otimes_{\ell=1}^N X_\ell^{Q(\ell,s)} \right) U_{\vec{\alpha}}^{t,(\vec{X})}(T_0) \left( \otimes_{\ell=1}^N X_\ell^{Q(\ell,s)} \right)^\dagger. \quad (8.48)$$

It remains to show that the above construction achieves in general the desired arbitrary-order noise suppression, similar to the two-qubit case. Our strategy is to first show the result for a *fixed* pair of qubits for which generalized displacement anti-symmetry at scale  $\tau_s$  holds, in the sense of equation (8.42), and then generalize the argument by noticing that, by construction, equation (8.47) is satisfied for at least one  $s$  for every  $\ell, \ell'$  pair. Given pair  $(\ell, \ell')$ , one then has

$$\begin{aligned} -F_{Z_\ell, Z_{\ell'}}^{(2)}(\omega_1, \omega_2, T) &= \sum_{q=0}^{2^{N-s-1}-1} \int_{q\tau_s}^{(q+1)\tau_s} dt_1 \int_{q\tau_s}^{t_1} dt_2 y_\ell(t_1) y_{\ell'}(t_2) e^{i\vec{\omega} \cdot \vec{t}} \\ &\quad + \sum_{q>r=0}^{2^{N-s-1}-1} \int_{q\tau_s}^{(q+1)\tau_s} dt_1 \int_{r\tau_s}^{(r+1)\tau_s} dt_2 y_\ell(t_1) y_{\ell'}(t_2) e^{i\vec{\omega} \cdot \vec{t}} \\ &= \sum_{q=0}^{2^{N-s-2}-1} \int_0^{\tau_s} dt_1 \int_0^{t_1} dt_2 \left( e^{iq(\omega_1+\omega_2)\tau_s} y_\ell(q\tau_s + t_1) y_{\ell'}(q\tau_s + t_2) e^{i\vec{\omega} \cdot \vec{t}} \right. \\ &\quad \left. + e^{i(2q-1)(\omega_1+\omega_2)\tau_s} y_\ell((2q-1)\tau_s + t_1) y_{\ell'}((2q-1)\tau_s + t_2) e^{i\vec{\omega} \cdot \vec{t}} \right) \\ &\quad + \sum_{q>r=0}^{2^{N-s-1}-1} \int_{q\tau_s}^{(q+1)\tau_s} dt_1 \int_{r\tau_s}^{(r+1)\tau_s} dt_2 y_\ell(t_1) y_{\ell'}(t_2) e^{i\vec{\omega} \cdot \vec{t}}. \end{aligned}$$

Each integral in the second summation is just a time-translated version of  $F^{(1)}(\omega_1, \tau_s) F^{(1)}(\omega_2, \tau_s)$ , while the first summation can be simplified by invoking displacement anti-symmetry:

$$\begin{aligned} &\sum_{q=0}^{2^{N-s-2}-1} \left( e^{iq(\omega_1+\omega_2)\tau_s} \int_0^{\tau_s} dt_1 \int_0^{t_1} dt_2 y_\ell(q\tau_s + t_1) y_{\ell'}(q\tau_s + t_2) e^{i\vec{\omega} \cdot \vec{t}} \right. \\ &\quad \left. + e^{i(2q-1)(\omega_1+\omega_2)\tau_s} \int_0^{\tau_s} dt_1 \int_0^{t_1} dt_2 y_\ell((2q-1)\tau_s + t_1) y_{\ell'}((2q-1)\tau_s + t_2) e^{i\vec{\omega} \cdot \vec{t}} \right) = \\ &\sum_{q=0}^{2^{N-s-2}-1} (e^{iq(\omega_1+\omega_2)\tau_s} - e^{i(2q-1)(\omega_1+\omega_2)\tau_s}) \int_0^{\tau_s} dt_1 \int_0^{t_1} dt_2 y_\ell(q\tau_s + t_1) y_{\ell'}(q\tau_s + t_2) e^{i\vec{\omega} \cdot \vec{t}}, \end{aligned}$$

which vanishes when  $\omega_1 + \omega_2 = 0$ , as relevant to stationary noise. Accordingly, in the absence of a time-dependent direct Ising coupling, generalized displacement-antisymmetry-enhanced DD achieves CO and FO equal to  $\alpha = \min\{\alpha_\ell\}$ , as desired.

## Example and resource scaling

We illustrate the above general construction in the simplest non-trivial multi-qubit setting,  $N = 3$ , in which case we have

$$P^{(3)}(\ell, s) = \begin{pmatrix} 0 & 0 \\ 1 & 0 \\ 0 & 1 \end{pmatrix}, \quad Q^{(3)} = \begin{pmatrix} 0 & 0 & 0 & 0 \\ 1 & 0 & 1 & 0 \\ 1 & 0 & 0 & 1 \end{pmatrix}.$$

Explicitly, the following set of symmetries are enforced by  $P^{(3)}$ : at time scales  $\tau_0$ , for  $t \in [T/2 - m\tau_0, T/2 - (m-1)\tau_0]$ , we have

$$\begin{aligned} y_1(t) &= (+1) y_1((2m-1)\tau_0 + t), \\ y_2(t) &= (-1) y_2((2m-1)\tau_0 + t), \\ y_3(t) &= (+1) y_3((2m-1)\tau_0 + t), \end{aligned}$$

for  $m = 1, 2$ , while at time scale  $\tau_1 = 2\tau_0$ ,  $t \in [T/2 - m\tau_1, T/2 - (m-1)\tau_1]$ , we have

$$\begin{aligned} y_1(t) &= (+1) y_1(\tau_1 + t), \\ y_2(t) &= (+1) y_2(\tau_1 + t), \\ y_3(t) &= (-1) y_3(\tau_1 + t), \end{aligned}$$

for  $m = 1$ . Starting from  $y_3(t)$ , for instance, and with  $\tau_0 = T/4$ , these conditions require

$$\begin{aligned} y_3(t) &= (+1) y_3(T/4 + t), \quad t \in [T/4, T/2], \\ y_3(t) &= (+1) y_3(3T/4 + t), \quad t \in [0, T/4] \\ y_3(t) &= (-1) y_3(T/2 + t), \quad t \in [0, T/2], \end{aligned}$$

which may be simultaneously obeyed by the pattern

$$y_3(t) = -y_3(T/4 + t) = -y_3(T/2 + t) = y_3(3T/4 + t), \quad t \in [0, T/4],$$

see figure 8.6. With  $T_0 = T/4$ , we may then build an enhanced DD sequence using equation (8.48) and the (independent) base sequence  $U_{\vec{\alpha}}^{(\vec{X})}(T/4) = U_{\alpha_1}^{(X_1)} \times U_{\alpha_2}^{(X_2)} \times U_{\alpha_3}^{(X_3)}(T/4)$ . Explicitly:

$$U_{\vec{\alpha}}^{d,(\vec{X})}(T) = X_3 X_2 U_{\vec{\alpha}}^{(\vec{X})}(T/4) X_3 X_2 U_{\vec{\alpha}}^{(\vec{X})}(T/4) X_2 U_{\vec{\alpha}}^{(\vec{X})}(T/4) X_2 X_3 U_{\vec{\alpha}}^{(\vec{X})}(T/4) X_3.$$

As in section 8.2.2, let  $n(\alpha_\ell) \geq n(\alpha)$  denote the number of pulses in a single-qubit DD sequence achieving CO  $\alpha_\ell$ , with  $n_P^{\text{tot}}(N) = \prod_{\ell=1}^N n(\alpha_\ell) \geq [n(\alpha)]^N$  for multi-qubit CDD or NUDD. For a sequence that incorporates generalized displacement anti-symmetry, the required number of pulses grows instead as  $n_P^{d,\text{tot}}(N) = 2^{N-1} \sum_{\ell=1}^N n(\alpha_\ell) \geq 2^{N-1} N n(\alpha)$ . While this is still exponential in  $N$ , it may translate into a significant resource reduction:

$$\frac{n_P^{d,\text{tot}}(N)}{n_P^{\text{tot}}(N)} \geq \frac{N 2^{N-1} n(\alpha)}{[n(\alpha)]^N} = \frac{N}{[n(\alpha)/2]^{N-1}},$$

which represents an *exponential reduction* in the required pulse number whenever  $\alpha > 1$ .

Beside affording a smaller total pulse number, the presence of displacement anti-symmetry also implies less stringent requirements on the minimum switching time of the corresponding protocols. For instance, the minimum switching time for a multi-qubit NUDD sequence

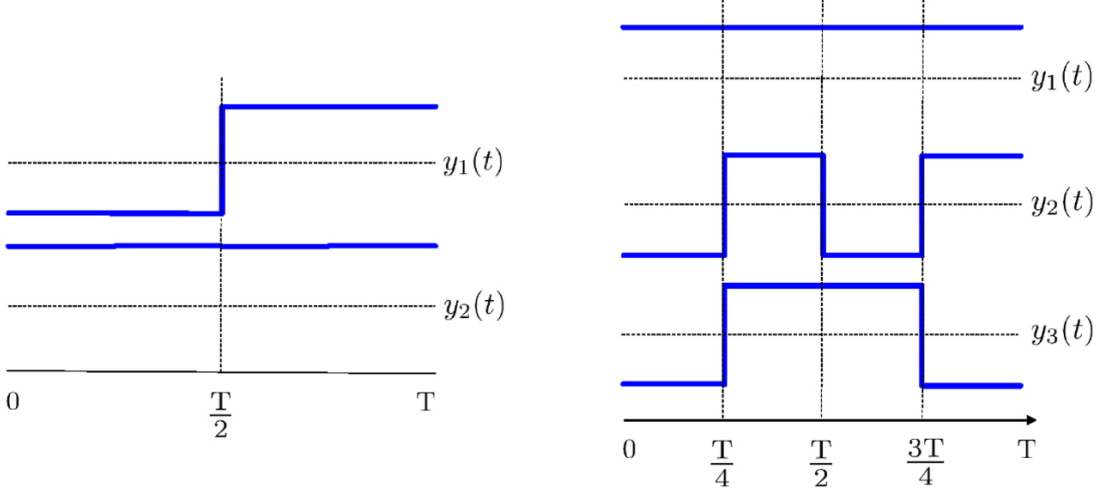


Figure 8.6: Schematic representation of the sign pattern induced in each of the  $y_\ell(t)$  by the displacement anti-symmetry for two (left panel) vs three (right panel) qubits. For example, for  $N = 3$ :  $y_3(t) = -y_3(T/4 + t) = -y_3(T/2 + t) = y_3(3T/4 + t)$ ,  $t \in [0, T/4]$ .

achieving minimum CO  $\alpha$  scales as  $\tau_\alpha^N \sim (1/\alpha^2)^N$ , whereas an enhanced  $\text{UDD}_\alpha^{d,(X_1 \dots X_N)}$  sequence built out of equation (8.48) has minimum switching time scaling as  $\tau_\alpha^N = \tau_\alpha/2^{N-1} \sim (1/\alpha^2)^N (\alpha^2/2)^{N-1}$ ; that is, our sequences also have an *exponentially larger minimum switching time*, making them potentially more amenable to experimental implementation in multi-qubit systems.

As in the two-qubit case, the above advantages in terms of pulse number and timing constraints are meaningful only so long as an arbitrarily high CO/FO is achievable, which in our noise model is possible only when no fluctuating direct coupling is present. Even if the latter is non-zero, however, it is beneficial to incorporate displacement anti-symmetry in NUDD or  $\overset{\circ}{U}'_{\alpha, \dots, \alpha}^{(X_1, \dots, X_N)}$  sequences which can achieve arbitrary CO: by doing so, the enhanced sequences  $\overset{\circ}{U}_{\alpha_1, \dots, \alpha_N}^{d,(X_1, \dots, X_N)}$  and  $\overset{\circ}{U}'_{\alpha, \dots, \alpha}^{d,(X_1, \dots, X_N)}$  achieve *both* CO and FO equal to  $\alpha$  for the most general version of the noise model under consideration. It is also worth noting that, out of the multi-qubit sequences described in section 8.2.2, the multi-qubit  $\overset{\circ}{\text{CDD}}'_{(\alpha, \dots, \alpha)}^{(X_1, \dots, X_2)}(T_\alpha)$  already has a form of displacement anti-symmetry built in. This is easily seen by noticing that  $\overset{\circ}{\text{CDD}}'_{(\alpha, \dots, \alpha)}^{(X_1, \dots, X_2)}(T_\alpha)$  may be thought of as the result of imposing anti-symmetry on a sequence  $\overset{\circ}{\text{CDD}}'_{(\alpha-1, \dots, \alpha-1)}^{(X_1, \dots, X_2)}(T_{\alpha-1})$  using an ‘enlarged’  $P^{(N)}$  matrix, with  $N \times N$  entries, given by

$$\tilde{P}^{(N)} = \begin{pmatrix} 1 & \dots & 1 & 1 & 1 \\ 1 & \dots & 1 & 1 & 0 \\ 1 & \dots & 1 & 0 & 0 \\ & & \dots & & \\ 1 & \dots & 0 & 0 & 0 \end{pmatrix}.$$

The concatenated structure results in the ‘enlarged’ displacement anti-symmetry and guarantees FO  $\Phi = \alpha$  using  $n_P^{\text{tot}} = 2^{2N(\alpha+1)}$  pulses. While the latter is exponentially larger than for  $U_\alpha^{d,(X_1 \dots X_2)}$  sequences (which use  $2^{N-1} N n(\alpha)$  pulses), multi-qubit CDD is capable of suppressing an arbitrary (direct and induced) coupling term. As we shall see next, displacement anti-symmetry is also the key to establishing our results for long-term storage of multiple qubits, hence our results will apply in particular to  $\overset{\circ}{\text{CDD}}'_{(\alpha, \dots, \alpha)}^{(X_1, \dots, X_2)}(T)$  sequences.

## 8.4 Dynamical decoupling vs. multi-qubit dephasing noise: long-time storage

If the promised benefits of QIP are to be fully realized, techniques that enable high-fidelity preservation of arbitrary quantum states for *extended time periods* (i.e., periods longer than those over which DD protocols have been traditionally designed to be effective) must be available. For example, in a quantum computer it may be necessary to store information at error rates well below the threshold value in idle qubits, while additional processing tasks are carried out in parallel on other qubits. Furthermore, in order minimize negative effects on total processing time, this stored information should, ideally, be accessible ‘on-demand’. For these reasons, we now turn attention to the problem of high-fidelity long-time storage of information, under realistic timing and access-latency constraints. That is, we are not solely interested in protecting an arbitrary multi-qubit state for a fixed (potentially arbitrarily long) storage time  $T$ , but also in being able to retrieve it on demand, with guaranteed high fidelity and sufficiently small access latency.

This problem was studied for a single-qubit exposed to Gaussian dephasing noise in [105], where a systematic approach to meet the above requirements was proposed, based on periodic repetition of a high-order DD ‘base’ sequence  $U_\alpha^{(X_1)}(T_p)$  – resulting in total storage time  $T = MT_p$  and access latency capped at  $T_p \ll T$ . Provided that the relevant noise spectrum decays to zero sufficiently rapidly at high frequency (ideally, with a ‘hard cutoff’ of the form  $S(\omega) \propto \omega^s \Theta(\omega - \omega_c)$ ), the key observation is that the long-time limiting value of the qubit coherence need not be zero; rather, coherence (hence fidelity) may be made to ‘plateau’ at a controllable limiting value by appropriately choosing the base DD sequence, so that the following conditions are obeyed:

$$\omega_c T_p < 2\pi, \quad s + 2\alpha > 1. \quad (8.49)$$

Qualitatively speaking, the first of these conditions ensures that no substantial high-frequency noise is present, above  $\omega_c = 2\pi/T_p$ , that would otherwise be amplified by the sharp ‘resonance peaks’ appearing in the relevant FF as a consequence of the periodic repetition. The second removes any singularity at zero frequency, thus curtailing the damaging effects of low-frequency noise in the long-time limit.

Here, we show how this result can be extended beyond the single-qubit Gaussian scenario, by identifying conditions that ensure, in principle, a *fidelity plateau* for stationary multi-qubit dephasing from classical and/or spin-boson (Gaussian and non-Gaussian) noise sources. The starting point is to recall that the expression for the system’s reduced dynamics, equation (8.34), does not make any special assumption on the statistical properties of the noise beyond those imposed by stationarity and the spin-boson algebra, along with the standard initial system-bath factorization. Thus, we may separately analyze each of the factors in equation (8.34) in order to derive plateau conditions for classical and quantum noise sources independently.

### 8.4.1 Fidelity plateau conditions for multi-qubit classical stationary dephasing

Let us first derive the conditions that must be satisfied in order to engineer a fidelity plateau in a multi-qubit system, subject to classical noise contributions only (as a reminder, these contributions are described by the fluctuations of single-qubit and two-qubit energies,  $\zeta'_\ell(t)$  and  $\eta'_{\ell,\ell'}(t)$ ). Specifically, we would like to show that when the control protocol consists of  $M$  repetitions of a base DD sequence with duration  $T_p$ , all classical contributions to the decay  $e^{-Z_{a,b}(T)}$ , namely,

the contributions given by

$$\langle e^{\sum_{\ell, \ell'} \Delta[a_\ell + a_{\ell'}, b_\ell + b_{\ell'}] \bar{\eta}'_{\ell, \ell'}(T)} \times e^{\sum_{\ell} \Delta[a_\ell, b_\ell] \bar{\zeta}'_\ell(T)} \rangle_c,$$

may be made to approach a *constant nonzero* value in the large- $M$  limit (formally, as  $M \rightarrow \infty$ ). Equivalently, we require that the *arguments* of these exponential terms not diverge as the number of sequence repetitions becomes large. From the cumulant expansion in equation (8.38), one sees that it suffices to show that each  $k$ -th order cumulant

$$C^{(k)}(\bar{\zeta}'_{\ell_1}(T) \cdots \bar{\zeta}'_{\ell_j}(T), \bar{\eta}'_{p_{j+1}}(T) \cdots \bar{\eta}'_{p_k}(T))_c \quad (8.50)$$

approaches a finite constant value in such a limit, for every  $j = 0, \dots, k$ . We do this by recalling that the effect of a base DD sequence on the classical noise contributions (and, therefore, on the corresponding cumulants) is captured entirely by the filter functions  $G_{Z_\ell}^{(1)}(\omega_\ell, T_p)$  and  $G_{Z_\ell Z_{\ell'}}^{(1)}(\omega_{\ell, \ell'}, T_p)$ , and noting that these first-order FFs obey a simple composition rule under repetition [105]:

$$G_{Z_\ell}^{(1)}(\omega_\ell, T = MT_p) = \frac{1 - e^{iM\omega_\ell T_p}}{1 - e^{i\omega_\ell T_p}} G_{Z_\ell}^{(1)}(\omega_\ell, T_p),$$

and similarly for  $G_{Z_\ell Z_{\ell'}}^{(1)}(\omega_{\ell, \ell'}, T = MT_p)$ . Defining the index vector

$$\vec{L}_{[k]} = \{L_r\} \equiv (\ell_1, \dots, \ell_j, p_{j+1}, \dots, p_k)$$

as a  $k$ -component vector with entries  $L_r$ , direct calculation yields:

$$\begin{aligned} & C^{(k)}(\bar{\zeta}_{\ell_1}(T) \cdots \bar{\zeta}_{\ell_j}(T), \bar{\eta}_{p_{j+1}}(T) \cdots \bar{\eta}_{p_k}(T))_c \\ &= \int_{-\infty}^{\infty} \frac{d\vec{\omega}_{[k-1]}}{(2\pi)^{k-1}} \left( \prod_{r=1}^{k-1} \frac{\sin(M\omega_{L_r} T_p/2)}{\sin(\omega_{L_r} T_p/2)} \right) G_{Z_{\ell_1}}^{(1)}(\omega_{L_1}, T_p) \cdots G_{Z_{\ell_{k-1}} Z_{\ell'_{k-1}}}^{(1)}(\omega_{L_{k-1}}, T_p) \end{aligned} \quad (8.51)$$

$$\times G_{Z_{\ell_k} Z_{\ell'_k}}^{(1)} \left( - \sum_{r=1}^{k-1} \omega_{L_r}, T_p \right) \frac{\sin \left( M \left( \sum_{r=1}^{k-1} \omega_{L_r} \right) \frac{T_p}{2} \right)}{\sin \left( \left( \sum_{r=1}^{k-1} \omega_{L_r} \right) \frac{T_p}{2} \right)} S_{\ell_1, \dots, \ell_j, p_{j+1}, \dots, p_k}^{\zeta, \eta}(\omega_{L_1}, \dots, \omega_{L_{k-1}}). \quad (8.52)$$

Upon making the change of variables  $M\omega_{L_r} T_p/2 \mapsto \omega_{L_r}$  and taking the large- $M$  limit, the product of ratios of sin functions in equation (8.51) may be replaced by a product of sinc functions, which approaches a multi-dimensional frequency comb with peaks of height  $\mathcal{O}(M)$  at  $\omega_{L_r} = q_{L_r} 2\pi/T$ ,  $q_{L_r} \in \mathbb{Z}$ . In order for the above  $k$ th-order cumulant to have a finite value, one must then avoid the  $\mathcal{O}(M)$  divergences at the peaks located at every

$$\vec{\omega}_{[k]}(\vec{q}) = \frac{2\pi}{T_p} \left( q_{L_1}, \dots, q_{L_{k-1}}, - \sum_{r=1}^{k-1} q_{L_r} \right). \quad (8.53)$$

In practice, meeting this requirement is impossible, since no DD sequence is known, such that its FFs have a high-order zero for *all*  $\{q_{L_r}\}$ , as required. However, building on the single-qubit case [105], it is unrealistic to expect that a plateau regime may emerge at all, unless the noise is sufficiently ‘well-behaved’ at high frequencies. Let us work in the simplest (idealized) scenario, where a hard frequency cutoff exists for each frequency variable, such that the power spectra may be Taylor-expanded around the  $\vec{\omega} = 0 = \vec{q}$  as follows:

$$S_{L_1, \dots, L_k}^{\zeta, \eta}(\omega_{L_1}, \dots, \omega_{L_{k-1}}) = \prod_{r=1}^{k-1} \omega_r^{s_{L_r}} \Theta(|\omega_{L_r} - \omega_{c, L_r}|), \quad (8.54)$$

where  $\omega_{c,L_r}$  is a high-frequency cutoff parameter and  $s_{L_r}$  characterizes the power-law behavior as  $\omega_{L_r} \rightarrow 0$ . Similarly, we assume that the low-frequency behavior of the relevant FFs reads

$$G_{Z_\ell}^{(1)}(\omega_{L_r}, T) \sim \mathcal{O}(\omega_{L_r}^{\alpha_{L_r}}), \quad G_{Z_\ell, Z_{\ell'}}^{(1)}(\omega_{L_r, L_{r'}}, T) \sim \mathcal{O}(\omega_{L_r}^{\alpha_{L_r}}), \quad (8.55)$$

in terms of the CO  $\alpha_{L_r}$  corresponding to each frequency variable. By demanding that, in analogy to equation (8.49),  $\omega_{c,L_r} T_p < 2\pi$ , for all  $L_r$ , we may then ensure that there are *no* high-frequency noise components at any of the resonant frequencies, so that *only* the divergence at  $\{q_{L_r}\} = 0$  contributes to the  $k$ -th order cumulant. The strategy is then to decompose the integral in equations (8.51)-(8.52) into a sum of integrals over hypercubes of side  $2\pi/T_p$  centered around  $\vec{q} = 0$  and, as in [105], to make sure that the dependence upon each frequency variable is sufficiently well-behaved close to zero for the corresponding integration to be convergent. That is, we require that each frequency integration admits a power law  $\omega_{L_r}^x$ , with  $x > -1$ , close to zero. Direct calculation then yields the following conditions:

$$\omega_{c,L_r} T_p < 2\pi, \quad \sum_{r=1}^{k-1} s_{L_r} + \sum_{r=1}^k \alpha_{L_r} > 1, \quad \forall \{L_r\}, \forall k \quad (8.56)$$

Being motivated by essentially the same physical requirements, these conditions are entirely analogous to those given in equation (8.49) for the single-qubit case.

Accordingly, a plateau behavior may be engineered by choosing a base DD sequence such that all first-order FFs  $G_{L_r}^{(1)}(\omega_{L_r}, T)$  and  $G_{Z_\ell, Z_{\ell'}}^{(1)}(\omega_{L_r}, T)$  have zeroes of sufficiently high order at each  $\omega_{L_r} = 0$ . Suitable choices were described in section 8.3. We note, in particular, that collective as well as independent single-qubit sequences suffice as long as no direct Ising coupling is present [ $\eta'_{\ell,\ell'}(t) \equiv 0$ ], otherwise sequences built out of composition (such as NUDD or multi-qubit CDD) will be required to ensure high CO  $\alpha_{p_j} = \alpha_{\ell,\ell'}$ . Still, since only first-order FFs are involved, displacement anti-symmetry does not play an essential role. This contrasts with the case where bosonic noise sources are present, as we shall see in section 8.4.2.

The conditions in equation (8.56) contain, as a special case, the ones derived in [105] for a single qubit exposed to zero-mean stationary Gaussian noise, due to either a classical source or a quantum bosonic environment. In such simple cases, with  $k = 2$  and  $\vec{L}_{[2]} = (1, 1)$ , there is only one power spectrum – namely,  $S_{1,1}^\zeta(\omega, -\omega) \equiv S^\zeta(\omega)$  or, respectively,  $S_{1,1}^{B,+}(\omega) = \pi J(\omega) \coth(\beta\omega/2)$ ,  $\omega \geq 0$ , hence our conditions translate into  $2\alpha_1 + s_1 > 1$  and  $\omega_{c,1} T_p < 2\pi$ , in agreement with equation (8.49). Since, for a single qubit, dephasing evolution is *fully* characterized by first-order FFs  $G_{L_r}^{(1)}(\omega_{L_r}, T)$ , the plateau conditions in equation (8.56) apply, in fact, to the more general scenario where noise is *non-Gaussian*.

Paradigmatic examples of classical non-Gaussian dephasing arise when a qubit is exposed to random telegraph noise [205] or is non-linearly coupled to a Gaussian noise source, e.g.,  $\zeta(t) = [\xi(t)]^2$ , with  $\xi(t)$  Gaussian as for a qubit operated at an optimal point [206]. Consider, for illustration, the latter case. If the power spectra  $S_{1,1}^\xi(\omega)$  of  $\xi(t)$  has a cutoff  $\omega_c \equiv \Lambda$ , it follows that  $S_1^\zeta(\omega_1, \dots, \omega_{k-1})$  has a cutoff at  $2\Lambda$  for all  $k$ . To see this, observe that  $\langle \zeta(t_1) \cdots \zeta(t_k) \rangle = \langle \xi(t_1)\xi(t_1) \cdots \xi(t_k)\xi(t_k) \rangle$  can be written, by virtue of the Gaussianity of  $\xi(t)$ , as a sum of terms of the form  $\langle \xi(t_{i_1})\xi(t_{i_2}) \cdots \langle \xi(t_{i_{k-1}})\xi(t_{i_k}) \rangle \rangle$ , where  $i_s \in [1, \dots, k]$ . After Fourier transforming, direct calculation shows that each of these terms is of the form

$$\begin{aligned} \int_{-\infty}^{\infty} d\omega_s S^\xi(\omega_s) S^\xi(\omega_s - \omega_{i_1}) \cdots S^\xi(\omega_s - \omega_{i_1} - \omega_{i_2} - \cdots - \omega_{i_{s-1}}) \delta(\omega_{i_1} + \cdots + \omega_{i_s}) \\ \times S^\xi(\omega_{i_s+1}) \cdots S^\xi(\omega_{i_k}) \delta_{\omega_{i_{s+1}}} \cdots \delta_{\omega_{i_k}}, \quad 1 \leq s \leq k. \end{aligned}$$

Because of the assumed cutoff in  $S^\xi(\omega)$ , it then follows that the integral is non-vanishing for  $\omega_s \in [-\Lambda, \Lambda]$ , and as long as  $-\Lambda \leq \omega_s - \omega_{i_1} \leq \Lambda$ ,  $-\Lambda \leq \omega_s - \omega_{i_1} - \omega_{i_2} \leq \Lambda$ ,  $\dots$ ,  $-\Lambda \leq$

$\omega_s - \omega_{i_1} - \cdots - \omega_{i_s} \leq \Lambda$ . Therefore,  $\omega_{i_1}$  can at most be  $2\Lambda$ ,  $\omega_{i_2} \in [-2\Lambda, 2\Lambda]$ , and so on. That is, any high-order spectra of  $\zeta(t)$  has a cutoff of at most  $2\Lambda$  in all its frequency variables and, furthermore, is stationary, that is,  $\omega_1 + \cdots + \omega_k = 0$ , at order  $k$ . Also notice that from the form of the above expressions we may infer that the functional dependence with respect to the frequencies is such that  $\sum_r s_{L_r}$  grows at most linearly with  $k$ , making it possible for the plateau constraints to be satisfied.

For bosonic noise, stationarity demands that  $[\rho_B, H_B] = 0$ , hence  $\rho_B$  is diagonal in the multi-mode Fock basis. A simple example of non-Gaussian dephasing arises when  $\rho_B$  is a mixture of thermal (Gaussian) components at different temperatures, e.g.,  $\rho_B = w_1\rho_{\beta_1} + w_2\rho_{\beta_2}$ , with  $\sum_i w_i = 1$  [185]. While detailed analysis is beyond the scope of this work, and may be most meaningfully carried out for a concrete qubit device, our approach provides in each case sufficient conditions for a coherence plateau to be engineered in principle.

### 8.4.2 Fidelity plateau conditions for multi-qubit classical plus spin-boson dephasing

Multi-qubit dephasing arising from combined classical and quantum bosonic noise sources may be analyzed by generalizing the strategy of section 8.4.1. Again, given the convenient form of equation (8.34), it is possible to analyze the additional effect of the spin-boson interaction by analyzing the contribution of the factors resulting from a quantum average. In order to guarantee the existence of a fidelity plateau for this more general case, it is necessary to ensure that the exponents of the additional decay terms, arising from quantum bosonic noise sources, also do not diverge as  $M \rightarrow \infty$ . Hence, in the large  $M$  limit, we require that, at order  $k$  in the cumulant expansion (recall equation (8.9) and the stationarity assumption),

$$\int_{-\infty}^{\infty} \frac{d\vec{\omega}_{[k-1]}}{(2\pi)^{k-1}} S_{\ell_1, \dots, \ell_k}^B(\omega_1, \dots, \omega_{k-1}) G_{Z_{\ell_1}}^{(1)}(\omega_1, t) \cdots G_{Z_{\ell_k}}^{(1)}(-\sum_{r=1}^{k-1} \omega_r, t) \longrightarrow \text{constant}, \quad (8.57)$$

$$\int_{-\infty}^{\infty} \frac{d\omega}{2\pi} S_{\ell, \ell'}^{B,-}(\omega) G_{Z_\ell}^{(1)}(\omega, T) G_{Z_{\ell'}}^{(1)}(-\omega, T) \longrightarrow \text{constant}, \quad (8.58)$$

$$\int_{-\infty}^{\infty} \frac{d\omega}{2\pi} S_{\ell, \ell'}^{B,-}(\omega) G_{Z_\ell, Z_{\ell'}}^{(2)}(\omega, -\omega, T) \longrightarrow \text{constant}. \quad (8.59)$$

It is straightforward to determine plateau conditions for equations (8.57)-(8.58) by following a similar analysis to the one used for classical noise, as the equations are basically the same. In particular, we also demand a hard cut-off for the quantum noise spectra, namely,

$$S_{\ell_1, \dots, \ell_k}^B(\omega_{\ell_1}, \dots, \omega_{\ell_{k-1}}) \sim \prod_{r=1}^{k-1} \mathcal{O}(\omega_{\ell_r}^{\tilde{s}_{\ell_r}}) \Theta(|\omega_{\ell_r} - \omega_{c, \ell_r}|),$$

$$S_{\ell, \ell'}^{B,-}(\omega) \sim \mathcal{O}(\omega^{\tilde{s}_{\ell, \ell'}}) \Theta(|\omega - \omega_{c, -}|),$$

where  $\tilde{s}_{\ell_r}$  and  $\tilde{s}_{\ell, \ell'}$  characterize the relevant low-frequency power-law behaviors and  $\omega_{c, \ell_r}, \omega_{c, -}$  are high-frequency cut-offs. A similar analysis to the classical case then leads to

$$\omega_{c,r} T_p < 2\pi, \forall r, \quad \omega_{c,-} T_p < 2\pi, \quad (8.60)$$

$$\sum_{r=1}^{k-1} \tilde{s}_{\ell_r} + \sum_{r=1}^k \alpha_{\ell_r} > 1, \forall k, \quad \tilde{s}_{\ell_r, \ell_{r'}}^{-} + \alpha_{\ell_r} + \alpha_{\ell_{r'}} > 1, \forall r \neq r'. \quad (8.61)$$

Obtaining plateau conditions for equation (8.59) requires more work. Using the periodicity

of  $y_\ell(t)$  over  $T = MT_p$ , we may rewrite

$$\begin{aligned} 2iG_{Z_\ell, Z_{\ell'}}^{(2)}(\omega, -\omega, T) &= G_{Z_\ell}^{(1)}(\omega, T_p)G_{Z_{\ell'}}^{(1)}(-\omega, T_p) \frac{e^{iM\omega T_p} - e^{-iM\omega T_p} - M(e^{i\omega T_p} - e^{-i\omega T_p})}{(e^{i\omega T_p/2} - e^{-i\omega T_p/2})^2} \\ &\quad + M 2iG_{Z_\ell, Z_{\ell'}}^{(2)}(\omega, -\omega, T_p), \end{aligned} \quad (8.62)$$

which, however, includes contributions with an *explicit linear M-dependence*. Accordingly,  $G_{Z_\ell, Z_{\ell'}}^{(2)}(\omega, -\omega, T)$  grows with  $M$  and, in the  $M \rightarrow \infty$  limit we are interested in, it diverges. One would like to show that under appropriate symmetry of  $y_\ell(t)$ , and consequently of the FFs in each  $T_p$  interval, the terms linear in  $M$  vanish. As it turns out, the displacement anti-symmetry comes to our aid here as well, leading to the desired cancellations, as we show below. We stress that the linear  $M$ -dependence is a generic feature, and unless additional symmetry is built into the applied control sequence, it necessarily leads to a divergence, forbidding the existence of a plateau regime. For example, repeating a high-order multi-qubit NUDD sequence without demanding further structure will *not* lead to a fidelity plateau in the presence of quantum noise, whereas a displacement anti-symmetry-enhanced NUDD sequence will achieve it in principle, provided that the appropriate conditions are obeyed.

## Two-qubit setting

To illustrate how the displacement anti-symmetry comes into play, let us analyze the two-qubit case first. Recall that displacement anti-symmetry can be built into any control sequence by the construction detailed in equation (8.48). The specific choice of base sequence depends on the noise model: as noted, in the presence of time-dependent direct coupling multi-qubit high-order DD sequences, such as CDD or NUDD, are needed, while if this coupling vanishes we may employ the more efficient multi-qubit sequences described in equations (8.43)-(8.44). Regardless, imposing displacement anti-symmetry over  $T_p$ , one finds that

$$\begin{aligned} G_{Z_\ell}^{(1)}(\omega, T_p) &= (1 - e^{i\omega T_p/2}) G_{Z_\ell}^{(1)}(\omega, T_p/2), \\ G_{Z_{\ell'}}^{(1)}(\omega, T_p) &= (1 + e^{i\omega T_p/2}) G_{Z_{\ell'}}^{(1)}(\omega, T_p/2), \\ 2iG_{Z_\ell, Z_{\ell'}}^{(2)}(\omega, -\omega, T_p) &= -2 \cos(\omega T_p/2) G_{Z_\ell}^{(1)}(\omega, T_p/2) G_{Z_{\ell'}}^{(1)}(-\omega, T_p/2). \end{aligned}$$

Collecting all the terms proportional to  $M$  in equation (8.62) leads then to

$$G_{Z_\ell}^{(1)}\left(\omega, \frac{T_p}{2}\right)G_{Z_{\ell'}}^{(1)}\left(-\omega, \frac{T_p}{2}\right)\left[\cos(\omega T_p/2) - \frac{e^{i\omega T_p} - e^{-i\omega T_p}}{2(e^{i\omega T_p/2} - e^{-i\omega T_p/2})^2} 2i \sin(\omega T_p/2)\right] = 0, \quad (8.63)$$

which leaves us with

$$\begin{aligned} 2iG_{Z_\ell, Z_{\ell'}}^{(2)}(\omega, -\omega, T) &= G_{Z_\ell}^{(1)}(\omega, T_p)G_{Z_{\ell'}}^{(1)}(-\omega, T_p) \frac{e^{iM\omega T_p} - e^{-iM\omega T_p}}{(e^{i\omega T_p/2} - e^{-i\omega T_p/2})^2} \\ &= -G_{Z_\ell}^{(1)}(\omega, T_p/2)G_{Z_{\ell'}}^{(1)}(-\omega, T_p/2) \frac{\sin(M\omega T_p)}{\sin(\omega T_p/2)}. \end{aligned}$$

By exploiting this structure, the relevant integral in equation (8.59) becomes:

$$\begin{aligned} \int_{-\infty}^{\infty} \frac{d\omega}{2\pi} S_{\ell, \ell'}^{B, -}(\omega) 2iG_{Z_\ell, Z_{\ell'}}^{(2)}(\omega, -\omega, T) &= 2i \sum_{r=-\infty}^{\infty} \int_{(2r-1)\pi/T_p}^{(2r+1)\pi/T_p} \frac{d\omega}{2\pi} S_{\ell, \ell'}^{B, -}(\omega) G_{Z_\ell, Z_{\ell'}}^{(2)}(\omega, -\omega, T) \\ &= - \sum_{r=-\infty}^{\infty} \int_{(2r-1)\pi/T_p}^{(2r+1)\pi/T_p} \frac{d\omega}{2\pi} S_{\ell, \ell'}^{B, -}(\omega) G_{Z_\ell}^{(1)}(\omega, T_p/2) G_{Z_{\ell'}}^{(1)}(-\omega, T_p/2) \frac{\sin(M\omega T_p)}{\sin(\omega T_p/2)} \\ &\xrightarrow{\text{large } M} -\frac{2}{T_p} \sum_{r=-\infty}^{\infty} \frac{(-1)^r}{2\pi} S_{\ell, \ell'}^{B, -}\left(\frac{2r\pi}{T_p}\right) G_{Z_\ell}^{(1)}\left(\frac{2r\pi}{T_p}, \frac{T_p}{2}\right) G_{Z_{\ell'}}^{(1)}\left(-\frac{2r\pi}{T_p}, \frac{T_p}{2}\right). \end{aligned}$$

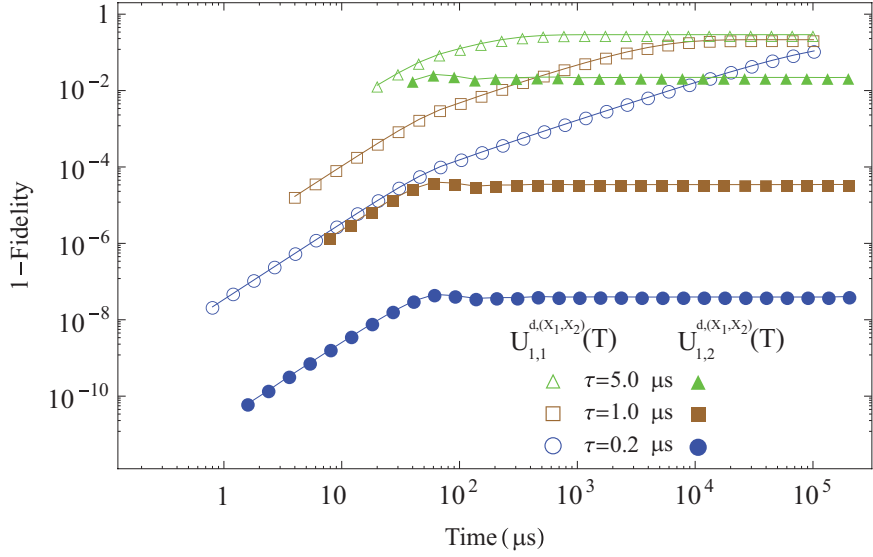


**Figure 8.7:** Emergence of a fidelity plateau under sequence repetition in the long-time limit. Two DD sequences incorporating displacement anti-symmetry are considered,  $U_{1,1}^{d,(X_1,X_2)}(T)$  and  $U_{1,2}^{d,(X_1,X_2)}(T)$  (empty vs. filled symbols), operating at different minimum pulse intervals,  $\tau = 0.2, 1.0, 5.0 \mu\text{s}$ . A purely Gaussian bosonic spectrum in the low-temperature limit is assumed [ $\coth(\beta\omega/2) \simeq 1$ ], of the form  $S_{Z_1,Z_2}^B(\omega) = 2\pi e^{i\omega t_{1,2}} \omega_c (\omega/\omega_c)^{-2} \Theta(|\omega - \omega_c|)$ , with  $\omega_c = 2\pi 10^4 \text{ Hz}$  and  $t_{1,2} = 10^{-2} \text{ s}$ . The fidelity is calculated using equation (8.64), by averaging over  $10^3$  random pure initial states of the form  $|\Psi\rangle = \sum_{a=0}^3 c_a |a_1 a_2\rangle$ , where for simplicity we have assumed real coefficients  $c_1 \equiv \cos \theta$ ,  $c_2 \equiv \sin \theta \cos \theta'$ ,  $c_3 \equiv \sin \theta \sin \theta' \cos \theta''$ ,  $c_4 \equiv \sin \theta \sin \theta' \sin \theta''$ , with  $\theta, \theta' \in [0, \pi]$  and  $\theta'' \in [0, 2\pi]$  uniformly random.

Assuming that equations (8.60)-(8.61) are satisfied, the two-qubit displacement anti-symmetry guarantees that the contribution due to the bath-induced coupling term is finite, as desired, without imposing additional constraints on the COs  $\{\alpha_{L_r}\}$ .

To better appreciate the role of the plateau conditions in the presence of the quantum bath, consider two DD sequences on which the displacement anti-symmetry is imposed:

$$\begin{aligned} \text{CDD}_{1,1}^{d,(X_1,X_2)}(T) &= \text{CDD}_1^{(X_1)} \times \text{CDD}_1^{(X_2)}(T/2) X_2 \left( \text{CDD}_1^{(X_1)} \times \text{CDD}_1^{(X_2)}(T/2) \right) X_2, \\ \text{CDD}_{1,2}^{d,(X_1,X_2)}(T) &= \text{CDD}_1^{(X_1)} \times \text{CDD}_2^{(X_2)}(T/2) X_2 \left( \text{CDD}_1^{(X_1)} \times \text{CDD}_2^{(X_2)}(T/2) \right) X_2. \end{aligned}$$

Representative results for the fidelity behavior when these are applied to two qubits subject to quantum Gaussian noise with a sub-Ohmic spectrum is shown in figure 8.7, for a value of the transit time  $t_{1,2}$  corresponding to generic (neither collective nor independent) coupling strengths. For any two-qubit initial pure state  $\rho(0) \equiv |\Psi\rangle\langle\Psi|$ , the fidelity is computed as

$$F(T = MT_p) = \langle \Psi | \rho(MT_p) | \Psi \rangle = \sum_{a,b} |\rho_{a,b}(0)|^2 e^{-\chi_{a,b}(MT_p)} \cos[\phi_{a,b}(MT_p)], \quad (8.64)$$

in terms of the appropriate decay and phase terms (see 8.7 for explicit expressions). Only one of the sequences satisfies the plateau conditions, and indeed the plateau is seen to appear only for such a sequence. Also, notice that the value at which the fidelity saturates, i.e., the quality of the plateau, deteriorates as  $\tau$  (hence  $T_p$ ) increases and approaches the upper bound imposed by equation (8.60).

Figure 8.8 further illustrates how the control protocol incorporating displacement antisymmetry is also the only one exhibiting *model robustness*, namely, the only one guaranteeing that the plateau may be achieved for arbitrary spin-boson couplings. Specifically, a protocol with displacement anti-symmetry (built out of  $U_{1,2}^{d,(X_1,X_2)}(T)$ ), one with mirror anti-symmetry (built out of  $U_2^{(X_1)} \times U_3^{(X_2)}(T)$ ), and a non-selective control protocol ( $U_2^{(X_1 X_2)}(T)$ ) are tested against the same Gaussian noise spectrum of figure 8.7 for different values of the transit time – equivalently, different spatial separation between the two qubits. In the  $t_{1,2} \rightarrow \infty$  limit, which corresponds to private baths, all strategies work equally well, as expected. In the opposite limit of a collective coupling,  $t_{1,2} \rightarrow 0$ , the non-selective control protocol fails to achieve a plateau since it cannot make  $G_{Z_1, Z_2}^{(2)}(\omega, -\omega, T)$  finite as  $M \rightarrow \infty$ . In the general case ( $0 < t_{1,2} < \infty$ ), only the displacement anti-symmetry enhanced protocol achieves a high-fidelity plateau.

## Multi-qubit setting

In order to extend the approach to the  $N$ -qubit setting, the key step is to show that, once the generalized displacement anti-symmetry introduced in section 8.3.3 is imposed, a cancellation analog to equation (8.63) holds. Consider the terms proportional to  $M$  arising in  $G_{Z_\ell, Z_{\ell'}}^{(2)}(\omega, -\omega, T)$  for each qubit pair [see equation (8.62)], and let  $\max\{\ell, \ell'\} = \ell$  without loss of generality. Since, for the matrix defined in equation (8.46),  $P^{(N)}(\ell, s) = \delta_{s,\ell-1}$ , to every qubit  $\ell > 1$  let us associate  $N_{\ell-1} = 2^{N-(\ell-1)}$  and intervals of length  $\tau_{\ell-1}$ , such that  $\tau_{\ell-1} N_{\ell-1} = T_p$ . By dividing all integrals into sub-integrals over length- $\tau_{\ell-1}$  intervals and using the properties of  $P^{(N)}(\ell, s)$ , direct calculation shows that for every  $\ell > \ell'$  the terms linear in  $M$  reduce to

$$G_{Z_\ell}^{(1)}(\omega, \tau_{\ell-1}) G_{Z_{\ell'}}^{(1)}(-\omega, \tau_{\ell-1}) \left[ \sum_{r=1}^{N_{\ell-1}-1} \sum_{s=0}^{r-1} \left( (-1)^r e^{i(r-s)\omega\tau_{\ell-1}} - (-1)^s e^{i(s-r)\omega\tau_{\ell-1}} \right) \right. \\ \left. - \left( \sum_{r=0}^{N_{\ell-1}-1} \sum_{s=0}^{N_{\ell-1}-1} (-1)^r e^{i(r-s)\omega\tau_{\ell-1}} \frac{e^{i\omega T_p} - e^{-i\omega T_p}}{(e^{i\omega T_p/2} - e^{-i\omega T_p/2})^2} \right) \right] = 0.$$

Consequently, for any  $\ell \neq \ell'$ , we may re-express

$$2iG_{Z_\ell, Z_{\ell'}}^{(2)}(\omega, -\omega, T) = G_{Z_\ell}^{(1)}(\omega, T_p) G_{Z_{\ell'}}^{(1)}(-\omega, T_p) \frac{e^{iM\omega T_p} - e^{-iM\omega T_p}}{(e^{i\omega T_p/2} - e^{-i\omega T_p/2})^2} \\ = G_{Z_\ell}^{(1)}(\omega, \tau_{\ell-1}) G_{Z_{\ell'}}^{(1)}(-\omega, \tau_{\ell-1}) \left[ \frac{-2i \sin^2(\frac{\omega T_p}{2})}{\sin(\omega\tau_{\ell-1})} \times \frac{e^{iM\omega T_p} - e^{-iM\omega T_p}}{(e^{i\omega T_p/2} - e^{-i\omega T_p/2})^2} \right] \\ = -G_{Z_\ell}^{(1)}(\omega, \tau_{\ell-1}) G_{Z_{\ell'}}^{(1)}(-\omega, \tau_{\ell-1}) \left[ \frac{\sin(M\omega T_p)}{\sin(\omega\tau_{\ell-1})} \right]. \quad (8.65)$$

It then follows that the generalized displacement anti-symmetry guarantees that, in the large- $M$  limit, any contribution due to bath-induced qubit coupling,

$$2i \int_{-\infty}^{\infty} \frac{d\omega}{2\pi} S_{\ell, \ell'}^{B, -}(\omega) G_{Z_\ell, Z_{\ell'}}^{(2)}(\omega, -\omega, T) = \\ - \frac{N_{\ell-1}}{T_p} \sum_{r=-\infty}^{\infty} \frac{(-1)^r}{2\pi} S_{\ell, \ell'}^{B, -}\left(\frac{r\pi}{\tau_{\ell-1}}\right) G_{Z_\ell}^{(1)}\left(\frac{r\pi}{\tau_{\ell-1}}, \tau_{\ell-1}\right) G_{Z_{\ell'}}^{(1)}\left(-\frac{r\pi}{\tau_{\ell-1}}, \tau_{\ell-1}\right),$$

is finite. Thus, a plateau regime may still exist, provided that the conditions identified for the two-qubit case, equations (8.60)-(8.61) remain valid. Remarkably, this result does not depend on the specific choice of base sequence, but only on the displacement anti-symmetry, further highlighting its fundamental role in multi-qubit control protocols for dephasing noise.

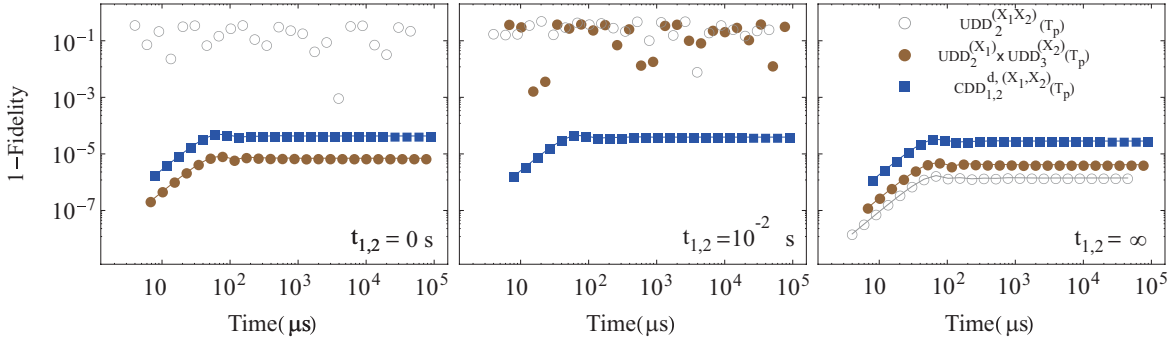


Figure 8.8: Comparison between different protocols in achieving a fidelity plateau: non-selective control ( $UDD_2^{(X_1 X_2)}(T_p)$ , empty symbols), sequences with mirror anti-symmetry ( $UDD_2^{(X_1)} \times UDD_3^{(X_2)}(T_p)$ , filled brown symbols), and with displacement anti-symmetry ( $CDD_{1,2}^{d,(X_1 X_2)}(T_p)$ , filled blue symbols). Only displacement anti-symmetry-enhanced DD achieves a plateau in the general case (middle panel). The fidelity loss, calculated by averaging over  $10^3$  random pure initial states as in figure 8.7, is plotted as a function of total time for the same Gaussian spin-boson noise spectrum  $S_{Z_1, Z_2}^B(\omega)$  considered therein, for representative values of the transit time  $t_{1,2}$ . In each case,  $T_p$  is fixed by the choice of minimum switching time, assumed here to be  $\tau = 1\mu\text{s}$ , so that the appropriate plateau condition is met.

## 8.5 Further considerations

### 8.5.1 Controlled entanglement generation and storage

Quantum entanglement is a crucial resource for QIP and hence devising ways to reliably generate and store it is an particularly important task. Entanglement may be achieved directly, via tunable or always-on couplings between qubits or, if the latter are not readily available, *indirectly*, with the aid of a common quantum environment. Various schemes for indirect generation of bipartite entanglement, as well as weaker quantum correlations quantified by discord, have been proposed [194, 195, 207]. Once created, such quantum correlations have to be stored (e.g., to be later used for quantum tasks of interest), and protected from unwanted decoherence. Several ways to do this have been invoked, e.g., employing the quantum Zeno effect [208], quantum feedback [209, 210], and DD control [211].

While the emphasis of existing work is on two-qubit settings and bipartite entanglement, the formalism we've developed allows for the generation and storage of *multi-partite entanglement* with high-fidelity for an extended time. Let us assume a multi-qubit Hamiltonian that includes classical and bosonic dephasing, as in equations (8.2)-(8.3), with vanishing direct coupling,  $d_{\ell,\ell'} = 0 = \eta_{\ell,\ell'}$  (or else one could just use that to create entanglement), and no assumption on the initial bath state (in particular, no thermal equilibrium). Our proposed strategy consists of two steps:

*Stage 1: Entanglement generation.* This can be achieved by using  $M_g$  repetitions, each of duration  $T_p$ , of a high-order multi-qubit DD sequence such as CDD or NUDD *without displacement anti-symmetry*. In this way, the contribution of all dephasing terms is suppressed to high order, except for the one stemming from the induced coupling term – which grows linearly with  $M_g$  [recall equation (8.62)]. As noted, the induced coupling is ruled by  $S_{\ell,\ell'}^{B,-}(\omega)$  and, as such, it does not depend on  $\rho_B$  but only on the actual dephasing Hamiltonian, in particular the spectral density function  $J(\omega)$ . The fact that the protocol is independent of  $\rho_B$  is an important

prerequisite for generating entanglement *on demand*, which may be achieved provided that accurate knowledge of the relevant power spectra  $S_{\ell,\ell'}^{B,-}(\omega)$  is available. In principle, this may be obtained by extending noise spectroscopy protocols for single-qubit [141, 185] and two-qubit classical dephasing [212] to general multi-qubit dephasing [185].

*Stage 2: Entanglement storage.* Once the state of the multi-qubit system after time  $T_g = M_g T_p$  is sufficiently close to an entangled state of interest, we may switch to a DD sequence *with displacement anti-symmetry*, in order to achieve protection for long storage times, say,  $T_s = M_s T'_p$ , provided that the plateau conditions of equations (8.60)-(8.60) are satisfied, and where we allow for the duration of the storage base sequence to differ, in general. Basically, the displacement anti-symmetry acts like an on/off switch for entanglement generation. There is, however, an important subtlety in the analysis that must be pointed out. In our derivation of the the plateau conditions, we relied on the assumption that the initial joint state was of the form  $\rho_S \otimes \rho_B$ ; this need not be the case at the end of the entanglement generation stage, with  $\rho_{SB}(T_g)$  involving entanglement between  $S$  and  $B$  in general (hence making  $\rho_S(T_g)$  mixed). To move forward, it is necessary to re-examine the derivation when the total evolution time  $T$  is divided in two consecutive stages, without and with displacement anti-symmetry, respectively. One can see that:

$$\begin{aligned} G_{O_a}^{(1)}(\omega, T) &= G_{O_a}^{(1)}(\omega, M_g T_p) + e^{i\omega M_g T_p} G_{O_a}^{(1)}(\omega, M_s T'_p), \quad O_a \in \{Z_\ell, Z_\ell Z_{\ell'}\}, \\ 2i G_{Z_\ell, Z_{\ell'}}^{(2)}(\omega_1, \omega_2, T) &= 2i G_{Z_\ell, Z_{\ell'}}^{(2)}(\omega_1, \omega_2, M_g T_p) + 2i G_{Z_\ell, Z_{\ell'}}^{(2)}(\omega_1, \omega_2, M_s T'_p) \\ &\quad + e^{i\omega_1 M_g T_p} G_{Z_\ell}^{(1)}(\omega_1, M_s T'_p) G_{Z_{\ell'}}^{(1)}(\omega_2, M_g T_p). \end{aligned}$$

By using these expressions in equations (8.57)-(8.59), each product of FFs, say with  $k$  factors, becomes a sum of products which are *at most*  $\mathcal{O}(M_s^k)$ . Since we showed that  $\mathcal{O}(M_s^k)$  terms are finite if the plateau conditions hold, it follows that terms with lower order in  $M_s$  are also finite.

By employing the above two-step control strategy, we can conclude that, for any finite number  $M_g$  of entanglement-generation cycles, it is possible to store the resulting multi-qubit entanglement with high fidelity for an arbitrary number  $M_s$  of storage cycles, in principle. A number of important aspects require additional detailed analysis – notably, the degree of purity and nature of the multipartite entangled states reachable over time under the assumed dephasing Hamiltonian, along with consideration of relevant time scales and resource scaling. While we leave this to a separate investigation, indirect ‘environment-assisted’ generation and storage of multi-qubit states close to paradigmatic entangled states of interest (such as W and GHZ states) would be especially interesting, and would complement ongoing efforts on steady-state entanglement generation using engineered dissipation, see e.g. [213, 214, 215].

### 8.5.2 Realistic considerations

It is important to note that, while the noise model assumed in equations (8.2)-(8.3) represents a simplified version of the actual dynamics of any real quantum system, it does encompass dominant sources of decoherence in a variety of systems of relevance to QIP. Classical fluctuations, like the one- and two-body stochastic processes  $\zeta_\ell(t)$  and  $\eta_{\ell,\ell'}(t)$ , provide an effective description of dephasing when the effects of back-action from the system on the environment are negligible. In the simplest case, the noise takes the form of fluctuations in an externally applied field, as it does for magnetic-field fluctuations in trapped-ions [32, 125, 126], or in NMR qubits [142]. More generally, so long as appropriate conditions are satisfied (e.g., effective high temperature), classical processes may be used to approximate the dephasing effects of more complex interactions – ranging from background charge, magnetic flux, and critical current fluctuations in superconducting qubits [53, 216, 93], to interactions between nuclear spins and their surrounding spin environment in NMR [171], and interactions between singlet-triplet electron spin states

in quantum dots and, again, their surrounding nuclear-spin bath [90, 161, 91, 217, 76]. We note also that control imperfections, such as fluctuations in the frequency of a master oscillator, often result in effective dephasing that can be accurately modeled as classical noise [32, 127, 218].

The quantum contributions to our noise Hamiltonian describe a dephasing interaction between the multi-qubit system and a bosonic environment of quantum oscillators. Such interactions, in the form of lattice vibrational modes, arise naturally in solid-state systems. A prominent example is the coupling between excitonic qubits in quantum dots and acoustic vibrations, which has been identified as the dominant source of dephasing in this type of system [221, 222, 223, 224, 225]. Even beyond oscillator environments, the linear spin-boson model has been widely applied to describe open-system dynamics in situations where the system-environment coupling is weak enough for a linear approximation to be valid [226]. For example, the dephasing effects of current and voltage fluctuations in Josephson junction qubits are accurately described in terms of spin-boson interactions [227].

It is often the case that the noise is generated by a large number of independent, weakly coupled sources, and can therefore be assumed to be Gaussian. Generic noise, however, is non-Gaussian; in particular, as mentioned in section 8.4.1, the assumption of Gaussianity breaks down for qubits operated at an optimal point [206], as well as for strongly coupled bistable fluctuators of the sort that generate  $1/f$  in Josephson nano-circuits [205, 53]. For quantum environments, both the initial state and the nature of the interaction with the system will determine whether the noise is Gaussian or not [185]. In these cases, the interplay between generalized FFs and higher-order noise spectra needs to be carefully considered.

Despite the broad applicability of the dephasing noise model on which we have based our analysis, it necessarily neglects important aspects that will affect the evolution of the system in reality. In particular, it is generally true that interactions between a quantum system and its environment will generate both dephasing and relaxation effects, with associated characteristic time scales  $T_2$  and  $T_1$ , respectively. The multi-qubit DD protocols we have presented are designed to address dephasing effects only, and are therefore not expected to be effective if ‘off-axis’ noise effects are significant over the desired storage time. In such cases, multi-axis DD protocols are necessary to counter both dephasing and relaxation effects simultaneously, and it is an interesting open question to determine the extent to which suitable variants of generalized displacement anti-symmetry may possibly still prove beneficial. That being acknowledged, for most of the above-mentioned QIP settings, an appreciable separation between dephasing and relaxation times exists (that is,  $T_1 \gg T_2$ ), and dephasing effects provide the dominant source of error up to very long storage times. In these systems, relaxation will not be a significant factor limiting the validity of our results, including those pertaining to long-time quantum storage [105]. By contrast, if the dephasing noise is strongly Markovian, the lack of temporal correlations will limit the usefulness of the proposed protocols. However, as already remarked in section 8.2.1, this holds for DD techniques generally, and it is well understood that significant Markovian error contributions must be countered using closed-loop quantum error correction strategies [156].

Even if the above conditions are obeyed, the simplifying assumption of the existence of a hard noise cutoff  $\omega_{c,L_r}$  for each noise spectrum frequencies  $\omega_{L_r}$ , made in section 8.4.1, will hardly be met in realistic scenarios. The purpose of this assumption was to avoid the singular behavior associated with the resonant frequencies defined by equation (8.53). In the absence of these cutoffs, the contribution of any noise at these frequencies will be amplified in a way that grows linearly with the number  $M$  of base sequence repetitions, ultimately making a long-time plateau unsustainable. However, building on the quantitative analysis carried out for the single-qubit case [105], if the noise beyond the resonant frequencies decays sufficiently rapidly, one can expect the errors associated with high frequency noise to grow slowly with  $M$ . As in the single-qubit case, we expect that this may still allow for the maintenance of a fidelity plateau

for storage times that are still sufficiently long to be practically useful.

Beside deviations from the assumed decoherence model, realistic control scenarios will inevitably face a number of technological limitations and imperfections. While the precise nature and extent of the discrepancies resulting the simplifying assumption of perfect control resources we have made will depend on the particular physical system being investigated, it is worthwhile highlighting those features that may have the greatest potential to limit the efficacy of the proposed quantum storage protocols across all potential QIP platforms. First, it is clear that any real control pulse has a non-zero duration. As a result, the application of each pulse in a DD sequence will introduce depolarization errors, in addition to a purely dephasing effect. It will not then be possible to describe the modulating influence of a pulse sequence in terms of uniaxial switching functions of the form exemplified in equation (8.22), and, consequently, the Magnus expansion for the controlled propagator  $\tilde{U}_e(T)$  will no longer exactly truncate. Strictly speaking, although it is possible to design sequences of finite-width pulses that achieve a non-zero CO [61], the (infinite-level-Magnus) FO  $\Phi^{[\infty]}$  of any DD protocols for a two-axis decoherence model will be zero [43]. Generally, one may expect this problem to become more significant as the number of applied pulses increases.

For short-term state preservation and relatively small numbers of qubits  $N$ , errors introduced by finite-duration pulses need not be a major concern, as the low-FO contributions may be negligible, so that the ‘effective’ FO  $\Phi^{[\kappa]}$  for finite order  $\kappa$  remains sufficiently high [228, 43]. For long-term memory and/or large  $N$ , however, the accumulation of pulse-induced errors may significantly reduce the attainable fidelity and the duration of any plateau. There are two readily apparent approaches to addressing this problem, which will likely have to be used in tandem in practical dephasing settings. The first, and a motivation for this work, is to use DD protocols that utilize the minimum number of pulses to achieve a desired level of error suppression for a given dephasing environment and system size  $N$ . The second is to replace ‘primitive’ DD pulses with dynamically corrected gates or composite pulses [68, 54, 102, 143, 228], so that error cancellation is maintained *during* the duration of all pulses, up to a sufficiently high order. For single-qubit storage, this approach has been shown to successfully counter pulse-width effects which would otherwise prevent or degrade a coherence plateau [105]. While a quantitative (numerical) analysis of a specific multi-qubit system is beyond our current scope, we expect similar techniques to maintain their usefulness, with the caveat that different COs may be required for different qubits, in order for the overall sign patterns required by displacement anti-symmetry to be maintained.

Lastly, another important source of control error arises from limited timing resolution and ‘jitter’. This may take the form of imprecision in the timing of the individual pulses that comprise a DD sequence. As the analysis in [47] implies, even when pulses are assumed to have vanishing duration, and imprecision is restricted to small rounding errors in the timing of each pulse, the actual CO and FO will go to zero. For short-term storage, this issue is most serious for optimized sequences, such as those based on UDD, which are known to be particularly sensitive to pulse placement. For long-term storage, two main effects may be attributable to timing errors in the multi-qubit case. The first effect, similar to the single-qubit setting analyzed in [105], is premature or belated memory access time. The long-time memory protocols discussed in section 8.4 are designed to allow for high-fidelity access to stored information only at integer multiples of the base sequence time, i.e., when  $T = MT_p$ , with access latency capped at  $T_p \ll T$ . If there is some small timing offset  $\delta t$ , so that  $T = MT_p + \delta t$ , the sub-optimal access time can have a similar effect on fidelity as pulse timing imprecision. The second effect, distinctive of the multi-qubit scenario, is breaking the generalized displacement anti-symmetry that is necessary for a plateau regime to exist. A full quantitative analysis of timing errors is necessarily highly system-dependent and, again, beyond our scope. We nevertheless include in 8.8 a qualitative analysis of symmetry-breaking effects on plateau emergence, based on a tim-

ing error model which, despite its oversimplified nature, is analytically tractable and captures the essential idea. Ultimately, as anticipated at the single-qubit level [105], this analysis reinforces how it is essential that DD protocols, particularly those intended for long-time storage, be clocked by high-resolution (sub-ps) timing systems with minimum jitter.

## 8.6 Conclusion

We have provided criteria for the design of effective and efficient control protocols for the preservation of arbitrary multi-qubit states in a relevant class of dephasing models, that combines the effects of classical noise and a linear interaction with a bosonic bath, not necessarily in thermal equilibrium. Under the assumption that (nearly) instantaneous DD pulses may be selectively applied to arbitrary subsets of qubits, we showed that the reduced dynamics of a multi-qubit system can be expressed in terms of a hierarchy of noise spectra – that capture the statistical properties of quantum and classical dephasing sources in the frequency domain – and of a small set of first- and second-order FFs – that describe the modulating effect of the applied control. These results allow for a relatively straightforward, exact characterization of the performance of an arbitrary DD protocol in both the time and frequency domains, and serve as the starting point for the derivation of conditions for the construction of resource-efficient high-order DD protocols.

Specifically, we showed that multi-qubit DD sequences may be constructed that are able to achieve high-order error suppression using exponentially fewer pulses than the most efficient existing protocols, so long as any direct qubit-qubit coupling is constant. This reduction in pulse number offers tremendous practical advantages in terms of the required minimum switching time and the cumulative effect of pulse errors. The improvement in efficiency derives from the property of *displacement anti-symmetry* with which the new protocols are endowed. Importantly, through the imposition of this form of temporal symmetry, it is also possible to ensure that a sequence achieves maximal filtering order in the frequency domain. This contrasts with previously proposed multi-qubit protocols based on nesting and concatenation, for which maximum filtering order cannot always be guaranteed.

We also demonstrated that the method of producing long-time quantum memory via DD sequence repetition, described previously for single-qubit systems under Gaussian noise, can be generalized to multi-qubit systems possibly subject to general non-Gaussian noise. For strictly classical, Gaussian noise on  $N$  qubits, the conditions for engineering the required fidelity plateau are a natural extension of those derived for the single-qubit case [105]. However, when a quantum spin-boson interaction is included, the fidelity plateau cannot be maintained unless additional structure is imposed on the base sequence from the outset. We found that those sequences possessing displacement anti-symmetry have the necessary structure and, therefore, can be used to generate a fidelity plateau in a combined classical and quantum noise environment. On the basis of these observations, we have outlined a simple switched control protocol for the generation and storage of entangled multi-qubit states.

The central role of that the displacement anti-symmetry plays in suppressing the effects of noise associated with the genuinely quantum (non-commuting) nature of the bath points to its relevance for characterizing bath-induced spatial correlations, along with their impact on the implementation of quantum technologies. By comparing the response of two qubits to different control sequences, for instance, it is now possible in principle to discriminate between a classical or a quantum bath with Gaussian statistics. This may have important implications for quantum verification and validation protocols and, ultimately, fault-tolerant quantum computing architectures in the presence of bath-induced spatial correlations. While exploring the usefulness of displacement anti-symmetry beyond the class of open quantum systems examined here

is a natural direction for further investigation, we anticipate immediate applications of our enhanced DD sequences in the context of multi-qubit noise spectroscopy for correlated dephasing environments [212, 185].

*Acknowledgements:* It is a pleasure to thank Kaveh Khodjasteh for early contributions, as well as Michael Biercuk and Leigh Norris for valuable discussions on different aspects of this work. TJG gratefully acknowledges hospitality from the Department of Physics and Astronomy at Dartmouth College, where part of his work was performed. We acknowledge support from the US Army Research Office under contracts No. W911NF-11-1-0068 and W911NF-14-1-0682, and from the Constance and Walter Burke Special Project Fund in Quantum Information Science.

## 8.7 Appendix A: Controlled two-qubit dynamics under Gaussian dephasing

To exemplify the formalism presented in section 8.2.3, let us consider in detail a two-qubit system undergoing stationary zero-mean Gaussian dephasing due to combined classical and quantum bosonic sources. With reference to equation (8.27), the relevant generalized FFs are  $G_{Z_1}^{(1)}(\omega, T)$ ,  $G_{Z_2}^{(1)}(\omega, T)$ ,  $G_{Z_1 Z_2}^{(1)}(\omega, T)$ , and  $G_{Z_1, Z_2}^{(2)}(\omega, -\omega, T)$ . The interaction-picture two-qubit dynamics is given by

$$\langle \rho(T) \rangle_{c,q} = \sum_{\{a_1, a_2, b_1, b_2 | a_\ell, b_\ell = 0, 1\}} e^{-\chi_{a_1 a_2, b_1 b_2}(T) + i \phi_{a_1 a_2, b_1 b_2}(T)} \rho_{a_1 a_2, b_1 b_2}(0) |a_1, a_2\rangle \langle b_1, b_2|,$$

where the decay and phase evolution are determined by the real and imaginary part of the noise second-order cumulants, respectively. Specifically, the decay contribution includes *all* the classical-noise effects [equation (8.35)] plus, from the quantum noise, a contribution that it is identical to what one would find under a private-bath assumption [first term in equation (8.36)]:

$$-\chi_{ab}(T) = \left\langle \left( \Delta[|a|, |b|] \bar{\eta}'_{1,2}(T) + \sum_\ell \Delta[a_\ell, b_\ell] \bar{\zeta}'_\ell(T) \right)^2 \right\rangle_c + \left\langle \left( \sum_\ell \Delta[a_\ell, b_\ell] \bar{B}_\ell(T) \right)^2 \right\rangle_q.$$

Non-commutativity of the bath operators,  $[B_\ell(t), B_{\ell'}(t')] \neq 0$ , is responsible for additional non-trivial phase evolution in certain off-diagonal density-matrix elements:

$$i\phi_{ab}(T) = \Delta[|a|, |b|] \underbrace{(\bar{R}_{12}(T) + \bar{R}_{21}(T))}_{\equiv i\phi^0} + \Delta[a_1 + b_2, a_2 + b_1] \underbrace{\frac{[\bar{B}_1(T), \bar{B}_2(T)]}{2}}_{\equiv i\phi^1},$$

where  $|a| \equiv \sum_\ell a_\ell$  and we have explicitly identified two distinct contributions: (i)  $i\phi^0$ , resulting from the second-order Magnus term; (ii)  $i\phi^1$ , originating from the partial trace over the quantum bath. Thanks to the bosonic algebra, and at variance with  $\chi_{ab}(T)$ ,  $\phi_{ab}(T)$  depends only on the Hamiltonian and not on  $\rho_B$  (in particular,  $\phi_{ab}(T)$  is temperature-independent).<sup>5</sup>

The presence of the  $\Delta[\cdot, \cdot]$  function in the above equations implies that not all noise sources contribute to the evolution of a given density-matrix element. By making the following natural identifications,

$$-\chi_{12,\ell} = \langle \bar{\eta}'_{1,2}(T) \bar{\zeta}'_\ell(T) \rangle, \quad (8.66)$$

---

<sup>5</sup>Classical non-Gaussian noise can also contribute to phase evolution, if odd-order cumulants are non-zero. For classical plus quantum non-Gaussian noise, i.e., when high-order cumulants of  $B_\ell(t)$ ,  $\eta_{\ell,\ell'}(t)$  and/or  $\zeta_\ell(t)$  exist, all factors in equation (8.34) may contribute to  $\phi_{ab}(t)$  and it becomes hard to isolate classical vs quantum effects.

$$-\chi_{12,12} = \frac{1}{2} \langle \bar{\eta}'_{1,2}(T) \bar{\eta}'_{1,2}(T) \rangle, \quad (8.67)$$

$$-\chi_{\ell,\ell} = \frac{1}{2} \langle \bar{\zeta}'_\ell(T) \bar{\zeta}'_\ell(T) \rangle + \langle \bar{B}_\ell(T)^2 \rangle_q, \quad (8.68)$$

and

$$-\chi_{1,2} = \frac{1}{2} \langle 2\bar{\zeta}'_1(T) \bar{\zeta}'_2(T) \rangle + \langle \bar{B}_1(T) \bar{B}_2(T) + \bar{B}_2(T) \bar{B}_1(T) \rangle_q, \quad (8.69)$$

the decay pattern has the following form:

$$e^{-\chi_{a,b}(T)} \sim \begin{pmatrix} \cdot & e^{-\chi_{12,12}-\chi_{2,2}-\chi_{12,2}} & e^{-\chi_{12,12}-\chi_{1,1}-\chi_{12,1}} & e^{-\chi_{1,1}-\chi_{2,2}-\chi_{1,2}} \\ e^{-\chi_{12,12}-\chi_{2,2}-\chi_{12,2}} & \cdot & e^{-\chi_{1,1}-\chi_{2,2}+\chi_{1,2}} & e^{-\chi_{12,12}+\chi_{12,1}-\chi_{1,1}} \\ e^{-\chi_{12,12}-\chi_{12,1}-\chi_{1,1}} & e^{-\chi_{1,1}-\chi_{2,2}+\chi_{1,2}} & \cdot & e^{-\chi_{12,12}-\chi_{2,2}+\chi_{12,2}} \\ e^{-\chi_{1,1}-\chi_{2,2}-\chi_{1,2}} & e^{-\chi_{12,12}+\chi_{12,1}-\chi_{1,1}} & e^{-\chi_{12,12}-\chi_{2,2}+\chi_{12,2}} & \cdot \end{pmatrix},$$

where  $\cdot$  stands for an identity action. While the diagonal entries (populations) are unaffected by the dephasing noise, off-diagonal terms decay according to different controlled decoherence functions, in the absence of special symmetries.<sup>6</sup> Similarly, the phase evolution is not the same for all the off-diagonal coherence elements. Rather, the diagonal and anti-diagonal entries do not exhibit phase evolution, whereas all other elements gain a time-dependent phase according to the following pattern:

$$e^{-i\phi_{a,b}(T)} \sim \begin{pmatrix} \cdot & e^{i(\phi^0-\phi^1)} & e^{i(\phi^0+\phi^1)} & \cdot \\ e^{-i(\phi^0-\phi^1)} & \cdot & \cdot & e^{-i(\phi^0+\phi^1)} \\ e^{-i(\phi^0+\phi^1)} & \cdot & \cdot & e^{-i(\phi^0-\phi^1)} \\ \cdot & e^{i(\phi^0+\phi^1)} & e^{i(\phi^0-\phi^1)} & \cdot \end{pmatrix}.$$

A paradigmatic situation is a pure Gaussian two-qubit spin-boson model under DD, in which case the classical average in the above expression for  $\chi_{ab}(T)$  vanishes and one has

$$-\chi_{ab}(T) = \sum_{\ell=1,2} \Delta[a_\ell, b_\ell]^2 \langle \bar{B}_\ell(T)^2 \rangle_q + \Delta[a_2, b_2] \Delta[a_1, b_1] \langle \bar{B}_2(T) \bar{B}_1(T) + \bar{B}_1(T) \bar{B}_2(T) \rangle_q,$$

with single- and two-qubit contributions given by

$$\langle \bar{B}_\ell(T)^2 \rangle_q = - \int_{-\infty}^{\infty} \frac{d\omega}{2\pi} G_{Z_\ell}^{(1)}(\omega, T) G_{Z_\ell}^{(1)}(-\omega, T) S_{\ell,\ell}^B(\omega) = -2 \int_0^{\infty} \frac{d\omega}{2\pi} |G_{Z_\ell}^{(1)}(\omega, T)|^2 S_{\ell,\ell}^{B,+}(\omega), \quad (8.70)$$

$$\langle \bar{B}_2(T) \bar{B}_1(T) + \bar{B}_1(T) \bar{B}_2(T) \rangle_q = 2 \int_0^{\infty} \frac{d\omega}{2\pi} \text{Re}[G_{Z_2}^{(1)}(\omega, T) G_{Z_1}^{(1)}(-\omega, T) S_{2,1}^{B,+}(\omega)], \quad (8.71)$$

that is, they are determined by an integral of the overlap between a product of FFs, purely dependent on the control, and the noise power spectra  $S_{\ell,\ell'}^{B,+}(\omega)$ . Thanks to the stationary zero-mean assumptions, note that no single FF  $G_{Z_\ell}^{(1)}(\omega, t)$  contributes to the reduced dynamics, but only  $G_{Z_\ell}^{(1)}(\omega, T) G_{Z_\ell}^{(1)}(-\omega, T) = |G_{Z_\ell}^{(1)}(\omega, T)|^2$ . Since the latter is an even function of frequency, rewriting the integral in equation (8.70) as one over the non-negative axis makes it clear that only  $J(\omega) \coth(\beta\omega/2)$  contributes. Similarly, the symmetry properties highlighted in equation (8.16) allow to cast the contribution to  $\chi_{ab}(T)$  in equation (8.71) in a form where it is manifestly real.

---

<sup>6</sup>It is easy to verify that, for collective dephasing, qubit-permutation symmetry implies that  $\chi_{1,1} = \chi_{2,2} = \chi_{1,2}/2$ , in agreement with decoherence-free subspace theory [156].

The two terms contributing to the controlled phase evolution  $i\phi_{ab}(T)$  may likewise be expressed as overlap integrals, except that the purely quantum noise spectra,  $S_{\ell,\ell'}^{B,-}(\omega)$ , which arises from bath non-commutativity, is the relevant one in this case. Explicitly,

$$\begin{aligned} i\phi^0(T) &= -i \int_{-\infty}^{\infty} \frac{d\omega}{2\pi} G_{Z_1,Z_2}^{(2)}(\omega, -\omega, T) S_{1,2}^{B,-}(\omega) \\ &= -2i \int_0^{\infty} \frac{d\omega}{2\pi} \text{Im}[iG_{Z_1,Z_2}^{(2)}(\omega, -\omega, T) S_{1,2}^{B,-}(\omega)], \end{aligned} \quad (8.72)$$

$$\begin{aligned} i\phi^1(T) &= \frac{1}{2} \int_{-\infty}^{\infty} \frac{d\omega}{2\pi} G_{Z_1}^{(1)}(\omega, T) G_{Z_2}^{(1)}(-\omega, T) S_{1,2}^{B,-}(\omega) \\ &= i \int_0^{\infty} \frac{d\omega}{2\pi} \text{Im}[G_{Z_1}^{(1)}(\omega, T) G_{Z_2}^{(1)}(-\omega, T) S_{1,2}^{B,-}(\omega)], \end{aligned} \quad (8.73)$$

where we have used the anti-symmetry property of  $S_{1,2}^{B,-}(-\omega)$ , given in equation (8.16), together with the relationships

$$iG_{1,2}^{(2)}(\omega, -\omega, T) = [iG_{1,2}^{(2)}(-\omega, \omega, T)]^*, \quad [G_{Z_1}^{(1)}(\omega, T) G_{Z_2}^{(1)}(-\omega, T)]^* = G_{Z_1}^{(1)}(-\omega, T) G_{Z_2}^{(1)}(\omega, T),$$

which follow directly from the definition. Written in the form of equations (8.72)-(8.73), it is manifest that  $i\phi^{0,1}$  are purely imaginary, as expected.

As anticipated, we remark that the special case of free dynamics may be recovered as a limiting case, by letting the control switching functions  $y_\ell(t) \equiv 1$  for all  $\ell, t$ , which yields

$$\begin{aligned} G_{Z_\ell}^{(1)}(\omega, T) G_{Z_\ell}^{(1)}(-\omega, T) &= G_{Z_1}^{(1)}(\omega, T) G_{Z_2}^{(1)}(-\omega, T) = \frac{2[1 - \cos(\omega T)]}{\omega^2}, \\ G_{Z_1,Z_2}^{(2)}(\omega, -\omega, T) &= -\frac{\omega T - \sin(\omega T)}{\omega^2}. \end{aligned}$$

One may then verify that our expressions recovers existing results obtained for both two- and multi-qubit free spin-boson dephasing dynamics, see e.g. [188, 194].

## 8.8 Appendix B: Two-qubit fidelity plateau under symmetry breaking timing errors

A qualitative understanding of the effect of timing errors on long-time multi-qubit storage may be obtained by focusing on how they influence the underlying displacement anti-symmetry, and how the resulting deviation from the ideal anti-symmetry condition may in turn affect the plateau. In order to isolate and analyze this effect, we assume all pulses are perfect with the exception of the pulses that generate the displacement anti-symmetry.

Consider, as an example, the use of CDD<sub>1</sub> on qubit one and CDD<sub>2</sub> on qubit 2 as base sequences. One can generate a displacement anti-symmetric sequence  $U_{1,2}^{d,(X_1,X_2)}(T_p)$ , as described in the main text [recall in particular equations (8.43)-(8.44)], by applying two consecutive CDD<sub>1</sub> sequences of length  $T_p/2$  on qubit one, while doing the same with CDD<sub>2</sub> for qubit 2, but conjugating the second half by an X pulse. In the ideal, error-free case, this gives rise to

the following control switching functions:

$$y_1(t) = \begin{cases} -1 & \text{for } 0 < t \leq \frac{T_p}{4} \\ +1 & \text{for } \frac{T_p}{4} < t \leq \frac{T_p}{2} \\ -1 & \text{for } \frac{T_p}{2} < t \leq 3\frac{T_p}{2} \\ +1 & \text{for } 3\frac{T_p}{2} < t \leq T_p \end{cases}, \quad y_2(t) = \begin{cases} -1 & \text{for } 0 < t \leq \frac{T_p}{8} \\ +1 & \text{for } \frac{T_p}{8} < t \leq 3\frac{T_p}{8} \\ -1 & \text{for } 3\frac{T_p}{8} < t \leq 4\frac{T_p}{8} \\ +1 & \text{for } 4\frac{T_p}{8} < t \leq 5\frac{T_p}{8} \\ -1 & \text{for } 5\frac{T_p}{8} < t \leq 7\frac{T_p}{8} \\ +1 & \text{for } 7\frac{T_p}{8} < t \leq T_p \end{cases}. \quad (8.74)$$

Mathematically, the cleanest way to analyze the effect of a deviation from an ideal displacement anti-symmetry is to introduce a timing error. We introduce this via a deviation from the ideal pulse timing which is a fraction  $\delta$  of the minimum switching time used in the sequence, i.e., the middle  $X_2$  pulse inducing the displacement anti-symmetry is applied at a time  $T_p/4 + \delta \times T_p/8$ . Under this error model, the control switching functions become

$$\tilde{y}_1(t) = \begin{cases} -1 & \text{for } 0 < t \leq \frac{T_p}{4} \\ +1 & \text{for } \frac{T_p}{4} < t \leq \frac{T_p}{2} \\ -1 & \text{for } \frac{T_p}{2} < t \leq 3\frac{T_p}{2} \\ +1 & \text{for } 3\frac{T_p}{2} < t \leq T_p \end{cases}, \quad \tilde{y}_2(t) = \begin{cases} -1 & \text{for } 0 < t \leq \frac{T_p}{8} \\ +1 & \text{for } \frac{T_p}{8} < t \leq 3\frac{T_p}{8} \\ -1 & \text{for } 3\frac{T_p}{8} < t \leq T_p(\frac{1}{2} + \frac{\delta}{8}) \\ +1 & \text{for } T_p(\frac{1}{2} + \frac{\delta}{8}) < t \leq 5\frac{T_p}{8} \\ -1 & \text{for } 5\frac{T_p}{8} < t \leq 7\frac{T_p}{8} \\ +1 & \text{for } 7\frac{T_p}{8} < t \leq T_p \end{cases}, \quad (8.75)$$

which can be more compactly rewritten as

$$\begin{aligned} \tilde{y}_1(t) &= y_1(t), \\ \tilde{y}_2(t) &= y_2(t) - 2\Theta(t - T_p/2)\Theta(T_p/2 + \delta T_p/8 - t), \end{aligned}$$

where, as in the main text,  $\Theta(\cdot)$  denotes the Heaviside step function.

It is then possible to rewrite the relevant equation determining the emergence of the plateau including quantum bosonic noise [equation (8.62) in the main text] by using the noisy filters, thereby computing the corrections induced by a non-zero  $\delta$ . One finds then the noisy FFs

$$\begin{aligned} \tilde{F}_{Z_1}^{(1)}(\omega, T) &= F_{Z_2}^{(1)}(\omega, -\omega, T), \\ \tilde{F}_{Z_2}^{(1)}(\omega, T) &= F_{Z_2}^{(1)}(\omega, -\omega, T) + 2i \int_{T_p/4}^{T_p(\frac{4+\delta}{8})} ds e^{i\omega s}, \\ \tilde{F}_{Z_1, Z_2}^{(2)}(\omega, -\omega, T) &= F_{Z_1, Z_2}^{(2)}(\omega, -\omega, T) \\ &\quad + 2 \int_0^T ds_1 \int_0^{s_1} ds_2 y_1(s_1) e^{i\omega(s_1-s_2)} \Theta(t - T_p/2) \Theta(T_p(\frac{4+\delta}{8})), \\ \tilde{F}_{Z_2, Z_1}^{(2)}(\omega, -\omega, T) &= F_{Z_2, Z_1}^{(2)}(\omega, -\omega, T) + 2 \int_{T_p/2}^{T_p(\frac{4+\delta}{8})} ds_1 \int_0^{s_1} ds_2 y_1(s_2) e^{i\omega(s_1-s_2)}, \end{aligned}$$

which can be combined to obtain the following expression, up the leading-order frequency contributions:

$$2i\tilde{G}_{Z_\ell, Z_{\ell'}}^{(2)}(\omega, -\omega, T = MT_p) = 2iG_{Z_\ell, Z_{\ell'}}^{(2)}(\omega, -\omega, T) - M \left( i \frac{\delta^2 T_p^2}{16} + \frac{\omega \delta^3 T_p^3}{384} \right) + \mathcal{O}(\omega^2), \quad (8.76)$$

from which the noisy version of equation (8.62) follows. The effect of such timing errors is illustrated in figure 8.9, for the same two-qubit system and low-temperature Gaussian bosonic

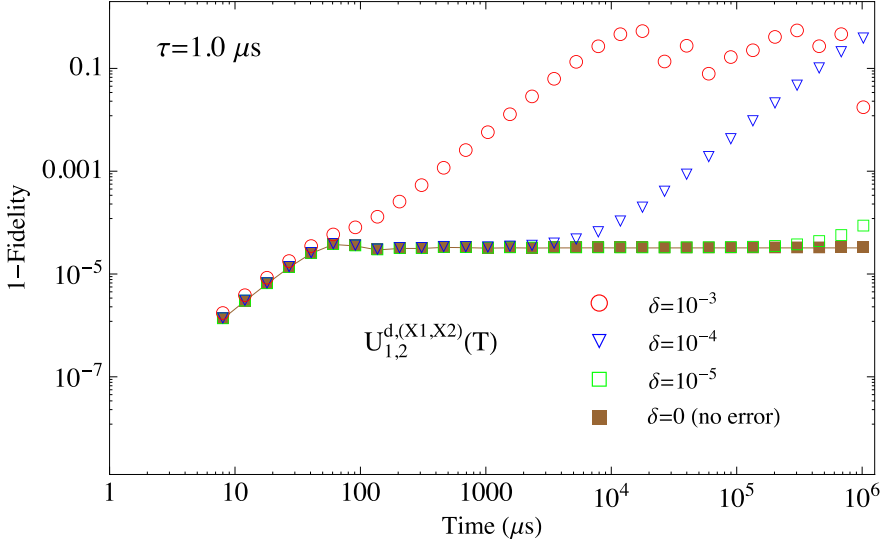


Figure 8.9: *Effect of timing errors on the emergence and duration of a fidelity plateau for two qubits, under the DD sequence  $U_{1,2}^{d,(X_1,X_2)}(T)$  incorporating displacement anti-symmetry and operating at minimum switching time  $\tau = 1.0 \mu\text{s}$ , as considered in figure 8.7 in the ideal case  $\delta = 0$  (filled brown symbols). The behavior for increasing error parameter  $\delta$  is shown, corresponding to a stronger breaking of the displacement anti-symmetry.*

spectrum analyzed in figure 8.7 of the main text. As one may expect, in the presence of such errors (and qualitatively similarly to the effect of other control imperfections [105]), it is no longer possible to generate an indefinitely long fidelity plateau. Indeed, for violations of the anti-symmetry condition that are relatively large compared to the relevant switching time ( $\delta \gtrsim 10^3$ ), it becomes difficult to identify a plateau at all. For sufficiently small violations, on the other hand, it is still possible to engineer a clear plateau that can be sustained for a significant number  $M$  of base-sequence repetitions. Thus, while the magnitude of any control errors plays an important role in determining the viability of an extended fidelity plateau, the mere existence of such imperfections need not, in itself, prohibit the generation and maintenance of a practically useful long-time quantum memory. As stressed in the main text, these results underline the need for high-precision control engineering in QIP.

# Chapter 9

## Phase-modulated decoupling and error suppression in qubit-oscillator systems

We present a scheme designed to suppress the dominant source of infidelity in entangling gates between quantum systems coupled through intermediate bosonic oscillator modes. Such systems are particularly susceptible to residual qubit-oscillator entanglement at the conclusion of a gate period, which reduces the fidelity of the target entangling operation. We demonstrate how the exclusive use of discrete shifts in the phase of the field moderating the qubit-oscillator interaction is sufficient to both ensure multiple oscillator modes are decoupled and to suppress the effects of fluctuations in the driving field. This approach is amenable to a wide variety of technical implementations including geometric phase gates in superconducting qubits and the Molmer-Sorensen gate for trapped ions. We present detailed example protocols tailored to trapped-ion experiments and demonstrate that our approach has the potential to enable multi-qubit gate implementation with a significant reduction in technical complexity relative to previously demonstrated protocols.

The contents of this chapter have been published as: T. Green and M. J. Biercuk, “Phase-modulated decoupling and error suppression in qubit-oscillator systems”, *Physical Review Letters* **114**, 120502 (2015). This work follows on from section 8.5.1 of the last chapter, in which entanglement generation was briefly discussed. Here we show that, in a more controlled environment, entangling operations can be generated much more efficiently and reliably.

### 9.1 Introduction

A key requirement for scalable QIP is the ability to controllably produce high-fidelity multi-particle entanglement on demand. This is accomplished in experimental systems using a variety of techniques, but a prominent approach relies on the realization of an indirect interaction between basic quantum systems (here qubits) mediated by bosonic oscillator modes [229, 230, 231, 232, 233, 234]. A significant source of infidelity in these experiments is the presence of residual qubit-oscillator entanglement at the conclusion of an interaction period, leading to decoherence and a degradation of the fidelity of entanglement generation. Therefore, the ability to effectively and efficiently disentangle qubits from bosonic modes is vital for many modern experimental implementations of entangling QIP operations.

In this chapter, we describe a simple technique to decouple qubits from multiple intermediary bosonic modes in order to improve entangling-gate fidelity. The technique is based solely on

technologically simple, discrete shifts in the phase of the field that mediates the qubit-oscillator coupling. We present a generalized theoretical framework permitting construction of protocols providing suppression of residual qubit-oscillator couplings in a densely packed mode structure. In addition to ensuring that all excited modes are decoupled under ideal operating conditions, we demonstrate how the same framework allows decoupling of each mode to arbitrary order when noise leads to imperfect evolution of the composite system. We first present a generic description of the method and then demonstrate its application in the context of Molmer-Sorensen (MS) gates for trapped-ion qubit pairs embedded in a linear chain [235], where residual coupling of ion internal states to multiple modes of motion leads to reduced gate fidelity. This method complements existing optimal-control techniques [236, 237], but reduces technical complexity in gate implementation, permits suppression of noise in the drive, and has the potential to achieve the same decoupling operation in a shorter time.

## 9.2 Theoretical model

We model the dynamical evolution of a compound system of  $N$  qubits ( $\mathcal{S}$ ) coupled to  $M$  bosonic oscillator modes ( $\mathcal{B}$ ) via the interaction Hamiltonian

$$H_{\mathcal{S}\mathcal{B}}(t) = i\hbar \sum_{\mu=1}^N \sigma_{\varsigma}^{\mu} \sum_{k=1}^M \left( \gamma_k^{\mu}(t) a_k^{\dagger} - \gamma_k^{\mu*}(t) a_k \right). \quad (9.1)$$

Here  $\sigma_{\varsigma}^{\mu}$  is a Pauli spin operator acting on the state of the  $\mu$ -th qubit, in a ‘direction’ defined by the subscript  $\varsigma \in \{x, y, z\}$ , while  $a_k^{\dagger}$  ( $a_k$ ) acts on  $\mathcal{B}$  creating (annihilating) a single bosonic excitation of the  $k$ -th oscillator mode. Each of the complex-valued functions  $\gamma_k^{\mu}(t)$  has the general form

$$\gamma_k^{\mu}(t) = f_k^{\mu} e^{i\delta_k t} r(t; \tau), \quad (9.2)$$

where  $\delta_k$  is the excitation frequency of the  $k$ -th mode and the coupling constant  $f_k^{\mu}$  quantifies the strength of its interaction with the  $\mu$ -th qubit. The function  $r(t; \tau) = \Theta[t]\Theta[\tau-t]e^{-i\phi(t)}$  represents an externally controlled temporal modulation of the coupling phase  $\phi(t)$ , implemented over an interval  $t \in [0, \tau]$ . During this time, the Hamiltonian (9.1) is effectively ‘switched on’, generating the unitary operation

$$U(\tau) = \exp \left\{ \sum_{\mu=1}^N \sigma_{\varsigma}^{\mu} B_{\mu}(\tau) + i \sum_{\mu, \nu=1}^N \varphi_{\mu\nu}(\tau) \sigma_{\varsigma}^{\mu} \sigma_{\varsigma}^{\nu} \right\}. \quad (9.3)$$

For  $N > 1$ ,  $\varphi_{\mu\nu}(\tau) \equiv \sum_k \text{Im} \int_0^{\tau} dt_1 \int_0^{t_1} dt_2 \gamma_k^{\mu}(t_1) \gamma_k^{\nu*}(t_2)$  represents an effective coupling between qubits  $\mu$  and  $\nu$  ( $\mu \neq \nu$ ) that arises due to the state-dependent displacement of the oscillator system in phase-space, given by

$$B_{\mu}(\tau) \equiv \sum_{k=1}^M [f_k^{\mu} \alpha_k(\tau) a_k^{\dagger} - f_k^{\mu*} \alpha_k^*(\tau) a_k], \quad (9.4)$$

where

$$\alpha_k(\tau) \equiv \int_0^{\infty} dt e^{i\delta_k t} r(t; \tau). \quad (9.5)$$

While the coupling interaction presented here is generic, it is frequently executed using a controlled periodic driving field. In this context, the excitation frequency  $\delta_k$  is realized via a detuning between the frequency of the driving field and a sideband associated with the  $k$ -th motional

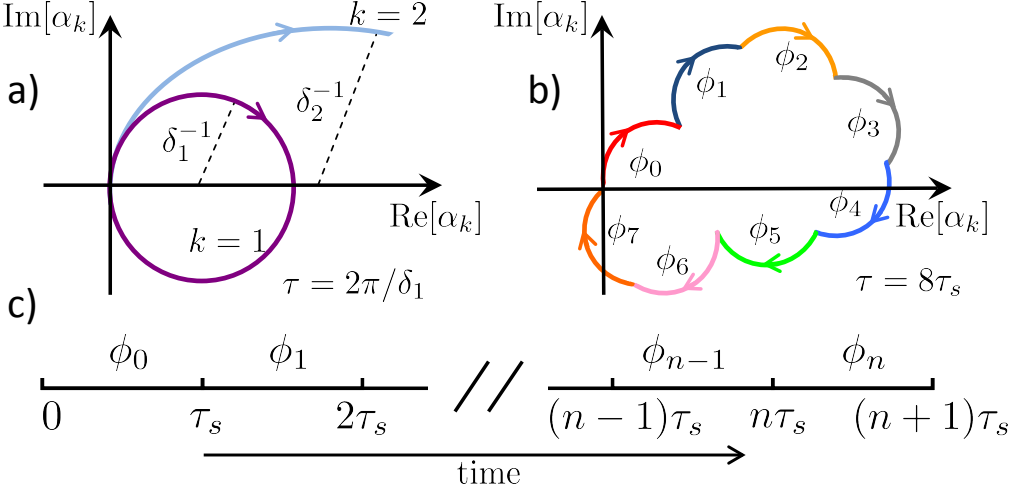


Figure 9.1: a) Schematic plots of  $\alpha_k(t)$ ,  $0 \leq t \leq \tau$ , for two modes,  $k = 1, 2$ . Each path represents  $N$  phase-space trajectories  $\alpha_k^\mu(t) = f_k^\mu \alpha_k(t)$ , for  $\mu = 1, \dots, N$ . Here  $\tau = 2\pi/\delta_1$ , so that the path labeled  $k = 1$  closes. b) An illustrative example of single closed path, generated by an eight-interval, piecewise-constant phase modulation sequence. c) Timing schematic for piecewise-constant phase modulation sequence, comprising a total of  $n$  instantaneous phase shifts. For the general  $M$  mode decoupling sequence (9.9)  $n = 2^M - 1$ .

mode (formally due to a transformation to the interaction picture with respect to the free Hamiltonian). The coupling strength  $f_k^\mu$  is determined by the magnitude of the field, and  $\phi(t)$  by its phase.

Any residual qubit-oscillator entanglement at time  $\tau$  will result in qubit decoherence and must, therefore, be suppressed in order to achieve a high-fidelity entangling operation. Complete qubit-oscillator decoupling occurs if

$$\alpha_k(\tau) \equiv \int_0^\infty dt e^{i\delta_k t} r(t; \tau) = 0 \quad (9.6)$$

for  $k = 1, \dots, M$ . Each of the time-parameterized functions  $\alpha_k(t)$ ,  $0 \leq t \leq \tau$ , defines a set of  $N$  phase space trajectories  $\alpha_k^\mu(t) = f_k^\mu \alpha_k(t)$ , for  $\mu = 1, \dots, N$ , associated with the  $k$ -th oscillator mode (figure 9.1). These trajectories vary in extent and orientation, according to the complex coupling constant  $f_k^\mu$ . However, by satisfying the condition (9.6) all trajectories are closed at  $t = \tau$ .

Decoupling from any particular mode  $k$  can be achieved by fixing the control phase at a constant value (which can be taken to be zero) and setting the total operation time and coupling-drive detuning such that  $\delta_k \tau = 2\pi j$ , for  $j \in \{1, 2, \dots\}$  (figure 9.1a). Simultaneous decoupling from any of the remaining modes is possible only if the associated detunings are commensurate with  $\delta_k$ . This can be difficult to engineer, even approximately, for more than one additional mode without the need to resort to undesirably long gate times [236, 237].

Modulation of the relevant control, as demonstrated recently [237], provides a path to simultaneously realizing the decoupling condition for multiple modes, and any of the parameters of the driving field may in principle be varied in time in order to achieve the necessary condition. Unlike previous work, our method fixes both the frequency of the drive (hence  $\delta_k$ ) as well as the coupling strength  $f_k^\mu$  during the interaction period, and treats only the drive phase  $\phi(t)$  as a tunable parameter. In the following, we demonstrate that the freedom to modulate  $\phi(t)$  via

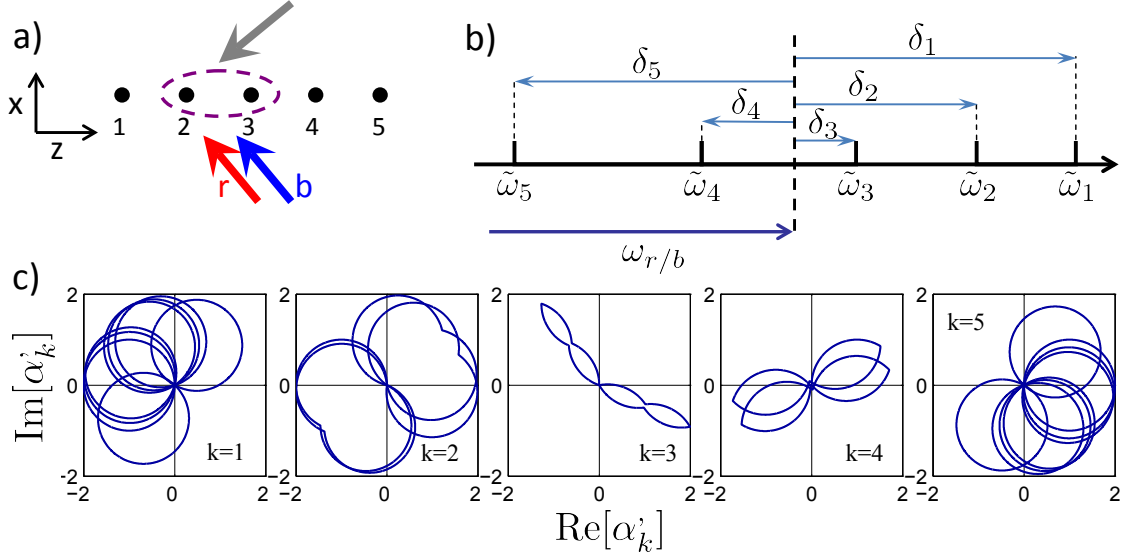


Figure 9.2: a) Raman laser geometry for a MS gate applied to 2 ions in a 5 ion chain in which only transverse ( $x$ -direction) phonon modes are excited. The red ( $r$ ) and blue ( $b$ ) Raman fields have frequencies  $\omega_r/b$  and phases  $\phi_{r/b}$ . b) Detuning diagram for 5 excited TP modes,  $\tilde{\omega}_k = \omega_0 \pm \omega_k$  (+ for  $\omega_b$  and - for  $\omega_r$ ), where  $\omega_0$  is the hyperfine qubit level splitting. c) Closed paths,  $\alpha'_k \equiv |\delta_k| \alpha_k(t)$ ,  $0 \leq t \leq \tau$ , (normalized by  $|\delta_k|$ ) for the detunings shown in b), generated by 7 discrete phase shifts.

discrete shifts, easily implemented using state-of-the-art digital frequency synthesis technology, may be used to impose a commensurate periodicity on the full set of phase-space paths so that they all close simultaneously at an (in principle) arbitrary time  $\tau$ .

The key to the method lies in the observation that any open phase space trajectory may be closed by repeating the sequence that produced it, with an appropriate overall phase shift. To describe this process of ‘phase-compensated’ concatenation mathematically, we define a family of *nonlinear* operators  $R_\delta$ , parameterized by the real number  $\delta$ , that act to extend any phase modulation sequence  $r(t; \tau')$ , defined over the interval  $[0, \tau']$ , to the interval  $[0, 2\tau']$  in the following way

$$R_\delta r(t; \tau') = r(t; \tau') + e^{-i(\delta\tau' - \pi)} r(t - \tau'; \tau'). \quad (9.7)$$

The function  $r(t; 2\tau') \equiv R_{\delta_k} r(t; \tau')$  then describes a sequence for which  $\alpha_k(2\tau') = 0$ .

The qubit system may be simultaneously decoupled from all  $M$  modes by implementing the piecewise-constant phase modulation sequence

$$r_{\delta_M \dots \delta_1}(t; 2^M \tau_s) \equiv R_{\delta_M} \dots R_{\delta_1} r_0(t; \tau_s), \quad (9.8)$$

starting with the trivial ‘no-operation’ base sequence  $r_0(t; \tau_s) = \Theta[t] \Theta[\tau_s - t]$ , for which  $\phi(t) \equiv 0$  over an arbitrary interval  $[0, \tau_s]$ . This sequence, applied over discrete timesteps of duration  $\tau_s$ , indexed by  $\ell$ , may be written explicitly as

$$r_{\delta_M \dots \delta_1}(t; 2^M \tau_s) = \sum_{\ell=0}^{2^M-1} r_0(t - \ell\tau_s; \tau_s) e^{-i\phi_\ell} \quad (9.9)$$

where

$$\phi_\ell = \sum_{j=0}^q \varepsilon_j(\ell) 2^j \delta_{j+1} \tau_s - s(\ell) \pi \quad (9.10)$$

is the requisite phase value for the time interval  $[\ell\tau_s, (\ell + 1)\tau_s]$  (see figure 9.1c). In this expression,  $\varepsilon_q(\ell)\varepsilon_{q-1}(\ell)\dots\varepsilon_0(\ell)$  is the binary representation of  $\ell$  and  $s(\ell) \equiv \sum_{j=0}^q \varepsilon_j(\ell)$  is its Hamming weight. As an example, the binary representation of  $\ell = 6$  is 110, so that  $q = 2$ ,  $\varepsilon_0(\ell) = 0$ ,  $\varepsilon_1(\ell) = 1$ ,  $\varepsilon_2(\ell) = 1$ , and  $s(\ell)=2$ . The resulting ‘entangling phases’  $\varphi_{\mu\nu}$  can then be calculated for these phase values (see *Appendix*), and the strength of the driving field adjusted to generate target values  $\varphi_{\mu\nu}^{(0)}$ , for  $\mu, \nu = 1, \dots, N$  and  $\mu \neq \nu$ .

Ideally, the decoupling condition (9.6) should also be met in the presence of time-domain variations in the coupling parameters defining phase-space trajectories. When only a single oscillator mode is coupled to the qubit system, discrete bivalued phase modulation in the form of simple binary ( $\pm 1$ ) concatenated dynamical decoupling (CDD) sequences [64, 46] has been shown to suppress errors due to thermal dissipation [238] and static detuning offsets [167]. In terms of our formalism, these sequences are generated by recursive application of the operator  $R_0 \equiv R_{\delta=0}$  to the simple no-operation base sequence  $r_0(t; \tau_s)$ , with the proviso that the step time  $\tau_s$  is chosen to coincide with the periodic evolution of the mode, i.e.,  $\delta_k \tau_s = 2\pi j$ , for  $j = \{1, 2, \dots\}$ .

The restriction on the allowable values of  $\tau_s$  leads to proscription against direct application of CDD sequences for multiple modes. We observe that by relaxing the binary-valued constraint on  $\phi(t)$ , phase compensated CDD sequences, targeting noise associated with *particular modes*, may be realized. Specifically, we consider noise that may be represented by a function  $\beta_k(t)$  that modifies the spin-oscillator coupling via  $\gamma_k^\mu(t) \rightarrow \gamma_k^\mu(t)\beta_k(t)$  (the subscript  $k$  allows for the possibility of mode dependence.) This model encompasses a number of important noise sources, including: frequency ( $\delta_k$ ) errors, thermal dissipation of oscillator modes and fluctuations in the strength of the qubit-oscillator interaction. We suppose that in the weak/slowly varying noise limit  $\beta_k(t)$  may be approximated by a  $p$ -th order polynomial

$$\beta_k^{(p)}(t) = \sum_{j=0}^p \beta_{k,j} t^j. \quad (9.11)$$

In the presence of such noise, the decoupling condition for the  $k$ -th mode *to order*  $p + 1$  is

$$\alpha_k^{(p+1)}(\tau) \equiv \int_0^\infty dt e^{i\delta_k t} r(t; \tau) \beta_k^{(p)}(t) = 0. \quad (9.12)$$

for  $p \geq 0$ .

Mathematically, binary CDD sequences are essentially time-domain representations of finite iterations of the infinite Thue-Morse (TM) sequence [239, 240]. From the perspective of noise suppression, the most interesting property of the TM sequence is that the  $(p + 1)$ -th iteration  $r(t; 2^{p+1}\tau_s) \equiv R_0^{p+1}r_0(t; \tau_s)$  is orthogonal to any  $p$ -th degree polynomial  $\beta^{(p)}(t) = \sum_{j=0}^p \beta_j t^j$ , i.e.,  $\int_0^\infty dt r(t; 2^{p+1}\tau_s) \beta^{(p)}(t) = 0$  [241]. Using this insight, and despite the fact that we have relaxed the binary-value restriction on  $\phi(t)$ , it can be shown (see *Appendix*) that the phase-compensated TM/CDD sequence

$$r(t; (n + 1)\tau_s) \equiv R_{\delta_k}^{p+1}r_0(t; \tau_s) = \sum_{\ell=0}^n r_0(t - \ell\tau_s; \tau_s) e^{-i\phi_\ell}, \quad (9.13)$$

where  $n = 2^{p+1} - 1$  and  $\phi_\ell = \ell\delta_k\tau_s - s(\ell)\pi$ , will achieve  $\alpha_k^{(p+1)}(2^{p+1}\tau_s) = 0$ .

The general properties of concatenated control sequences may now be brought to bear in providing simultaneous high-order mode decoupling in the presence of time-varying coupling parameters. To suppress noise across multiple modes, one may construct a phase modulation sequence of the general form  $R_{\delta_{k_q}} \dots R_{\delta_{k_2}} R_{\delta_{k_1}} r_0(t; \tau_s)$ , where the *order of error suppression*

Interval	Phase
$\ell$	$\phi_\ell$
0	0
1	$\delta_1 \tau_s - \pi = \pi$
2	$2\delta_2 \tau_s - \pi \simeq 1.694\pi$
3	$\delta_1 \tau_s + 2\delta_2 \tau_s - 2\pi \simeq 1.694\pi$
4	$4\delta_3 \tau_s - \pi \simeq 0.4803\pi$
5	$\delta_1 \tau_s + 4\delta_3 \tau_s - 2\pi \simeq 1.4803\pi$
6	$2\delta_2 \tau_s + 4\delta_3 \tau_s - 2\pi \simeq 2.175\pi$
7	$\delta_1 \tau_s + 2\delta_2 \tau_s + 4\delta_3 \tau_s - 3\pi \simeq 3.175\pi$

Table 9.1: *Example phase-modulation sequence.*

associated with mode  $k_i$  is determined by the number of times  $k_i$  appears in the sequence indices  $(k_1, k_2, \dots, k_q)$ . For example,  $R_{\delta_3} R_{\delta_2} R_{\delta_3} R_{\delta_1} r_0(t; \tau_s)$  will close all trajectories associated with the first three modes, providing additional error suppression to second order for mode  $k = 3$ . The order in which the operators are best applied will depend on the properties of the noise: in particular the extent to which the noise varies with  $k$ . Vitally, in the presence of any such modulation protocol it remains possible to analytically calculate the entangling phase  $\varphi_{\mu\nu}(\tau)$  for arbitrary qubit-pair  $\mu - \nu$  and to adjust  $f_k^{\mu(\nu)}$  appropriately.

### 9.3 Entangling phases for a piecewise-constant phase-modulation sequence

A piecewise-constant phase-modulation sequence defined over  $n + 1$  subintervals  $\ell = 0, \dots, n$ , each of equal duration  $\tau_s$ , is described by the function

$$r(t; (n+1)\tau_s) = \sum_{\ell=0}^{2^M-1} r_0(t - \ell\tau_s; \tau_s) e^{-i\phi_\ell}. \quad (9.14)$$

Substituting this into the expression for the ‘entangling phase’

$$\varphi_{\mu\nu}(\tau) = \sum_k \text{Im} \int_0^\tau dt_1 \int_0^{t_1} dt_2 \gamma_k^\mu(t_1) \gamma_k^{\nu*}(t_2), \quad (9.15)$$

where  $\gamma_k^\mu(t) = f_k^\mu e^{i\delta_k t} r(t; \tau)$ , we find that

$$\varphi_{\mu\nu}(\tau) = \sum_k \frac{1}{\delta_k^2} \{2(1 - \cos \delta_k \tau_s) A_k^{\mu\nu} + B_k^{\mu\nu}\} \quad (9.16)$$

with

$$A_k^{\mu\nu} \equiv \sum_{\ell=1}^n \sum_{\ell' < \ell} \text{Im} \left\{ f_k^\mu f_k^{\nu*} e^{i[(\ell-\ell')\delta_k \tau_s - \phi_\ell + \phi_{\ell'}]} \right\} \quad (9.17)$$

and

$$B_k^{\mu\nu} \equiv (n+1)\text{Im} \left\{ f_k^\mu f_k^{\nu*} (i\delta_k \tau_s - e^{i\delta_k \tau_s} + 1) \right\}. \quad (9.18)$$

## 9.4 Example implementation

For concreteness, we now consider the task of entangling the internal states of a pair of adjacent trapped ions embedded in an  $N > 2$  ion chain. Under certain simplifying assumptions, the effect of a state-dependent force generated by a bichromatic light field is well described by the Hamiltonian (9.1) [230, 242, 243]. Effective spin-1/2 manifolds realized within the electronic states of each of the ions comprise the system of qubits  $\mathcal{S}$ , and the shared vibrational modes of the ions in a confining potential constitute the oscillator system  $\mathcal{B}$ . The qubit-oscillator coupling strength  $f_k^\mu$  is proportional to the amplitude of the Raman fields (see *Appendix* for further details). The relevant control phase  $\phi(t)$  is determined by the difference between the phases of the red and blue Raman fields, and can be varied without altering the spin-dependence of the entangling gate. Most importantly, in this setting,  $\phi(t)$  inherits all the flexibility and precision provided by modern laser control systems. In particular, the discrete phase shifts required for the basic decoupling sequence (9.9) can be implemented quasi-instantaneously and with high accuracy using standard optical modulators driven by radiofrequency sources.

In implementing a Molmer-Sorensen (MS) entangling gate [230], in particular, the target ions are simultaneously illuminated by two off-resonant Raman laser fields with beat notes symmetrically detuned from motional sidebands on the qubit carrier frequency  $\omega_0$  such that  $\delta_k = \omega_b - (\omega_0 + \omega_k) = (\omega_0 - \omega_k) - \omega_r$ . Here  $\omega_k$  denotes the frequency of the  $k$ -th motional mode and the subscripts  $b/r$  denote the blue ( $b$ ) and red ( $r$ ) Raman sidebands. This bichromatic field creates state-dependent forces on the illuminated ions that generate an effective interaction between the otherwise independent internal ion states [230, 242, 243]. The qubit-oscillator coupling strength  $f_k^\mu = -i\Omega_\mu \eta_{\mu,k}/2$  is determined by the Rabi frequency  $\Omega_\mu$ , which is itself proportional to the common amplitude of the Raman fields, and by the dimensionless Lamb-Dicke parameter  $\eta_{\mu,k}$  [248].

The spin dependence of the gate (i.e., the subscript  $\varsigma$  in equation (9.1)) is decided by sum  $\phi_s(t) = [\phi_b(t) + \phi_r(t)]/2$  of the phases of the red and blue Raman fields, while the control phase  $\phi(t)$  (usually called the ‘motional phase’) is given by their difference  $\phi(t) = [\phi_b(t) - \phi_r(t)]/2$ . By ensuring that the red and blue phases always have opposite sign, the control phase  $\phi(t) \equiv \phi_b(t) = -\phi_r(t)$  and can be varied without altering the spin dependence (here  $\varsigma = x$ ).

Assuming a common Rabi rate  $\Omega = \Omega_1 = \Omega_2$ , the time-evolution operator for the two-qubit MS gate with piece-constant phase-modulation is

$$U(\tau) = \exp \left\{ \sum_{\mu=1}^2 \sigma_x^\mu B_\mu(\tau) + 2i\varphi_{12}(\tau) \sigma_x^1 \sigma_x^2 \right\} \quad (9.19)$$

where  $B_\mu(\tau) \equiv \sum_{k,\ell} [\alpha_{k,\ell}^\mu(\tau) a_k^\dagger - \alpha_{k,\ell}^{\mu*}(\tau) a_k]$ , where

$$\alpha_{k,\ell}^\mu(\tau) \equiv -\frac{\Omega \eta_{\mu,k}}{2\delta_k} e^{i(\delta_k \tau_s - \phi_\ell)} (e^{i\delta_k \tau_s} - 1). \quad (9.20)$$

The entangling phase  $\varphi_{12}(\tau)$  is given by equation (9.16), where now

$$A_k^{12} = \frac{\Omega^2 \eta_{k,1} \eta_{k,2}}{4} \sum_{\ell=1}^n \sum_{\ell' < \ell} \sin[(\ell - \ell') \delta_k \tau_s - \phi_\ell + \phi_{\ell'}] \quad (9.21)$$

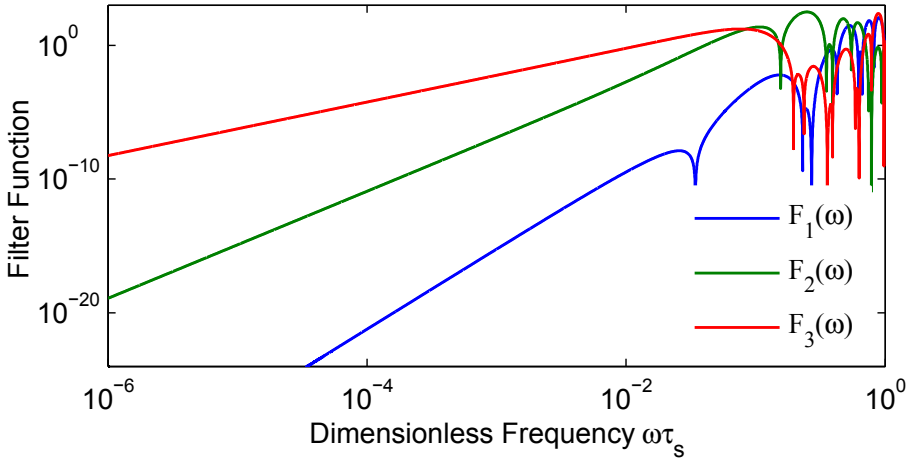


Figure 9.3: *Laser amplitude noise filter functions for 3 excited oscillator modes  $k = 1, 2, 3$ . The effect of the noise on the coupling to each mode is suppressed to third order for  $k = 1$  ( $F_1(\omega) \propto \omega^3$  as  $\omega \rightarrow 0$ ), second order for  $k = 2$  ( $F_2(\omega) \propto \omega^2$ ), and first order for  $k = 3$  ( $F_3(\omega) \propto \omega$ ).*

and

$$B_k^{12} = (n+1) \frac{\Omega^2 \eta_{k,1} \eta_{k,2}}{4} (\delta_k \tau_s - \sin \delta_k \tau_s). \quad (9.22)$$

Figure 9.2. shows closed mode trajectories representing the complete decoupling of a pair of  $^{171}\text{Yb}^+$  hyperfine qubits from five excited transverse phonon modes [244], using phase-shifts derived from equation (9.9). In this illustrative example, we set the laser frequencies so that two modes have commensurate detunings and choose  $\tau_s = 2\pi/\delta_{1,5}$  to match the period of the associated phase space evolution. In this way, a sequence of only  $n = 7$  phase shifts is required to decouple the qubits from all 5 modes, rather than the more general sequence of  $n = 31$  phase shifts. Table 9.1 lists the eight phase values  $\phi_\ell$ , for  $\ell = 0, \dots, 7$ , calculated using equation (9.9) and assuming equivalent physical parameters to recent demonstrations of multimode decoupling using optimized amplitude modulation [237]. Execution of this sequence results in the complete decoupling of a pair of  $^{171}\text{Yb}^+$  hyperfine qubits from five excited transverse phonon (TP) modes. The associated detunings are  $\delta_k = 2\pi \times \{59.77\text{kHz}, 40.26\text{kHz}, 11.06\text{kHz}, -20.07\text{kHz}, -59.77\text{kHz}\}$ . The laser frequencies have been chosen such that modes  $k = 1, 5$  have equal detunings and  $\tau_s = 2\pi/\delta_{1,5}$  matches the period of the associated phase space evolution.

The resulting phase-modulated gate has duration  $\tau \sim 140 \mu\text{s}$  which compares favorably with the reported value of  $\tau = 190 \mu\text{s}$ , while obviating considerations of nonlinear amplitude responses in optical modulators and rf amplifiers. Faster gate times may be achieved, at the expense of a greater number of phase shifts, by allowing  $\tau_s$  to vary arbitrarily. This freedom to vary the step time the step time may also be used to ‘tune’ the phase-modulation protocol with the aim of mitigating additional decoherence effects that, while not accounted for in the model Hamiltonian, will nonetheless negatively impact gate fidelity in practice.

We also demonstrate the effectiveness of phase modulation sequences in suppressing decoupling errors induced by laser amplitude noise, a prominent time-dependent gate error. We assume that a pair of qubits to be entangled is initially in an ‘evenly weighted’ separable pure state, such as

$$|11\rangle_z = (|00\rangle_x + |11\rangle_x - |01\rangle_x - |10\rangle_x)/2 \quad (9.23)$$

(the subscripts indicate the particular eigenbasis) and then quantify the extent of residual entanglement between the internal and vibrational ion states by calculating the linear entropy or ‘purity loss’

$$\bar{P} \equiv 1 - \text{Tr}[\rho_S^2(\tau)], \quad (9.24)$$

where  $\rho_S(\tau)$  is the final qubit state obtained by tracing out the vibrational degrees of freedom [245, 246].

The laser amplitude instability is modeled as a time-dependent contribution to the Rabi rate  $\Omega(t) = \Omega_0 + \Omega_e(t)$ , where  $\Omega_0$  is the ideal value and  $\Omega_e(t)$  represents the noise (we assume the Rabi rate is the same for the two adjacent ions). As  $\Omega_e(t)$  is a stochastic process, we average over the ensemble of noise realizations ( $\mathbb{E}[\dots]$ ) to obtain our final metric (see *Appendix* for a derivation)

$$\mathbb{E}[\bar{P}] \approx \frac{1}{8\pi} \int_{-\infty}^{\infty} d\omega S_{\Omega_e}(\omega) F(\omega) \quad (9.25)$$

Here,  $S_{\Omega_e}(\omega)$  represents the power spectral density of amplitude fluctuations as a function of frequency  $\omega$ . This expression assumes the weak noise limit in which only the first-order effect of amplitude fluctuations is significant, and assumes that phase modulation results in complete decoupling in the *absence* of noise.

The effect of the phase modulation is captured by the expression

$$F(\omega) \equiv \sum_k D_k F_k(\omega), \quad (9.26)$$

with  $D_k$  a constant. The ‘modal filter function’

$$F_k(\omega) \equiv \left| \int_0^{\infty} dt e^{i(\omega+\delta_k)t} r(t; \tau) \right|^2 \quad (9.27)$$

provides a frequency-domain representation of the phase modulation sequence  $r(t; \tau)$ , following insights presented in [49, 108]. It captures the effectiveness of the phase-modulation protocol in suppressing laser amplitude noise for different modes; a higher ‘slope’ on a log-log plot indicates higher order ( $p$ ) suppression of time-dependent fluctuations. This general filter-function framework provides a formalism for assessing the robustness of complex control protocols against arbitrary time-varying noise. The approach has recently been validated by a range of single-qubit experiments [32, 228], and has been extended here to qubit-oscillator and qubit-qubit interactions.

In figure 9.3 we plot  $F_k(\omega)$  calculated for specific, but arbitrarily chosen, orders associated with each of three modes,  $k = 1, 2, 3$ . By increasing the level of concatenation for specific modes we are able to improve qubit-oscillator decoupling through the suppression of low-frequency amplitude fluctuations *while simultaneously ensuring all modes are efficiently decoupled*. In general,  $D_k$  depends on the initial qubit state  $|\phi_0\rangle$  and the effective temperature, in addition to the frequency of the  $k$ -th mode  $\omega_k$ . Here, where we consider only the collective zero temperature limit and the particular initial state  $|\phi_0\rangle = |11\rangle_z$ .

## 9.5 Conclusion

In summary, we have presented a unified framework for improving entangling gate fidelity in qubit-oscillator systems by ensuring efficient decoupling of intermediary bosonic modes. Our framework permits simultaneous decoupling of multiple oscillator modes using only sequences of discrete phase shifts, and may also be combined with concatenation procedures to include

robustness against time-dependent control noise. The approach complements and provides substantial benefits relative to existing techniques, leveraging the technical simplicity of phase modulation in RF electronics. It also mitigates the need to account for nonlinearities in the response of modulating hardware (such as acousto-optic modulators for laser beams) or variations in residual light shifts endemic to Raman-mediated trapped-ion gates. Overall we hope that this phase-modulation approach to improving entangling gate fidelities will prove useful in a range of quantum information settings across different qubit-oscillator systems. We are also excited by the possibility that similar approaches may be employed to effectively modify the entangling phase between different qubits in a multipartite system, or be employed to improve the performance of quantum-enhanced sensors [247].

*Acknowledgements:* The authors thank L. Viola, S.-W. Lee, G. Paz-Silva, and K. R. Brown for useful discussions on dynamical decoupling as well as C. Monroe and J. Kim for useful discussions of motional mode structure and decoupling in linear ion traps. This work partially supported by the Australian Research Council Centre of Excellence for Engineered Quantum Systems CE110001013, the Office of the Director of National Intelligence (ODNI), Intelligence Advanced Research Projects Activity (IARPA), through the Army Research Office, the Lockheed Martin Corporation, and a private grant from Hugh and Anne Harley.

## 9.6 Appendix

### Phase compensated TM sequences

The  $\ell$ -th element of the infinite Thue-Morse (TM) sequence  $(\mathfrak{T}_\ell)_{\ell \geq 0}$ , defined over the two letter alphabet  $\{-1, 1\}$ , is given by  $\mathfrak{T}_\ell = (-1)^{s(\ell)}$ , where  $s(\ell)$  is the Hamming weight of the binary representation of the integer  $\ell$ . Successive finite iterations of the sequence may be generated in the time domain through repeated application of the operator  $R_0$  to the function  $r_0(t; \tau_s)$  (see main text for definitions). The  $(p+1)$ -th iteration

$$r(t; 2^{p+1}\tau_s) \equiv R_0^{p+1} r_0(t; \tau_s) \quad (9.28)$$

is orthogonal to any  $p$ -th degree polynomial  $\beta^{(p)}(t) = \sum_{j=0}^p \beta_j t^j$ , i.e.,  $\int_0^\infty dt r(t; 2^{p+1}\tau_s) \beta^{(p)}(t) = 0$ . This is a special case of the more general result that

$$\int_0^\infty dt e^{i\delta t} r(t; 2^{p+1}\tau_s) \beta^{(p)}(t) = 0 \quad (9.29)$$

where  $r(t; 2^{p+1}\tau_s) \equiv R_\delta^{p+1} r_0(t; \tau_s)$ , which we prove by induction.

Showing the result to be true for  $p = 0$  is simply a matter of direct substitution into (9.29). Now assume (9.29) holds for  $p = q$ , where  $q$  is an arbitrary positive integer. In that case, it must hold for the  $q$ -th degree polynomial  $\beta^{(q)}(t) \equiv \beta^{(q+1)}(t) - \beta^{(q+1)}(t + 2^{q+1}\tau_s)$ . That is,

$$\begin{aligned} & \int_0^\infty dt e^{i\delta t} r(t; 2^{q+1}\tau_s) \beta^{(q+1)}(t) \\ & - \int_0^\infty dt e^{i\delta t} r(t; 2^{q+1}\tau_s) \beta^{(q+1)}(t + 2^{q+1}\tau_s) = 0 \end{aligned} \quad (9.30)$$

Making the substitution  $t \rightarrow t + 2^{q+1}\tau_s$  in the second integral, we find that we can write

$$\int_0^\infty dt e^{i\delta t} r(t; 2^{q+2}\tau_s) \beta^{(q+1)}(t) = 0 \quad (9.31)$$

where  $r(t; 2^{q+2}\tau_s) \equiv R_\delta^{q+2}r_0(t; \tau_s)$ . Thus, if (9.29) holds for  $q$ , it also holds for  $q + 1$  and the proof is complete.

To implement the MS gate, the target ions are simultaneously illuminated by two off-resonant Raman laser fields with beat notes symmetrically detuned from motional sidebands on the qubit carrier frequency  $\omega_0$  such that  $\delta_k = \omega_b - (\omega_0 + \omega_k) = (\omega_0 - \omega_k) - \omega_r$ . Here  $\omega_k$  denotes the frequency of the  $k$ -th motional mode and the subscripts  $b/r$  denote the blue ( $b$ ) and red ( $r$ ) Raman sidebands. This bichromatic field creates state-dependent forces on the illuminated ions that generate an effective interaction between the otherwise independent internal ion states [230, 242, 243]. The qubit-oscillator coupling strength  $f_k^\mu = -i\Omega_\mu\eta_{\mu,k}/2$  is determined by the Rabi frequency  $\Omega_\mu$ , which is itself proportional to the common amplitude of the Raman fields, and by the dimensionless Lamb-Dicke parameter  $\eta_{\mu,k}$  [248].

The spin dependence of the gate (i.e., the subscript  $\varsigma$  in equation (9.1)) is decided by sum  $\phi_s(t) = [\phi_b(t) + \phi_r(t)]/2$  of the phases of the red and blue Raman fields, while the control phase  $\phi(t)$  (usually called the ‘motional phase’) is given by their difference  $\phi(t) = [\phi_b(t) - \phi_r(t)]/2$ . By ensuring that the red and blue phases always have opposite sign, the control phase  $\phi(t) \equiv \phi_b(t) = -\phi_r(t)$  and can be varied without altering the spin dependence (here  $\varsigma = x$ ).

Assuming a common Rabi rate  $\Omega = \Omega_1 = \Omega_2$ , the time-evolution operator for the two-qubit MS gate with piece-constant phase-modulation is

$$U(\tau) = \exp \left\{ \sum_{\mu=1}^2 \sigma_x^\mu B_\mu(\tau) + 2i\varphi_{12}(\tau) \sigma_x^1 \sigma_x^2 \right\} \quad (9.32)$$

where  $B_\mu(\tau) \equiv \sum_{k,\ell} [\alpha_{k,\ell}^\mu(\tau) a_k^\dagger - \alpha_{k,\ell}^{\mu*}(\tau) a_k]$ , where

$$\alpha_{k,\ell}^\mu(\tau) \equiv -\frac{\Omega\eta_{\mu,k}}{2\delta_k} e^{i(\delta_k\tau_s - \phi_\ell)} (e^{i\delta_k\tau_s} - 1). \quad (9.33)$$

The entangling phase  $\varphi_{12}(\tau)$  is given by equation (9.16), where now

$$A_k^{12} = \frac{\Omega^2 \eta_{k,1} \eta_{k,2}}{4} \sum_{\ell=1}^n \sum_{\ell' < \ell} \sin[(\ell - \ell')\delta_k\tau_s - \phi_\ell + \phi_{\ell'}] \quad (9.34)$$

and

$$B_k^{12} = (n+1) \frac{\Omega^2 \eta_{k,1} \eta_{k,2}}{4} (\delta_k\tau_s - \sin \delta_k\tau_s). \quad (9.35)$$

## Ensemble average purity loss

The MS time-evolution operator (in the  $\varsigma = x$  basis) may be written as  $U(\tau) = U_1(\tau)U_2(\tau)$ , where

$$U_1(\tau) = \exp \left\{ \sum_{\mu} \sigma_x^\mu \sum_k [\alpha_k^\mu(\tau) a_k^\dagger - \alpha_k^{\mu*}(\tau) a_k] \right\} \quad (9.36)$$

and  $U_2(\tau) = e^{i\varphi(\tau)\sigma_x^1\sigma_x^2}$ . Here

$$\alpha_k^\mu(\tau) = \frac{-i\eta_k^\mu}{2} \int_0^\infty dt \Omega(t) e^{i\delta_k t} r(t; \tau) \quad (9.37)$$

and

$$\varphi(\tau) = \frac{1}{2} \sum_k \eta_k^\mu \eta_k^\nu \int_0^\tau dt_1 \Omega(t_1) \int_0^{t_1} dt_2 \Omega(t_2) \sin[\delta_k(t_1 - t_2) - (\phi(t_1) - \phi(t_2))] \quad (9.38)$$

We assume that the combined qubit-oscillator system is in a separable initial state  $|\psi_0\rangle\langle\psi_0| \otimes \rho_B$ , where

$$|\psi_0\rangle = \sum_{ij} c_{ij} |ij\rangle_x \quad (9.39)$$

is a pure two-qubit state (expanded in the  $x$  basis.). The final state is  $\rho_S(\tau) = U_2(\tau)\tilde{\rho}_S(\tau)U_2^\dagger(\tau)$ , where we've defined

$$\tilde{\rho}_S(\tau) \equiv \text{Tr}_B \left[ U_1(\tau) |\psi_0\rangle\langle\psi_0| \otimes \rho_B U_1^\dagger(\tau) \right] \quad (9.40)$$

Using the cyclic property of the trace, the purity loss may be written as  $\bar{P} = 1 - \text{Tr}[\tilde{\rho}_S^2(\tau)]$ . Substituting the expansion (9.39) and assuming the oscillator system is in a state  $\rho_B = \prod_k \rho_k$ , where  $\rho_k = e^{-\hbar\omega_k a_k^\dagger a_k / (k_B T_k)} / \text{Tr}_k[e^{-\hbar\omega_k a_k^\dagger a_k / (k_B T_k)}]$  ( $T_k$  is the effective temperature of the  $k$ -th mode), we can write

$$\tilde{\rho}_S = \sum_{ijlm} c_{ij} c_{lm}^* |ij\rangle\langle lm| e^{i\{s_m s_i - s_l s_j\} \sum_k \text{Im}(\alpha_k^1 \alpha_k^{2*})} e^{-\chi_{ijlm}} \quad (9.41)$$

where  $\chi_{ijlm} = \sum_k |\tilde{\alpha}_k|^2 \coth[\hbar\omega_k / (2k_B T_k)]/2$ ,  $\tilde{\alpha}_k = (s_i - s_l)\alpha_k^1(\tau) + (s_j - s_m)\alpha_k^2(\tau)$  and  $s_i = (-1)^i$  (the eigenvalue of  $\sigma_x$  for the state  $|i\rangle_x$ ). From this, we find that

$$\bar{P} = 1 - \sum_{ijlm} |c_{ij}|^2 |c_{lm}|^2 e^{-2\chi_{ijlm}} \quad (9.42)$$

We now write the noisy Rabi rate (which is assumed to be real) as  $\Omega(t) = \Omega_0 + \Omega_e(t)$ , where the function  $\Omega_e(t)$  describes fluctuations about the ideal value  $\Omega_0$ . Further, we consider only phase modulation sequences for which perfect decoupling would occur in the absence of noise, i.e.,  $\alpha_k^\mu(\tau) = 0$ , for  $\mu = 1, 2$  and  $k = 1, \dots, M$ , when  $\Omega_e(t) = 0$ . In that case,

$$\alpha_k^\mu(\tau) = \frac{-i\eta_k^\mu}{2} \int_0^\infty dt \Omega_e(t) e^{i\delta_k t} r(t; \tau) \quad (9.43)$$

and the exponent  $\chi_{ijlm}$  depends only on the noise  $\Omega_e(t)$  and not on  $\Omega_0$ .

We average over an ensemble of noise realizations to obtain the ensemble average ( $\mathbb{E}[\dots]$ ) purity loss

$$\mathbb{E}[\bar{P}] = 1 - \sum_{ijlm} |c_{ij}|^2 |c_{lm}|^2 \mathbb{E}[e^{-2\chi_{ijlm}}]. \quad (9.44)$$

Using the inequality  $e^x \geq 1 + x$ , we see that

$$\mathbb{E}[\bar{P}] \leq 1 - \sum_{ijlm} |c_{ij}|^2 |c_{lm}|^2 \mathbb{E}[\chi_{ijlm}] \quad (9.45)$$

providing an upper bound on the purity loss. In the limit of weak noise the inequality approaches equality, giving an approximate weak noise expression for purity loss. To make the noise dependence explicit, we need to evaluate the quantities

$$\mathbb{E}[\chi_{ijlm}] = \frac{1}{2} \sum_k \mathbb{E}[(s_i - s_l)\alpha_k^1(\tau) + (s_j - s_m)\alpha_k^2(\tau)]^2 \coth[\hbar\omega_k / (2k_B T_k)] \quad (9.46)$$

To do so, we first introduce  $S_{\Omega_e}(\omega)$ ; the power spectral density of the Rabi rate fluctuations

$$\mathbb{E}[\Omega_e(t_1)\Omega_e(t_2)] = \frac{1}{2\pi} \int_{-\infty}^{\infty} d\omega S_{\Omega_e}(\omega) e^{i\omega(t_1 - t_2)}. \quad (9.47)$$

From (9.45) and (9.46), we then arrive at the weak noise approximation for the purity loss

$$\mathbb{E}[\bar{P}] \approx \frac{1}{8\pi} \int_{-\infty}^{\infty} d\omega S_{\Omega_e}(\omega) F(\omega) \quad (9.48)$$

where  $F(\omega) = \sum_k D_k F_k(\omega)$

$$D_k = \sum_{ijlm} |c_{ij}|^2 |c_{lm}|^2 \left| (s_i - s_l) \eta_k^1 + (s_j - s_m) \eta_k^2 \right|^2 \coth [\hbar\omega_k / (2k_B T_k)] \quad (9.49)$$

and  $F_k(\omega) = \left| \int_0^\infty e^{i(\omega+\delta_k)t} r(t; \tau) \right|^2$ .

# Chapter 10

## Conclusion

The design and implementation of high-fidelity quantum control operations that are resistant to error is a necessary condition for the realization of practical QIP devices, as are techniques for evaluating the performance of such operations. In this thesis, we've sought to make progress towards meeting these conditions via the presentation of novel methods for both modeling and suppressing errors in QIP systems. We've considered a general class of control protocols and settings, covering state preservation and nontrivial quantum information processing tasks in both single and multi-qubit QIP systems. The work was undertaken with the intention of making the proposed methods useful and accessible to experimentalists. We therefore chose to emphasize the intuitive and experimentally relevant view of error-robust control operations as noise filters, acting to remove detrimental frequency-domain contributions to environmental and control noise. This also allowed us to make a number of interesting and useful connections to concepts in classical control theory and signal processing.

The first half of the thesis focused on the frequency-domain analysis of the effects of classical time-dependent universal noise on single-qubit systems. We described an efficient and accessible analytical approach to modeling the effects of such noise. This enabled the evaluation of arbitrary single-qubit control operations in terms of spectral characteristics of the noise and a set of *generalized filter functions* representing the action of the control. The utility and widespread applicability of this theoretical ‘toolkit’ was demonstrated by applying it to a number of important and interesting problems that had not previously been addressed from a filtering perspective. We modeled the effect of finite operation time on single-qubit control operations, comparing the performance of simple, primitive gates and error-robust dynamically corrected gates (DCGs). We also extended the standard ‘bang bang’ dynamical decoupling filter function formalism to include first order noise/pulse-width effects. In addition, we were able to quantify the extent to which existing composite pulses, devised to correct for static control errors, remain effective in time-dependent non-Markovian noise environments. These analytic results were supported by brute-force numerical simulation and experiments conducted on ‘bath-engineered’ ion trap systems, and shown to be accurate over a surprisingly wide range of parameter values.

In the latter half of the work, we obtained a number of new and important results that generalize the utility of state-preserving ‘bang-bang’ DD sequences. We showed that a high-fidelity, single-qubit quantum memory could be created via the repetition of a base DD sequence, and that this memory remains viable in the presence of realistic experimental imperfections. We also showed that, in particular noise environments, multi-qubit DD sequences can be devised that ensure maximum high-order error suppression in both the time and the frequency domains, using exponentially fewer pulses than sequences designed for arbitrary noise environments. In the last chapter, we presented a framework for improving entangling gate fidelity in qubit-

oscillator systems by efficiently decoupling intermediary bosonic modes after a predetermined interaction time. This framework enables simultaneous decoupling of multiple oscillator modes using sequences of discrete, quasi-instantaneous phase shifts. These sequences can then be concatenated to create robustness against time-dependent control noise. This phase-modulation approach complements and provides substantial benefits relative to existing techniques, leveraging the technical simplicity of phase modulation in RF electronics. Taken together, we hope that the modeling techniques and error suppressing protocols presented in this thesis will constitute a significant contribution to the existing literature on control and error suppression techniques in QIP systems.

# References

- [1] B. Schumacher, M. Westmoreland, *Quantum Processes, Systems & Information* (Cambridge University Press, Cambridge, 2010).
- [2] A. Peres, *Quantum Theory: Concepts and Methods* (Kluwer Academic Publishers, New York, 2002).
- [3] C. A. Fuchs, *arXiv:quant-ph/0205039* (2002).
- [4] C. E. Shannon, *Bell System Tech. J.* **27**, 379 (1948).
- [5] A. M. Turing, *Proc. Lond. Math.* **42**, 230 (1936).
- [6] M. A. Nielsen and I. L. Chuang, *Quantum Computation and Quantum Information: 10th Anniversary Edition* (Cambridge University Press, Cambridge, 2010).
- [7] M. A. Schlosshauer, *Decoherence and the Quantum-To-Classical Transition* (Springer, 2008).
- [8] E. Joos, H. D. Zeh, C. Kiefer, D. Giulini, J. Kupsch and I.-O. Stamatescu, *Decoherence and the Appearance of a Classical World in Quantum Theory* (Springer, New York, 2003).
- [9] M. Brune, E. Hagley, J. Dreyer, X. Maitre, C. Wunderlich, J. M. Raimond and S. Haroche, *Phys. Rev. Lett.* **77**, 4887 (1996).
- [10] S. Haroche, *Physica Scripta* **T76**, 159 (1998).
- [11] Q. A. Turchette, C. J. Myatt, B. E. King, C. A. Sackett, D. Kielpinski, W. M. Itano et al., *Phys. Rev. A* **62**, 053807 (2000).
- [12] W. Wootters and W. Zurek, *Nature* **299**, 802 (1982).
- [13] D. Dieks, *Phys. Lett. A* **92**, 271 (1982).
- [14] Shor, P. W., *Phys. Rev. A* **52**, 2493 (1995).
- [15] Steane, A. M., *Phys. Rev. Lett.* **77** 793 (1996).
- [16] Laflamme, R., Miquel, C., Pas, J. P., and Zurek, W. H., *Phys. Rev. Lett.* **77**, 198 (1996).
- [17] E. Knill, R. Laflamme, and W. H. Zurek, *Math., Phys. and Eng. Sci.* **454**, 365 (1998).
- [18] P. Aliferis, D. Gottesman and J. Preskill, *Quant. Info. and Comp.* (2009).
- [19] E. L. Hahn, *Phys. Rev.* **80**, 580 (1950).
- [20] U. Haeberlen and J. S. Waugh, *Phys. Rev.* **175**, 453 (1968).

- [21] U. Haeberlen, *High Resolution NMR in Solids: Selective Averaging* (Academic Press, New York, 1976).
- [22] C.-T. Chen, *Linear System Theory & Design: Third Edition* (Oxford University Press, New York, 1999).
- [23] W. L. Brogan, *Modern Control Theory: Third Edition* (Prentice-Hall International, 1991).
- [24] J. G. Proakis and D. G. Manolakis, *Digital Signal Processing: 3rd Edition* (Prentice-Hall International, 1996).
- [25] S. Kochen and E. Specker, *J. Math. Mech.* **17**, 59 (1967).
- [26] E. Prugovecki, *Quantum Mechanics in Hilbert Space: 2nd Edition* (Academic Press, New York, 1981).
- [27] M. Born, *Z. Phys.* **37**, 863 (1926).
- [28] F. Schwabl, *Advanced Quantum Mechanics: Fourth Edition* (Springer-Verlag, Berlin, 2008).
- [29] J. J. Sakurai, *Modern Quantum Mechanics* (Addison-Wesley, 1994).
- [30] H. P. Breuer and F. Petruccione, *The Theory of Open Quantum Systems* (Oxford University Press, USA, 2002).
- [31] W. H. Zurek, *Phys. Today* **44**, 36 (1991).
- [32] M. J. Biercuk, H. Uys, A. P. VanDevender, N. Shiga, W. M. Itano and J. J. Bollinger, *Nature* **458**, 996 (2009).
- [33] J. M. Martinis, S. Nam, J. Aumentado, K. M. Lang and C. Urbina, *Phys. Rev. B* **47**, 094510 (2003).
- [34] D. J. Tannor, *Introduction to Quantum Mechanics: A Time-Dependent Perspective* (University Science Books, 2007).
- [35] J. A. Gubner, *Probability and Random Processes for Electrical and Computer Engineers* (Cambridge University Press, 2006).
- [36] S. L. Miller and D. Childers, *Probability and Random Processes: With Applications to Signal Processing and Communications* (Elsevier, 2012).
- [37] E. Fraval, M. J. Sellars and J. J. Longdell, *Phys. Rev. Lett.* **95**, 030506 (2009).
- [38] J. J. L. Morton, A. M. Tyryshkin, R. M. Brown, S. Shankar, B. W. Lovett, A. Ardavan, T. Schenkel, E. E. Haller, J. W. Ager and S. A. Lyon, *Nature* **455**, 1085 (2008).
- [39] S. Damodarakurup, M. Lucamarini, G. D. Giuseppe, D. Vitali and P. Tombesi, *Nature* **458**, 996 (2009).
- [40] S. Dong and I. R. Peterson, *IET Control Theory & Applications* **4**, 2651 (2010).
- [41] D. D'Alessandro, *Introduction to Quantum Control & Dynamics* (Chapman & Hall/CRC, Boca Raton, 2008).
- [42] C. P. Koch, *J. Phys.: Condens. Matter* **28**, 213001 (2016).

- [43] G. A. Paz-Silva and L. Viola, *Phys. Rev. Lett.* **113**, 250501 (2014).
- [44] M. W. Reinsch, *J. Math. Phys.* **41**, 2434 (2000).
- [45] D. A. Lidar, P. Zanardi and K. Khodjasteh, *Phys. Rev. A* **78**, 012308 (2008).
- [46] K. Khodjasteh and D. A. Lidar, *Phys. Rev. A* **75**, 062310 (2007).
- [47] M. J. Biercuk, A. C. Doherty and H. Uys, *J Phys. B* **44**, 154002 (2011).
- [48] L. Viola and S. Lloyd, *Phys. Rev. A* **58**, 2733 (1998).
- [49] A. G. Kofman and G. Kurizki, *Phys. Rev. Lett.* **87**, 270405 (2001).
- [50] G. Gordon and G. Kurizki, *Phys. Rev. A* **76**, 042310 (2007).
- [51] G. Gordon, G. Kurizki and D. A. Lidar, *Phys. Rev. Lett.* **101**, 010403 (2008).
- [52] G. S. Uhrig, *New J. Phys.* **10**, 083024 (2008).
- [53] L. Cywinski, R. M. Lutchyn, C. P. Nave and S. Das Sarma, *Phys. Rev. B* **77**, 174509 (2008).
- [54] K. Khodjasteh, D. A. Lidar and L. Viola, *Phys. Rev. Lett.* **104**, 090501 (2010).
- [55] K. Khodjasteh and L. Viola, *Phys. Rev. A* **80**, 032314 (2009).
- [56] K. Khodjasteh and D. A. Lidar, *Phys. Rev. A* **78**, 012355 (2008).
- [57] P. Zanardi, *Phys. Lett. A* **258**, 77 (1999).
- [58] L. Viola, E. Knill and S. Lloyd, *Phys. Rev. Lett.* **82**, 2417 (1999).
- [59] J. Kempe, D. Bacon, D. A. Lidar and K. B. Whaley, *Phys. Rev. A* **63**, 042307 (2001).
- [60] L. Viola, E. Knill and S. Lloyd, *Phys. Rev. Lett.* **83**, 4888 (1999).
- [61] L. Viola and E. Knill, *Phys. Rev. Lett.* **90**, 037901 (2003).
- [62] D. Vitali and P. Tombesi, *Phys. Rev. A* **59**, 4178 (1999).
- [63] M. S. Byrd and D. A. Lidar, *Phys. Rev. A* **67**, 012324 (2003).
- [64] K. Khodjasteh and D. A. Lidar, *Phys. Rev. Lett.* **99**, 180501 (2005).
- [65] W. Yao, R. B. Liu and L. J. Sham, *Phys. Rev. Lett.* **98**, 077602 (2007).
- [66] P. Kuopanportti, M. Mottonen, V. Bergholmand, O.-P. Saira, J. Zhang and K. B. Whaley, *Phys. Rev. A* **77**, 032334 (2008).
- [67] G. S. Uhrig, *Phys. Rev. Lett.* **98**, 100504 (2007).
- [68] K. Khodjasteh and L. Viola, *Phys. Rev. Lett.* **102**, 080501 (2009).
- [69] W. Magnus, *Pure Appl. Math.* **7**, 649 (1954).
- [70] S. Blanes, F. Casas, J. A. Oteo and J. Ros, *Phys. Rep.* **470**, 151 (2009).
- [71] B. Schumacher, *Phys. Rev. A* **54**, 2614 (1996).

- [72] K. Khodjasteh, T. Erdelyi and L. Viola, *Phys. Rev. A* **83**, 020305R (2011).
- [73] A. G. Kofman and G. Kurizki, *Phys. Rev. Lett.* **93**, 130406 (2004).
- [74] J. Clausen, G. Bensky and G. Kurizki, *Phys. Rev. Lett.* **104**, 040401 (2010).
- [75] D. Hayes, K. Khodjasteh, L. Viola and M. J. Biercuk, *Phys. Rev. A* **84**, 062323 (2011).
- [76] M. J. Biercuk and H. Bluhm, *Phys. Rev. B* **83**, 235316 (2011).
- [77] T. J. Tarn, G. Huang and J. W. Clark, *Math. Modeling* **1**, 109 (1980).
- [78] G. M. Huang, T. J. Tarn and J. W. Clark, *J. Math. Phys.* **24**, 2608 (1983).
- [79] J. W. Clark, D. G. Lucarelli and T. J. Tarn, *Int. J. Mod. Phys. B* **17**, 5397 (2003).
- [80] L. Bouten, R. Van Handel and M. R. James, *SIAM J. Control Optim.* **46**, 2199 (2007).
- [81] H. I. Nurdin, M. R. James and I. R. Petersen, *Automatica* **45**, 1837 (2009).
- [82] H. M. Wiseman and G. J. Milburn, *Quantum Measurement and Control* (Cambridge University Press, Cambridge, 2010).
- [83] D. D'Alessandro, *Introduction to Quantum Control and Dynamics* (Taylor & Francis, Boca Raton, 2007).
- [84] P. Aliferis, D. Gottesman and J. Preskill, *Quant. Info. and Comp.* (2009).
- [85] A. G. Kofman and G. Kurizki, *Phys. Rev. Lett.* **93**, 130406 (2004).
- [86] M. Ban, *Journal of Modern Optics* **45**, 2315 (1998).
- [87] J. T. Merrill and K. R. Brown, *Adv. Chem. Phys.* **154**, 241 (2014).
- [88] M. J. Biercuk, H. Uys, A. P. VanDevender, N. Shiga, W. M. Itano, Wayne M. and J. J. Bollinger, *Phys. Rev. A* **79**, 062324 (2009).
- [89] G. de Lange, Z. H. Wang, D. Rist, V. V. Dobrovitski, R. Hanson, *Science* **330**, 60 (2010).
- [90] H. Bluhm and S. Foletti and I. Neder and M. Rudner and D. Mahalu and V. Umansky and A. Yacoby, *Nature Physics* **7**, 109 (2010).
- [91] J. Medford, L. Cywiński, C. Barthel, C. M. Marcus, M. P. Hanson, A. C. Gossard and S. Das Sarma, *Phys. Rev. Lett.* **108**, 086802 (2012).
- [92] G. de Lange, D. Rist, V. V. Dobrovitski, R. Hanson, *Phys. Rev. Lett.* **106**, 080802 (2011).
- [93] J. Bylander, S. Gustavsson, F. Yan, F. Yoshihara, K. Harrabi, G. Fitch, D. G. Cory, Y. Nakamura, J.- S. Tsai and W. D. Oliver, *Nat. Phys.* **7**, 565 (2011).
- [94] S. Kotler, N. Akerman, Y. Glickman, A. Keselman and R. Ozeri, *Nature* **473**, 61 (2011).
- [95] M. S. Byrd and D. A. Lidar, *Quantum Information Processing* **1**, 19 (2002).
- [96] S. Pasini and G. S. Uhrig, *J. Phys. A: Math. Theor.* **41**, 312005 (2008).
- [97] B. Fauseweh, S. Pasini and G. S. Uhrig, *Phys. Rev. A* **85**, 022310 (2012).

- [98] W. K. Tung, *Group Theory in Physics* (World Scientific, 1985).
- [99] H. K. Ng, D. A. Lidar and J. Preskill, *Phys. Rev. A* **84**, 012305 (2011).
- [100] T. J. Green, H. Uys and M. J. Biercuk, *Phys. Rev. Lett.* **109**, 020501 (2012).
- [101] M. H. Levitt, *Prog. NMR Spectrosc.* **18**, 61 (1986).
- [102] A. M. Souza, G. A. Alvarez and D. Suter, *Phys. Rev. Lett.* **106**, 240501 (2011).
- [103] L. Viola, *private communication* (2012).
- [104] H. Y. Carr and E. M. Purcell, *Phys. Rev.* **94**, 630 (1954).
- [105] K. Khodjasteh, J. Sastrawan, D. Hayes, T. J. Green, M. J. Biercuk and L. Viola, *Nature Commun.* **4**, 2045 (2013).
- [106] P. C. Moan, J. A. Oteo and J. Ros, *J. Phys. A: Math. Gen.* **32**, 5133 (1999).
- [107] K. Spindler, *Abstract Algebra with Applications - Volume 1* (Marcel Dekker, Inc., 1994).
- [108] T. J. Green, J. Sastrawan, H. Uys and M. J. Biercuk, *New J. Phys.* **15**, 095004 (2013).
- [109] M. H. Levitt and R. Freeman, *J. Magn. Reson.* **43**, 65 (1981).
- [110] S. Wimperis, *J. Magn. Reson.* **109**, 221 (1994).
- [111] K. R. Brown, A. W. Harrow, and I. L. Chuang, *Phys. Rev. A* **70**, 052318 (2004); **72**, 039905(E) (2005).
- [112] S. Odedra, M. J. Thriplleton and S. Wimperis, *J. Magn. Reson.* **225**, 81 (2012).
- [113] Y. Tomita, J. T. Merrill and K. R. Brown, *New J. Phys.* **12**, 015002 (2010).
- [114] M. Bando, T. Ichikawa, Y. Kondo and M. Nakahara, *J. Phys. Soc. Jpn.* **82**, 014004 (2013).
- [115] G. H. Low, T. J. Yoder and I. L. Chuang, *arXiv:1307.2211* (2013).
- [116] D. Leibfried, R. Blatt, C. Monroe and D. Wineland, *Rev. Mod. Phys.* **75**, 281 (2003); H. Haffner, C. Roos and R. Blatt, *Phys. Rep.* **469**, 155 (2008); N. Timoney, V. Elman, S. Glaser, C. Weiss, M. Johanning, W. Neuhauser and C. Wunderlich, *Phys. Rev. A* **77**, 052334 (2008); W. Rakreungdet, J. H. Lee, K. F. Lee, B. E. Mischuck, E. Montano and P. S. Jessen, *ibid.* **79**, 022316 (2009); C. M. Shappert et al., *New J. Phys.* **15**, 083053 (2013); J. T. Merrill et al., *arXiv:1401.1121v1*.
- [117] J. J. L. Morton, A. M. Tyryshkin, A. Ardavan, K. Porfyrakis, S. A. Lyon and G. A. D. Briggs, *Phys. Rev. Lett.* **95**, 200501 (2005); I. Chiorescu, Y. Nakamura, C. J. P. M. Harmans and J. E. Mooij, *Science* **299**, 1869 (2003); J. Clarke and F. K. Wilhelm, *Nature* **453**, 1031 (2008).
- [118] S. Montangero, T. Calarco and R. Fazio, *Phys. Rev. Lett.* **99**, 170501 (2007).
- [119] K. Khodjasteh, H. Bluhm, and L. Viola, *Phys. Rev. A* **86**, 042329 (2012).
- [120] R. L. Kosut, M. D. Grace and C. Brif, *Phys. Rev. A* **88**, 052326 (2013).
- [121] M. Mottonen, R. de Sousa, J. Zhang and K. B. Whaley, *Phys. Rev. A* **73**, 022332 (2006).

- [122] Z. Chen, J. G. Bohnet, J. M. Weiner, and J. K. Thompson, *Phys. Rev. A* **86**, 032313 (2012).
- [123] X. Wang, L. S. Bishop, E. Barnes, J. P. Kestner and S. Das Sarma, *Phys. Rev. A* **89**, 022310 (2014).
- [124] S. G. Schirmer, *Lagrangian and Hamiltonian Methods for Nonlinear Control 2006, Lect. Notes Control Info. Sci.*, edited by F. Allguwer et al., Vol. 366 (Springer, Berlin, 2007).
- [125] H. Uys, M. J. Biercuk and J. J. Bollinger, *Phys. Rev. Lett.* **103**, 040501 (2009).
- [126] D. J. Szwer, S. C. Webster, A. M. Steane and D. M. Lucas, *J. Phys. B* **44**, 025501 (2011).
- [127] A. Soare, H. Ball, D. Hayes, X. Zhen, M. C. Jarratt, H. Uys and M. J. Biercuk, *Phys. Rev. A* **89**, 042329 (2014).
- [128] H. K. Cummins, G. Llewellyn and J. A. Jones, *Phys. Rev. A* **67**, 042308 (2003).
- [129] R. Ghanem and P. Spanos, *Stochastic Finite Elements: A Spectral Approach* (Springer, London, 2012).
- [130] N. Kasdin, *Proc. IEEE* **83**, 802 (1995); G. Stefanou and M. Papadrakakis, *Comput. Methods Appl. Mech. Eng* **196**, 2465 (2007).
- [131] J. A. Jones, *Phys. Rev. A* **87**, 052317 (2013).
- [132] M. B. Weissman, *Rev. Mod. Phys.* **60**, 537 (1988).
- [133] E. Paladino, L. Faoro, G. Falci and R. Fazio, *Phys. Rev. Lett.* **88**, 228304 (2002); L. Faoro and L. B. Ioffe, *ibid.* **100**, 227005 (2008).
- [134] L. Faoro and L. Viola, *Phys. Rev. Lett.* **92**, 117905 (2004).
- [135] J. F. Harris, *Proc. IEEE* **66**, 51 (1978); J. Thom, G. Wilpers, E. Riis and A. G. Sinclair, *Opt. Express* **21**, 18712 (2013).
- [136] P. Sengupta and L. P. Pryadko, *Phys. Rev. Lett.* **95**, 037202 (2005).
- [137] A. Smith et. al., *Phys. Rev. Lett.* **111**, 170502 (2013).
- [138] F. Dolde et. al., *Nature Phys.* **7**, 459 (2011).
- [139] G. Kucsko et. al., *Nature* **500**, 54 (2013).
- [140] A. Cooper, E. Magesan, H. Yum and P. Cappellaro, *Nature Comms.* **5**, 3141 (2014).
- [141] G. A. Alvarez and D. Suter, *Phys. Rev. Lett.* **107**, 230501 (2011).
- [142] L. M. K. Vandersypen and I. Chuang, *Rev. Mod. Phys.* **76**, 1037 (2004).
- [143] C. Kabytayev, T. J. Green, K. Khodjasteh, M. J. Biercuk, L. Viola and K. R. Brown, *Phys. Rev. A* **90**, 012316 (2016).
- [144] X. Wang et. al., *Nature Comms.* **3**, 997 (2012).
- [145] F. Ticozzi, K. Nishio and C. Altafini, *IEEE Trans. Auto. Control* **58**, 74 (2013).
- [146] K. G. Beauchamp, *Walsh Functions and their Applications* (Academic Press, 1975).

- [147] P. Owrutsky and N. Khaneja, *arXiv:1204.006* (2012).
- [148] N. C. Jones, T. D. Ladd and B. H. Fong, *New J. Phys.* **14**, 093045 (2012).
- [149] C. Barthel, J. Medford, C. M. Marcus, M. P. Hanson and A. C. Gossard, *Phys. Rev. Lett.* **336**, 266808 (2010).
- [150] G.-Q. Liu, H. C. Po, J. Du, R. B. Liu and X. Y. Pan, *Nat. Comms.* **4**, 2254 (2013).
- [151] A. M. Souza, G. A. Alvarez and D. Suter, *Phys. Rev. A* **86**, 050301 (2012).
- [152] T. van der Sar et al., *Nature* **484**, 82 (2012).
- [153] Z.-K. Su and S.-J. Jiang, *Journal of Physics B: Atomic, Molecular and Optical Physics* **45**, 025502 (2012).
- [154] T. J. Green and M. J. Biercuk, *Phys. Rev. Lett.* **114**, 120502 (2015).
- [155] K. J. Horadam, *Hadamard Matrices and their Applications* (Princeton University Press, 2007).
- [156] D. A. Lidar and T. A. Brun, *Quantum Error Correction* (Cambridge University Press, 2013).
- [157] S. Olmschenk et al., *Phys. Rev. A* **76**, 052314 (2007).
- [158] Y. Sagi, I. Almog and N. Davidson, *Phys. Rev. Lett.* **105**, 053201 (2010).
- [159] I. Almog, Y. Sagi, G. Gordon, G. Bensky, G. Kurizki and N. Davidson, *J. Mod. Phys.* **44**, 154006 (2011).
- [160] S. Foletti, H. Bluhm, D. Mahalu, V. Umansky and A. Yacoby, *Nature Phys.* **5**, 903 (2009).
- [161] M. D. Schulman, O. E. Dial, S. P. Harvey, H. Bluhm, V. Umansky and A. Yacoby, *Science* **336**, 202 (2011).
- [162] A. M. Tyryshkin, Z.-H. Wang, W. Zhang, E. E. Haller, J. W. Ager, V. V. Dobrovitski and S. A. Lyon, *arXiv:1011.1903* (2010).
- [163] Z.-H. Wang, W. Zhang, A. M. Tyryshkin, S. A. Lyon, J. W. Ager, E. E. Haller and V. V. Dobrovitski, *Phys. Rev. B* **85**, 085206 (2012).
- [164] C. A. Ryan, J. S. Hodges and D. G. Cory, *Phys. Rev. Lett.* **105**, 200402 (2010).
- [165] B. Naydenov, F. Dolde, L. T. Hall, C. Shin, H. Fedder, L. C. L. Hollenberg, F. Jelezko and J. Wrachtrup, *Phys. Rev. B* **83**, 081201(R) (2011).
- [166] Z.-H. Wang, G. de Lange, D. Riste, R. Hanson and V. V. Dobrovitski, *Phys. Rev. B* **85**, 155204 (2012).
- [167] D. Hayes, S. M. Clark, S. Debnath, D. Hucul, I. V. Inlek, K. W. Lee, Q. Quraishi and C. Monroe, *Phys. Rev. Lett.* **109**, 020503 (2012).
- [168] M. Palma, K.-A. Suominen and A. K. Ekert, *Proc. R. Soc. London A* **452**, 567 (1996).
- [169] T. Hodgson, L. Viola and I. D'Amico, *Phys. Rev. A* **81**, 062321 (2010).

- [170] T. Yuge, S. Sasaki and Y. Hirayama, *Phys. Rev. Lett.* **107**, 170504 (2011).
- [171] A. Ajoy, G. A. Álvarez and D. Suter, *Phys. Rev. A* **83**, 032303 (2012).
- [172] J. Rutman, *Proc. IEEE* **66**, 1048 (1978).
- [173] G. S. Uhrig and D. A. Lidar, *Phys. Rev. A* **82**, 012301 (2010).
- [174] L. Viola and E. Knill, *Phys. Rev. Lett.* **94**, 060502 (2005).
- [175] L. F. Santos and L. Viola, *Phys. Rev. Lett.* **97**, 150501 (2006).
- [176] L.-M. Duan and C. Monroe, *Rev. Mod. Phys.* **82**, 1209 (2010).
- [177] G. A. Álvarez, M. A. Souza and D. Suter, *Phys. Rev. A* **85**, 052324 (2012).
- [178] L.-M. Duan and G.-C. Guo, *Phys. Rev. A* **57**, 737 (1998).
- [179] J. M. Martinis, *arXiv:1510.01406* (2015).
- [180] R. Kueng, D. M. Long, A. C. Doherty and S. T. Flammia, *arXiv:1510.05653* (2015).
- [181] H. Ball, T. M. Stace, S. T. Flammia and M. J. Biercuk, *Phys. Rev. A* **93**, 022303 (2016).
- [182] A. Leggett, S. Chakravarty, A. Dorsey, M. Fisher, A. Garg and W. Zwerger, *Rev. Mod. Phys.* **59**, 1 (1987).
- [183] R. Doll, D. Zueco, M. Wubs, S. Kohler and P. Hänggi, *Chem. Phys.* **347**, 243 (2008).
- [184] H.-K. Ng and J. Preskill, *Phys. Rev. A* **79**, 032318 (2009).
- [185] L. M. Norris, G. Paz-Silva and L. Viola, *Phys. Rev. Lett.* **116**, 150503 (2016).
- [186] Z.-Y. Wang and R.-B. Liu, 2011 *Phys. Rev. A* **83**, 022306 (2011).
- [187] W. J. Kuo, G. Quiroz, G. A. Paz-Silva and D. A. Lidar, *J. Math. Phys.* **53**, 122207 (2012).
- [188] J.-H. Reina, L. Quiroga and N.-F. Johnson, *Phys. Rev. A* , 032326 (2002)
- [189] K. Kim, H.-J. Lee, D. Ahn and S.-W. Hwang, *J. Korean Phys. Soc.* **37**, 496 (2000).
- [190] Y. Hu, Z.-W. Zhou, J.-M. Cai and G.-C. Guo, *Phys. Rev. A* **75**, 052327 (2007).
- [191] Z.-K. Su and S.-J. Jiang, *J. Phys. B: At. Mol. Opt. Phys.* **45**, 025502 (2012).
- [192] Y. Pan, H.-T. Song and Z.-R. Xi, *J. Phys. B: At. Mol. Opt. Phys.* **45**, 205504 (2012).
- [193] H. Song, Y. Pan and Z. Xi, *Int. J. Quant. Inf.* **11**, 1350012 (2013).
- [194] D. Braun, *Phys. Rev. Lett.* **89**, 277901 (2002).
- [195] S. Oh and J. Kim, *Phys. Rev. A* **73**, 062306 (2006).
- [196] E. M. Fortunato, L. Viola, J. Hodges, G. Teklemariam and D. G. Cory, *New J. Phys.* **4**, 5 (2002).
- [197] R. Kubo, *J. Phys. Soc. Japan* **17**, 1100 (1962).
- [198] D. Brillinger, *Ann. Math. Stat.* **36**, 1351 (1965).

- [199] T. E. Hodgson, L. Viola and I. D’Amico, *Phys. Rev. B* **78**, 165311 (2008).
- [200] J. Jing, R. Li, J.-Q. You and T. Yu, *Phys. Rev. A* **91**, 022109 (2015).
- [201] L. F. Santos and L. Viola, *New J. Phys.* **10**, 083009 (2008).
- [202] G. A. Paz-Silva and D. A. Lidar, *Sci. Rep.* **3**, 1530 (2013).
- [203] S. Pasini and G. S. Uhrig, *Phys. Rev. A* **81**, 012309 (2010).
- [204] C. Uchiyama, *Phys. Rev. A* **66**, 032313 (2002).
- [205] E. Paladino, Y. M. Galperin, G. Falci and B. L. Altshuler, *Rev. Mod. Phys.* **86**, 361 (2014).
- [206] L. Cywiński, *Phys. Rev. A* **90**, 042307 (2014).
- [207] J. Krzywda and K. Roszak, *Sci. Rep.* **6**, 23753 (2016).
- [208] S. Maniscalco, F. Francica, R. L. Zaffino, N. Lo Gullo and F. Plastina, *Phys. Rev. Lett.* **100**, 090503 (2008).
- [209] S. Mancini and J. Wang, *Eur. Phys. J. D* **32**, 257 (2005).
- [210] N. Yamamoto, K. Tsumura and S. Hara, *Automatica* **43**, 981 (2007).
- [211] R. Lo Franco, A. D’Arrigo, G. Falci, G. Compagno and E. Paladino, *Phys. Rev. B* **90**, 054304 (2014).
- [212] P. Szańkowski, M. Trippenbach and L. Cywiński, *Phys. Rev. B* **77**, 174509 (2016).
- [213] F. Ticozzi and L. Viola, *Quantum Inf. & Comp.* **14**, 0265 (2014).
- [214] C. Aron, M. Kulkarni and H. E. Türeci, *Phys. Rev. X* **6**, 011032 (2016).
- [215] F. Reiter, D. Reeb and A. S. Sørensen, *arXiv:1501.06611* (2015).
- [216] Y. Nakamura, Y. A. Pashkin, T. Yamamoto and J. S. Tsai, *Phys. Rev. Lett.* **88**, 047901 (2002).
- [217] A. Johnson, J. Petta, J. Taylor, A. Yacoby and M. Lukin, *Nature* **435**, 925 (2005).
- [218] H. Ball, W. D. Oliver and M. J. Biercuk, *arXiv:1602.04551* (2016).
- [219] B. Krummheuer, V. M. Axt and T. Kuhn, *Phys. Rev. B* **65**, 195313 (2002).
- [220] A. Vagov, V. M. Axt and T. Kuhn, *Phys. Rev. B* **66**, 165312 (2002).
- [221] B. Krummheuer, V. M. Axt and T. Kuhn, *Phys. Rev. B* **65**, 195313 (2002).
- [222] A. Vagov, V. M. Axt and T. Kuhn, *Phys. Rev. B* **66**, 165312 (2002).
- [223] K. Roszak K and P. Machnikowski, *Phys. Rev. A* **73**, 022313 (2006).
- [224] F. Lastra, S. A. Reyes and S. Wallentowitz, *J. Phys. B* **45**, 015504 (2011).
- [225] O. Cotlet and B. W. Lovett, *New J. Phys.* **16**, 103016 (2014).
- [226] N. V. Prokofev and P. C. E. Stamp, *Rep. Prog. Phys.* **63**, 669 (2000). 63, 669726 (2000).

- [227] A. Shnirman, Y. Makhlin and G. Shon, *Phys. Scr.* **T102**, 147 (2002).
- [228] A. Soare, H. Ball, D. Hayes, J. Sastrawan, M. C. Jarratt, J. J. McLoughlin, X. Zhen, T. J. Green and M. J. Biercuk, *Nature Phys.* **10**, 825 (2014).
- [229] C. Monroe, D. M. Meekhof, B. E. King, W. M. Itano and D. J. Wineland, *Phys. Rev. Lett.* **75**, 4714 (1995).
- [230] A. Sorensen and K. Molmer, *Phys. Rev. Lett.* **82**, 1971 (1999).
- [231] G. J. Milburn, S. Schneider and D. F. V. James, *Fortschr. Phys.* **48**, 801 (2000).
- [232] X.-L. Feng, Z. Wang, C. Wu, L. C. Kwek, C. M. Lai and C. H. Oh, *Phys. Rev. A* **75**, 052312 (2007).
- [233] J. Majer, J. M. Chow, J. M. Gambetta, J. Koch, B. R. Johnson, J. A. Schreier, L. Frunzio, D. I. Schuster, A. A. Houck, A. Wallraff, A. Blais, M. H. Devoret, S. M. Girvin and R. J. Schoelkopf, *Nature* **449**, 443 (2007).
- [234] A. Albrecht, A. Retzker, F. Jelezko and M. B. Plenio, *New J. Phys.* **15**, 083014 (2013).
- [235] C. Monroe C, R. Raussendorf, A. Ruthven, K. R. Brown, P. Maunz, L.-M. Duan and J. Kim, *Phys. Rev. A* **89**, 022317 (2014).
- [236] K. Kim, M.-S. Chang, R. Islam, S. Korenblit, L.-M. Duan and C. Monroe, *Phys. Rev. Lett.* **103**, 120502 (2009).
- [237] T. Choi, S. Debnath, T. A. Manning, C. Figgatt, Z.-X. Gong, L.-M. Duan and C. Monroe, *Phys. Rev. Lett.* **112**, 190502 (2014).
- [238] L.-X. Cen and P. Zanardi, *Phys. Rev. A* **71**, 060307 (2005).
- [239] J.-P. Allouche J. and Shallit, *Automatic Sequences: Theory, Applications, Generalizations* (Cambridge University Press, Cambridge, 2003).
- [240] C. Mauduit, *Period. Math. Hungar.* **43**, 137 (2001).
- [241] R. M. Richman, *Complex Systems* **13**, 381 (2001).
- [242] P. J. Lee, K.-A. Brickman, L. Deslauriers, P. C. Haljan, L.-M. Duan and C. Monroe, *J. Opt. B: Quantum Semiclass. Opt.* **7**, S371 (2005).
- [243] K.-A. Brickman Soderberg and C. Monroe, *Rep. Prog. Phys.* **73**, 036401 (2010).
- [244] S.-L. Zhu, C. Monroe and L.-M. Duan, *Phys. Rev. Lett.* **97**, 050505 (2006).
- [245] C. Tsallis, *J. Stat. Phys.* **52**, 479 (1988).
- [246] J. Audretsch, *Entangled systems: new directions in quantum physics.* (Wiley-VCH, 2007).
- [247] K. E. Khosla, M. R. Vanner, W. P. Bowen and G. J. Milburn, *New J. Phys.* **15**, 043025 (2013).
- [248] D. J. Wineland, C. Monroe, W. M. Itano, D. Leibfried, B. E. King and D. M. Meekhof, *J. Res. Natl. Inst. Stand. Technol.* **103**, 259 (1998).